Application of Representation Theory to Magnetic and Structural Phase Transitions

Zoso Luke Davies
UCL

Degree of Doctor of Chemistry
June 2009

"It is surmounting difficulties that makes heroes."

Louis Pasture

Declaration

I, Zoso Luke Davies, confirm that the work presented in this thesis is my own. Where information has been derived from other sources, I confirm that this has been indicated in the thesis.

"Brevity is the best recommendation of speech, whether in a senator or an orator."

Marcus Tulius Cicero (106-43 BC)

Abstract

The tools of representation theory offer us a powerful insight in those terms in a system's Hamiltonian which cause it to become ordered. Such is its power that, in many fields, the vocabulary of representations has become conventional; crystallography remains a notable exception. This thesis develops the existing methods for applying representation theory to symmetry lowering phase transitions in crystalline systems, and presents examples of its use.

The opening section reviews the foundations and previous applications of representation theory to magnetic and structural phase transitions. Complimentary to the mathematical framework is a discussion of the physical interpretation of irreducible representations and basis vectors, the building blocks of any system model constructed in this way. Symmetry arguments are used to qualitatively discuss the symmetry breaking in ferroelectric materials and the role of phase factors in the loss of centro-symmetry.

The body of this work is concerned with developing fast, reliable and repeatable methods for applying representation theory to displacive transitions. Calculation of a system's basis vectors requires both a reliable method, and suitable starting resources. In this section, the first verifiable validation of the tables of Kovalev is presented, along with a strategy for determining the appropriate set of trial functions for use with the method of projection operators. Further, a new module in SARA*h*-Refine has been written which performs basis vector refinement of powder diffraction data to facilitate quantitative analysis using these techniques.

Finally, the techniques of representation theory are applied to two experimental investigations: iron oxyborate and potassium selenate. The use of a single symmetry framework to discuss the structural, magnetic and charge-ordering transitions in these systems demonstrate the power of this technique. Representation theory provides a bridge between structure and properties; this work aims to strengthen the foundations of that bridge.

"Nanos gigantum humeris insidentes."

"Dwarves standing on the shoulders of giants."

Latin saying

Acknowledgements

I would like to thank all those who took interest in my work during the last three years, and those who encouraged me before then. In particular I would like to thank Andrew for taking me on as his student, and the rest of G19 for not mentioning that I snore.

"A good gulp of hot whiskey at bedtime - it's not very scientific but it helps."

Alexander Flemming

Dedication

To Pat, Coral, and Kate; my three non-scientists.

Contents

List of Tables

List of Figures

KEY

General Notation

$\vec{x}, \vec{y}, \vec{z}$	A vector
$\mathbb{A}, \mathbb{B}, \mathbb{C}$	A set
$\mathbb{A}_x$	A subset
$n(\mathbb{A})$	The order of the set $\mathbb{A}$
$\mathfrak{M}, \mathfrak{N}, \mathfrak{O}$	A matrix
$\mathfrak{M}_{ab}$	The ab'th element of a matrix
$\mathscr{F}, \mathscr{G}, \mathscr{H}$	A field

Specific Notation

$\vec{k}$	The k-vector
$\mathscr{C}$	Field of complex numbers
$\mathbb{Z}$	Set of all integers
Γ^ν	The ν'th irreducible representation
$\mathfrak{d}^\nu(g)$	The matrix representation of g in Γ^ν
d^ν	The dimension of the ν'th irreducible representation
$\mathbb{T}$	The set of primitive translation operations
E	The identity operation
I	The inversion operation

Boolean Operators

iff	If and only if	$\therefore$	Therefore
$\exists$	There exists	$\forall$	For all
$\subset$	Subset	$\in$	Is a member of
$\longmapsto$	Maps to	$\otimes$	Direct product

CHAPTER 1

The evolution of crystal symmetry

"I like to recall [M. von Laue's] question as to which results derived in the present volume I considered the most important . . . I have come to agree with his answer that the recognition that almost all rules of spectroscopy follow from the symmetry of the problem is the most remarkable result"

E. Wigner

1.1. Introduction

Symmetry is integral to many areas of science, drastically simplifying problems in fields as diverse as density functional theory and X-ray diffraction (e.g. van Leeuwen, 1998; Buxton, 1976). Almost all selection rules of spectroscopy are defined by symmetry, and without it the field of diffraction would probably not exist. The 230 space groups that comprise the classical symmetries of a crystal have been known for over 100 years, and their application to crystallography is covered in detail in the International Tables for Crystallography - A (2002). However, there are an ever increasing number of systems that cannot be fully described using space groups, and for which we must extend our concepts of symmetry.

In this chapter, we review how diffraction experiments have driven the evolution of symmetry theory and look at some existing extensions of the space group formalism: the magnetic and superspace groups. Representation theory is introduced as the

most general treatment of symmetry groups, and we state the aims of this thesis in extending the use of representation theory in crystallography.

1.2. Symmetry and diffraction

X-rays were first observed by Crookes, who noticed that shadows formed on photographic plates placed near cathode ray tubes. Despite investigations by Tesla and Hertz, it was Röntgen who first recognized X-rays to be a form of electromagnetic wave (Röntgen, 1894); they are sometimes referred to as Röntgen rays. In 1912 Ewald completed his doctoral thesis on the optical properties of periodic arrays of isotropic resonators (Ewald, 1912). Upon hearing of Ewald's results, von Laue realized that crystals were precisely such a medium, and that X-rays were of an appropriate wavelength to be diffracted by them. Under von Laue's direction, Freidrich and Knipping performed the first X-ray scattering experiment upon a single crystal in 1912 (Friedrich, 1912).

It was immediately apparent that the internal structure of a crystal would determine the nature of the diffraction pattern, but it took much longer for it to be accepted that a diffraction pattern could determine the positions of atoms within a crystal. One of the key problems to overcome in determining crystal structures from diffraction patterns was the "phase problem", whose solution in the 1950s led to the award of a Nobel prize in chemistry to Hauptman (1985, 1990). Hauptman's key breakthrough was the realization that: although the X-rays are diffracted by the electron density function (EDF) of a crystal, it is sufficient to determine the atomic positions which can be approximated to the maxima in the EDF; and that the EDF is non-negative everywhere. Indeed, simple structures were already being solved under the basis of these restrictions, without them being formally stated or recognized.

While crystallography had been a growing science for some years, famously it was the Braggs who first used X-ray diffraction to study the internal structure of crystalline

materials. When the Braggs first began to publish the structures they had determined from experiment (Bragg, 1913; 1914), Fedorov wrote a number of papers emphasizing that *all* the determined structures belonged to the groups he had derived more than 20 years earlier (Fedorov; 1885, 1891)[1]. W. L. Bragg said of Fedorov's preceding work (Bragg, 1958):

> *Fedorov was then to me an almost legendary being who had worked out the 230 crystal classes.*
>
> *Few people at that time were interested in crystallography. Such interest as did exist was in the outer forms of crystals, not in their inner structure. When I started analysing crystals with X-rays, I knew nothing at all about their geometry. It was wonderful for us to discover that great men like Fedorov and Barlow, whom I also got to know, had studied the inner geometry of crystals and provided a sure theoretical basis for our work.*

The space groups were formalized in the Tables for X-ray crystallography (1952) and redefined more recently in the International tables for Crystallography (2002). However, they are fundamentally unchanged since their first publication[2].

1.2.1. Frieze and plane groups

The diffraction pattern of aperiodic systems consists of diffuse scattering, and the information that can be extracted is limited (Welberry, 1976). The greatest amount of information is obtained from diffraction experiments upon systems that are periodic; in a static (time independent) system this is usually associated with translational

[1]The space groups were derived simultaneously by Schöenflies (1891), and soon after by Barlow (1894) who used a different method.
[2]The groups differ only in their choice of axis, origin, or generating elements. The complete groups contain the same symmetry operations when in the same axis system.

symmetry. Frieze and plane groups describe the symmetry of systems that are periodic in one, or two dimensions respectively.

There are 7 frieze groups and 17 plane groups, which follows from the "crystallographic restriction". This restriction states that there exists a vector, $\vec{\eta}$, whose modulus (length) is smaller than that of any element, $\vec{t_i}$, of the group of translational symmetry operators, $\mathbb{T}$:

$$\exists \vec{\eta} : |\vec{\eta}| < |\vec{t_i}| \qquad \forall t_i \in \mathbb{T}, \qquad 0 \neq \eta \in \mathbb{R} \tag{1.1}$$

Another way of stating the restriction is that the translational period of the system must be non-zero, and so there exists a "unit cell" of non-zero area which is repeated throughout the plane. If a space shows translational periodicity along some axis, then the smallest translation along that axis which leaves the system invariant is denoted a; the minimal translation along any other periodic axis is denoted b, c, etc. In crystallography it is conventional to use these minimal translations as the axis system. The span of the minimal translations[3] forms the group $\mathbb{T}$; the translational symmetry group. The crystallographic restriction also limits the possible symmetry operations (combinations of rotations and inversion) that are compatible with a given lattice (Coexter, 1989).

The frieze and plane groups are perhaps best known for their use in works by M. C. Escher, such as the examples in Fig.1.1[4]. In science they are most commonly encountered in soft-matter systems (e.g. Löwen, 2001), though there are examples of solid-state systems showing pseudo one- or two-dimensional symmetry which are expected to show exotic and unusual physics such as high-T_c superconductivity (e.g. Haldane, 1980; Yeom, 1999; Kageyama 1999).

[3]Here span has a technical meaning: it refers to all linear combinations of the axes with integer coefficients. See section 2.8.

[4]All M.C. Escher works ©2009 The M.C. Escher Company - the Netherlands. All rights reserved. Used by permission.

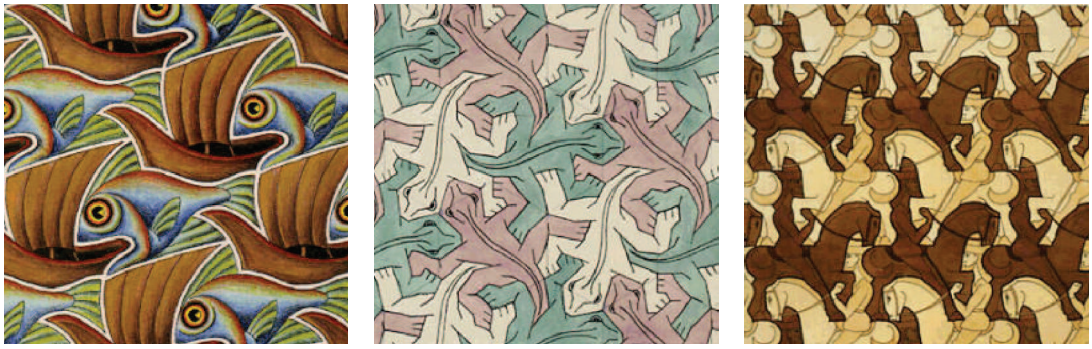

*p*1 *p*3 *pg*

FIGURE 1.1. Some M.C. Escher wallpapers and their plane groups, in this example we disregard the colour when determining symmetry. Taken, with permission, from *www.mcescher.com*

1.2.2. Space groups

Crystalline systems show a periodic arrangement of atoms in three dimensions (or more, as we shall see shortly). The periodic directions are usually employed as the crystallographic axes, and their span defines a lattice. The relative orientations and periods of the translational symmetries define seven crystal systems[5] (Table 1.1).

System	Angles	Lengths
Triclinic	$\alpha \neq \beta \neq \gamma$	$\lvert a\rvert \neq \lvert b\rvert \neq \lvert c\rvert$
Monoclinic	$\alpha = \beta = 90° \neq \gamma$	$\lvert a\rvert \neq \lvert b\rvert \neq \lvert c\rvert$
Othorhombic	$\alpha = \beta = \gamma = 90°$	$\lvert a\rvert \neq \lvert b\rvert \neq \lvert c\rvert$
Tetragonal	$\alpha = \beta = \gamma = 90°$	$\lvert a\rvert = \lvert b\rvert \neq \lvert c\rvert$
Cubic	$\alpha = \beta = \gamma = 90°$	$\lvert a\rvert = \lvert b\rvert = \lvert c\rvert$
Hexagonal	$\alpha = \beta = 90°, \gamma = 60°$	$\lvert a\rvert = \lvert b\rvert \neq \lvert c\rvert$
Trigonal	$\alpha = \beta = \gamma \neq 90°$	$\lvert a\rvert = \lvert b\rvert = \lvert c\rvert$

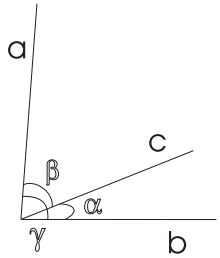

TABLE 1.1. The crystal systems (de Wolf, 1985; International Tables, 2002).

These classes can be extended by convoluting their group of translational operators $\mathbb{T}$ with linear combinations of the "centring" translations: $\frac{a}{2}$, $\frac{b}{2}$, $\frac{c}{2}$. This procedure generates the Bravais lattices, named after mathematician Auguste Bravais who demonstrated in 1850 that there are only 14 unique lattices[6] (Bravais, 1850).

[5]The number of crystal classes can vary by definition; in minerology the the trigonal class is considered to be part of the hexagonal family. Further, an alternate subset of the hexagonal family is the rhombohedral class (Buerger, 1970; de Wolf, 1985).
[6]More strictly, there are 14 unique lattices *up to isomorphism* (See Appendix 2).

There are 32 point groups which are symmetry groups of one or more Bravais lattices, combining these with the 14 Bravais lattice generates 73 *symmorphic* space groups: the space groups lacking screw axes and glide planes. If glide planes and screw-rotation axes are included in the analysis, then a new set of *non-symmorphic* space groups are generated. In total there are 230 different space groups.

1.3. Extending the space groups

The crystallographic space groups are a complete and comprehensive set of symmetry information for triply-periodic systems. However, if we wish to consider properties of an atom other than its position, for example charge or magnetic moment, then we need to extend this formalism to include other types of symmetry operator. Indeed, even in analysis of atomic positions, the space groups have proven insufficient in an increasingly large family of structures: the incommensurate crystals.

1.3.1. Magnetic space groups

With the advent of neutron diffraction, experimentalists were able to gain greater insight into the structure of materials. In particular, because they possess quantum mechanical spin, neutrons distinguish between identical nuclei having non-identical magnetic moments, revealing the presence of long-range magnetic order. Like nuclear order, the magnetic structure only gives rise to diffraction peaks when it is periodic.

Neutrons were discovered by Chadwick in 1932 (Chadwick; 1932a, 1932b), and were found to be chargeless particles, having approximately the weight of a proton and a spin of $\frac{1}{2}$. The first neutron diffraction experiments were performed by E. O. Wollan in 1945 (Wollen, 1948), who was later joined by Clifford Shull (Wollen, 1949). In 1949 Shull was able to experimentally demonstrate the antiferromagnetic ordering of MnO (Shull, 1949) using neutron diffraction. This was the first experimental evidence of antiferromagnetic ordering as predicted by Néel (Néel, 1932), and contributed to

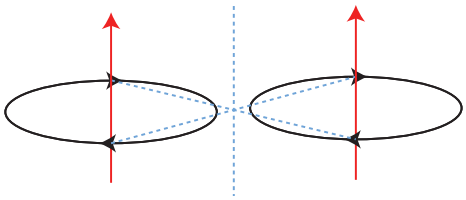

FIGURE 1.2. A magnetic moment shares some of the symmetry of a current loop: it is invariant under inversion of space; inversion of time causes the current loop to run in the opposite sense, reversing the magnetic moment.

Shull's sharing of the Nobel Prize in Physics (1994). It demonstrated the power of neutron diffraction as a tool for exploring magnetic ordering in crystals, and neutrons remain the main probe of magnetic structures.

Many of the systems elucidated by early magnetic diffraction studies had simple magnetic structures: either the magnetic structure had the periodicity of the crystal lattice; or one or more of the cell parameters were doubled. The doubling of the minimal translation in one or more directions corresponds to a loss of translational symmetry, and other symmetry elements can be lost as well. In a Néel antiferromagnet, these "lost" symmetry operations leave the atomic lattice invariant, but invert the spin everywhere.

Magnetic moments are unusual in the sense that they transform as *axial*-vectors; they are invariant under inversion of space, but change sign under an inversion of time (Fig. 1.2). Atomic positions are defined by polar-vectors which change sign under inversion of space, but not under inversion of time. Thus, it is possible to imagine an operation (such as time-reversal) that inverts all the magnetic moments without moving any of the atoms. Combinations of the "time-inversion" operator with those symmetry operations of the lattice which invert the magnetic structure, generates new symmetry operations which leave the magnetic lattice unchanged (Fig.1.3).

The process of combining space group elements with the operation of "time-reversal" generates a new set of space groups; variously denoted as the magnetic, Shubnikov, or the black and white space groups. Extensive work on this problem was performed

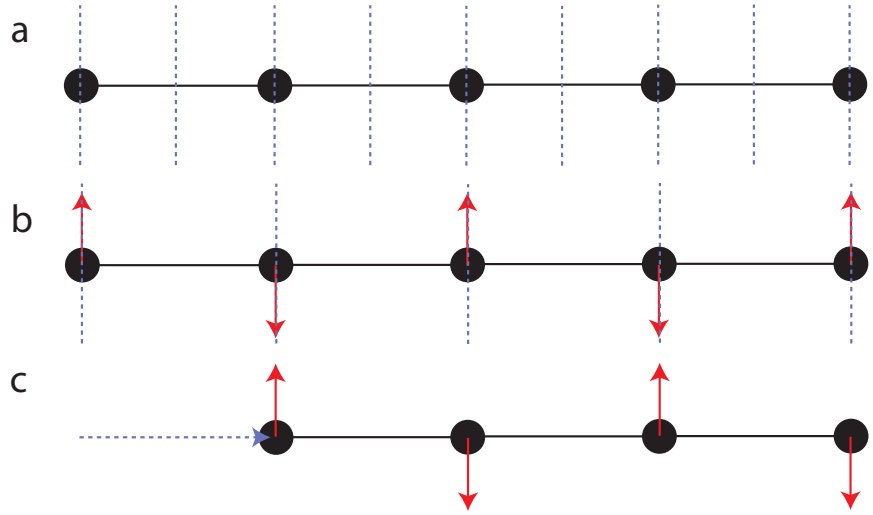

FIGURE 1.3. (a) Part of an infinite line of atoms, the blue dashed lines indicate some of the reflection symmetries of this system. (b) If the atoms become magnetically ordered the symmetry of the system may be lowered, here some of the reflection planes have been "lost". (c) The "lost" operations, such as the translation shown, invert the magnetic structure. Combination of these operations with inversion of the magnetic moments everywhere forms new symmetry operations of the magnetic lattice.

by Belov, Shubnikov, and Opechowski (Belov, 1955; Shubnikov, 1964; Opechowski, 1965), who determined and enumerated the 1651 two-coloured space groups[7]. The derivation of these groups is relatively straight forward (e.g. Cracknell, 1969); each operation of the space group either leaves the magnetic structure invariant or inverted, and operations which invert the structure are primed. Enumeration of all possible magnetic space groups is achieved by listing all the ways to prime half of the generating operators, along with combinations of either the translational group, or some sub-group of translations which is exactly half the size (the other half, of course, being primed). The difficulty, as with deriving the original space groups, lies in determining which of the magnetic groups generated in this way are equivalent.

The formalism of coloured space groups can only represent systems for which the atomic property (here a magnetic moment, but in general any property) has two possible states, represented by the colours black and white. For more complex ordering one would require a different colour for each possible state, and the magnetic

[7]This includes the so-called "grey" groups; groups that describe paramagnetic structures.

symmetries would quickly grow to an unmanageable number. Further, the formalism is only able to represent systems with a finitely large unit cell, a problem that is discussed now.

1.3.2. Incommensurate structures

It is the periodic nature of crystals that gives rise to discrete spots in their diffraction patterns. Usually the pattern of spots is indexible by three vectors: $\vec{h}, \vec{k}, \vec{l}$. The vectors $\vec{h}, \vec{k}, \vec{l}$ define the periodicity of the diffraction pattern in *reciprocal*-space, and are related to the periodic directions in the crystal by:

$$\vec{a}.\vec{h} = \vec{b}.\vec{k} = \vec{c}.\vec{l} = 2\pi \tag{1.2}$$

The γ-phase of Na_2CO_3 is, therefore, unusual in that each point in its diffraction pattern has one or more pairs of "satellite" peaks which can not be indexed using three vectors. In 1964 de Wolff *et. al.* determined that the diffraction pattern contained a *fourth* periodicity, not commensurate with the main lattice (Brouns, 1964). Examples of structural distortions commensurate with the underlying lattice were widely known, and could be described by an enlarged "supercell". However, for a system in which the distortion is incommensurate with the main lattice, the supercell is infinitely large. Such crystals lack pure translational[8] symmetry, yet still give rise to discrete diffraction peaks as they are periodic in *four* (or more) dimensions. In total, the analysis of Na_2CO_3 took nearly 40 years to complete (Dušek, 2003).

It was shown by Janner and Janssen (Janner, 1977) that although systems such as γ-Na_2CO_3 appear to have no symmetry, their structures could be related to space groups embedded in a space of higher dimensionality (Brown, 1978). This formalism is termed superspace group theory, and has been developed by Janner and Janssen (Janner; 1983a, 1983b, 1983c). In superspace group theory the average structure has

[8]Translation-identity.

the symmetry of a space group, but the system is distorted by a periodic modulation. These perturbations take the form of plane waves:

$$\vec{u}(\vec{n}, \vec{r}_j) = \vec{f}_{\vec{r}_j}(\vec{k})e^{i\vec{k}.\vec{n}} \tag{1.3}$$

The amplitude of the wave at the position of the j'th atom, in the n'th unit cell is defined relative to the position of the j'th atom in every other unit cell by the exponential term; the displacement of the atom is parallel to the vector $\vec{f}_{r_j}$. $\vec{k}$ is termed the propagation vector (Janner and Janssen use $\vec{q}$ with the same meaning) and is perpendicular to the wave-fronts of the plane wave.

In magnetic space groups, "lost" symmetry operations are restored by combination with "time-reversal"; an operation which transforms the magnetic moment. Similarly, incommensurate structures are symmetric under combinations of the space group elements with operators that transform the distortion at each atom. We term these transformations of the distortion "phasing" as they correspond to a change in the phase of the plane-wave defining it. The $(3 + n)$ dimensional periodicity of such lattices diffracts X-rays in the same manner as undistorted crystals, but now the patterns are indexed by $(3 + n)$ integers.

While super space groups are a well founded formalism they are also limited. First, super-space groups only consider incommensurate structures. Any commensurate distortion can be expressed as a simple crystal with an enlarged super-cell and so the space group/super space group approach creates an artificial divide between commensurate and incommensurate structures. In fact, as we shall see in the next chapter, this divide is only appropriate when the k-vector lies on a high-symmetry point of the Brillouin zone:

E.g.

There is no difference, formally, between the rational k-vector $(\frac{1}{5}, 0, 0)$

and the irrational k-vector $(\frac{1}{\sqrt{2}}, 0, 0)$. However, super space groups would not consider the $\vec{k} = (\frac{1}{5}, 0, 0)$ case.

The second shortcoming of super-space groups is that they are only concerned with defining the structure of the incommensurate phase, but not the distortion from which it arises. However, to understand the energy terms that drive a phase transitions we should consider the symmetry of the distortion itself. Third, the plane-wave can only be transformed by "phasing", chapter 2 will show that this corresponds to distortions with the symmetry of a one-dimensional irreducible representation. Hence, super-symmetry is not able to fully describe every possible symmetry of higher-dimensional spaces[9].

Finally, super space groups are only concerned with structural distortions. In fact, many properties, such as magnetic- and charge-ordering, can show incommensurate periodicity (e.g. Boehm, 2003; Loudon, 2005; Janssen, 2006; Sánchez, 2008). To fully understand a system all the ordering phenomena should be considered in a single symmetry framework, particularly for systems showing multiple ordering phenomena such as magneto-ferroics (Fiebig, 2005). What is required is a more general symmetry framework that encompasses both commensurate and incommensurate structures, and many types of ordered phenomena.

1.4. Representation theory

Magnetic neutron diffraction underwent its own revelation with the discovery of complex magnetic ordering. In 1952 Néel's model of antiferromagnetism in ferrites was challenged by Yafet who asserted that there were ordered spin arrangements which were neither parallel nor anti-parallel, but that they might have a triangular arrangement (Yafet, 1952). Kaplan extended this idea by demonstrating that helical

[9]This does not imply that super space groups can not define every possible *structure*. However, use of a artificially lower symmetry to describe complex order-phenomena involves a loss of symmetry information.

ordering was possible in systems of competing exchange interactions (Kaplan, 1959); this work elucidated the puzzling diffraction pattern of chromium (Corliss, 1959). Magnetic ordering of this sort was as insoluble to the formalism of magnetic space groups as incommensurate structures were to space groups, and became a driving force behind the extension of magnetic space groups.

Much of the work on ordered complex magnetism was developed by Bertaut, who sought to define magnetic configurations using eigenfunctions of a system's spin Hamiltonian (Bertaut, 1962). He developed his "matrix method" of solving spin configurations into full representation analysis, a mathematical method, and showed that the magnetic space groups formed a sub-set of the symmetries that could be expressed using representation theory (Bertaut; 1968, 1981)[10]. This technique defines magnetic ordering using "basis vectors": complex vectors that define the magnetic moment at each atom. Magnetic basis-vectors are equivalent to the normal modes used in vibrational spectroscopy, and are derived using the same techniques.

The interpretation of magnetic neutron diffraction data using representation theory, and the description of phase transitions with basis vectors was developed further by Izyumov, Naïsh, and Syromyatnikov (Izyumov; 1990, 1991). Central to the application of representation theory to crystals was the work of Kovalev (Kovalev, 1993) and Miller and Love (1967) in tabulating the irreducible representations of all possible k-vectors for every space group. Representation theory is becoming the technique of choice for analysing magnetic structures, particularly from powder-diffraction data (e.g. Wills, 2001, 2005; Arkenbout, 2006), and a number of programs have been developed for its application, such as SARAh (Wills, 2000) and Fullprof (Rodríguez-Carjaval, 2001).

A major advantage of representation theory is its ability to express any ordered property, commensurate or incommensurate, using k-vectors. Bertaut demonstrated that

[10]The magnetic point groups comprise exactly those groups generated by the one-dimensional, real irreducible representations of the crystallographic point groups.

representation theory could express both magnetic and electronic ordering within a *single* symmetry framework, elucidating the mixed terms in magneto-electric systems. In fact, it is entirely general and can be applied to magnetic ordering, structural distortions, charge ordering and other phenomena such as quadrupolar ordering (Sikora, 2008). Further, it differs from superspace groups in that it is explicitly concerned with the order-phenomena driving a phase transition.

1.5. Landau theory

Perhaps the most important contributions to the discussion of symmetry in phase transitions were made by the work of Landau and colleagues (Landau and Lifshitz 1958, Lyubarskii 1960, Anderson and Blount 1965, Haas 1965). Their work on the energy expansion of systems close to critical points gave rise to a number of results including the following theory of second-order phase transitions:

> Every second order phase transition must occur according to a single irreducible representation. [11]

This statement is not completely true; other irreducible representations can be part of higher-order terms in the Landau expansion of a phase transition (Dimmock, 1963). However, Landau's work has created a strong incentive to directly analyse the symmetry of a system's distortion during a phase change as it provides significant insight into the transition energetics. Landau-type expansions of a system's free-energy are now standard (e.g. Harris, 2004; Chandra, 2007; Tagantsev, 2008)

[11] The full symmetry arguments are somewhat more involved (Dimmock 1963, Ascher 1966, Birman 1966).

In chapter 3 we shall see that the relationship between symmetry adapted functions and the energetics of phase transitions runs much deeper than simple Landau theory. The language of symmetry describes the eigenspaces of the Hamiltonian, a fact exploited in spectroscopy when labelling the energy levels of a system.

1.6. Aims and conclusions

In this chapter we have briefly reviewed the use of symmetry in physical chemistry. As more complex and interesting materials are investigated, our theoretical understanding of these systems needs to evolve and grow. While magnetic and super space groups extend our symmetry framework, they are still too limiting for many systems. Further, they fail to describe the phenomena driving phase transitions as they are only concerned with the product of a phase transition. Representation theory is the most general and complete description of possible symmetries, and it explicitly defines the order-phenomena causing a phase transition. What remains is the development of tools to apply its methods to problems in crystallography.

The use of representation theory is already well established in analysing magnetic structures and, in particular, magnetic powder diffraction data. However, it is not limited to analysis of magnetic phenomena and constitutes a symmetry framework for all phase transitions including charge ordering and displacive phase transitions. The aims of this thesis are:

(1) To develop a reliable method of generating all the basis-vectors of a system.
(2) To develop a method for analysing structural transitions using powder diffraction data, parameterized in terms of basis vectors.
(3) To investigate a number of phase transitions using representation theory.

In the next chapter we touch upon the mathematical foundations of representation theory, and in chapter 3 discuss how basis vectors are related to the Hamiltonian of a

system. Chapter 4 explores important empirical results that can be derived from very simple symmetry arguments and an understanding of irreducible representations and basis vectors. The reliability of methods for deriving the basis vectors of a system are developed in chapters 5 and 6, before we present a SARA*h*-Refinement module developed for use in analysing displacive phase transitions from powder diffraction data in chapter 7. Finally, chapters 8 and 9 explore two experimental systems: iron oxyborate and potassium selenate.

References

[1] Anderson, P. W, and Blount, E. I. (1965). *Phys. Rev. Lett.*, **14**, 217.

[2] Arkenbout, A. H. *et. al* (2006). *Phys. Rev. B*, **74**, 184431.

[3] Ascher, E. (1966). *Phys. Lett.*, **20**, 352.

[4] Barlow, W. (1894). *Z. Kristallogr. Mineral.*, **23**, 1-63.

[5] Belov, N. V., Neronova, N. N., and Smirnova, T. S. (1955). *Tr. Inst. Kristallogr. Akad. Nauk. SSSR*, **11**, 33.

[6] Bertaut, E. F. (1962). *J. App. Phys.*, **33**, 1138.

[7] Bertaut, E. F. (1968). *Acta Cryst. A*, **24**, 217.

[8] Bertaut, E. F. (1981). *J. Mag. Mag. Materials*, **24**, 267.

[9] Buerger, M. J. (1970). *Contemporary Crystallography*, **McGraw-Hill** (New York).

[10] Birman, J. L. (1966). *Phys. Rev. Lett.*, **17**, 1216-9.

[11] Boehm, M., Roessli, B., Wills, A. S., *et. al.* (2003). *Phys. Rev. B*, **68**, 024405.

[12] Bragg, W. L. (1913). *Proc. Roy. Soc. A*, **89** (610), 248.

[13] Bragg, W. L. (1914). *Proc. Roy. Soc. A*, **89** (613), 468.

[14] Bragg, W. L. (14 May 1958). *Private communications.*

[15] Brouns, E., Visser, J. W., and de Wolff, P. M. (1964). *Acta Cryst.*, **17**, 614.

[16] Brown, H. *et. al.* (1978). *Crystallographic Groups of Four-Dimensional Space*, **John Wiley & Sons**, (New York).

[17] Bravais, A. (1850). *Journal de l' 'Ecole Polytechnique*, **19**, 1.

[18] Buxton, B. F. *et. al.* (1976). *Phil. Trans. Roy. Soc. A*, **281** (1301), 171.

[19] Corliss, L. M., Hastings, J. M. and Weiss, R. J. (1959). *Phys. Rev. Lett.*, **3**, 211.

[20] Chadwick, J. (1932a). *Nature*, **129**, 312.

[21] Chadwick, J. (1932b). *Proc. Roy. Soc. A*, **136**, 692.

[22] Chandra, P. and Littlewood, B. (2007). *A Landau Primer for Ferroelectrics*, **Springer**, (Berlin / Heidelberg).

[23] Coxeter, H. S. M. (1989). *Introduction to Geometry (second ed.)*, **John Wiley and Sons**.

[24] Cracknell, A. P. (1969). *Rep. Prog. Phys.*, **32**, 633.

[25] de Wolf, P. M. *et. al.* (1985). *Acta. Crys. A*, **41**, 278.

[26] Dimmock, J. O. (1963). *Phys. Rev.*, **130**(4), 1337.

[27] Dušek, M. *et al.* (2001). *J. Appl. Cryst.*, **34**, 398.

[28] Dušek, M., Chapuis, G., Meyer M. and Petříček, V. (2003). *Acta Cryst. B*, **59**, 337.

[29] Escher, M. C. *www.mcescher.com*, Official M.C.Escher Website.

[30] Ewald, P. P. (1912). *PhD. Dissertation*, **Ludwig Maximillian University of Munich**.

[31] Fedorov, E. S. (1885). *Trans. Mineral. Soc.*, **21**, 240.

[32] Fedorov, E. S. (1891). *Trans. Mineral. Sot.*, **28**, 146.

[33] Fedorov, E. S. (1890). *The Symmetry of Regular Systems of Figures.* **Academy of Sciences** (St Petersburg). (In Russian.)

[34] Fedorov, E. S. (1912). *Trans. of the Mining Institute.*, **5**, 54.

[35] Fiebig, M. (2005). *J. Phys. D*, **38**, 123.

[36] Friedrich, W., Knipping, P., and von Laue, M. (1912). *M. Sber. bayer. math. phys. Klasse, (Kgl.) Akad. Wiss.*, 303 (Munich).

[37] Haas, C. (1965). *Phys. Rev. A*, **140**, 638.

[38] Haldane, F. D. M. (1980). *Phys. Rev. Lett.* **45**, 1358.

[39] Harris, A. B., *et al.* (2004). *Phys. Rev. B*, **69**, 094409.

[40] Hauptman, H. A. (1985). *"Direct Methods and Anomalous Dispersion"*, **Nobel Lecture**, http://nobelprize.org/nobel_prizes/chemistry/laureates/1985/hauptman-lecture.html.

[41] Hauptman, H. A. (1990). *Struct. Chem.*, **6**, 617.

[42] *International tables for crystallography. Vol. A.*, 5th edition. (2002). Ed. T. Hahn, **Springer** (Dordrecht).

[43] *International tables for X-ray Crystallography, Vol. A* (1952). Ed. N. F. M Henry and K. Lonsdale, **Kynoch Press** (Birmigham).

[44] Izyumov, Y. A and Syromyatnikov, V. N. (1990). *Phase Transitions and Crystal Symmetry*, **Kluwer Academic Publishers** (Dordrecht).

[45] Izyumov, Y. A. and Naish, V. E. (1991) *Neutron Diffraction of Magnetic Materials*, **Consultants Bureau** (New York and London).

[46] Janner, A. and Janssen, T. (1977). *Phys. Rev. B*, **15**(2), 643.

[47] Janner, A. and Janssen, T. (1983a). *Acta Crsyt. A*, **39**, 658.

[48] Janner, A. and Janssen, T. (1983b). *Acta Crsyt. A*, **39**, 667.

[49] Janner, A. and Janssen, T. (1983c). *Acta Crsyt. A*, **39**, 671.

[50] Kaplan, T. A. (1959) *Phys. Rev.*, **116**, 888.

[51] Janssen, T., Schobinger-Papamantellos, P. (2006). *Zeit. f ur Krist.*, **221**, 732.

[52] Kageyama, H. *et. al.* (1999). *Phys. Rev. Lett.*, **82** (15) 3168.

[53] Kovalev, O. V. (1993). *Representations of the Crystallographic Space Groups: Irreducible representations, Induced representations and Corepresentations*, (2nd Ed). Ed. H. T. Stokes and D. M. Hatch, **Gordon and Breach Science Publishers** (London).

[54] Landau, L. D., and Liftshitz, E. M. (1958). *Statistical Physics* **Oxford** (Pergamon Press).

[55] Loudon, J. C.,*et. al.* (2005). *Phys. Rev. Lett.*, **94**, 097202.

[56] Löwen, H. (2001). *J. Phys.: Condens. Matter*, **13** R415.

[57] Lyubarskii, G. Ya. (1960). *The Application of Group Theory in Physics*, **Oxford** (Pergamon Press).

[58] Miller, S. C., and Love, W. F. (1967). *Tables of Irreducible Representations of Space Groups and Co-representations of Magnetic Space Groups*, **Pruett.** (Boulder, Col.).

[59] Opechowski, W. and Guccione, R. (1965). *Magnetism*, Ed. G. T. Rado and H. Suhl, **Academic Press.** (New York).

[60] Rodríguez-Carvajal, J. (2001) *Fullprof News* **January**,

[61] Röntgen, W.C. (1894). *Zur Geschichte der Physik an der Universitaet Wuerzburg.*

[62] Sánchez, D., Caldern, M. J., Snchez-Bentez, J., Williams, A. J., Attfield, J. P., Midgley, P. A., Mathur, N. D. (2008). *Physical Review B*, **77**, 092411.

[63] Schöenflies, A. (1891). *Krystallsysteme und Krystallstructur.* **Teuber** (Leipzig).

[64] Shubnikov, A. V., Belov, N. V. *et. al.* (1964). *Colored Symmetry, edited by W. J. Holser*, **Macmillan** (New York).

[65] Shull, C. G. and Smart, J. Samuel (1949). *Phys. Rev.*, **76**, 1256.

[66] Sikora, W., *et. al.* (2008). *J. Phys.: Conf.* **104** 012023.

[67] Tagantsev, A. K. (2008). *Ferroelectrics*, **375**, 19.

[68] van Leeuwen, R. (1998). *Phys. Rev. Lett.*, **80**, 1280.

[69] Wigner, E. P. (1959). *Group Theory and its application to the quantum mechanics of atomic spectra*, **Academic Press Inc.** (London).

[70] Wills, A. S. (2000). *Physica B*, **276**, 680.

[71] Wills, A. S. (2001). *Appl. Phys. A*, **74**, 856.

[72] Wills, A. S. (2005). *J. Mater. Chem.*, **15**, 245.

[73] Wollan, E. O. and Shull, C. G. (1948). *Phys. Rev*, **73**, 810.

[74] Wollan, E. O., Davidson, W. L. and Shull, C. G. (1949). *Phys. Rev.*, **75**, 1348.

[75] Yafet, Y. and Kittel, C. (1952) *Phys. Rev.*, **87**, 290.

[76] Yeom, H. W. *et. al.* (1999). *Phys. Rev. Lett.* **82**, 4898.

[77] Welberry, T. R. (1985). *Rep. Prog. Phys.*, **48**, 1543.

CHAPTER 2

Representation theory: A mathematical review

"I can not conclude this brief account of the early history of direct methods of X-ray crystallography without also describing the reception this work received at the hands of the crystallographic community. This was, simply, extreme scepticism if not outright hostility. In hindsight I think this reaction was due, first, to the strong mathematical flavour of this early work."

H. A. Hauptman, History of X-Ray Crystallography

2.1. Introduction

In this thesis we aim to develop the use of representation theory for describing crystalline systems, and their phase transitions. The first step towards our goal is to derive, from group and representation theory, a set of tools with which we can reliably calculate the basis vectors that will describe phase transitions and ordering phenomena. In this chapter we construct a mathematical framework for describing systems using vectors and matrices, and derive two key equations: the reduction and projection operators. Discussion of what basis vectors represent and their relationship to the Hamiltonian is left until the next chapter.

2.2. Sets and Groups

Representation theory is a sub discipline of group theory, and in this section we review the basic principles of set and group theory.

A set, $\mathbb{G}$, is a collection of elements, $\{g_1, ..., g_n\}$, such as vectors, operators, or other sets. The number of elements in the set $\mathbb{G}$ is termed the *order* of the set, $n(\mathbb{G})$. A group, $(\mathbb{G}, \circ)$, is a set and a binary law of composition, $\circ$, which satisfies four axioms:

- **Closure :** $a \circ b = c \in \mathbb{G} \qquad \forall a, b \in \mathbb{G}$

  The product of any two elements of the group, under the law of composition, is always an element of the group.

- **Associativity :** $(a \circ b) \circ c = a \circ (b \circ c) \qquad \forall a, b, c \in \mathbb{G}$

  The law of composition is associative.

- **Identity :** $\exists E \in \mathbb{G} : a \circ E = E \circ a = a \qquad \forall a \in \mathbb{G}$

  There is an element E which leaves every other element unchanged under the law of composition. This element is called the *identity*, it *commutes* with every element of the group and it is unique.

- **Inverse :** $\exists a^{-1} \in \mathbb{G} : a^{-1} \circ a = a \circ a^{-1} = E \qquad \forall a \in \mathbb{G}$

  For every element in of $\mathbb{G}$ there exists some element a^{-1}, also in $\mathbb{G}$, with which its product is the identity. This element is called the inverse of a, and is also unique.

Some groups have the additional property of commutation, and are termed *abelian*. Non-commutative groups are referred to as *non-abelian*.

- **Commutation :** $a \circ b = b \circ a \qquad \forall a, b \in \mathbb{G}$

  The product of two elements of the group, under the law of composition, is the same regardless of the order in which they are combined.

Except for reasons of clarity, groups will be referred to by their sets, and the operator symbol is dropped in equations throughout the remainder of this thesis.

I.e. When a, b are members of a group then ab should be read as $a \circ b$.

2.2.1. Subgroups and cosets

Imagine two sets $\mathbb{G}_n$ and $\mathbb{G}$, if every element in $\mathbb{G}_n$ is also an element of $\mathbb{G}$ then it is referred to as a *subset* of $\mathbb{G}_n$.

$$\mathbb{G}_n \subset \mathbb{G} \qquad \text{iff} \qquad g \in \mathbb{G} \qquad \forall g \in \mathbb{G}_n \tag{2.1}$$

If both $(\mathbb{G}, \circ)$ and $(\mathbb{G}_n, \circ)$ form groups, then $\mathbb{G}_n$ is termed a sub-group of $\mathbb{G}$. All groups contain the two trivial sub-groups:

$$\begin{aligned} \mathbb{G}_n &= \{E\} \\ \mathbb{G}_n &= \mathbb{G} \end{aligned} \tag{2.2}$$

Consider a set $\mathbb{G}$ with a subgroup $\mathbb{G}_n$. The operation $g\mathbb{G}_n$ denotes the action of applying g to every element in $\mathbb{G}_n$, and the resulting set of elements is termed the left-coset.

$$g\mathbb{G}_n = \sum_{g_i \in \mathbb{G}_n} g g_i \tag{2.3}$$

By Lagrange's theorem (Appendix 1), all cosets of a subgroup (including $E\mathbb{G}_k$) have the same order and they partition $\mathbb{G}$: each element of the group appears in exactly one coset of a subgroup. It follows that the ratio the orders of a group and its subgroup must be an integer:

$$\frac{n(\mathbb{G})}{n(\mathbb{G}_k)} = a \in \mathbb{Z} \tag{2.4}$$

A trivial, but important, result is that every coset of $\mathbb{G}$ is $\mathbb{G}$:

$$g\mathbb{G} = \mathbb{G}, \qquad \forall g \in \mathbb{G} \tag{2.5}$$

2.2.2. Conjugacy

Two elements of a group g_i, g_j are said to be conjugate if there is some element $g_k \in \mathbb{G}$ that relates them in the following way:

$$g_i = g_k^{-1} g_j g_k \tag{2.6}$$

More generally, two subgroups $\mathbb{G}_i$,$\mathbb{G}_j$ are conjugate if:

$$\exists g \in \mathbb{G} : g^{-1}\mathbb{G}_i g = \mathbb{G}_j \tag{2.7}$$

This is an important relationship as conjugate (sub)groups are *isomorphic*; they have the same number of elements and the same group structure. Conjugate groups are often referred to as being *similar*, and their conjugacy relationship is termed a *similarity transformation*.

2.3. Matrix representations of a group

There are several ways to represent abstract groups, the simplest being a multiplication table. Consider the group $(\mathbb{G}, \times)$, where $\mathbb{G} = \{x^2 = y^2 = E; xy = yx\}$, we can represent all possible combinations of its elements in a table:

	E	x	y	xy
E	E	x	y	xy
x	x	E	xy	y
y	y	xy	E	x
xy	xy	y	x	E

This approach to defining a group quickly becomes unmanageable as the group grows in size and complexity. One alternative is to use a set of invertible matrices to represent elements of the group. For example, our group could be described by the following matrices:

$$E = \begin{pmatrix} 1 & 0 \\ 0 & 1 \end{pmatrix}, \qquad x = \begin{pmatrix} -1 & 0 \\ 0 & -1 \end{pmatrix}, \qquad y = \begin{pmatrix} 0 & 1 \\ 1 & 0 \end{pmatrix}, \qquad xy = \begin{pmatrix} 0 & -1 \\ -1 & 0 \end{pmatrix}$$

Such a equivalence is called a map (Appendix 2), as each element of the group has been mapped to a matrix:

$$F : E \mapsto \begin{pmatrix} 1 & 0 \\ 0 & 1 \end{pmatrix}, \qquad F : x \mapsto \begin{pmatrix} -1 & 0 \\ 0 & -1 \end{pmatrix}$$

$$F : y \mapsto \begin{pmatrix} 0 & 1 \\ 1 & 0 \end{pmatrix}, \qquad F : xy \mapsto \begin{pmatrix} 0 & -1 \\ -1 & 0 \end{pmatrix}$$

Some maps preserve the structure of a group: the multiplication tables of the range and the image are isomorphic. A map with this property is said to be *homomorphic*, a homomorphism, or a representation. More formally, a homomorphic map has the property that the product of the images of two elements in $\mathbb{G}$ is always equal to the image of their product.

$$\begin{gathered} F : g \mapsto \mathfrak{T}(g) \\ \mathfrak{T}(g_i) \circ \mathfrak{T}(g_j) = \mathfrak{T}(g_i \circ g_j) \qquad \forall g_i, g_j \in \mathbb{G} \end{gathered} \tag{2.8}$$

For a general matrix representation there will exist some matrix $\mathfrak{A}$, which simultaneously transforms every matrix, $\mathfrak{T}(g)$, to the same block-diagonal form. Representations for which the matrix $\mathfrak{A}$ does not exist are said to be *irreducible* and have special significance.

$$\mathfrak{A}^{-1}\mathfrak{T}(g)\mathfrak{A} = \begin{pmatrix} & & & \dots & 0 & \dots & 0 \\ & \mathfrak{d}^{\alpha}(g) & & \dots & \vdots & & \vdots \\ & & & \dots & 0 & \dots & 0 \\ & & & & & & \\ \vdots & \vdots & \vdots & & & \vdots & \vdots & \vdots \\ & & & & & & \\ 0 & \dots & 0 & \dots & & & \\ \vdots & & \vdots & \dots & & \mathfrak{d}^{\zeta}(g) & \\ 0 & \dots & 0 & \dots & & & \end{pmatrix} \tag{2.9}$$

2.3.1. Representation theory

Representation theory seeks to solve the following problem:

> How many independent ways can we represent a finite group $\mathbb{G}$ as a group of invertible matrices?

A representation Γ of the group $\mathbb{G}$ is a homomorphism of $\mathbb{G}$ to the group of invertible matrices under matrix multiplication. The matrix representations $\mathfrak{T}(g)$ and $\mathfrak{T}'(g)$ are independent if there is no matrix $\mathfrak{A}$ which satisfies the following:

$$\mathfrak{T}(g) = \mathfrak{A}^{-1}\mathfrak{T}'(g)\mathfrak{A} \qquad \forall g \in \mathbb{G} \tag{2.10}$$

Independent matrix representations are termed irreducible representations (IRs), Γ_ν. Every representation of a group consist of some linear combination of irreducible representations (Maschke's theorem, Appendix 3), and these correspond to the blocks of the block-diagonalized matrix in Eq. 2.9:

$$\Gamma = \oplus \sum_i C^\nu \Gamma_\nu \tag{2.11}$$

2.3.2. Orthogonality properties of irreducible representations

Irreducible representations have a number of useful orthogonality properties, derived from Schur's Lemma (Appendix 4):

> *If* $\mathfrak{d}(g)$ *and* $\mathfrak{d}'(g)$ *are matrices from two irreducible matrix representations of a group* $\mathbb{G}$*, and there is some matrix* $\mathfrak{A}$ *such that:*
>
> $$\mathfrak{d}(g)\mathfrak{A} = \mathfrak{A}\mathfrak{d}'(g), \qquad \forall g \in \mathbb{G}$$
>
> *Then either* $\mathfrak{A} = 0$*, or* $\mathfrak{d}$ *and* $\mathfrak{d}$*' are equivalent and* $\mathfrak{A} = n.I$*, where* n *is some constant.*

This lemma also tells us, indirectly, that any matrix which commutes with the matrices of an irreducible representation is a linear multiple of the identity matrix. We make use of this form of the lemma in chapter 3.

Making use of this lemma, we can derive the orthogonality properties of irreducible representations. Consider the square matrix $\mathfrak{A} = \sum_{g\in\mathbb{G}} \mathfrak{d}^\nu(g)\mathfrak{X}\mathfrak{d}^\mu(g^{-1})$, constructed from the matrices of two representations Γ_ν, and Γ_μ and an arbitrary matrix $\mathfrak{X}$, all of order d^n. This matrix obeys the condition of Shur's lemma when left-multiplied by $\mathfrak{d}^\nu(h)$, where h is some element of $\mathbb{G}$:

$$\begin{aligned}
\mathfrak{d}^\nu(h)\mathfrak{A} &= \sum_{g\in\mathbb{G}} \mathfrak{d}^\nu(h)\mathfrak{d}^\nu(g)\mathfrak{X}\mathfrak{d}^\mu(g^{-1}) \\
&= \sum_{g\in\mathbb{G}} \mathfrak{d}^\nu(h)\mathfrak{d}^\nu(g)\mathfrak{X}\mathfrak{d}^\mu(g^{-1})\mathfrak{d}^\mu(h^{-1})\mathfrak{d}^\mu(h) \\
&= \left(\sum_{g\in\mathbb{G}} \mathfrak{d}^\nu(hg)\mathfrak{X}\mathfrak{d}^\mu(g^{-1}h^{-1})\right)\mathfrak{d}^\mu(h) \\
&= \left(\sum_{g\in\mathbb{G}} \mathfrak{d}^\nu(g)\mathfrak{X}\mathfrak{d}^\mu(g^{-1})\right)\mathfrak{d}^\mu(h) \\
&= \mathfrak{A}\mathfrak{d}^\mu(h)
\end{aligned} \tag{2.12}$$

The second last equality holds because, for a fixed h, both summations are over the whole of $\mathbb{G}$[1]. For the case $\nu = \mu$, Schur's lemma states that $\mathfrak{A} = \lambda I$, where λ will depend upon our choice of $\mathfrak{X}$. λ is determined by choosing $\mathfrak{X}$ to have a single non-zero element, $\mathfrak{X}_{lm} = 1$ and expanding the matrix-multiplication that defines $\mathfrak{A}$.

$$\begin{aligned}
\mathfrak{A}_{ij} &= \lambda\delta_{ij} \\
&= \sum_{g\in\mathbb{G}} [\mathfrak{d}^{\nu}(g)\mathfrak{X}\mathfrak{d}^{\mu}(g^{-1})]_{ij} \\
&= \sum_{g}\sum_{a} \mathfrak{d}^{\nu}_{ia}(g)(\mathfrak{X}\mathfrak{d}^{\nu}(g^{-1}))_{aj} \\
&= \sum_{g}\sum_{a}\sum_{b} \mathfrak{d}^{\nu}_{ia}(g)\mathfrak{X}_{ab}\mathfrak{d}^{\nu}_{bj}(g^{-1}) \\
\therefore \lambda\delta_{ij} &= \sum_{g} \mathfrak{d}^{\nu}_{il}(g)\mathfrak{d}^{\nu}_{mj}(g^{-1})
\end{aligned} \tag{2.13}$$

Putting $j = i$ and summing over all i:

$$\begin{aligned}
\sum_{i}\sum_{g} \mathfrak{d}^{\nu}_{il}(g)\mathfrak{d}^{\nu}_{mi}(g^{-1}) &= d^n\lambda \\
\sum_{g} \mathfrak{d}^{\nu}_{ml}(g^{-1}g) = \sum_{g} \mathfrak{d}^{\nu}_{ml}(E) &= \sum_{g} \delta_{ml} \\
&= n(\mathbb{G})\delta_{ml} \\
\therefore \lambda &= \frac{n(\mathbb{G})}{d^n}\delta_{lm} \\
\therefore \sum_{g} \mathfrak{d}^{\nu}_{il}(g)\mathfrak{d}^{\nu}_{mj}(g^{-1}) &= \frac{n(\mathbb{G})}{d^n}\delta_{lm}\delta_{ij}
\end{aligned} \tag{2.14}$$

Finally, consider the case that $\nu \neq \mu$, now $\mathfrak{A} = 0$. Eq. 2.13 can be rewritten to include this condition:

$$\sum_{g} \mathfrak{d}^{\nu}_{il}(g)\mathfrak{d}^{\mu}_{mj}(g^{-1}) = \lambda\delta_{ij}\delta_{\nu\mu} \tag{2.15}$$

[1]Recall from section 2.2.1 that $\sum_{g\in\mathbb{G}} hg = h\mathbb{G}$, and that every left coset of a group is the group itself: $h\mathbb{G} = \mathbb{G}$.

Thus, our orthogonality relationship becomes:

$$\therefore \sum_{g} \mathfrak{d}^{\nu}_{il}(g)\mathfrak{d}^{\mu}_{mj}(g^{-1}) = \frac{n(\mathbb{G})}{n}\delta_{lm}\delta_{ij}\delta_{\nu\mu} \tag{2.16}$$

This is sometimes referred to as the Great Orthogonality Theorem.

2.4. The reduction operator

While it is possible to reduce a general representation, Γ, to block-diagonal form using a similarity transform of the type $\mathfrak{A}\Gamma\mathfrak{A}^{-1}$, in general $\mathfrak{A}$ is not of interest and its determination is arduous. Our interest lies in determining the block-diagonalized representation matrices, and this is equivalent to knowing the coefficients of each irreducible representation in the linear expansion:

$$\Gamma = \oplus \sum_{\nu} C^{\nu}\Gamma_{\nu} \tag{2.17}$$

Ideally, we would find all the coefficients, C^{ν}, without calculating $\mathfrak{A}$. In this section the reduction operator is derived from the orthogonality properties of irreducible representations, with which we can achieve this goal.

The orthogonality relations of IRs are summarized by Eq. 2.16:

$$\sum_{g_i \in \mathbb{G}} \mathfrak{d}^{\mu}_{il}(g_i)\mathfrak{d}^{\nu}_{mj}(g_i^{-1}) = \frac{|\mathbb{G}|}{d^{\mu}}\delta_{\mu,\nu}\delta_{i,j}\delta_{l,m}$$

Here $|\mathbb{G}|$ has the same meaning as $n(\mathbb{G})$. From this, the reduction operator is derived by putting $l = i$, $m = j$ and summing over all i and j. The sum over the spine of a matrix is termed the *trace* or *character* of the matrix, and is denoted χ.

$$\begin{aligned}\sum_i \sum_j \sum_{g_i \in \mathbb{G}} \mathfrak{d}^{\mu}_{ii}(g_i)\mathfrak{d}^{\nu}_{jj}(g_i^{-1}) &= \sum_i \sum_j \frac{|\mathbb{G}|}{d^{\mu}} \delta_{\mu,\nu}\delta_{i,j} \\ \sum_{g_i \in \mathbb{G}} \chi^{\mu}(g_i)\chi^{\nu}(g_i^{-1}) &= |\mathbb{G}|\delta_{\mu,\nu} \\ \frac{1}{|\mathbb{G}|}\sum_{g_i \in \mathbb{G}} \chi^{\mu}(g_i)\chi^{\nu}(g_i^{-1}) &= \delta_{\mu,\nu}\end{aligned} \tag{2.18}$$

The action of the reduction operator can be seen by replacing Γ_μ with some reducible representation $\chi(g_i) = \oplus \sum_\mu C^\mu \chi^\mu(g_i)$. For a particular Γ_ν the reduction operator will determine C^ν:

$$\begin{aligned}\frac{1}{|\mathbb{G}|}\sum_{g_i \in \mathbb{G}} \chi(g_i)\chi^{\nu}(g_i^{-1}) &= \frac{1}{|\mathbb{G}|}\sum_{g_i \in \mathbb{G}} \sum_{\mu} C^{\mu}\chi^{\mu}(g_i)\chi^{\nu}(g_i^{-1}) \\ &= \sum_{\mu} C^{\mu}\frac{1}{|\mathbb{G}|}\sum_{g_i \in \mathbb{G}} \chi^{\mu}(g_i)\chi^{\nu}(g_i^{-1}) \\ &= \sum_{\mu} C^{\mu}\delta_{\mu,\nu} = C^{\nu}\end{aligned} \tag{2.19}$$

Hence, by applying this operator over all Γ_ν, we can determine the coefficients of the irreducible representations.

2.5. Fields and vector spaces

Before a matrix representation of the symmetry group can be constructed, we need to understand the space upon which it acts, and the axis system used to define that space. In conventional crystallography the space of interest is a vector space, and the position of every atom of the crystal is defined by a vector.

A field is a structure in which the operations of addition, subtraction, multiplication and division (except by zero) are defined; examples are the field of real numbers, $\mathscr{R}$, and the field of complex numbers, $\mathscr{C}$. A vector space V over a field $\mathscr{F}$, is a set on which two operations, vector addition and scalar multiplication, are defined.

The 2- and 3-dimensional Euclidian spaces are the most familiar examples of vector spaces and the behaviour of geometric vectors under addition and scalar multiplication is a strong, intuitive model for vector spaces. Within these spaces, vectors are ordered pairs or triples of real numbers, respectively.

2.6. Affine spaces

In affine geometry there is no notion of length or angle, instead points in space, denoted over a field $\mathscr{F}$, are subtracted to generate vectors. Thus, an affine space is a vector space without a fixed origin; physical space is an affine space.

2.6.1. Affine transformations

An affine transformation is a map between two affine spaces and is comprised of a linear transformation h_i, typically a rotation, followed by a translation[2] α_i:

$$x \mapsto \alpha_i + h_i x \tag{2.20}$$

An affine transformation preserves co-linearity and ratios of distance, and is usually denoted $(\alpha_i|h_i)$ in crystallography. This follows the mathematical convention of applying operations from right to left.

If the affine space is of finite dimension n, then h_i is represented by an $n \times n$ matrix $\mathfrak{T}(h_i)$, α_i by an $n \times 1$ vector $\vec{\alpha}_i$, and the operator $(\alpha_i|h_i)$ is represented by the augmented matrix:

$$\begin{pmatrix} \mathfrak{T}(h_i) & \vec{\alpha}_i \\ 0...0 & 1 \end{pmatrix} \tag{2.21}$$

[2]Note that α is an *operator* which acts upon a vector by adding to it the *vector* $\vec{\alpha}$.

2.7. The affine representation of space groups

Crystals are highly symmetric systems[3], consisting of (ideally) infinite lattices of atoms. A crystal is defined by an infinite set of vectors, each defining the position of an atom, having some set of symmetry operations that map the set of vectors to itself. The nature of a crystal lattice is such that this set of vectors is generated from a finite sub-set of those positions and repeated application of the symmetry operations. In particular, every proper crystal is invariant under a set of translations:

$$\mathbb{T} = \{((0,0,0)|E), ((0,0,1)|E), \ldots, ((a,b,c)|E)\}, \qquad \forall a,b,c \in \mathbb{Z} \tag{2.22}$$

The vectors (a,b,c) are defined in the crystallographic axes: a right-handed axis system parallel to the directions of translational symmetry.

The crystallographic symmetry groups are the direct product of the group of translations, and a smaller group of symmetry operations $\mathbb{G}_0$ which is termed the *transversal*.

$$\mathbb{G} = \mathbb{G}_0 \otimes \mathbb{T} \tag{2.23}$$

All symmetry operations of the crystallographic space groups leave an affine (physical) space unchanged; they are affine operations upon 3-dimensional space. Hence, we can define them with 4×4 augmented matrices.

2.8. Span and basis

The span of a set of vectors $\vec{p} \in \mathbb{P}$, over a field $\mathscr{F}$, is the intersection of all spaces containing that set:

$$\text{Span}(\vec{p}_1, ..., \vec{p}_n) = \{\lambda_1\vec{p}_1 + ... + \lambda_n\vec{p}_n \| \lambda_1, ..., \lambda_n \in \mathscr{F}\} \tag{2.24}$$

[3]Even $P1$ systems are infinitely symmetric under a set of translations.

More simply: a set spans all linear combinations of its elements. If none of the vectors in $\mathbb{P}$ can be removed without changing the span of $\mathbb{P}$ then the vectors $\vec{p} \in \mathbb{P}$ are said to be linearly independent, and they form a *basis* for the space they span; every vector in their span can be written as a unique linear combination of the set elements. Using Zorn's lemma (Appendix 5) it can be shown that any vector space has a basis, and that all bases of a vector space have the same cardinality (the order of the basis set). Thus, all vector spaces are isomorphic if they have the same cardinal number. This is an important result; it allows us to select any basis we desire, provided it has the correct size, without changing the space.

2.8.1. Basis transformation in affine spaces

A point, R, in a 3-dimensional vector space, is defined relative to the origin by the scalar product of a basis $\vec{a_1}, \vec{a_2}, \vec{a_3}$ and a co-ordinate vector, $\vec{p}$.

$$\begin{aligned} R = (\vec{a_1}, \vec{a_2}, \vec{a_3}).\vec{p} &= (\vec{a_1}, \vec{a_2}, \vec{a_3}). \begin{pmatrix} x \\ y \\ z \end{pmatrix} \\ &= x\vec{a_1} + y\vec{a_2} + z\vec{a_3} \end{aligned} \tag{2.25}$$

Let $\mathfrak{P}$ be an invertible matrix of dimension 4, representing some transformation of the basis. All vector spaces, and thus all affine spaces, are isomorphic if they are of the same cardinality. If $\mathfrak{P}$ is chosen such that this is true, then the new basis defines an isomorphic space and R must be unchanged. It is shown in Appendix 6 that:

$$R = (\vec{a_1}, \vec{a_2}, \vec{a_3}, 1). \begin{pmatrix} x \\ y \\ z \\ 1 \end{pmatrix} = (\vec{a_1}, \vec{a_2}, \vec{a_3}, 1)\mathfrak{P}.\mathfrak{P}^{-1} \begin{pmatrix} x \\ y \\ z \\ 1 \end{pmatrix} \tag{2.26}$$

Where the vectors have been augmented so that the matrix $\mathfrak{P}$ can act upon them. Comparing Eq. 2.26 with 2.25, we see that the basis is now $(\vec{a_1}, \vec{a_2}, \vec{a_3}, 1)\mathfrak{P}$, and the vector defining R has been transformed to $\mathfrak{P}^{-1}\vec{p}$. Note that $\vec{p}$ and $\mathfrak{P}^{-1}\vec{p}$ refer to the same point in space, but using two different axis systems. In crystallography the matrix $\mathfrak{P}^{-1}$ is usually denoted $\mathfrak{Q}$.

Consider a matrix $\mathfrak{W}(g_i)$ that represents some affine transformation $(\alpha_i|h_i)$ acting upon a co-ordinate vector $\vec{p}$, in the basis $(\vec{a_1}, \vec{a_2}, \vec{a_3})$. In order to transform a co-ordinate vector to a new axis with some transformation $\mathfrak{P}$ then $\mathfrak{W}(g_i)$ must change in two ways. First, the operator must act upon a vector defined in original axis system; in the new axis system the co-ordinate vector has become $\mathfrak{Q}\vec{p}$ so the vector is pre-multiplied by $\mathfrak{P}$:

$$\begin{aligned} \mathfrak{W}(g_i)\mathfrak{P} \times \mathfrak{Q}\vec{p} &= \mathfrak{W}(g_i)\mathfrak{W}(E)\vec{p} \\ &= \mathfrak{W}(g_i)\vec{p} \end{aligned} \tag{2.27}$$

Second, the result vector must be in the new basis, requiring the product to be post-multiplied by $\mathfrak{P}$. Combining these two steps we derive an expression for the operator matrix in the new axis system:

$$\begin{aligned} \mathfrak{Q}(\mathfrak{W}(g_i)\mathfrak{W}(E)\vec{p}) &= \mathfrak{Q}\mathfrak{W}(g_i)\mathfrak{P} \times \mathfrak{Q}\vec{p} \\ \therefore \mathfrak{P} : \mathfrak{W}(g_i) &\mapsto \mathfrak{Q}\mathfrak{W}(g_i)\mathfrak{P} \end{aligned} \tag{2.28}$$

Strictly, $\mathfrak{P}$ maps the vector space to itself with a new basis, however, we can summarize its action using a series of maps. While the position is unchanged, the basis set and co-ordinate vectors are transformed, as is every matrix representation of the symmetry operations.

$$\begin{aligned} R &\mapsto R \\ (\vec{a_1}, \vec{a_2}, \vec{a_3}) &\mapsto (\vec{a_1}, \vec{a_2}, \vec{a_3})\mathfrak{P} \\ \vec{p} &\mapsto \mathfrak{P}^{-1}\vec{p} \\ \mathfrak{W}(i) &\mapsto \mathfrak{P}^{-1}\mathfrak{W}(g_i)\mathfrak{P} \end{aligned} \tag{2.29}$$

2.9. Describing ordered properties using vector fields

If we wish to define some property upon the atoms within a crystal, such as a displacement or magnetic moment, then a space larger than the vector-space is necessary. A vector-field is such a space, and which places a vector $\vec{v}_R$ at each point R defining some property. The dimensionality of $\vec{v}_R$ determines the types of physical properties it can describe. 1-dimensional vectors define properties such as temperature or electron density, while 3-dimensional vectors define properties such as magnetic moments and atomic motion.

Our goal is to build a representation of the system's vector field, and from this derive matrix representations of its symmetry operations. Once these are constructed, application of the reduction formula will determine the IRs spanned by the system and its basis vectors (BVs). First, we discuss the symmetry of vector-fields.

2.9.1. Little groups

In general, the symmetry of a vector-field will be lower than that of the lattice which defines the atomic positions. In particular, the translational symmetry of the property may differ from that of the lattice. In section 3.3, we shall see that the appropriate translational symmetry for vector fields of a crystal is defined by:

$$\begin{aligned} g_{trans} &: R \longmapsto R + \alpha \\ g_{trans} &: \vec{v}_R \longmapsto e^{-2\pi i \vec{k}.\vec{\alpha}}.\vec{v}_R \end{aligned} \tag{2.30}$$

The vector $\vec{k}$, called the k-vector or propagation vector, is characteristic of the vector field and defines the periodicity of the vector-field in reciprocal space, relative to the crystal lattice.

> i.e.
> $\vec{k} = (\frac{1}{2}, 0, 0)$ defines a property field with a period of half that of the lattice in reciprocal space, or twice the period in direct space. A k-vector of $(0, 0, 0)$ defines a wave with the same period as the lattice in direct space.

Because a lattice consists of discrete points, many $\vec{k}$ are equivalent and by convention $\vec{k}$ is chose to lie within the first Brilluoin zone. Any k-vector outside the first Brillouin zone defines the same translational behaviour as some equivalent $\vec{k}$ within the first Brilluoin zone.

$$\begin{aligned} g_{trans} : \vec{v}_R &\longmapsto e^{-2\pi i(\vec{k}+(a,b,c)).\vec{\alpha}}.\vec{v}_R \\ &= e^{-2\pi i\vec{k}.\vec{\alpha}}.\vec{v}_R e^{-2\pi(a,b,c).\vec{\alpha}} \\ &= e^{-2\pi i\vec{k}.\vec{\alpha}} \qquad \forall a, b, c \in \mathbb{Z} \end{aligned} \tag{2.31}$$

This relationship occurs because both (a, b, c) and $\vec{\alpha}_{trans}$ are integer triples, and so their dot product must also be an integer.

For systems in which the vectors $\vec{v}_R$ show long-range order, the transversal of the system is not $\mathbb{G}_0$ but some sub group $\mathbb{G}_k$, defined by $\vec{k}$. There exists a surjective homomorphism from g_i to its linear transformation h_i, generating a group $\mathbb{H}$ which is a *point* group.

$$\begin{aligned} f : \mathbb{G} &\longmapsto \mathbb{H} \\ f : g &\longmapsto h \end{aligned} \tag{2.32}$$

The subgroup $\mathbb{G}_k$ is defined by the action of this map's image upon the vector $\vec{k}$. It consists of all those elements whose point-operation transforms $\vec{k}$ into itself, plus or minus some primitive translation:

$$f(g) : \vec{k} \mapsto t + \vec{k} \qquad t \in \mathbb{T}, \quad \forall g \in \mathbb{G}_{\vec{k}} \tag{2.33}$$

2.9.2. The star of $\vec{k}$

In general $\mathbb{G}_k$ will be smaller than $\mathbb{G}_0$ and we can divide up $\mathbb{G}_0$ into left cosets of $\mathbb{G}_k$. If $h\mathbb{G}_k$ is a coset, then h is termed the coset generating element. The set of all coset generating elements itself generates the "star" of $\vec{k}$, $\vec{k} + h_1\vec{k} + ...$ (Fig. 2.9.2). The symmetry groups of the each arm of the star are equivalent, and defined by the similarity transforms:

$$\mathbb{G}_{h_i k} = h_i^{-1}\mathbb{G}_k h_i \tag{2.34}$$

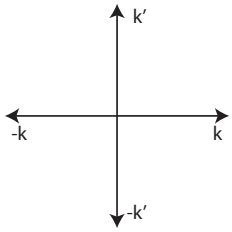

FIGURE 2.1. The "star" of $\vec{k}$ under the symmetry group C_4, this star has four arms. For the special case that $\vec{k} = (\frac{a}{2}, \frac{b}{2}, \frac{c}{2},)$ where $a, b, c = 0, 1$, then $\vec{k} \equiv -\vec{k}$ and the star will have only two inequivalent arms.

2.9.3. Orbits

Every position R in a crystal generates an infinite number of symmetry equivalent positions upon repeated application of the crystal's symmetry operations. The orbit of R is the set of vectors generated from R by $\mathbb{G}_0$, then translated so that every

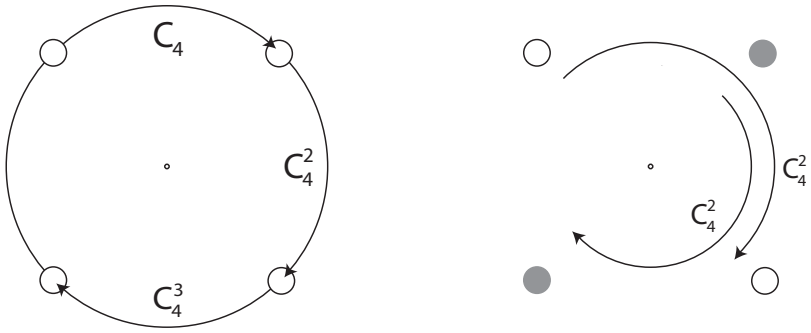

FIGURE 2.2. A general point has four images under the group generated by C_{4z}, the z-axis being perpendicular to the page (left). For $\vec{k} = (\frac{1}{2}, 0, 0)$, the little group consists of only two operations: E, C_{4z}^2 and does not generate every image. When this is the case, the positions are split into distinct orbits (right): within each orbits, the little group generates every position.

fractional co-ordinate lies in the range $[0, 1]$ (termed the 0^{th} unit cell). As $\mathbb{G}_k < \mathbb{G}_0$ it is not uncommon for the orbit of R under the operations of $\mathbb{G}_k$ to be smaller than its orbit under $\mathbb{G}$. When this happens the symmetry equivalent positions of R are split into several distinct orbits. The principles of orbit-splitting are demonstrated using a simple example in Fig. 2.9.3.

2.10. Representations of the system and its symmetry operators

Having determined the appropriate symmetry group and space for defining our system property, we are ready to build a vector representation of the crystal and matrices to represent its symmetry properties. Consider a position R, having an orbit of size m in a 3-dimensional vector field. This system can be described by a vector $\vec{\Phi}_k$ of dimension $3m$, which can be written as a sum of vectors $\vec{\phi}_k^{j\beta}$ for which every element is 0, apart from the $j\beta$'th. In this notation the j denotes the j'th position in R's orbit under $\mathbb{G}_k$; β denotes the β'th component of the property vector $\vec{v}_j$. This generates a

vector that defines the property every position equivalent to R:

$$\vec{\Phi}_k = \sum_{j\beta} \vec{\phi}_k^{j\beta} \tag{2.35}$$

Consider $g \in \mathbb{G}_k$ acting on a position r_j, with property vector $\vec{v}_j$:

$$\begin{aligned} &g : r_j \longmapsto \alpha(g) + hr_j = r_i + \vec{a}_{ij}(g) \qquad \vec{a}_{ij}(g) \in \mathbb{T} \\ &g : \vec{v}_j \longmapsto h_g \vec{v}_j \end{aligned} \tag{2.36}$$

In general the image of the atom, $hr_j + \vec{\alpha}_{ij}(g)$, will lie outside the 0^{th} unit cell. It will also be related to some position r_i, in the 0^{th} unit cell, by a vector $\vec{a}_{ij}(g)$ which is a translation symmetry of the space group.[4]

A symmetry operation, therefore, has three effects upon an particular atomic position: the permutation of the position vector r_j to the symmetry equivalent position r_i in the 0^{th} cell; the rotation of the property vector, $\vec{v}_j$, upon that position; and a translation of the image out of the 0^{th} cell, that phases the property[5] according to $e^{-2\pi i \vec{k}.\vec{a}_{ij}(g)}$. This is summarized by the equations:

$$\begin{aligned} \mathfrak{T}(g)\phi^{j\beta} &= e^{-2\pi i \vec{k}.\vec{a_{ij}}(g)} \sum_{\gamma} \mathfrak{D}_{\gamma\beta}(h_g)\vec{\phi}^{i\gamma} \\ \mathfrak{T}_{i\gamma,j\beta}(g) &= e^{-2\pi i \vec{k}.\vec{a_{ij}}(g)} \mathfrak{D}_{\gamma\beta}(h_g)\delta_{r_i,gr_j} \end{aligned} \tag{2.37}$$

$\mathfrak{T}(g)$ is a matrix representation of $g = (\alpha_g|h_g)$ acting upon the system vector $\vec{\Phi} = \sum_{j\beta} \vec{\phi}_k^{j\beta}$, $\mathfrak{D}(h_g)$ is the matrix representation of h_g and $\mathfrak{D}_{\gamma\beta}(h_g)$ its $\gamma\beta$'th element. The delta-function δ_{r_i,gr_j} determines wether the image of gr_j is equivalent to r_i. It is defined by:

$$\delta_{r_i,gr_j} = \begin{cases} 1 & (gr_i - r_j) \in \mathbb{T} \\ 0 & (gr_i - r_j) \notin \mathbb{T} \end{cases} \tag{2.38}$$

[4]This vector is, misleadingly, referred to as the *returning* vector by Izyumov. Misleading because it does not return us to the 0^{th}, but actually takes us out of it.
[5]Recall the effect of a translation upon the property, as defined by Eq. 2.31

Thus, we have derived an explicit form for the matrices that represent the symmetry operations of our vector field.

2.10.1. Reduction of the space group representation

Although construction of $\mathfrak{T}(g)$ is possible, it is also laborious. Determination of the IRs spanned by a system representation can be significantly simplified with a little consideration. For a representation of the group $\mathbb{G}_k$, the diagonal elements of $\mathfrak{T}(g)$ are derived from Eq. 2.37:

$$\begin{aligned} \mathfrak{T}_{i\gamma,j\beta}(g) &= e^{-2\pi i k \vec{a_{ij}}(g)} \mathfrak{D}_{\gamma\beta}(h_g) \delta_{r_j, g r_j} \\ \chi^{\vec{k}}(g) &= \sum_{i\gamma} \mathfrak{T}_{i\gamma,i\gamma}(g) \\ &= \sum_{i} e^{-2\pi i k \vec{a_{ii}}(g)} \delta_{r_i, g r_i} \sum_{\gamma} \mathfrak{D}_{\gamma\gamma}(h_g) \end{aligned} \tag{2.39}$$

This implies that $\chi^{\vec{k}}(g)$ can be split into two terms:

$$\begin{aligned} \chi^{\vec{k}}(g) &= \chi^{\vec{k}}_{Perm}(g) \chi^{\vec{k}}(h_g) \\ \chi^{\vec{k}}_{\mathrm{Perm}}(g) &= \sum_{j} e^{-2\pi i \vec{k}.\vec{a_{jj}}(g)} \delta_{r_j, g r_j} \\ \chi^{\vec{k}}(h_g) &= \sum_{\gamma} \mathfrak{D}_{\gamma\gamma}(h_g) \end{aligned} \tag{2.40}$$

The first term, $\chi^{\vec{k}}_{\mathrm{Perm}}(g)$, is the character of a matrix representing the permutation of the position vectors about the orbit of R. The term $\chi^{\vec{k}}(h_g)$ is the character of the matrix representation of h_g. Therefore, to find the IRs spanned by a crystal's vector field it is sufficient to determine the character of these simpler representations, and then apply the reduction operator to their product.

Example. Consider simple group $\mathbb{G}_k = \{E, I\}$, $\vec{k} = (0, 0, \frac{1}{2})$. The h-matrices for these operations acting upon a polar vector have characters $\chi(E) = 3$ and $\chi(I) = -3$.

$$\Gamma_{Rot}(E) = \begin{pmatrix} 1 & 0 & 0 \\ 0 & 1 & 0 \\ 0 & 0 & 1 \end{pmatrix} \qquad \Gamma_{Rot}(I) = \begin{pmatrix} \bar{1} & 0 & 0 \\ 0 & \bar{1} & 0 \\ 0 & 0 & \bar{1} \end{pmatrix} \tag{2.41}$$

If our system has a single atom at $(0, 0, 0.25)$, then its orbit under $\mathbb{G}_k$ consists of the positions $(0, 0, 0.25)$ and $(0, 0, 0.75)$ in the 0^{th} cell. The identity operation leaves both points unmoved, and so can be represented by a permutation matrix of character 2:

$$\Gamma_{Perm}(E) = \begin{pmatrix} 1 & 0 \\ 0 & 1 \end{pmatrix} \tag{2.42}$$

Inversion transforms the point $(0, 0, 0.25)$ into the point $(0, 0, -0.25)$, which we relate to the 0^{th} cell by writing it as $(0, 0, 0.75)$ - $(0, 0, 1)$. Similarly the image of the point $(0, 0, 0.75)$ under inversion is $(0, 0, 0.25)$ - $(0, 0, 1)$. These translations correspond to a phasing of the field by a factor of $e^{-2\pi i(0,0,\frac{1}{2})(0,0,1)} = e^{-\pi i} = -1$. Hence, the permutation representation of inversion has a character of 0 and the form:

$$\Gamma_{Perm}(I) = \begin{pmatrix} 0 & -1 \\ -1 & 0 \end{pmatrix} \tag{2.43}$$

With this information, application of Eq. 2.40 generates the characters of this representation: $\chi^{\vec{k}}(E) = 3 \times 2 = 6$; and $\chi^{\vec{k}}(i) = -3 \times 0 = 0$. The IRs for this group are:

	E	C_2
Γ_1	1	1
Γ_2	1	-1

(2.44)

Using the reduction operator, we determine that our system spans the representations $\Gamma = 3\Gamma_1 + 3\Gamma_2$. Hence, we have deduced the reduction of our system representation without having to calculate the representation matrices in full, or diagonalize them.

2.10.2. The action of matrix representations upon the system vector

Consider the action of a representation, $\mathfrak{T}(g)$, upon the state vector Φ_i (defined in section 2.10). The new vector is expressible as a linear combination of some basis of the space: $\langle\psi_1, \psi_2, ..., \psi_n|$.

$$g\Phi = \mathfrak{T}(g)\vec{\Phi} = \sum_{j=1}^{n} \mathfrak{D}_{ji}(g)\psi_j \tag{2.45}$$

It should be shown that Eq. 2.45 is a valid definition for the action of symmetry operators upon the system vector. We do this by showing that it is consistent with $\mathfrak{T}(g)$ being a representation of $\mathbb{G}$, and first by showing that $\mathfrak{D}(g)$ form a representation[6] of $\mathbb{G}$:

$$\begin{aligned}
(g_2 \circ g_1)\Phi &= \sum_{k=1}^{n} \mathfrak{D}_{ki}(g_2 \circ g_1)\psi_k \\
g_2 g_1 \Phi &= g_2 \sum_{n} \mathfrak{D}_{ji}(g_1)\psi_j \\
&= \sum_{k=1}^{n}\sum_{j=1}^{n} \mathfrak{D}_{ji}(g_1)\mathfrak{D}_{kj}(g_2)\psi_k \\
&= \sum_{k=1}^{n} \left(\sum_{j=1}^{n} \mathfrak{D}_{kj}(g_2)\mathfrak{D}_{ji}(g_1) \right) \psi_k \\
\therefore \sum_{k=1}^{n} \psi_k \mathfrak{D}_{ki}(g_2 \circ g_1) &= \sum_{k=1}^{n} \left(\sum_{j=1}^{n} \mathfrak{D}_{kj}(g_2)\mathfrak{D}_{ji}(g_1) \right) \psi_k \\
\mathfrak{D}_{ki}(g_2 \circ g_1) &= \sum_{j=1}^{n} \mathfrak{D}_{kj}(g_2)\mathfrak{D}_{ji}(g_1) \\
\therefore \mathfrak{D}(g_2 \circ g_1) &= \mathfrak{D}(g_2)\mathfrak{D}(g_1)
\end{aligned} \tag{2.46}$$

[6]This proof only holds for linear operators, and therefore does not apply to the anti-linear operators discussed in section 3.6.

Knowing that the matrices $\mathfrak{D}(g)$ form a representation of $\mathbb{G}$ is sufficient to show that the matrices $\mathfrak{T}(g)$ also form a representation of $\mathbb{G}_k$.

$$\begin{aligned}
\mathfrak{T}(g_2)\mathfrak{T}(g_1)\Phi &= \mathfrak{T}(g_2)\sum_{j}^{n}\psi_j\mathfrak{D}_{ji}(g_1) \\
&= \sum_{k=1}^{n}\sum_{j=1}^{n}\psi_k\mathfrak{D}_{kj}(g_2)\mathfrak{D}_{ji}(g_1) \\
&= \sum_{k=1}^{n}\psi_k\left(\sum_{j=1}^{n}\mathfrak{D}_{kj}(g_2)\mathfrak{D}_{ji}(g_1)\right) \\
\mathfrak{D}_{ki}(g_2\circ g_1) &= \sum_{j=1}^{n}\mathfrak{D}_{kj}(g_2)\mathfrak{D}_{ji}(g_1) \\
\therefore \mathfrak{T}(g_2)\mathfrak{T}(g_1)\Phi &= \sum_{k}\psi_k\mathfrak{D}_{ki}(g_2\circ g_1) \\
&= \mathfrak{T}(g_2\circ g_1)\Phi
\end{aligned} \tag{2.47}$$

Thus, Eq. 2.45 forms our definition of how matrix representations of symmetry operations transform a system-vector.

2.11. Basis vectors and their calculation

Having constructed and deconstructed a representation of the crystal to determine the irreducible representations spanned, what remains is to project out the basis vectors. This is done using the method of projection operators, which we now discuss.

We define the set of vectors $\langle\phi_1^\nu,\phi_2^\nu,\ldots,\phi_n^\nu|$ as the basis vectors for the representation Γ_ν of $\mathbb{G}$ such that:

$$\mathfrak{T}(g)\phi_s^\nu = \sum_{t=1}^{d^\nu}\phi_t^\nu\mathfrak{d}_{ts}^\nu(g) \tag{2.48}$$

This is Eq. 2.45 when $\mathfrak{D}_{ji}(g)=\mathfrak{d}_{ts}^\nu(g)$; we are free to make this substitution as the matrices $\mathfrak{D}(g)$ form a representation of the group. Thus, we define basis-vectors by restricting $\mathfrak{D}_{ji}(g)$ to being an irreducible representation of g in Γ_ν. A set of basis

vectors that transform as in 2.48 are termed a 'basis-set", and the symmetric basis for a system is a set of basis-sets; this is used explicitly in chapter 6.

Like the reduction operator, the projection operator derives from Schur's lemma. We seek to derive a set of basis vectors which observe the following relations:

$$\begin{aligned} \mathfrak{T}(g_i)\phi_i^\nu &= \sum_j^{d^\nu} \mathfrak{d}_{ji}^\nu(g_i)\phi_j^\nu \\ \sum_{g_i\in\mathbb{G}} \mathfrak{d}_{ij}^\mu(g_i)\mathfrak{d}_{ml}^\nu(g_i^{-1}) &= \frac{|\mathbb{G}|}{d^\mu}\delta_{\mu,\nu}\delta_{l,j}\delta_{m,i} \end{aligned} \tag{2.49}$$

Multiplying both sides of the orthogonality relation by $\mathfrak{d}_{ml}^\mu(g_i^{-1})$ and summing over all the operations of the group derives the projection operator, W_{ml}^μ.

$$\begin{aligned} \sum_{g_i\in\mathbb{G}} \mathfrak{d}_{ml}^\mu(g_i^{-1})\mathfrak{T}(g_i)\phi_i^\nu &= \sum_{g_i\in\mathbb{G}}\sum_j^{d^\nu} \mathfrak{d}_{ml}^\mu(g_i^{-1})\mathfrak{d}_{ji}^\nu(g)\phi_j^\nu \\ &= \sum_j^{d^\nu} \frac{|\mathbb{G}|}{d^\mu}\phi_j^\nu\delta_{\mu,\nu}\delta_{l,j}\delta_{m,i} \\ &= \frac{|\mathbb{G}|}{d^\mu}\phi_l^\nu\delta_{\mu,\nu}\delta_{m,i} \end{aligned} \tag{2.50}$$

$$\begin{aligned} W_{ml}^\mu\phi_i^\nu &= \frac{d^\mu}{|\mathbb{G}|}\sum_{g_i\in\mathbb{G}} \mathfrak{d}_{ml}^\mu(g_i^{-1})\mathfrak{T}(g_i)\phi_i^\nu \\ &= \phi_l^\nu\delta_{\mu,\nu}\delta_{m,i} \end{aligned} \tag{2.51}$$

When a vector of the basis set (ϕ_m^ν) is known, then the whole basis set is generated by applying W_{ml} over all l:

$$W_{ml}^\nu\phi_m^\nu = \phi_l^\nu \tag{2.52}$$

However, in general none of the basis vectors are known, and we must consider the action of the projection operator upon a trial vector[7], $\phi = \sum_\nu \sum_i^{d^\nu} C_i^\nu \psi_i^\nu$:

$$\begin{aligned} W_{ml}^\mu \phi &= \sum_\nu \sum_i^{d^\nu} C_i^\nu W_{ml}^\mu \psi_i^\nu \\ &= \sum_\nu \sum_i^{d^\nu} C_i^\nu \psi_l^\mu \delta_{m,i} \delta_{\mu,\nu} \\ &= C_m^\mu \psi_l^\mu \end{aligned} \tag{2.53}$$

The action of the projection operator is to take the component of ϕ along ψ_m^μ and transform it into ψ_l^μ; all the other components are transformed to zero.

When the IRs spanned by a system are known we can use the method of projection operators to generate all the basis vectors by varying l, m, μ and ϕ. Varying l generates new members of the same basis-set, while varying the other parameters generate new basis sets.

2.12. Unitary matrices

When a matrix is the conjugate transpose of its inverse, then it is said to be *unitary*:

$$\mathfrak{d}_{ml}(g_s) = \mathfrak{d}_{lm}^*(g_s^{-1}) \tag{2.54}$$

An IR composed of unitary matrices is, itself, unitary. It is usual to assume that IRs used in representation theory are unitary, and under this assumption the projection and reduction operators can be rewritten:

$$W_{lm}^{\mu *} = \frac{d^\mu}{|\mathbb{G}|} \sum_{g_s} \mathfrak{d}_{lm}^{\mu *}(g_s) \mathfrak{T}(g_s) \tag{2.55}$$

$$\frac{1}{|\mathbb{G}|} \sum_{g_s \in \mathbb{G}} \chi^\nu(g_s) \chi^{\mu *}(g_s) = \delta_{\mu,\nu} \tag{2.56}$$

[7]Selection of appropriate trial vectors is discussed in chapter 6.

The projection and reduction operators are almost always used in the form above for convenience, and occasionally with the complex conjugation dropped if the IRs are know to be completely real. However, these equations are only valid when the IRs have been confirmed as being unitary. In chapter 5, the unitary character of the irreducible representations tabulated by Kovalev (1993) is confirmed for the first time.

2.13. The stabilizers method

An alternative set of reduction and projection operators have been derived by Izyumov (1960). Rather than considering the whole of the group $\mathbb{G}_k$, his method focuses upon the action of a special subgroup of $\mathbb{G}_k$ that "stabilizes" one of the atomic position vectors R_0. This approach is advantageous in computational work as it reduces the number of calculations, the concept of stabilizers is exploited in chapter 6. Here, we derive the stabilizer form of the reduction operator, without discussing Izyumov's alternative projection operator. The stabilizer projection involves the explicit generation of large matrices that are difficult to interpret, where as the method of projection operators are more intuitive and can be understood graphically (section 3.3).

Consider the sub-group $\mathbb{S}_0 \subset \mathbb{G}_k$, consisting of all those operations in $\mathbb{G}_k$ which permute some position vector r_0 into itself (within a primitive translation).

$$s : r_0 \longmapsto r_0 + t \qquad \forall s \in \mathbb{S}_0, t \in \mathbb{T} \tag{2.57}$$

$\mathbb{G}_k$ can be decomposed into left co-sets of $\mathbb{S}_0$:

$$\mathbb{G}_k = \mathbb{S}_0 + g_1\mathbb{S}_0 + g_2\mathbb{S}_0 + .. + g_n\mathbb{S}_0 \tag{2.58}$$

Further, we can generate all the positions in r_0's orbit by acting upon r_0 with a member of each left coset in turn:

$$g_1 \mathbb{S}_0 r_0 = g_1 r_0 = r_1 \tag{2.59}$$

There are n left cosets of order $n(\mathbb{S}_0)$, and from Lagrange's theorem:

$$n = \frac{n(\mathbb{G}_k)}{n(\mathbb{S}_0)} \tag{2.60}$$

Every position in the orbit of r_0 also has its own set of stabilizing elements $\mathbb{S}_j \subset \mathbb{G}_k$, which is conjugate to $\mathbb{S}_0$:

$$\begin{aligned} \mathbb{S}_1 r_1 = r_1 &= g_1 r_0 \\ &= g_j \mathbb{S}_0 r_0 \\ &= g_j \mathbb{S}_0 g_j^{-1} r_j \\ \therefore \mathbb{S}_1 &= g_j \mathbb{S}_0 g_j^{-1} \\ \therefore \mathbb{S}_0 &= g_j^{-1} \mathbb{S}_j g_j^1 \end{aligned} \tag{2.61}$$

Expanding Eq. 2.56, using Eq. 2.40:

$$\begin{aligned} n^\nu &= \frac{1}{n(\mathbb{G})} \sum_g \chi^{\vec{k}*}(g) \chi^{\vec{k}\nu}(g) \\ &= \frac{1}{n(\mathbb{G})} \sum_g \chi^{\vec{k}*}_{Perm}(g) \chi^{\vec{k}*}_h(g) \chi^{\vec{k}\nu}(g) \\ &= \frac{1}{n(\mathbb{G})} \sum_g \chi^{\vec{k}*}_h(g) \chi^{\vec{k}\nu}(g) \sum_j e^{-2\pi i \vec{k} \vec{a_{ij}}(g)} \delta_{r_j, g r_j} \end{aligned} \tag{2.62}$$

Here, we have used the idea of stabilizing elements to define the character of the permutation matrix: $\delta_{r_j, g r_j} = 0$ unless g stabilizes r_j. Using Eq. 2.61, we write all

stabilizers of r_j as similarity transformations of r_0, and rearrange the sum over r_j.

$$\begin{aligned}\sum_j e^{-2\pi i\vec{k}\vec{a_{ij}}(g)}\delta_{r_j,gr_j} &= \sum_j e^{-2\pi i\vec{k}.(gr_j-r_j)}\delta_{g_jr_0,gg_jr_0} \\ &= \sum_j e^{-2\pi i\vec{k}.(gg_jr_0-g_jr_0)}\delta_{g_jr_0,gg_jr_0} \\ &= \sum_j e^{-2\pi i\vec{k}g_j.(g_j^{-1}gg_jr_0-r_0)}\delta_{r_0,g_j^{-1}gg_jr_0} \\ &= \sum_j e^{-2\pi i\vec{k}g_j.(sr_0-r_0)}\delta_{r_0,sr_0}\end{aligned} \tag{2.63}$$

The last step is derived from Eq. 2.61, with $s \in \mathbb{S}_0$, $g \in \mathbb{S}_j$. Strictly, this is only valid when $g \in \mathbb{S}_j$, however $g \notin \mathbb{S}_j \leftrightarrow \delta_{r_j,gr_j} = 0$. To complete the derivation, we note that $g_j \in \mathbb{G}_k \Rightarrow g_j\vec{k} = \vec{k} + \vec{t}_{g\vec{k}}$, and $s \in \mathbb{S}_0 \Rightarrow sr_0 \mapsto r_0 + \vec{a}_{00}(s)$.

$$\begin{aligned}\sum_{r_j} e^{-2\pi ig_j\vec{k}.(sr_0-r_0)}\delta_{r_0,sr_0} &= \sum_{r_j} e^{-2\pi i(\vec{k}+\vec{t}_{g\vec{k}}).(\vec{a}_{00}(s))}\delta_{r_0,sr_0} \\ &= \sum_{r_j} e^{-2\pi i\vec{k}.(\vec{a}_{00}(s))}\delta_{r_0,sr_0}e^{-2\pi it_{g\vec{k}}.(\vec{a}_{00}(s))} \\ &= \sum_{r_j} e^{-2\pi i\vec{k}.(\vec{a}_{00}(s))}\delta_{r_0,sr_0}\end{aligned} \tag{2.64}$$

In a primitive setting both $\vec{t}_{gk}$ and $\vec{a}_{00}(s)$ are primitive translations: vectors comprised of integer elements. Hence, the dot-product $t_{g\vec{k}}.\vec{a}_{00}$ is an integer, and the term $e^{2\pi i\vec{t}_{gk}\vec{a}_{00}}(s)$ is always equal to 1. As a change of basis preserves the dot-product of two vectors, this holds for any choice of basis. The sum over r_j will multiply the exponential by the number of symmetry equivalent positions, known from Eq. 2.60.

$$
\begin{aligned}
n^v &= \frac{1}{n(\mathbb{G})} \sum_g \chi_h^{\vec{k}*}(g)\chi^{\vec{k}\nu}(g) \sum_j e^{-2\pi i \vec{k}.\vec{a_{ij}}(g)} \delta_{r_j, g r_j} \\
&= \frac{1}{n(\mathbb{G})} \sum_g \chi_h^{\vec{k}*}(g)\chi^{\vec{k}\nu}(g) \sum_j e^{-2\pi i \vec{k}.\vec{a}_{00}(s)} \delta_{r_0, s r_0} \\
&= \frac{1}{n(\mathbb{G})} \sum_g \chi_h^{\vec{k}*}(g)\chi^{\vec{k}\nu}(g) \frac{n(\mathbb{G})}{n(S_0)} e^{-2\pi i \vec{k}.\vec{a}_{00}(s)} \delta_{r_0, s r_0} \\
&= \frac{1}{n(S_0)} \sum_s \chi_s^{\vec{k}*}(s)\chi^{\vec{k}\nu}(s) e^{-2\pi i \vec{k}.\vec{a}_{00}(s)}
\end{aligned}
\tag{2.65}
$$

Therefore, to derive the irreducible representations spanned by this basis at R, one need only consider the elements that stabilize the point R, simplifying the calculations considerably. Revisiting the example from section 2.10.1, we can see that the order of the stabilizing group is 1, as is the character of the permutation representation when considering only stabilizing elements. Completing the calculations with the diminished IR tables generates the same reduction: $C^1 = \frac{1}{1} \times 3 \times 1 = 3 = C^2$.

2.14. Conclusions

This chapter has reviewed the foundations of representation theory and its application to crystalline systems. We have not only considered how to describe the positions of each atom in the crystal, but also properties upon that position. In this way, we can describe how a system changes during a phase change. Further, we have derived the reduction and projection operators; tools for constructing the basis vectors of the little group $\mathbb{G}_k$.

Though equipped with the tools to calculate the basis vectors of a system, we still lack the raw materials; IRs and trial functions. Chapter 5 will validate a reliable source of IRs with which to perform these calculations, and in chapter 6 the problem of what constitutes an appropriate set of trial functions is discussed. Before that,

chapter 3 will discuss how basis vectors relate to a system's Hamiltonian and how to construct completely real symmetry modes from complex basis vectors.

References

[1] Bradley, C. J. and Cracknell, A. P. (1972) *Mathematical Theory of Symmetry in Solids*, **Clarendon Press**.

[2] Hamermesh, M. (1964) *Group Theory and its Application to Physical Problems*, **Addison-Wesley Publishing Company**.

[3] Izyumov, Yu. A., Syromyatnikov, V. N. (1990) *Phase Transitions and Crystal Symmetry*, **Kluwer Academic Publishers**.

[4] Kovalev O. V., *Representations of the Crystallographic Space Groups: Irreducible representations, Induced representations and Corepresentations (2nd Ed)*, **Gordon and Breach Science Publishers** (Amsterdamn. 1993).

[5] Wigner, E. P., (1959) *Group Theory and its application to the quantum mechanics of atomic spectra*, **Academic Press Inc.**

CHAPTER 3

Representation theory: A physical interpretation

"I fear explanations explanatory of things explained"

Abraham Lincoln

3.1. Introduction

The advantages of using representation theory to describe phase transitions are two fold. First, representation theory is the only symmetry frame-work which fully describes all the possible symmetries of a crystal: a point developed by Bertaut (1968, 1981) with particular reference to magnetic structures. Second, the irreducible representations of a system are intimately related to the eigenvectors of its Hamiltonian. Using representation theory, to define how a system changes, indirectly probes the energy terms driving a phase transition.

In this chapter we derive Wigner's Theorem (Wigner, 1927), demonstrating the link between basis vectors and eigenspaces of a Hamiltonian. Then, the use of complex vectors to define completely real properties is considered, and this apparent contradiction resolved using Wigner's theory of anti-linear operations. This is followed by a discussion on the use of co-representations, and why work to derive new basis vectors from them is largely misguided. Finally, some of the qualitative arguments used in later chapters are developed.

3.2. Wigner's theorem

It is hard to overstate the importance of Wigner in bringing group theoretical techniques to physical problems, and a number of lengthy celebrations of his contributions have been made (e.g. Voight, 1995; Primas, 1997; Chayut, 2001). While his work has been widely applied in the fields of physics and mathematics, he was introduced to symmetry theory through crystallography by Weissenberg (Kuhn, 1965). This chapter will exploit two of Wigner's most celebrated results, beginning with a proof of his theorem concerning the subspaces of the Hamiltonian.

Wigner's theorem (Wigner, 1927), draws a link between the eigensubspaces of a Hamiltonian, and the representation of its symmetry group.

> *If* $\mathbb{G}$ *is the symmetry group of a Hamiltonian* H*, then every degenerate eigensubspace of* H *is invariant under* $\mathbb{G}$*.*
> *i.e. It constitutes a representation of* $\mathbb{G}$*.*

The eigensubspace of a_n is the span of all eigenvectors with eigenvalue a_n.

Proof of Wigner's theorem consists of three steps: determining the symmetry properties of operators that commute (the First theorem); showing that operators which commute have a common set of eigenfunctions (the Great theorem); and finally using these results to prove Wigner's theorem. We follow the proof presented by Pfister (2003, Supporting materials), supplementing the mathematics with a more detailed discussion.

3.2.1. The First theorem

If A, B are two operators that commute, then every eigensubspace of A is invariant under B and vice-versa

Proof

Let $|\psi_n\rangle$ be an eigenvector of A, eigenvalue a_n, then:

$$\begin{aligned} A(B|\psi_n\rangle) &= BA|\psi_n\rangle \\ &= Ba_n|\psi_n\rangle \\ &= a_n(B|\psi_n\rangle) \end{aligned} \tag{3.1}$$

This shows that $B|\psi_n\rangle$ is also an eigenvector of A. As this holds for any combination of the eigenvectors of a_n, this entire eigensubspace of A is invariant under B. Further, the argument holds for any eigenvalue a_n and so every eigensubspace of A is invariant under B. Trivially, we can reverse this argument with respect to A and B, proving the First theorem.

3.2.2. The Great theorem

If A, B commute, then we can always find a common eigenbasis.

The eigenbasis of an eigensubspace is the set of linearly independent eigenvectors from which it is constructed. The Great Theorem tells us that if the operators A, B commute then one can always find a common set of eigenvectors. This is already proven when a_n is non-degenerate; in this case a_n has only a single eigenvector, $|\psi_n\rangle$, and so $B|\psi_n\rangle$ must be parallel to it. When a_n is degenerate, there is an additional step in the proof.

Proof

Consider some matrix representation of A acting upon the vector:

$$|\Psi\rangle = \begin{pmatrix} |\psi_1\rangle \\ ... \\ |\psi_m\rangle \end{pmatrix} \tag{3.2}$$

Where $\psi_1 ... \psi_m$ are the eigenvectors of a_n. The action of A upon this subspace can be represented by the identity matrix:

$$A|\Psi\rangle = a_n \mathfrak{T}(E)|\Psi\rangle \tag{3.3}$$

Thus, any similarity transformation leaves A invariant:

$$\begin{aligned} \mathfrak{A}A\mathfrak{A}^{-1} = \mathfrak{A}a_n\mathfrak{T}(E)\mathfrak{A}^{-1} &= (a_n\mathfrak{T}(E))(\mathfrak{A}\mathfrak{A}^{-1}) \\ &= AE \\ &= A \end{aligned} \tag{3.4}$$

As A and B have the same eigensubspaces, there also exists a matrix representation of B upon $|\Psi\rangle$. The matrix representation of B can be diagonalized by some similarity transformation, $\mathfrak{A}^{-1}B\mathfrak{A}$, and this transformation will leave A and a_n unchanged. The diagonality of $\mathfrak{A}^{-1}B\mathfrak{A}$ implies that it transforms every $|\psi\rangle$ into itself. Hence, there exists some transformation of B under which it has the same eigenvectors as A.

3.2.3. Wigner's Theorem

Before First and Great theorems can be used in the proof of Wigner's theorem, we must show that a Hamiltonian commutes with its symmetry group. A symmetry operation of the Hamiltonian acts upon the system co-ordinates in such a way as to leave the Hamiltonian unchanged (Hammermesh, 1964):

$$gH(x) = H(g^{-1}x) = H(x) \tag{3.5}$$

By representing $H(x)\psi(x)$ with some function $\Phi(x)$ the Hamiltonian can be shown to commute with its symmetry functions:

$$\begin{aligned} g\Phi(x) &= \Phi(g^{-1}x) \\ \therefore gH(x)\psi(x) &= g\Phi(x) = \Phi(g^{-1}x) = H(g^{-1}x)\psi(g^{-1}x) \\ &= gH(x)g^{-1}g\psi(x) = gH(x)g^{-1}\psi(g^{-1}x) \\ \therefore gH(x)g^{-1} &= H(g^{-1}x) = H(x) \\ \therefore gH(x) &= H(x)g \end{aligned} \tag{3.6}$$

As H, $\mathbb{G}$ commute, they can be substituted for A, B in the First and Great theorems. Maschke's Theorem (Appendix 3) states that there exists a similarity transformation which block-diagonalizes every matrix $\mathfrak{T}(g)$ in $\mathbb{G}$, and the First Theorem states that the matrix representation of H must have the same block-diagonal form (the same invariant subspaces) as the matrices $\mathfrak{T}(g)$.

To complete the proof, we consider the individual matrix blocks. For the matrices $\mathfrak{T}(g)$, the blocks consist of the irreducible representations of $\mathbb{G}$. As H commutes with every g in $\mathbb{G}$ so must its matrix representation; indeed each block of the Hamiltonian matrix commutes with the corresponding block (irreducible representation) of the $\mathfrak{T}(g)$. Shur's lemma (Appendix 4) implies that any matrix which commutes with an irreducible representation of $\mathbb{G}$ must be some multiple of the identity, hence each block in the Hamiltonian matrix must be some multiple of an identity matrix.

The transformation that block-diagonalizes the representations of the symmetry operations simultaneously diagonalizes the Hamiltonian, demonstrating that: *the IR's of* $\mathbb{G}$ *correspond to eigensubspaces of the Hamiltonian.* This result is so well known as to be "hidden in plain view"; in many fields it is conventional to label energy levels with the irreducible representations that correspond to them (e.g. electronic and vibrational spectroscopy). Basis vectors transform as irreducible representations,

which themselves correspond to eigensubspaces of the Hamiltonian. As such, they have the symmetry of eigensubspaces, and defining a system property using basis vectors gives us insight into the energy terms under which it is ordering.

3.3. The structure of basis vectors

Wigner's theorem shows that basis vectors, by transforming as irreducible representations, capture the symmetry of terms in the Hamiltonian. However, it says nothing about their form or how to derive them, for this we must turn to Bloch's theorem (Bloch, 1928) and the method of projection operators.

Basis vectors represent long range order, in particular translational periodicity. In section 2.9.1 the translational symmetry of the vector-field representing our property was defined in the following way:

$$\begin{aligned} g_{trans} &: \vec{R} \mapsto \vec{R} + \alpha_{trans} \\ g_{trans} &: \vec{v}_R \longmapsto e^{-2\pi i \vec{k}.\vec{\alpha}_{trans}}.\vec{v}_R \end{aligned} \tag{3.7}$$

$\vec{R}$ is the position of some atom in the crystal, and v_R defines the system property at that point. Previously, no justification was given for the periodic nature of basis vectors, but this is a natural result of Wigner's theorem. Bloch's Theorem states that the wave-functions of periodic systems have the form:

$$\psi_{n\vec{k}} = u_{n\vec{k}}(R)e^{i\vec{q}.\vec{R}} \tag{3.8}$$

In this equation the term $e^{i\vec{k}.R}$ captures the translational symmetry of the wave function, while $u_{n\vec{k}}(R)$ is a function that defines the shape of the wave function. As basis vectors have the symmetry of the eigenfunctions, the basis vectors of crystals must have the same translational properties as these *Bloch waves*.

The form of Eq. 3.8 suggests a system property could defined using Bloch waves in which $u_{n\vec{k}}(R)$ is very simple:

$$\vec{v}_R = \vec{A}e^{-2\pi i\vec{k}.\vec{R}} \tag{3.9}$$

We have chosen $u_{n\vec{k}}(R) = \vec{A}$, a vector that defines the amplitude and the orientation of the property vector at a position in the 0^{th} primitive unit cell[1]. The property at the equivalent position in every other primitive cell is defined by its translational relationship to the 0^{th} cell.

Eq. 3.9 only applies to those positions which are related by translational symmetry, and not to other positions in an atom's orbit or atoms in other orbits. As our model is quite general, the entire system can be defined using a series of these simple Bloch waves upon each atom in the 0^{th} primitive unit cell. However, we might expect the Bloch waves of symmetry related positions within the 0^{th} unit cell to have well defined relationships. Indeed they do and these relations can be determined by consideration of how basis vectors are constructed using the method of projection operators.

Consider a crystal with space group $\mathbb{G} = \{E, C_2\} \otimes \mathbb{T}$, consisting of a single atom at the position R, ordering under $\vec{k} = (0, \frac{1}{2}, 0)$. For this k-vector, $\mathbb{G}_k = \mathbb{G}_0$ and has two IRs:

	E	C_2
Γ_1	1	1
Γ_2	1	-1

[1]The constant factor of -2π in the exponent denotes a change from the wave-vector $\vec{q}$ to the reduced wave-vector $\vec{k} = \frac{-\vec{q}}{2\pi}$ which is more convenient to work with in these calculations.

The unitary projection operator (section 2.12), acting on a trial vector ϕ, has the form:

$$W_{lm}^{\mu*}\phi = \frac{d^{\mu}}{|\mathbb{G}|}\sum_{g}\mathfrak{d}_{lm}^{\mu*}(g)\mathfrak{T}(g)\phi \tag{3.10}$$

It is important to note that, for any real system, the symmetry group considered when applying Eq. 3.10 is $\mathbb{G}_k$. Construction of a basis vector transforming as Γ_2 is illustrated in Fig. 3.1. (a)First, our trial function, consisting of a property vector $\vec{v}_R$ at the position $\vec{R}$, is transformed by the operation g to some new position $g\vec{R}$ with property $h\vec{v}_R$. (b)The image of the trial function is then multiplied by a complex number $\mathfrak{d}_{lm}^{2*}(g)$; the complex number "phases" the Bloch wave, translating it relative to the atomic-lattice . (c)This process is repeated over all $g \in \mathbb{G}_k$, and the sum of all the images forms a basis-vector . (d)The property at every other position in the crystal is defined by the basis vector's translational symmetry under $\vec{k}$.

Thus, the form of basis vectors is a set of Bloch-waves, with a single k-vector, upon every symmetry related position in an orbit under $\mathbb{G}_k$. The relative orientations and phases of the Bloch waves are strictly defined by the symmetry operations of the group and the irreducible representation from which it has been projected.

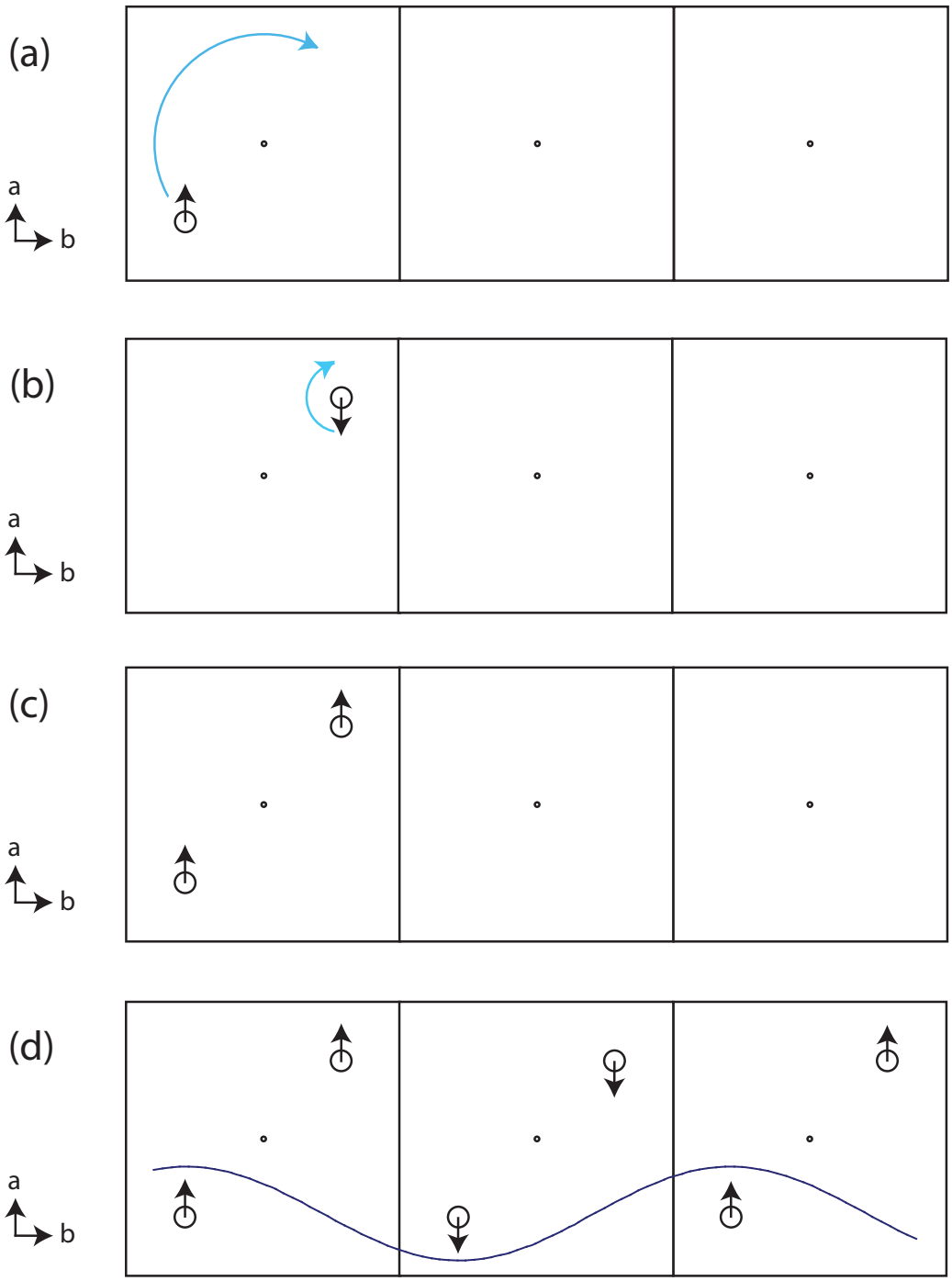

FIGURE 3.1. A graphical illustration of the method of projection operators. (a) A trial vector upon a single atom is transformed to a symmetry related position by the operation C_2. (b) The image is then multiplied by the matrix element $\mathfrak{d}^{2*}_{11}(C_2) = -1$. (c) The basis vector comprises the sum of all the images generated by the elements of $\mathbb{G}$. (d) The property vectors of equivalent positions outside the 0^{th} cell are defined according to the translational symmetry: $\psi(r_j) = e^{-2\pi\vec{k}.a_{ij}}$. In this example $\vec{k} = (0, \frac{1}{2}, 0)$

3.4. Constructing completely real basis vectors

In general, basis vectors derived from the method of projection operators are complex, as are their coefficients in the linear expansion of an ordered state. For many properties this represents an unphysical result, and the basis vectors must be brought into a form that is completely real everywhere. This is done by forming linear combinations of each basis vector with a basis vectors ordering under $-\vec{k}$. These basis vectors are the complex conjugates of the $+\vec{k}$ basis vectors (Wills, 2001):

$$\begin{aligned} \Psi &= \psi_{\vec{k}} + \psi_{-\vec{k}} \\ &= \psi_{\vec{k}} + \psi^*_{\vec{k}} \end{aligned} \tag{3.11}$$

This definition does not uniquely determine Ψ, as one must decide how to handle complex coefficients of ψ. There are two possibilities:

$$\begin{aligned} \Psi &= C\psi_{\vec{k}} + (C\psi_{\vec{k}})^* \\ &= C\psi_{\vec{k}} + C^*\psi^*_{\vec{k}} \qquad (3.12) \\ \Psi &= C\psi_{\vec{k}} + C\psi^*_{\vec{k}} \qquad (3.13) \end{aligned}$$

In the second case, Ψ will still be complex when C becomes complex. To achieve our aim of a completely real construction, we must either restrict C to being completely real or use the "standing wave" approach.

$$\Psi = C(\psi_{\vec{k}} + \psi^*_{\vec{k}}) + C^*(\psi_{\vec{k}} + \psi^*_{\vec{k}}) \tag{3.14}$$

In this section we consider the construction proposed in Eq. 3.12, termed the plane-wave construction as it behaves like a plane-wave when ψ is complex. In particular, the complexity of C in Eq. 3.12 is realized as a phasing of the wave; a translation of the property wave relative to the crystal lattice.

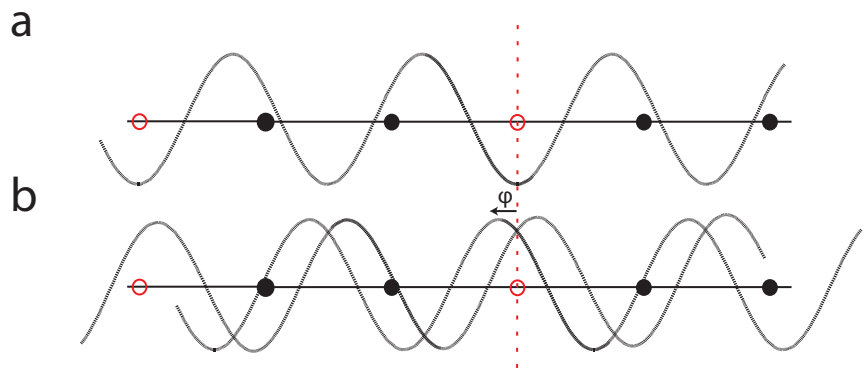

FIGURE 3.2. A graphical representation of symmetry breaking through phase displacement. A line of atoms is depicted by the filled and unfilled circles, and some axial-vector property by the cosinusoidal wave. In (a) both the atomic positions atoms and the property wave are symmetric under inversion about the unfilled red circles. In (b) a phase-displacement of the wave eliminates inversion symmetry. In (b), any inversion which leaves the lattice invariant transforms the spin density wave, and vice-versa.

The transformation properties of basis vectors are defined by the equation:

$$g\psi_i = \sum_i \mathfrak{d}_{ij}(g)\psi_j \tag{3.15}$$

From Eq. 3.15 it is clear that the symmetry of a basis vector is strictly defined by the irreducible representation from which it is projected. A plane-wave, as defined in Eq. 3.11, is inconsistent with this constraint when we allow the coefficients, C, to be complex. Figure 3.2 depicts a cosinusoidal basis vector representing a pseudo-vector property (Fig. 1.3), such as a spin-density wave, with the symmetry of a one-dimensional irreducible representation. In (a) the spin density wave is related to the lattice such that their inversion centres are coincident, and both lattice and spin density wave are invariant under the operation of inversion about the red circles. This relationship is encapsulated in the irreducible matrix representation of I (section 3.8):

$$\begin{aligned} I\Psi &= \mathfrak{d}(I)\Psi = \Psi \\ \therefore \mathfrak{d}(I) &= 1 \end{aligned} \tag{3.16}$$

A complex-coefficient of ψ displaces the wave relative to the lattice, and the symmetry of the system is changed (Fig 3.2b). For the displaced wave, the matrix representation of I is now:

$$\begin{aligned} Ie^{i\theta}\Psi &= e^{i\theta}\mathfrak{d}\Psi = e^{-i\theta}\Psi \\ \therefore \mathfrak{d}(I) &= e^{-2i\theta} \end{aligned} \tag{3.17}$$

While a completely-real construction of basis-vectors is required to describe physical systems, they must retain the symmetry properties of their constituent basis vectors. The plane-wave construction violates this rule, and therefore can not be used as a definition for completely real symmetry modes.

3.5. Standing wave constructions

The definition of how a system responds to complex basis vector coefficients given by 3.14 will be termed the standing wave construction. Standing waves differ from plane-waves in that they do not propagate through a system, instead complex coefficients of ψ modulate the amplitude of the mode. This is most readily demonstrated using the trigonometric form for standing waves.

$$\begin{aligned} C &= Ae^{i\omega} \\ \Psi &= C(\psi_{\vec{k}} + \psi^*_{\vec{k}}) + C^*(\psi_{\vec{k}} + \psi^*_{\vec{k}}) \\ &= A\cos(\omega)\cos(\vec{k}R) \end{aligned} \tag{3.18}$$

The term that transforms in space, $\cos(\vec{k}R)$, is unchanged by a complex coefficient, indicating that the wave does not move relative to the origin. This spatial invariance with respect to phase demonstrates that the symmetry of the standing-wave construction is not changed by complex coefficients of ψ (Figure 3.3). By constructing completely real basis vectors using the standing wave form, we ensure that they have the correct symmetry. Further, there is no need to consider complex coefficients of

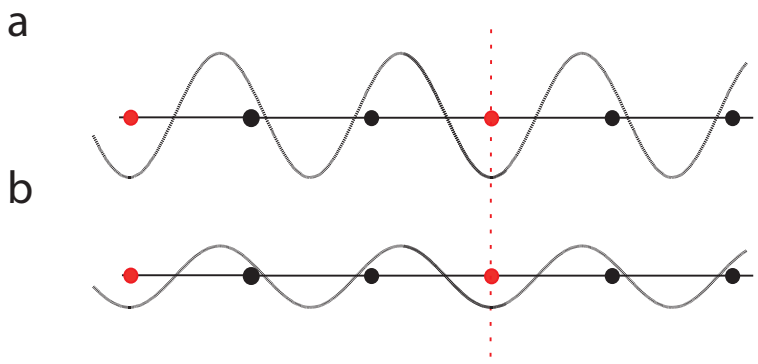

FIGURE 3.3. Figures (a) and (b) depict the same standing wave when ψ has coefficients 1, and $e^{\frac{\pi}{2}}$ respectively. The symmetry of a standing wave does not vary with the phase of the coefficient, instead complexity is indistinguishable from a change in the wave amplitude.

ψ, as they are indistinguishable from real coefficients when we form Ψ. Hence, we have restricted the coefficient of Ψ to being completely real, without restricting the coefficients of ψ. [2]

3.6. Anti-linear symmetry

Though we have determined how to construct completely real modes from complex basis vectors, it has not shown that the basis vectors of $\vec{k}$ and $-\vec{k}$ are degenerate. To show that both $-k$ and $-\vec{k}$ reside within the same eigensubspace of the Hamiltonian, requires consideration of the anti-linear symmetry operations of the Hamiltonian.

The invariance of a system's Hamiltonian under inversion of time was first discussed by Wigner (1959) and formalized through the theory of co-representations. He also derived a general framework for using anti-linear operations[3], and his results have been widely discussed throughout both the physics and mathematical communities

[2]In practise, it is usual to construct completely real symmetry modes as $\Psi = \psi_{\vec{k}} + \psi^*_{\vec{k}}$ and restrict the coefficients of Ψ. We have shown that does not cause a loss of generality in the results.
[3]More specifically, anti-*unitary* operations. Those anti-linear operations which leave the transition probability between any two states invariant: $|(\Phi_1, \Phi_2)| = |(K\Phi_1, K\Phi_2)|$

(e.g. Bargmann, 1964; Lajos, 1998; Jinxiu, 2006; Simona, 2008). While the importance of anti-linear symmetry has been recognized for many years (Landau, 1960; Bertaut, 1971), it is still relatively undiscussed in crystallography. Recently, it has received increasing attention (e.g Schweizer, 2005, 2007; Stewart, 2007; Radaelli, 2007; ; Harris, 2008a, 2008b), but a considerable amount of confusion about this symmetry remains in the literature.

One common misconception is that the degrees of freedom of a system can be reduced by consideration of anti-linear symmetry; this is not correct. When using basis vectors to define the structure of some ordered property of a system, the degrees of freedom are exactly the coefficients of the basis-vectors (which may be complex). If the property is defined by an n-dimensional vector and the unit-cell contains m atoms, then there are nm degrees of freedom. The only way to reduce the number of free parameters is to restrict them by making assumptions about the symmetry of the final structure[4]. The number of independent atoms in the system-vector depends only upon the assumptions made about the symmetry of the daughter phase, and not the symmetry operators of the parent phase.

3.6.1. Irreducible co-representations

Anti-linear operators behave in the following way:

$$Ka\psi = a^*K\psi \tag{3.19}$$

The most prominent example of an anti-linear operation is complex-conjugation. However, the choice of anti-unitary operator is relatively unconstrained and in crystallography it is conventionally chosen such that:

$$K : \vec{k} \mapsto -\vec{k} \tag{3.20}$$

[4]In fact, a system has nM degrees of freedom, where M is the total number of atoms in the system (and not just the unit cell). This is reduced to nm by the assumption that the daughter phase orders under some k-vector $\vec{k}$

This operation is equivalent to complex-conjugation, and the choice is useful as diffraction data can not determine whether a system orders under $\vec{k}$ or -$\vec{k}$.

The element K is referred to as the anti-unitary generating element. As the symmetry elements of a system must form a group, when we consider anti-linear symmetry we not only include K, but the set $K\mathbb{G}$: a set of anti-linear operations generated by K. When K is an element of $\mathbb{G}_k$, then $K\mathbb{G}_k = \mathbb{G}_k$ (section 2.2.1) and the little group is left unchanged. Otherwise, the symmetry group of a system is expanded to the union $\mathbb{G}_k \oplus K\mathbb{G}_k$, doubling its size.

Consideration of anti-linear operations enlarges the symmetry group of the system to the union $(\mathbb{G} \oplus K\mathbb{G})$[5]. As usual, matrix representations of this group can be reduced to a block-diagonal form, but now the blocks constitute irreducible co-representations (ICRs). The ICRs of a group are defined by the following relations:

$$\begin{aligned} \mathfrak{c}(u_1)\mathfrak{c}(u_1) &= \mathfrak{c}(u_1u_2) & \mathfrak{c}(u)\mathfrak{c}(a) &= \mathfrak{c}(ua) \\ \mathfrak{c}(a)\mathfrak{c}(u)^* &= \mathfrak{c}(au) & \mathfrak{c}(a_1)\mathfrak{c}(a_2)^* &= \mathfrak{c}(a_1a_2) \end{aligned} \tag{3.21}$$

The u are linear operations of $\mathbb{G}$, and the a are anti-linear operations of $K\mathbb{G}$; $\mathfrak{c}(g)$ is the irreducible co-representation of $g \in (\mathbb{G} \oplus K\mathbb{G})$. It is important to note that ICRs do *not* form representations of the group; as such we cannot use the reduction or projection operators during this type of analysis. The effect of anti-unitary symmetry upon the basis vectors is discussed in section 3.7.

Rigorous derivation of ICRs is lengthy (Wigner, 1959), but the method can be summarized as follows. Using the relations in Eq. 3.21, and Eq. 3.15 it is possible to construct the irreducible representations of $\mathbb{G}$ in two ways: $\mathfrak{d}(u)$ and $\mathfrak{d}(K^{-1}uK)$. From these three general types of ICR are derived.

[5]This is exactly analogous to the construction of magnetic space groups (section 1.3.1), in particular the grey-groups. For the non-grey groups $\mathbb{G}$ is replaced by some subgroup of $\mathbb{G}$ containing exactly half of the symmetry operations.

- *Type A*

  $\mathfrak{c}(u)$ is the same order as $\mathfrak{d}(u)$, and $\mathfrak{d}(u)$ is equivalent to $\mathfrak{d}(K^{-1}uK)$:

$$\begin{aligned} \mathfrak{d}(K^{-1}uK) &= \beta^{-1}\mathfrak{d}(u)\beta \\ \mathfrak{c}(u) &= \mathfrak{d}(u) \\ \mathfrak{c}(a) &= \mathfrak{d}(aK^{-1})\beta \end{aligned} \tag{3.22}$$

- *Type B*

  $\mathfrak{c}(u)$ is the twice the order of $\mathfrak{d}(u)$, and $\mathfrak{d}(u)$ is equivalent to $\mathfrak{d}(K^{-1}uK)$:

$$\begin{aligned} \mathfrak{d}(K^{-1}uK) &= \beta^{-1}\mathfrak{d}(u)\beta \\ \mathfrak{c}(u) &= \begin{pmatrix} \mathfrak{d}(u) & 0 \\ 0 & \mathfrak{d}(u) \end{pmatrix} \\ \mathfrak{c}(a) &= \begin{pmatrix} 0 & \mathfrak{d}(aK^{-1}) \\ -\mathfrak{d}(aK^{-1}) & 0 \end{pmatrix} \end{aligned} \tag{3.23}$$

- *Type C*

  $\mathfrak{c}(u)$ is the twice the order of $\mathfrak{d}(u)$; $\mathfrak{d}(u)$ and $\mathfrak{d}(K^{-1}uK)$ are inequivalent irreducible representations:

$$\begin{aligned} \mathfrak{c}(u) &= \begin{pmatrix} \mathfrak{d}(u) & 0 \\ 0 & \mathfrak{d}(K^{-1}uK)^* \end{pmatrix} \\ \mathfrak{c}(a) &= \begin{pmatrix} 0 & \mathfrak{d}(aK) \\ \mathfrak{d}(K^{-1}a)^* & 0 \end{pmatrix} \end{aligned} \tag{3.24}$$

Note that $K^{-1}uK, K^{-1}a, aK$ etc. are all members of $\mathbb{G}_k$, so we can fully determine the ICRs of a group from the IRs of $\mathbb{G}_k$.

3.6.2. Degeneracies from co-representations

Within Wigner's theorem we can replace IRs with ICRs (Wigner, 1959), and each type of ICR will have a distinct effect upon the degeneracies of a system. The simplest are type A ICRs, which mix a single IR of $\vec{k}$ and the same IR of $-\vec{k}$; this

generates new basis functions without creating additional degeneracies. Type B are constructed from equivalent IRs of $\vec{k}$ and $-\vec{k}$; within this space, an IR of $\vec{k}$ and $-\vec{k}$ become degenerate. Type C ICRs bring together inequivalent IRs, again representing $\vec{k}$ and $-\vec{k}$. Like type B ICRs, type C ICRs form new dengeracies between the IRs of $\pm\vec{k}$. For this type of ICR, a second-order phase transition involving *two* distinct IRs joined by anti-unitary symmetry would be possible (Landau theory, section 1.5).

Returning to the problem of completely real symmetry modes, inclusion of anti-linear symmetry is sufficient to justify the standing wave construction. For all types of ICR, both $\psi_{\vec{k}}$ and $\psi_{-\vec{k}}$ reside within the same eigensubspace and are therefore necessarily degenerate, as is any linear combination of their basis vectors. Hence, the construction of modes as described in section 3.5 does not mix eigensubspaces (energy levels).

3.6.3. Free phase-factors in anti-linear symmetry

One element of anti-linear symmetry that has, until recently, been overlooked are the free phase factors when choosing K and β (Stewart, 2007; Wills, 2009). Any choice of K could be replaced by an element that inverts $\vec{k}$ *and then adds a phase to the basis vector* (in the manner of super-space groups). Equally, β is restricted such that $\beta\beta^* = \pm 1$ leaving only its modulus defined.

It should be noted that these degrees of freedom are equivalent. Suppose that we chose $\beta = \omega$, so that $\mathfrak{c}(K) = \omega$. In this case, Eq. 3.15 states that, for a 1 dimensional ICR of type A, the effect of K is to phase the basis vector by ω:

$$K\psi = \omega\psi \tag{3.25}$$

If we now redefine K such that the operation itself phases the basis vector by $-\omega$ then the action of this new operation, K', will leave the basis vector unchanged. Hence, the representation of K' must be: $\mathfrak{c}(K') = 1$. As inversion symmetry can have an

important influence upon a systems properties (chapter 4), we usually ignore the free phase in K and consider, instead, the phase to reside within β. This free phase is important: it makes it impossible to uniquely define "co-basis vectors".

3.7. The effect of anti-linear symmetry upon a system's basis vectors

It has been suggested that anti-linear symmetry operations redefine a system's basis vectors and a significant body of work has discussed the use of basis vectors derived from co-representations (e.g. Kovalev 1980, 1983). In this section we use simple considerations to show that such an approach is largely misguided.

The definition of ICR matrices given in Eq. 3.21 makes it clear that, in general, ICRs do *not* form a representation of $\mathbb{G} \oplus K\mathbb{G}$, and so the projection or reduction operators can not be applied. Indeed the orthogonality properties of ICRs are quite distinct from those of simple IRs (Dimmock, 1963), and any attempts to derive general operators for ICRs (e.g. Kotzev, 1980) are "untenable" (Dimmock, 1963). When the ICR matrices are all completely real then they become representations once more, and in this case the projection operator can be used in the usual way. However, we shall see that this does not alter the system's basis vectors, except in the case of type A co-representations.

Type A ICRs are constructed from two equivalent IRs, one from each of $\mathbb{G}_k$ and $\mathbb{G}_{-k}$. Projection from them generates "co-basis vectors", ζ^ν, which are the direct sum of two basis vectors projected from IRs:

$$\zeta^\nu = \psi^\nu_{\vec{k}} + \mathfrak{c}(KK^{-1})\beta K\psi^\nu_{-\vec{k}} \tag{3.26}$$

The coefficient $\mathfrak{c}(KK^{-1})\beta$ comes directly from the definition of type A ICRs (Eq. 3.22) and $K\psi$ will be some other basis vector of the system, but *not* a new basis vector. Recognizing that $\mathfrak{c}(KK^{-1}) = \mathfrak{c}(E) = 1$ and that for completely real ICRs

$\beta = \pm 1$, it is possible to form the combinations $\zeta^{\nu}_{pm} = \psi^{\nu}_{\vec{k}} \pm K\psi^{\nu}{}_{-\vec{k}}$. This is analogous to the mixing of wave functions during bonding interactions.

It is important to note that, under the arguments of 3.6.3 these linear combinations are not unique. If we do not restrict the ICRs to being completely real, then there is a free phase factor between the cojoined basis vectors. Under the standing wave construction (section 3.5) this corresponds to a free amplitude, decoupling the magnitude of $\psi^{\nu}_{\vec{k}}$ and $\psi^{\nu}{}_{-\vec{k}}$. Hence, we cannot determine *a priori* the exact form of A-type co-basis vectors.

ICRs of type B and C bring four IRs into degeneracy: two IRs of $\mathbb{G}_k$ and two IRs of $\mathbb{G}_{-k}$. If we consider the form of the ICR matrices (Eq. 3.23 and 3.24) then it becomes clear that:

(1) For linear operators, the top-right and bottom-left quadrants are null.
(2) For anti-linear operators, the top-left and bottom-right quadrants are null.

Hence, depending upon which column of the matrices used, the matrix element for every element in either $\mathbb{G}$ or $K\mathbb{G}$ will be 0. During projection, half of the symmetry operations contribute nothing to the form of the "co basis vectors":

$$\begin{aligned} \zeta^{\nu} &= \psi^{\nu}_{k} + 0 \\ \zeta^{\nu} &= 0 + \psi^{\nu}_{-k} \end{aligned} \tag{3.27}$$

This implies that, under type B and C ICRs, anti-linear symmetry brings basis vectors of a system into degeneracy without changing their form

In conclusion, co-representations bring into degeneracy several basis sets of $\vec{k}$ and $-\vec{k}$. While this allows us to form linear combinations that are completely real, the form of a systems basis vectors are usually unchanged. Further, even in the case of completely type A ICRs, for which we can project new basis vectors, their form is not uniquely defined. To summarize these results, we present a simplified example.

Example:

Consider a simple system with symmetry $\mathbb{G} = \{E, C_{2x}, I, \sigma_{yz}\} \otimes \mathbb{T}$, ordering under $\vec{k} = (\frac{1}{3}, 0, 0)$. For this group, $\mathbb{G}_k = \{E, C_{2x}\}$ and has IRs:

	E	C_2
Γ_1	1	1
Γ_2	1	-1

(3.28)

Now consider the point $(0.25, 0.25, 0)$, which splits into two orbits under $\mathbb{G}_k$: $(0.25, 0.25, 0)$ and $(0.25, -0.25, 0)$; $(-0.25, -0.25, 0)$ and $(-0.25, 0.25, 0)$. These four positions will be denoted A_0, A_1, A_2 and A_3 respectively. If we wish to represent a polar vector property, then the basis vectors for this system are very simple: for each, the property vectors upon the two related positions are either parallel or anti-parallel. One such basis vector from each orbit is given, projected from a trial parallel to the a-axis.

$$\begin{aligned} \psi^2_{11}(A_0(\vec{x})) &= A_0(\vec{x}) + A_1(-\vec{x}) \\ \psi^2_{11}(A_2(\vec{x})) &= A_2(\vec{x}) + A_3(-\vec{x}) \end{aligned} \tag{3.29}$$

In this notation, the basis vector $\psi^\nu_{ij}(\phi)$ was projected from the ij^{th} elements of Γ_ν using the trial function ϕ. It consists of a series of property vectors $\vec{v}$ upon the positions A_n, denoted $A_n(\vec{v})$.

Rather than use the correct ICRs for this system, let's consider the possible scenarios. In this example, completely real type A ICRs would have the form:

	E	$C_{2\vec{x}}$	I	σ_{yz}
Γ_{1+1}	1	1	1	1
Γ_{1-1}	1	1	-1	-1
Γ_{2+2}	1	-1	1	-1
Γ_{2-2}	1	-1	-1	1

(3.30)

Projection from Γ_{2+2} and Γ_{2-2} generates basis vectors which are clearly linear combinations of those presented in Eq. 3.29.

$$\begin{aligned}\psi_{11}^{2-2}(A_0(\vec{x})) &= A_0(\vec{x}) + A_1(-\vec{x}) + A_2(\vec{x}) + A_3(-\vec{x}) \\ &= \psi_{11}^{2}(\vec{x}) + \psi_{11}^{2}(\vec{x}) \\ \psi_{11}^{2+2}(A_0(\vec{x})) &= A_0(\vec{x}) + A_1(-\vec{x}) + A_2(-\vec{x}) + A_3(\vec{x}) \\ &= \psi_{11}^{2}(\vec{x}) - \psi_{11}^{2}(\vec{x})\end{aligned} \tag{3.31}$$

Now let us consider the case of completely real type B ICRs, which would have the form:

	E	$C_{2\vec{x}}$	I	σ_{yz}
Γ_{1B}	$\begin{pmatrix} 1 & 0 \\ 0 & 1 \end{pmatrix}$	$\begin{pmatrix} -1 & 0 \\ 0 & -1 \end{pmatrix}$	$\begin{pmatrix} 0 & 1 \\ 1 & 0 \end{pmatrix}$	$\begin{pmatrix} 0 & -1 \\ -1 & 0 \end{pmatrix}$

(3.32)

Projection from Γ_{1B} generates the following basis vectors, identical to those in Eq. 3.29:

$$\begin{aligned}\psi_{11}^{1B}(A_0(\vec{x})) &= A_0(\vec{x}) + A_1(-\vec{x}) + 0 + 0 = \psi_{11}^{2}(A_0(\vec{x})) \\ \psi_{21}^{1B}(A_0(\vec{x})) &= A_2(\vec{x}) + A_3(-\vec{x}) + 0 + 0 = \psi_{11}^{2}(A_2(\vec{x}))\end{aligned} \tag{3.33}$$

These results, concerning the form of "co-basis vectors", are observed in calculations upon real systems (e.g. Samokhin, 2002; Schweizer, 2005).

3.8. Qualitative analysis of phase transitions using irreducible representations

While completely real basis vectors are required for any quantitative analysis, a great deal can be determined from qualitative arguments based upon the irreducible representations of a system. In particular, when we know the symmetry of the parent phase and the daughter phase, the IR symmetries that could bring about that phase transition can be deduced. These ideas have been used both explicitly and implicitly in previous work (e.g. Birman, 1966; Aroyo 1998).

The simplest approach is to start by solving a very similar problem; predicting the possible symmetries of the daughter phase using the irreducible representations of the parent phase.

The behaviour of a basis-vector under the symmetry operations is well defined Eq. 3.15:

$$g\psi_l^\nu = \sum_m \mathfrak{d}_{ml}(g)\psi_m^\nu$$

Under the symmetry operation g, the basis vector is transformed into a linear combination of the members of its basis set; the coefficients are defined by a single column of the irreducible matrix representation of g. The only symmetry operations of the little group $\mathbb{G}_k$ preserved by a distortion with the symmetry of a single IR are those that leave the distortion unchanged: i.e. those for which:

$$g\psi_l^\nu = \sum_m \mathfrak{d}_{ml}(g)\psi_m^\nu = \psi_l^\nu, \qquad l = 1, 2, \ldots, d^\nu \tag{3.34}$$

And it follows that:

$$\mathfrak{d}_{ml}(g) = \delta_{ml} \tag{3.35}$$

We conclude that the irreducible matrix representation of any preserved symmetry operation must be the identity matrix.

When the symmetry of the parent and daughter phase is known the above argument can be reversed; for a well defined group-subgroup relationship the system can only order under IRs in which every symmetry operation of the daughter-phase is represented by the identity matrix. Thus, we have a powerful tool for determining which irreducible representations can drive a phase-transitions between two known symmetries.

3.9. Conclusions

In this chapter we have shown the intimate relationship between a system's Hamiltonian and the irreducible representations of its symmetry group. Basis vectors have the symmetry of eigensubspaces and they represent families of Bloch waves with which it is possible to define a property showing a long-range order, characterized by a wave-vector $\vec{k}$. Further, by exploiting the anti-linear symmetry of a system, we have arrived at a method for constructing completely real modes from complex basis vectors that have the correct symmetry properties; this symmetry of a system is often over-looked and widely misunderstood.

Our discussion of irreducible co-representations has shown that, apart from the case of ICRs of type A, anti-linear symmetry does not alter a system's symmetry modes. Further, the "co-basis vectors" of type A ICRs are not uniquely defined because of the free-phase of β. Indeed, rather than new basis vectors, co-representational analysis defines new degeneracies: all types of ICR bring distinct energy subspaces of $\vec{k}$ and $-\vec{k}$ into coincidence.

Finally, we have developed qualitative arguments for defining phase-transitions using the irreducible representations of the parent phase. Understanding the symmetry information encoded in IRs allows us to predict either the symmetry of the daughter phase, or the distortion relating two phases. The qualitative arguments of sections 3.4 and 3.8 are used in the next chapter to gain considerable insight into magnetic and structural phase transitions in an important class of materials, magneto-electrics. More generally, an understanding of the symmetry of IRs will underline almost all of the work in this thesis.

References

[1] Aroyo, M. I. and J. M. Perez-Mato (1998). *Acta. Crys. A*, **54**, 19.

[2] Bertaut, E. F. (1968). *Acta Cryst.*, **A24**, 217.

[3] Bertaut, E. F. (1971). *J. Phys. Colloq. C*, **1** (32) 462-470.

[4] Bertaut, E. F. (1981). *J. Mag. Mag. Materials*, **24**, 267.

[5] Birman, J. L. (1966). *Phys. Rev. Lett.*, **17**, 1216.

[6] Bloch, F. (1928). *Zeit. f ur Physik*, **52**, 555-600.

[7] Bargmann, V. (1964). *J. Math. Phys.***5**, 862.

[8] Chayut, M. (2001). *J. Foundations of Chemistry*, **3**, 55.

[9] Dimmock, J. O. (1963). *J. Math. Phys.*, **4**, 1307.

[10] Hamermesh, M. (1964) *Group Theory and its Application to Physical Problems*, **Addison-Wesley Publishing Company**.

[11] Harris, A. B., Kenzelmann, M. (2008a) *Phys. Rev. Lett.* **100**, 089701 (2008).

[12] Harris, A. B., *et. al.* (2008b) *arXiv.org*, arXiv:0803.0945v1

[13] Jinxiu, L. (2006). *Frontiers of Mathematics in China*, **1**, 582.

[14] Kenzelmann, M. *et. al.* (2005). *Phys. Rev. Lett.*, **95**, 087206.

[15] Kunn, T. S. (1965). *Archives for the History of Quantum Physics*, (Philadelphia, PA).

[16] Kotzev, J. N., and Aroyo, M. I. (1980). *J. Phys. A*, **13**, 2275.

[17] Kovalev, O. V (1980). *Sov. J. Low Temp Phys.*, **6**, 44.

[18] Kovalev, O. V (1983). *Ukr. Phys. J.*, **28**, 1103.

[19] Lajos, M. (1998). *http://arxiv.org/abs/math/980803.*

[20] Landau, L.D., Lifshits, E.M. (1960). *Electrodynamics of Continuous Media*, **Pergamon Press**, Oxford.

[21] Pfister, O. (2003) *http://www.math.virginia.edu/Institute/MathSeminar2003_04_23.pdf.*

[22] Primas, H. and Esfeld, M. (1997). *http://philsci-archive.pitt.edu/archive/00001574/01/ReviewOfWigner%27sWork.pdf.*

[23] Radaelli, P. G. and Chapon, L. C. (2007) *Phys Rev B* **76**, 054428.

[24] Samokhin, K. V. (2002). *Phys, Rev. B*, **66**, 212509.

[25] Schweizer, J. (2005). *Comptes Rendus Physique*, **6**, 375.

[26] Schweizer, J., Villain, J. and Harris, A.B. (2007). *Phys. J. Appl. Phys.*, **38**, 41.

[27] Simona, R. *et. al.* (2008). *Phys. Lett. A*, **372**, 6847.

[28] Stewart, J. R. *et. al.* (2007). *J. Phys.: Con. Mat*, **19**, 145291.

[29] Voigt, E (1995). *Physics Today*, **December**, 40.

[30] Wigner, E. P. (1927). *Zeit. f ur Physik*, **43**, 624.

[31] Wigner, E. P. (1959) *Group Theory and its application to the quantum mechanics of atomic spectra*, **Academic Press Inc.**

[32] Wills, A. S. (2001). *Phys, Rev. B*, **63**, 064430.

[33] Wills, A. S. (2009). *Private communications*

CHAPTER 4

The role of phase dislocation in symmetry breaking

"I'm just going through a phase right now. Everybody goes through phases and all, don't they?"

J. D. Salinger

4.1. Introduction

Before turning our attention to quantitative methods of analysis in chapters 5, 6 and 7, it is worth pausing to discuss some important results that can be derived from purely qualitative symmetry arguments of the type used in sections 3.4 and 3.8. Ferroelectric systems are a classic example in which interesting new physical properties arise from a displacive phase transition. This chapter explores how "phase displacements" can give rise to ferroelectricity in multi-ferroic materials, and their interpretation in the representation theory formalism.

4.2. Ferroelectricity and centro-symmetry

Ferroelectric materials have a spontaneous electric polarisation and are of considerable technological interest in areas such as data storage (e.g. Spaldin 2005; Kanareykin, 2006). Their electric polarization often arises from a coherent displacement of ions within the structure, during a displacive phase transition. It is simple to show, using

symmetry considerations, that a ferroelectric material must lack inversion symmetry. The presence of inversion symmetry would require every displacement associated with a local electric dipole to have a matching displacement generating an opposed dipole (Fig. 4.1); the sum polarisation of such displacements would be nil. Therefore, the absence of centro-symmetry is a necessary, but not sufficient, condition upon the emergence of spontaneous electric polarisation (Harris, 2008a)[1]. As a result, the emergence of a ferroelectric phases is often characterized by a transition in which centro-symmetry is lost.

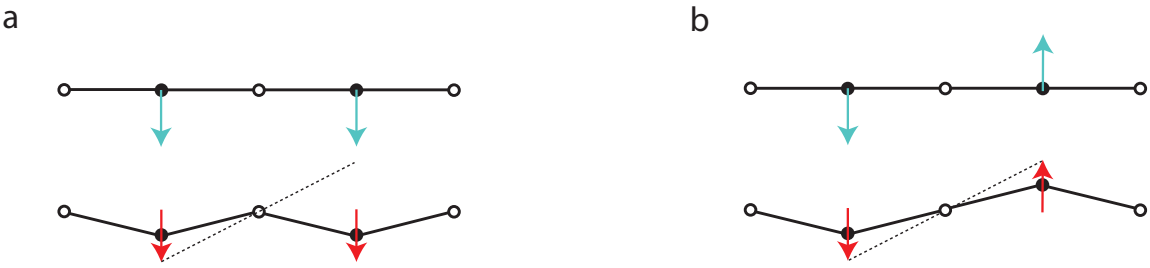

FIGURE 4.1. A simple model of two distortions (blue arrows): in (a) centro-symmetry about the white circles is destroyed; in (b) the distortion preserves centro-symmetry. Retention of centro-symmetry ensures that the electric dipoles (red arrows), at positions related by inversion, sum to zero.

4.2.1. Multi-ferroic materials, and the magneto-electric effect

Ferroelectric materials that are simultaneously magnetically ordered are one class of multi-ferroics: materials that show two or more simultaneous ferroic phenomena (ferroelectricity, ferroeleasticity, ferromagnetism). The coupling of internal magnetic and electric fields in such materials is termed the magneto-electric effect and has generated significant interest, as the ability to manipulate a material's magnetic field using an external electric field (and vice-versa) has potential application in technological areas such as data storage (e.g. Sakai, 2007; Vopsaroiu, 2007). Such materials are extremely rare, and their magneto-electric coupling is often weak (Khomskii, 2001).

[1]Other symmetry elements can forbid polarization to occur along certain directions

A new generation of materials, in which the centro-symmetry of the system is broken by magnetic ordering, with strong magneto-electric coupling has spurred the most recent work in this field. Systems such as $TbMnO_3$ (Kajimoto, 2004; Kenzelmann, 2005; Duque, 2006; Yamasaki, 2007) and $MnWO_4$ (Lautenschl ager, 1993; Heyer, 2006), are notable for their large magneto-electric coupling and complex, frustrated magnetic ordering (Kimura, 2003, 2006a; Hur, 2004; Eerenstein, 2006; Cheong, 2007).

For these "new" multi-ferroics the electric polarisation is intimately related to the symmetry of the magnetic ordering, emerging at magnetic phase transitions which are symmetry lowering. The distribution of magnetic moments throughout these materials can be described using spin-density waves (SDW), so-called because magnetism arises from the spin of unpaired electrons. One simple model for a spin-density wave is a plane wave of the form:

$$\psi = Ae^{2\pi(-k.\tau+\phi)} \tag{4.1}$$

In this description ϕ is an arbitrary phase-factor that defines the plane wave at the 0^{th} atom. A review of more detailed models of the magneto-electric effect, in the next section, shows that ϕ appears to have a central role to the emergence of ferro-electricity in these new multi-ferroic materials. The importance of this term has previously been touched upon by Chapon (2006, and Betouras (2007) who have shown that phase displacements can give rise ferroelectricity in two specific cases: a single commensurate SDW; and two incommensurate SDWs.

In this chapter we use symmetry arguments to explore the general role of phase displacements in symmetry-breaking, including systems that order under one or several commensurate or incommensurate spin density waves. We consider how these arguments can be interpreted when using representation theory to define the magnetic ordering of a system with basis vectors and derive simple rule for determining whether centro-symmetry is lost during phase transitions. Further, we use our model

of phase displacements to explain the relationship between the elipticity of magnetic spirals and electric polarisation observed in $TbMnO_3$.

4.3. Quantitative models of the ferroelectric effect

There exist several quantitative models of the magneto-electric effect in the literature. Kimura (2006b) broadly separates these into two exchange mechanisms: parallel spins are able to interact via super-exchange (SE) (Goodenough, 1963); while perpendicular spin components experience Dzyaloshinsky-Moriya (DM) interactions (Dzyaloshinsky, 1958; Moriya, 1960). These models vary in their detail, but share a common motif: in each, a phase displacement, ϕ, is key.

The works of Chapon (2006), Mostovoy (2006) and Betouras (2007) exemplify current models of the SE interaction and resulting electric polarisation. The quantitative elements of these works are summarized by the three equations:

$$\bar{P} = \gamma\chi_e M_1 M_2 [\vec{Q} \times [\vec{a}_1 \times \vec{a}_2]] \sin\phi \tag{4.2}$$

$$P^{ICM} = 4C\vec{S_3}.\vec{S_4}\cos(2\pi\left(\frac{1}{4}+\delta_z\right)z')\cos(2\pi\delta_x(1-x)).\cos(\epsilon)\sin\phi \tag{4.3}$$

$$p_0 = \frac{-\gamma q_m M_0^2}{2}\frac{e_1}{2e_0^2 - e^2}\sin(2\phi) \tag{4.4}$$

In each, the terms M_n are amplitudes of the magnetic components, $\vec{S}_n$ are spins on the n^{th} atom, and the other terms are constants. The term $\sin(n\phi)$ appears in all of these equations and corresponds to some form of phase displacement: in Eq. 4.4 the dislocation is between the SDW and the lattice; in the Eqs. 4.2 & 4.3 it defines a dislocation between two independent SDWs. Phase dislocation defines the presence, or absence, and magnitude of ferroelectric polarisation in these models

Alternate to super-exchange, spins can interact via the Dzyaloshinsky-Moriya mechanism. For a quantitative model of DM exchange we refer to the one-hole (Eq. 4.5) and two-hole (Eq. 4.6) models of Katsura (2005), and have expanded the vector product term:

$$\vec{P} \approxeq -\frac{eV}{3\Delta} I \frac{\vec{e}_{12} \times \hat{r} |\vec{e}_1||\vec{e}_2| \sin\theta_{12}}{|\cos\frac{\phi_{12}}{2}|} \tag{4.5}$$

$$\vec{P} \approxeq -\frac{4e}{9} \left(\frac{V}{\Delta}\right)^3 I \vec{e}_{12} \times \hat{r} |\vec{e}_1||\vec{e}_2| \sin\phi_{12} \tag{4.6}$$

$$\hat{r} \perp \hat{e}_1, \hat{e}_2$$

These models are derived from a quantum mechanical treatment of the Hamiltonian, and their physical interpretation is a "reverse" DM interaction in which magnetic exchange causes displacement of the atom mediating magnetic exchange. Again, a term involving ϕ is central to the emergence of net electric polarisation.

4.4. Phase dislocations of the spin-density wave

A function of ϕ appears ubiquitous in all of the quantitative models of the magnetoelectric effect. In this section, we develop simple qualitative symmetry arguments as to why this should be the case and what ϕ corresponds to. Symmetry analysis of phase dislocation will allow us to explain some interesting features in existing $TbMnO_3$ data, and develop a "selection" rule for the emergence of net electric polarisation.

Net polarisation arises from a uniform distortion of the crystal and so can be expected to arise from an homogenous interaction between spins. For DM type interactions the constant angular differential between interacting spins gives rise to a homogenous interaction along the chain. The spatially invariant term in SE interactions is less obvious. Simple spin-spin interaction has the form $(\vec{S}_i \cdot \vec{S}_j)$, where each of the spins is described by a spin-density wave of the form $\sin(k.\tau)$. For two colinear spins, with

a phase displacement ϕ, this expression separates into two terms:

$$\begin{aligned}\vec{S}_i \cdot \vec{S}_j &= \sin(k.\tau).\sin(k.\tau+\phi) \\ &= \cos\left(\frac{2k.\tau+\phi}{2}\right) - \cos\left(\frac{\phi}{2}\right)\end{aligned} \tag{4.7}$$

The second term in this expansion is a function of ϕ, but invariant with respect to any translation τ. Hence, it represents a spatially invariant interaction of the type from which ferroelectricity can arise. A physical interpretation of the SE and DM interactions are depicted in Figure 4.2.

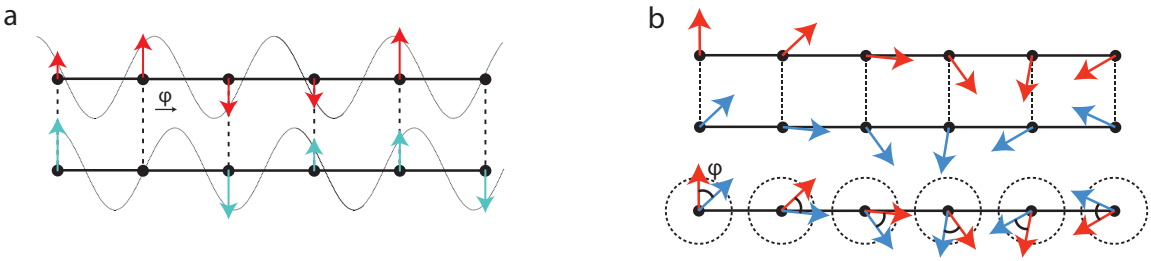

FIGURE 4.2. An illustration of phase-dislocation between interacting magnetic atoms. Each diagram depicts lines of magnetic atoms, interacting with their partner in the other line. (a) For colinear spins, phase displacement gives rise to interactions between spins of varying size and sign. (b) Phase separated spiralling spins are characterised by a constant angular differential, as depicted in the lower superposition (Davies, 2009).

For "new" multi-ferroics, it is magnetic order that destroys the centro-symmetry of the parent phase. In the quantitative expressions of section 4.3, this symmetry breaking is encapsulated by the term $\sin(n\phi)$; when $\sin(n\phi) = 0$ there is no net polarization. Hence, a phase-dislocation of the SDW is central to the symmetry breaking in magneto-ferroic materials. If we express the spin density wave as a plane-wave (Eq. 4.1), then ϕ represents the phase of the plane-wave at the 0^{th} atom. This can be interpreted as the displacement of the spin density wave's relative to the atomic lattice (Figure 4.3), breaking the symmetry of the system.

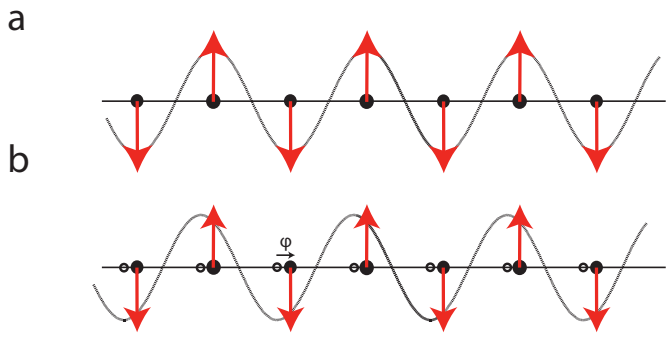

FIGURE 4.3. We can interpret a phase change of the SDW as a displacement of the wave relative to the lattice. The empty circles denote inversion centers of the spin density wave (axial-vector wave), which lie upon atomic positions in (a). In (b) a phase displacement of the wave has moved the symmetry centers away from the atomic positions.

4.4.1. Systems ordering a single spin-density wave

The symmetry of a multi-ferroic material is defined by the symmetry of the spin-density wave convoluted with the lattice; any symmetry operation must leave both wave and lattice invariant. The precise nature of this symmetry will depend, in part, upon ϕ; in particular, according to the equations of section 4.3, the system should be acentric except for special values of ϕ. For a system ordering under a single SDW, centro-symmetry of the system is preserved when both the wave and the lattice are simultaneously invariant under inversion about a single point. This occurs in two cases: when the components of the k-vector are all multiples of one-half, and the atoms lie upon inversion centers; or an inversion center of the lattice and the SDW are coincident.

The first condition arises from the symmetry of a sine function. When the k-vector consists of multiples of one half, then every lattice translation corresponds to a phase-factor of $n\pi$. In this case, the phase of the SDW at the 0^{th} atom is given by ϕ, and at every other position by $\phi + n\pi$, $n \in \mathbb{Z}$. Further, simple trigonometry reveals that:

$$\sin(\phi + \pi) = -\sin(\phi)$$

$$\therefore S_n = S_{-n} \qquad \forall\phi$$

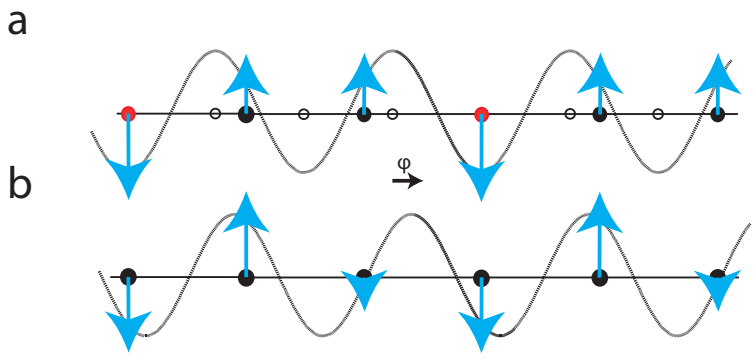

FIGURE 4.4. A line of magnetic atoms (black circles) whose moments (blue arrows) ordering under $\vec{k} = (\frac{1}{3}, 0, 0)$. In (a) the wave is related to the lattice in such a way that the system is centro-symmetric about the positions marked with red circles. In (b) this symmetry has been broken by the displacement of the wave relative to the lattice.

This shows that every position the SDW has a moment equal to $\pm$ the moment at the 0^{th} position for any value of ϕ. Hence, a phase dislocation cannot be distinguished from a change of the SDW's amplitude. The second condition simply restates that the SDW and lattice must share a common center of inversion, otherwise there is no inversion operation which leaves both the lattice and the SDW invariant.

When neither of these conditions are satisfied, the relative magnitudes of the SDW upon each atomic position varies with ϕ and the effect of a phase dislocation can be expressed by:

$$\sin(\theta + \phi) = \sin(\theta)\cos(\phi) + \cos(\theta)\sin(\theta) \tag{4.8}$$

For a general k-vector, the phase between two positions can take many values θ. Now, varying ϕ causes some moments to become larger, and others smaller, breaking centro-symmetry (Fig 4.4). Hence, phase displacements of the SDW form a simple mechanism for the emergence of spontaneous electric polarisation in systems ordering under a single, commensurate spin-density wave. This result was reached quantitatively by Betouras (2007).

4.4.2. Systems ordering under more than one spin-density wave

The arguments about a single, commensurate SDW can be extended to systems that order under an incommensurate SDW, or many SDWs of either type. The inversion centers of an incommensurate SDW are evenly distributed along lines passing through the inversion centers of the lattice. Hence, there will be at least one inversion center of the SDW that is, within experimental uncertainty, coincident with an inversion center of the lattice; an incommensurate spin density wave does not break inversion symmetry. When a system orders under several SDWs, then the inversion centers of all the SDWs must coincide with the inversion center of the lattice, and therefore with each other, hence ferroelectricity may arise when the waves are phase-displaced relative to each other (Chapon, 2006).

A special case of the symmetry breaking that can arises by phase separation of two SDWs is spiral ordering. The standard expression for a magnetic spiral is:

$$\vec{M} = M_1\vec{e}_1 \sin(\vec{k}.x) + M_2\vec{e}_2 \sin(\vec{k}.x) + M_3\vec{e}_3 \tag{4.9}$$

Where $\vec{e}_1$, $\vec{e}_2$, $\vec{e}_3$ are mutually orthogonal vectors and $\vec{k}$ is the propagation vector of magnetic order. This equation can be rewritten in a form that contains a phase dislocation between two perpendicular spin density waves:

$$M = M_1[(\vec{e}_1 + \vec{e}_2)\sin(\vec{k}.x) + (\vec{e}_1 - \vec{e}_2)\sin(\vec{k}.x + \phi)] + M_3 e_3 \tag{4.10}$$

The magnetisation M is defined as the sum of three components. Two are perpendicular sine waves, that are ϕ radians out of phase, and the third is a static term, present in magnetic cones. The effect of ϕ in Eq. 4.10 is demonstrated in Figure 4.5.

The phase term moderates the elipticity of the spiral, and its limiting values of $0 \mathrm{mod} \pi$ and $\frac{\pi}{2} \mathrm{mod} \pi$ gives rise to colinear ordering and circular spirals respectively[2].

[2]Here, "mod" refers to modular (or remainder) arithmetic. $a(\mathrm{mod}b)$ returns the remainder when a is divided by b

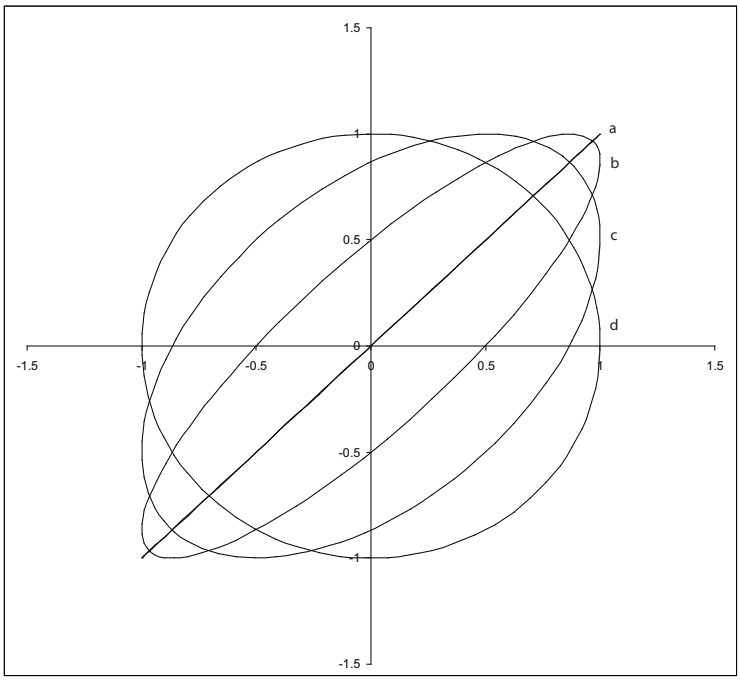

FIGURE 4.5. The eliptic curves defined by Eq. 4.10 for different values of ϕ: (a) $\phi = 0$; (b) $\phi = \frac{\pi}{6}$; (c) $\phi = \frac{\pi}{3}$; (d) $\phi = \frac{\pi}{2}$. In this example, the magnetization axes e_1, e_2 are parallel to the graph axes. The magnetic orbits evolve continuously with ϕ, which has the limiting values $0 \mathrm{mod} \pi$ and $\frac{\phi}{2} \mathrm{mod} \pi$. (Davies, 2009)

Ferroelectricity can arise from spiralling magnetic moments through DM-type interactions, appearing at the phase transition to spiral magnetic order. Such transitions are observed in the rare-earth manganates $RMnO_3$ (R=Tb, Dy) (Goto, 2004; Kimura, 2005; Cheong, 2007; Yamasaki, 2007) and $CoCrO_4$ (Yamasaki, 2006). This result is apparent from both Eqs. 4.5 and 4.6, and from the qualitative argument we have presented; colinear ordering implies that ϕ (and $\sin \phi$) are 0, and no polarisation is observed. In DM exchange, electric polarisation arises from the evolution of a phase difference between perpendicular SDWs.

We can use this qualitative model to make a simple prediction. The elipticity of the magnetic spiral (defined as the ratio of the shortest and longest diameters) is an almost linear function of ϕ (Figure 4.6). In the DM model polarization, is proportional

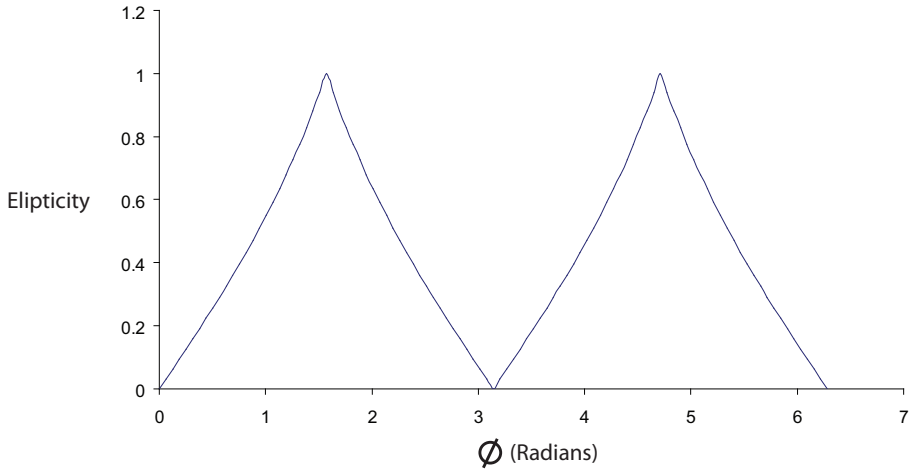

FIGURE 4.6. A plot of elipticity (vertical axis) against phase displacement ϕ, using the expressions in Eq. 4.10. We can see that the relationship is almost linear giving rise to a pseudo-proportionality between them.

to $\sin(\phi)$, therefore we can hypothesise that the polarization of such systems should be related to the elipticity of the magnetic spiral. This correlation between elipticity and electric polarization is clearly seen in the $TbMnO_3$ (Yamasaki (2007), Figure 4.7), supporting our hypothesis.

4.5. The meaning of phase in a basis-vector description

This chapter has discussed how phase dislocations of spin density waves can lower a symmetry's system. However, section 3.4 noted that the plane wave construction, used throughout this chapter, is not appropriate for basis vectors; precisely because their symmetry would change according to their phase. When using basis vectors to define the magnetic ordering of a system, phase displacements correspond to a lowering of symmetry. In the basis vector formalism this must arise from the presence of another basis vector of differing symmetry: a basis vector from another irreducible

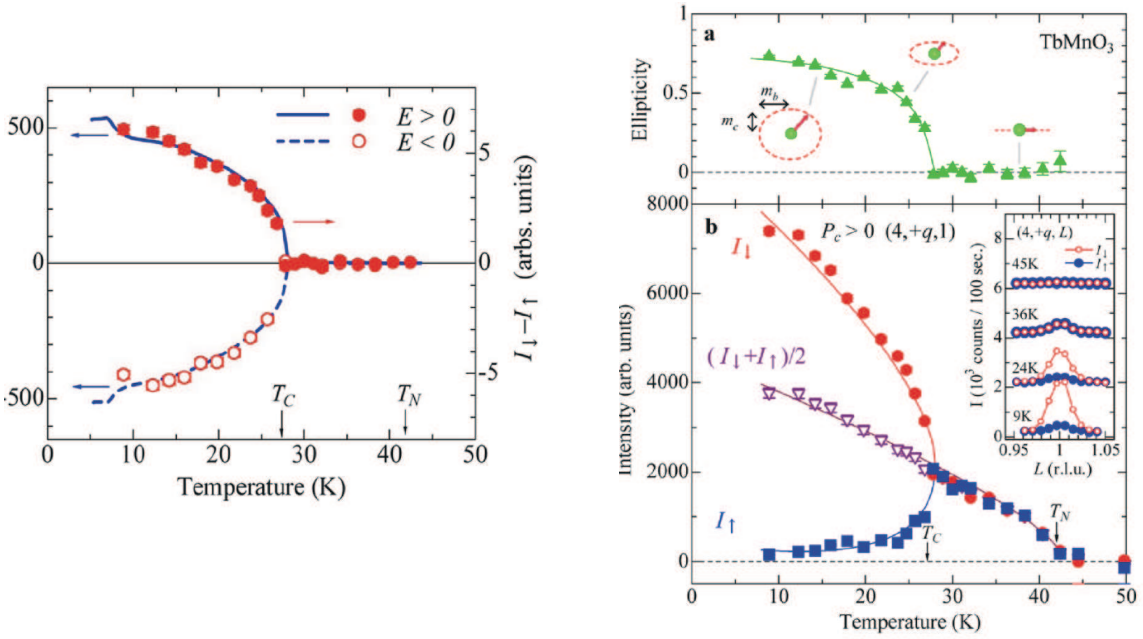

FIGURE 4.7. The plot in Figure 4.6 implies a pseudo-proportionality between spiral elipticity and ϕ, the phase displacement of two perpendicular spin density waves. As ϕ also determines the magnitude of electric polarisation in DM model of multiferroic materials, we predict a positive correlation between elipticity and ferroelectric polarisation. This prediction is supported by $TbMnO_3$ data collected (Yamasaki, 2007). On the left is a graph of polarisation against temperature, on the top right elipticity is plotted against temperature. The similarity is quite striking.

representation (or more strictly, ICR, section 3.6.1). Under representation theory, therefore, ϕ is interpreted as the perturbation of the magnetic order by a second irreducible representation.

$$\Phi = \psi^\nu + \delta\psi^\mu \tag{4.11}$$

Typically, materials which become ferroelectric at a magnetic phase transition do so in one of two ways. The first class undergo an incommensurate to commensurate magnetic transition, e.g. $HoMn_2O_5$ (Kimura, 2006c). Within our simple model, the emergence of ferroelectricity arises from the symmetry reduction when moving from an incommensurate to a displaced, commensurate SDW. In the second case, ferroelectricity appears at a colinear to spiral magnetic phase transition, such as in (Tb/Dy)MnO_3 (e.g. Goto, 2004; Kimura, 2005; Cheong, 2007; Yamasaki, 2007)

systems. Such materials are expected to obey DM-type interactions and symmetry breaking arises due to a second, phase dislocated, SDW.

In the language of representation theory these cases are equivalent. For both types of phase transition, ferroelectricity arises from the appearance of a second IR in the decomposition of the magnetic order[3]. The coefficient of the second irreducible representation determines the magnitude of the phase-dislocation, and hence the electric polarisation. This provides a qualitative explanation for the strong magneto-electric coupling in such materials; both the magnetic and electric polarization are determined by the magnitude of the "perturbation".

The importance of a second irreducible representation in the magnetic ordering has been derived quantitatively by Harris *et. al.* and is referred to as tri-linear coupling (Kenzelmann, 2005; Harris, 2008b). Under tri-linear coupling, net electric polarisation must arise from an interplay between two different irreducible representations, in exactly the manner described here through a purely qualitative approach.[4]

4.6. Symmetry breaking rules

The results of this chapter can be neatly summarized in a simple "selection rule" for multiferroic materials, to determine whether centro-symmetry is broken by the magnetic ordering. For these materials, I is in the parent phase transversal $\mathbb{G}_0$, and it must therefore either be in either $\mathbb{G}_k$ or form the anti-unitary generating element K. Following the arguments of section 3.8 it is simple to define a symmetry-rule for these transitions:

[3]There is also a change of k-vector in the incommensurate to commensurate transition, but unless $\vec{k}$ rests upon a symmetry point of the Brillouin zone this does not change $\mathbb{G}_k$. Hence it is considered to be equivalent except for the special case that $\vec{k}_{commensurate}$ lies on a high-symmetry point.
[4]Tri-linear coupling also explicitly includes the influence of the $-\vec{k}$ component of a basis-vector, discussed in sections 3.4 and 3.6.

> *Ferroelectricity can only arise when the inversion operator is not represented by an identity matrix in every irreducible (co)representation present in the magnetic ordering.*

For each IR identified as contributing to the magnetic ordering of a system, we should inspect the matrix representing the inversion operator and confirm that it is the identity matrix. If any one of them does not obey this restriction, the system can not be centro-symmetric. Further, as all the preceding arguments are entirely general, they are not restricted to systems ordering magnetically; they also hold for systems in which centro-symmetry is broken by charge ordering or other ordered phenomena.

4.7. Conclusions

In this chapter we have reviewed the role of symmetry breaking phase transitions in the emergence of ferroelectricity. From quantitative models in the literature we have extracted symmetry arguments that provide us with a simple and physically meaningful mechanism for symmetry breaking using the concept of phase dislocation. Consideration of phase factors allows the construction of simple models which explanation the emergence of ferroelectricity at incommensurate to commensurate and colinear to spiral magnetic phase transitions. These arguments have been distilled into a simple rule for determining if centro-symmetry is lost during at a phase transition. Of course, to apply this selection rule one must describe the phase transition using basis vectors and irreducible representations; in the following chapters we will develop the methods for reliably performing this analysis.

Our new approach to symmetry breaking in these materials also helps explain why their magneto-electric coupling is so strong: ferroelectricity arises from the presence of a second order parameter which determines both the magnetic structure and the

electric-polarization. It has also allowed us to explain the near proportionality of elipticity and polarization observed in $TbMnO_3$, and derive the symmetry elements of tri-linear coupling (Harris, 2008b) form purely qualitative arguments.

Much of the work presented in this chapter has been previously published in the proceedings of the Highly Frustrated Magnetism conference (Davies, 2009).

References

[1] Betouras, J. J., Giovanetti, G. and van der Brink, J. (2007). *Phys. Rev. Lett.* **98**, 257602.

[2] Chapon, L. C., *et al.* (2006). *Phys. Rev. Lett.* **96**, 097601.

[3] Cheong, S-W., and Mostovoy, M. (2007). *Nature Materials* **6**, 13.

[4] Davies, Z. L., Poole, A. and Wills, A. S. (2009). *J. Phys: Conference Series* **145**, 012072.

[5] Duque, J. S., *et al.* (2006). *Magnetics Conference, 2006.* **INTERMAG 2006**, 244.

[6] Dzyaloshinsky, I. (1958). *J. Phys. Chem. Solids* **4**, 241.

[7] Eerenstein, W., Mathur, N. D. and Scott, J. F. (2006). *Nature*, **442**, 759.

[8] Goodenough, J. B. (1963). *Magnetism and the Chemical Bond*, **John Wiley & Sons, New York**.

[9] Goto, T. *et al.* (2004). *Phys. Rev. Lett.*, **92**, 257201.

[10] Harris, A. B., *et al.* (2008a) *Physical Review* **B 78**, 014407.

[11] Harris, A. B., *et al.* (2008b) *arXiv.org*, arXiv:0803.0945v1

[12] Heyer, O. *et al.* (2006). *J. Phys. Condens. Matter*, **18** (39), L471.

[13] Hur, N. *et al.* (2004). *Nature*, **429**, 392.

[14] Kanareykin, A., *et al.* (2006). *AIP Conference Proceedings* **877**, 311.

[15] Iizumi, M., Axe, J. D. and Shirane, G. (1977). *Phys. Rev. B*, **15**, 4392.

[16] Kajimoto, R., *et al.* (2004). *Phys. Rev. B*, **70**, 012401.

[17] Katsura, H., Nagaosa, N. and Balatsky A. V. (2005). *Phys. Rev. Lett.* **95**, 057205.

[18] Khomskii, D. I. (2001). *Bull. Am. Phys. Soc.* **C**, 21.002.

[19] Kenzelmann, M. *et al.* (2005). *Phys. Rev. Lett.*, **95**, 087206.

[20] Kimura, T. *et al.* (2003). *Nature*, **426**, 55.

[21] Kimura, T. *et al.* (2005). *Phys. Rev. B*, **71**, 224425.

[22] Kimura T., Lashley, J. C., and Ramirez, A. P. (2006a). *Phys. Rev. B*, **73**, 220401.

[23] Kimura, T. (2006b). *JPSJ Online-News and Comments*

[24] Kimura, H. *et al.* (2006c). *http://arxiv.org/abs/cond-mat/0602226*

[25] Lautenschl ager, G. *et al.* (1993). *Phys. Rev. B*, **48**, 6087.

[26] Sakai, M. (2007). *Appl. Phys. Lett.*, **90**, 072903.

[27] Spaldin, N. A. and Fiebig, M. (2005). *Science*, **309** (July), 391.

[28] Stewart, J. R., Wills, A. S., Leavey, C. J., Rainford, B. D. and Ritter, C. (2007). *J. Phys.: Condens. Matter* **19**, 145291.

[29] Spaldin, N. A., and Fiebig, M. (2005) *Science* **309**, 15.

[30] Moriya, T. (1960). *Phys. Rev* **120**, 91.

[31] Mostovoy, M. (2006). *Phys. Rev. Lett.* **96**, 067601.

[32] Vopsaroiu, M. *et al* (2007). *J. Phys. D*, **40**, 5027.

[33] Wigner, E. P. (1959). *Group Theory and its application to the quantum mechanics of atomic spectra*, **Academic Press Inc., London**.

[34] Yamasaki, Y. *et al.*, *Phys. Rev. Lett.*, **96**, 207204.

[35] Yamasaki, Y. *et al* (2007). *Phys. Rev. Lett.* **98**, 147204.

CHAPTER 5

Irreducible representations: Validating the tables of Kovalev

The Captain... with a great effort, that made his face very red, pulled up the silver watch, which was so big, and so tight in his pocket, that it came out like a bung. "Walr," said the Captain, handing it over and shaking him heartily by the hand, "a parting gift, my lad. Put it back half an hour every morning, and about a quarter towards the afternoon, and its a watch thatll do you credit."

Charles Dickens, Dealings with the Firm of Dombey and Son, Ch. 19
Quoted in "Representations of the Crystallographic Space Groups"

5.1. Introduction

Having constructed a representation of some system, we can dissect it and construct a symmetric basis using the reduction and projection operators. To make use of this method we require access to a reliable source of irreducible representations, along with an appropriate set of trial functions. In this chapter we validate the tabulated source of irreducible representations collated by Kovalev (1993) for use with the crystallographic space groups and all little groups. We also confirm that the representations in these tables are unitary, and so can be used with the operators presented in section 2.12: the form in which the projection and reduction operators are most commonly encountered.

The International Tables for Crystallography, volume A (IT-A)(2002) form the most widely accepted definition of the crystallographic space groups. In contrast, there

is no such agreement over the representations of the space groups, and a number of alternate listings exist: Kovalev (1993), Miller and Love (1967), Bradley and Cracknell(1969), Zak (1969). This has lead to the use of conflicting notations, settings and vocabulary in the reporting of symmetry analysis work, causing unnecessary confusion and complication. The most widely used tables are those published by O.V. Kovalev in 1960, and since reprinted and translated into English. They are notable for their completeness, their independent validation and correction by the editors of the English translation, and because a digital form of the tables exists making them particularly convenient for use in computer programs.

A number of programmes have been developed based upon the tables of Kovalev, using the *unitary* form of the projection and reduction operators (Eq. 5.1), section 2.12): SARA*h* (Wills, 2000), MODY (Sikora, 2004), Isotropy (Stokes, 2002).

$$\begin{aligned} W_{ml}^{\mu*} &= \frac{d^{\mu}}{|\mathbb{G}|}\sum_{g_s}\mathfrak{d}_{lm}^{\mu*}(g_s)\mathfrak{T}(g_s) \\ \frac{1}{|\mathbb{G}|}\sum_{g_s\in\mathbb{G}}\chi^{\nu}(g_s)\chi^{\mu*}(g_s) &= \delta_{\mu,\nu} \end{aligned} \tag{5.1}$$

For all of these programs there exist example systems for which this method generates obviously wrong solutions (e.g non-integer coefficients for IRs in the reduction step); and the number of these systems has brought into question the validity of the tables of Kovalev. As the method of previous validations is undocumented (Stokes, 2007), it became necessary to validate independently the tables in order to better understand the problems encountered by these programs. In particular, we undertook the task of validating that the irreducible representations presented by Kovalev are unitary homomorphisms of the little groups they corresponded to. The use of incorrect IRs will, in general, produce basis vectors which do not have the desired symmetry properties and so the correctness of our IR tables is paramount.

5.2. Loaded irreducible representations

We have already encountered the irreducible representations (IRs) of a space group $\mathbb{G}$, and the small irreducible-representations (SIRs) of its little groups $\mathbb{G}_k$. In practice many little groups have SIRs which are identical except for a phase factor related to the translational component of each symmetry operation. Making use of this equivalence to reduce the size of his publication, Kovalev's lists only the Loaded IRs (LIRs), $\hat{\tau}_i$ of each group $\mathbb{G}_k$. The LIR, $\hat{\tau}_i$, of an operation $g_i = \{\alpha_i|h_i\}$ is related to its SIR, τ_i, in the following way:

$$\tau_i = \hat{\tau}_i.e^{-2\pi i\vec{k}.\vec{\alpha}_i} \tag{5.2}$$

The exponent is called the "load", and τ_i has the same meaning as $\mathfrak{d}(g_i)$ in the preceding chapters. In this chapter we will use Kovalev's notation (τ_i) to make any references to his work as clear as possible.

5.2.1. Composition of Loaded Irreducible Representations

Despite their name, LIRs are, in general, not a representation of the little group. However, they do have a law of composition derived from the homomorphism of SIRs. If τ_i is a representation of the operation $(\alpha_i|h_i)$ then:

$$\begin{aligned} \tau_i \times \tau_j &= \tau_{i\circ j} \\ \tau_{i\circ j} &= \{\alpha_i + h_i\alpha_j | h_i h_j\} \end{aligned} \tag{5.3}$$

Substituting this into Eq. 5.2:

$$\begin{aligned} \hat{\tau}_i.e^{-2\pi i\vec{k}.\vec{\alpha}_i} \times \hat{\tau}_j.e^{-2\pi i\vec{k}.\vec{\alpha}_j} &= \hat{\tau}_{i\circ j}.e^{-2\pi i\vec{k}.(\vec{\alpha}_i + h_i\times\vec{\alpha}_j)} \\ \hat{\tau}_i \times \hat{\tau}_j &= \hat{\tau}_{i\circ j}.e^{-2\pi i\vec{k}.(\vec{\alpha}_i + h_i\times\vec{\alpha}_j)}.e^{2\pi i\vec{k}.\vec{\alpha}_i}.e^{2\pi i\vec{k}.\vec{\alpha}_j} \\ &= \hat{\tau}_{i\circ j}.e^{-2\pi i\vec{k}.(\vec{\alpha}_i - \vec{\alpha}_j - \vec{\alpha}_i + h_i\times\vec{\alpha}_j)} \\ &= \hat{\tau}_{i\circ j}.e^{2\pi i\vec{k}.(\vec{\alpha}_j - h_i\times\vec{\alpha}_j)} \end{aligned} \tag{5.4}$$

The last line gives defines the "LIR-factor", $W = e^{2\pi i \vec{k}.(\vec{\alpha}_j - h_i \times \vec{\alpha}_j)}$, that is introduced by the non-homomorphism of LIRs. We make use of this relationship in validating the homomorphism of Kovalev's tables.

5.3. The KovCheck applet

Validation of the tables of Kovalev was performed upon the digital data set from SARA*h* (Wills, 2000)[1], using the custom utility "KovCheck" written in Visual Basic 6.0 (Microsoft, 1998). KovCheck has a simple GUI interface (Figure 5.1) in which the user can define a range of space groups to check, and some of the output details. The output is a text file that lists all of the calculations in which KovCheck determines that the LIR tables do not define an SIR which is a unitary homomorphism of the little group. There are also additional output options, such as a debugging mode which outputs details of every calculation regardless of the result.

The body of the KovCheck programme is a family of nested loops which loads the LIR matrices sequentially. The parent loop runs over a range of space groups and, for each space group, daughter-loops run over: the distinct k-vector types; all IRs for each k-vector; and all combinations of operators in $\mathbb{G}_k$. The code for KovChek is provided in the "Supporting materials" appendix, and a schematic overview of the programme is given in Figure 5.2. The following sections aim to give as much information as possible on the strategy employed, while keeping technical details of the code to a minimum.

[1] A small number corrections to these files were made when they were not consistent with the printed versions of the tables. These corrections have been incorporated into a new release of SARA*h*

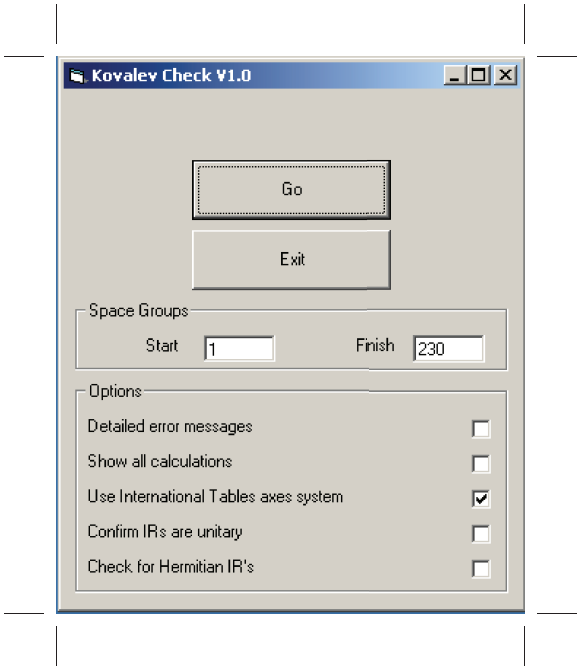

FIGURE 5.1. The Graphical User Interface for KovCheck. Users input a range of space groups to check, defined by the first and last space group fields. The checkboxes allow the user to toggle various output options such as the detail level on error reporting.

5.3.1. Validation of homomorphism

The strategy for validating homomorphism follows from the relationship derived in section 5.2.1. Two separate methods of generating the "LIR-factor", W, are compared to determine any inconsistencies between the tables and the law of composition (Eq. 5.4).

(1) The LIRs of two operators $g_i, g_j \in \mathbb{G}_k$ are multiplied to generate a product matrix, $\mathfrak{M}$. $\mathfrak{M}$ is expressed as the LIR of the product operator, g_{ioj}, multiplied by a coefficient: the "LIR-factor", W_1.

$$\hat{\tau}_i \times \hat{\tau}_j = \mathfrak{M} = W_1 \hat{\tau}_{product} \tag{5.5}$$

(2) The load is calculated according to Eq. 5.4.

$$W_2 = e^{2\pi i \vec{k}.(\vec{\alpha}_j - h_i \times \vec{\alpha}_j)} \tag{5.6}$$

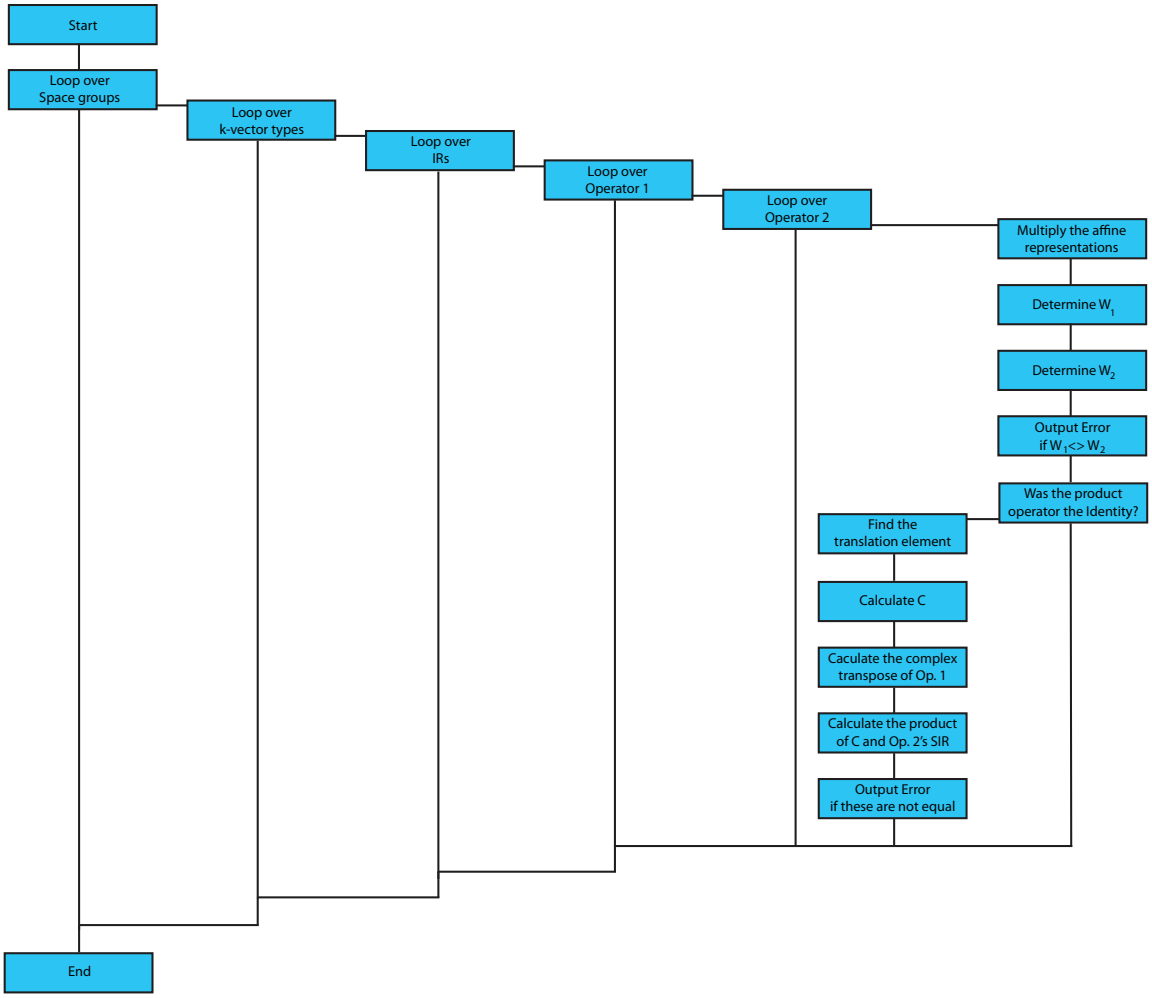

FIGURE 5.2. This flowchart depicts the various loops and steps in the KovCheck algorithm. The loops cycle over all combinations of space group, k-vector, irreducible representation and symmetry operators. In each loop the homomorphism and unitary nature of the SIR matrices is tested in the manner described in the text (section 5.3.1 and 5.3.2).

If, during a calculation, KovChek can not find a W_1 that satisfies Eq. 5.5, or if $W_1 \neq W_2$ then a homomorphism error code is printed to the output file along with details of the spacegroup, IR, and operators used

An example of the calculations performed is given below, with space groups $P2_12_12_1$. The operators are g_2 and g_4 (following Kovalev's notation) and $\vec{k}_{26} = (\frac{1}{2}, \frac{1}{2}, \frac{1}{2})$.

$$
\begin{aligned}
g_2 &: (\tfrac{1}{2}, \tfrac{1}{2}, 0|x, -y, -z) \\
g_4 &: (\tfrac{1}{2}, 0, \tfrac{1}{2}| - x, -y, z)
\end{aligned}
$$

$$
\begin{aligned}
\hat{\tau}_2 \times \hat{\tau}_4 &= \begin{pmatrix} i & 0 \\ 0 & -i \end{pmatrix} \begin{pmatrix} 0 & i \\ i & 0 \end{pmatrix} \\
&= \begin{pmatrix} 0 & -1 \\ 1 & 0 \end{pmatrix} \qquad\qquad \hat{\tau}_{2\circ 4} = \begin{pmatrix} 0 & 1 \\ -1 & 0 \end{pmatrix} \\
&= -1\hat{\tau}_{2\circ 4}
\end{aligned}
$$

$$
\begin{aligned}
e^{2\pi i\vec{k}.(\vec{\alpha}_4 - h_2 \times \vec{\alpha}_4)} &= e^{2\pi i(\frac{1}{2},\frac{1}{2},\frac{1}{2}).((\frac{1}{2},0,\frac{1}{2}) - h_2 \times (\frac{1}{2},0,-\frac{1}{2}))} \\
&= e^{2\pi i(\frac{1}{2},\frac{1}{2},\frac{1}{2}).((\frac{1}{2},0,\frac{1}{2}) - (\frac{1}{2},0,-\frac{1}{2}))} \\
&= e^{2\pi i(\frac{1}{2},\frac{1}{2},\frac{1}{2}).(0,0,1)} \\
&= e^{\pi i} \\
&= -1
\end{aligned}
$$

Hence, $W_1 = W_2 = -1$ and the LIR passes the homomorphism check in this example.

5.3.2. Confirmation of unitary SIR matrices

As with homomorphism, brute-force calculation was used to confirm that the tabulated LIRs correspond to unitary SIR matrices. For each symmetry element $g_1 \in \mathbb{G}_k$, KovCheck finds a symmetry element $g_2 \in \mathbb{G}_k$ such that $g_1 g_2$ is an identity-translation.

$$\mathfrak{T}(g_1) \times \mathfrak{T}(g_2) = \begin{vmatrix} 1 & 0 & 0 & T_x \\ 0 & 1 & 0 & T_y \\ 0 & 0 & 1 & T_z \\ 0 & 0 & 0 & 1 \end{vmatrix} \tag{5.7}$$

$$\mathfrak{d}(g_1)\mathfrak{d}(g_2) = C\mathfrak{d}(E)$$

$$\therefore \mathfrak{d}(g_2) = C\mathfrak{d}(g_1^{-1})$$

All translations are represented by $C\mathfrak{T}(E)$, where $C = e^{-2\pi\vec{k}.\vec{\alpha}}$, and their irreducible matrix representation is $C\mathfrak{d}(E)$.

$$C = \exp(2\pi\vec{k}. \begin{pmatrix} T_x \\ T_y \\ T_z \end{pmatrix}) \tag{5.8}$$

$$CC^* = 1$$

If the IR is unitary then the $C^*\mathfrak{d}(E)$ represents the inverse translation and, from the homomorphism of SIRs, combines with $\mathfrak{d}(g_2)$ to form $\mathfrak{d}(g_1^{-1})$. Further, for unitary representations, $\mathfrak{d}(g_1^{-1})$ is will be equal to the conjugate transpose $\mathfrak{d}^\dagger(g_1)$:

$$\begin{aligned} \therefore \mathfrak{d}(g_1^{-1}) &= C^*\mathfrak{d}(g_2) \\ &= \mathfrak{d}^\dagger(g_1) \\ \therefore \mathfrak{d}^\dagger(g_1) &= \mathfrak{d}(g_2) \times \exp\left(2\pi \times (k_x, k_y, k_y) \cdot \begin{pmatrix} T_x \\ T_y \\ T_z \end{pmatrix}\right) \end{aligned} \tag{5.9}$$

KovCheck tests the final equality explicitly, and outputs a unitary check error when it does not hold.

5.4. Results

The final version of KovCheck, and the input files, output no errors except for the few cases in which two equivalent forms of the same k-vector are included, but LIR tables have been tabulated for only one of them. This work shows that that the IRs presented in Kovalev's tables constitute unitary homomorphisms of the little groups $\mathbb{G}_k$ *under his definition of the space group operators*. This work therefore validates both the tables themselves and the use of projection and reduction techniques in computer codes based upon them.

5.5. Discussion

Kovalev's tabulated representations were verified as part of an effort to resolve problems in calculations based upon them. In doing so, we have found that (without exception) errors arise from how the calculations are performed and not the tables of Kovalev. The tables are entirely consistent *within those definitions laid out by Kovalev*; problems arise from user preference for the space group definitions laid out by the International Tables for Crystallography, A (IT-A) (2002). The transformation from these settings to Kovalev's alternative, but equally valid, definitions is not always performed correctly, causing the projection and reduction operators to fail.

The fundamental obstacle to moving correctly between the various axis systems is, in fact, a lack of clarity in Kovalev's tables as to which information is given in which setting. Thorough review of his work leads to the following conclusions:

- Kovalev's fundamental periods define his primitive lattice, and are listed in the Kovalev defined cubic/hexagonal axis system.
- The translational element of operators in the tri- and monoclinic space groups are defined in the Kovalev primitive axis systems; they are tabulated

as linear combinations of the fundamental reciprocal periods to indicate this. Operators for all other SGs are in the cubic/hexagonal axis system: these are tabulated as numbers.

- Where the Kovalev centred setting differs from the IT setting, Kovalev list transformations between them. However, when doing so, *Kovalev always refers to settings defined in the International tables for X-Ray Crystallography* (IT-X) (1952) rather than those in IT-A (2002).
- Due to differences in space groups definitions between in IT-X and IT-A, many of the current software programs available do not correctly transform co-ordinates and k-vectors from the IT-A settings to the Kovalev setting. An additional transformation from the IT-A setting to the IT-X setting is required *before* the transformations listed in Kovalev's work.
- The tables of Kovalev are, unsurprisingly, intolerant to redefinitions of the axes or the operators.

5.6. Conclusions

This work reinforces the earlier, indeterminate validation of Kovalev's tables; the LIR tables, combined with Kovalev's definition of the space group operators, proginate SIR matrices that are both unitary and homomorphic to the groups they represent. The validity of the tables, demonstrates that examples in which existing software fails to calculate the correct basis vectors usually arise from a failure to correctly transform the problem into Kovalev's setting. Used with care, Kovalev's tables form a complete and validated source of unitary irreducible representations for all the little groups of the crystallographic space groups.

Having sourced a complete and reliable set of irreducible representations, in the next chapter we discuss the other ingredient of basis-vector calculations: the selection of an appropriate set of trial functions. This will include a discussion of another

common problem in the calculation of basis vectors by software, projection of an incorrect number of solutions.

The validation of homomorphism has been previously published (Davies, 2008), while the check for unitary character has been submitted to a peer reviewed journal as part of a larger paper (Davies, 2009).

References

[1] Bradley, C. J. and Cracknell, A. P. (1972) *Mathematical Theory of Symmetry in Solids*, **Clarendon Press**.

[2] Davies, Z., Poole, A., and Wills, A. S. (2008). *J. Physics: Condensed Matter* **20**, 104232.

[3] Davies, Z. and Wills, A. S., (2009). *Submitted to: Acta Crystallographica A*.

[4] *International tables for crystallography. Vol. A. (5th edition.)* (2002). Ed. T. Hahn, **Springer**, Dordrecht.

[5] *International tables for X-Ray Crystallography, Vol. A* (1952). Ed. N. F. M Henry and K. Lonsdale, **Kynoch Press** (Birmigham, 1952).

[6] Izyumov, Yu. A. and Naish, V. E. (1921). *Neutron Diffraction of Magnetic Materials*, **Consultants Bureau**, New York and London.

[7] Kovalev, O. V. (1993). *Representations of the Crystallographic Space Groups: Irreducible representations, Induced representations and Corepresentations (2nd Ed)*, Ed. H. T. Stokes and D. M. Hatch, **Gordon and Breach Science Publishers** (London, 1993).

[8] Microsoft Visual Basic 6.0 for 32-bit Windows Development (1987-1998). *Microsoft Corp.*

[9] Miller, S.C. and Love, W. F. (1967) *Tables of Irreducible Representatatations and Co-Representations of Magnetic Space Groups* **Pruett Press**, Boulder.

[10] Sikora, W., Bialas, F. and Pytlik, L. (2004). *J. Apply. Cryst.*, **37**, 1015.

[11] Stokes, H. T. *Private communications* (2007).

[12] Stokes, H. T. and Hatch, D. M. (2002). *ISOTROPY*, stokes.byu.edu/isotropy.html (2002).

[13] Wills, A. S. (2000). *Physica B*, **276**, 680.

[14] Zak, J., Casher, A., Glück, M. and Gur, Y. (1969). *The irreducible Representations of Space Groups.* **New York**, Benjamin.

CHAPTER 6

Suitable trial functions for the method of projection operators

"Any man who can drive safely while kissing a pretty girl is simply not giving the kiss the attention it deserves."

Albert Einstein

6.1. Introduction

A reliable source of irreducible representations is just one of the ingredients required to generate the basis vectors of a system; the other is a *suitable* set of trial vectors. Prior to this work, the meaning of "suitable" has been left undefined and received little consideration. Indeed, the choice of trial functions is conspicuously absent in both textbooks and journal papers (e.g. Hamermesh, 1964; Bertaut 1962, 1981; Izyumov 1990,1991; Wills, 2005; Kenzelmann, 2006).

Explicit definition of what constitutes a suitable set of trial vectors is important because the calculation of basis vectors is arduous, making automation desirable, and any software applying the method of projection operators requires a defined set of trial functions. A number of such routines already exist (e.g MODY (Sikora, 2004), BASIREPS(Rodríguez-Carvajal, 2004), SARA*h*(Wills; 2000,2005))[1] and, for all of them, there exist a number of systems for which they derive an incorrect number of basis vectors. We will show that this can be resolved by a better choice of trial vectors.

[1]These are reviewed in section 7.3, along with other software.

Further, the selection of trial functions has implications beyond solving problems during calculation. The general method of representation theory, and in particular the projection of basis vectors, does not make allowance for the influce of an atoms local environment. One way we might better represent the role of local symmetry, and in particular covalent bonds, is through the choice of trial functions.

In this chapter, we present an example where the "standard" trial functions cause difficulties during computation of the basis vectors and derive a method for calculating "symmetry adapted trial functions". In particular, an *algorithm* for generating suitable trial functions is derived, allowing us to reliably automate the calculation of basis vectors using software. We also discuss how selection of trial functions can help represent the local anisotropy of an atom.

6.2. Properties of basis sets

Before considering some difficulties that may occur when using the method of projection operators, it is useful to remind ourselves about the properties of basis vectors. A *basis set*, $\{\psi_1^\nu, \psi_2^\nu, \ldots, \psi_{d^\nu}^\nu\}$, is defined by the relationship:

$$g\psi_l^\nu = \sum_{m=1}^{d^\nu} \mathfrak{d}_{ml}^\nu(g)\psi_m^\nu, \qquad \forall g \in \mathbb{G}_k \tag{6.1}$$

$\mathbb{G}_k$ is the little group of a system ordering under $\vec{k}$, $\mathfrak{d}^\nu(g)$ is the matrix representation of g in the irreducible representation Γ_ν, and d^ν is the order of Γ_ν.

Basis vectors are representations of a system's eigensubspaces, and Eq. 6.1 shows that each basis set must have the same order as the irreducible representation it is projected from. It is central to the correct application of representation theory that the set of all basis vectors is a *set of basis sets*, and that each basis set has the correct order. If this not the case, then the basis chosen can not have the correct symmetry properties.

6.3. Over-generation

Reduction of a system's representation to a linear combination of irreducible representations defines exactly the number of basis vectors we need to derive from each IR. When the method of projection operators defines more BVs than required, then the basis has been over-generated and some of the calculated BVs are linearly related[2]. The problem is, therefore, to reduce the set of solutions to one of the correct size while preserving all the desired symmetry properties.

The first step is to determine which basis vectors are equivalent. When the solutions occur in pairs, related by a complex coefficient $\psi_0 = l\psi_1$, the equivalence relationships are simple to determine. If three or more BVs are linearly related, then the relationship must be derived by the solution of simultaneous equations (with complex coefficients). However, determination of equivalencies is not sufficient to determine which of the basis vectors should can be discarded. An arbitrary elimination of equivalent solutions will not, in general, result in a set of basis sets.

When over-generation occurs, there are two problems to resolve. The first is how to identify complex linear relations of the type $\psi_0 = \sum_i^n l_i \psi i$ when $n > 1$; when $n = 0, 1$ equivalencies are quick and simple to determine.. Having determined which basis vectors are equivalent, we then require a elimination procedure that ensures only complete basis sets remain. Further, any solution should be simple to implement within a computational routine.

Rather than inspecting the projected basis vectors, we might instead consider the trial functions used to generate them. The projection operators derives a set of solutions of order d^ν or 0 for any trial vector[3]. As the size of each trial's image is fixed, over-generation must arise from *equivalent trial functions*. If, through judicious

[2]There is always some *linear* relationship. Any correct basis spans the entire eigensubspace; as such any other vector can be expressed as some linear combination of this basis.
[3]Varying over all i, with a fixed IR ν and column index j. See the end of section 6.5

choice of trial vectors, we can reduce all BV equivalencies to a relationship of the form $\psi_1 = l\psi_2$, then it becomes simple to determine which trial vectors generate equivalent solutions, and to eliminate all but one of them. Removing trial vectors, rather than basis vectors, ensures that a set of basis-sets is generated.

6.3.1. Symmetry Adapted Trial vectors

The trial vectors used within MODY, BASIREPS, SARA*h* and the majority of previous work are unit vectors that lie parallel to the crystallographic axis system. We will term these the "standard" trial functions, and they lead to over-generation in a significant number of systems. Our goal is to determine a method for constructing alternate trial functions, having the property that every basis vector projected from them is linearly related to exactly one or less of the other projected basis vectors. Such a set of trial vectors would make it trivial to identify any equivalent basis vectors, and hence eliminate equivalent trial vectors.

When two BVs are linearly related, then the property at each atomic position they describe has that same linear relationship. Thus, by controlling how the property at a single point is generated, we can control the relationships between basis vectors. Under the method of projection operators, the property at a single point is generated by the sum action of all the operators which generate that point from an initial position A_0; if we consider A_0 itself then these operators are the "stabilizers" of A_0, denoted $\mathbb{S}_0$.

$$s : A_0 \longmapsto A_0 + t \qquad t \in \mathbb{T}, \forall s \in \mathbb{S}_0$$

$$\begin{pmatrix} a_0 \\ b_0 \\ c_0 \end{pmatrix} A_0 = \frac{d^\mu}{|\mathbb{G}|} \sum_{g_i \in \mathbb{S}_0} \mathfrak{d}^\mu_{ml}(g_i^{-1}) \mathfrak{T}(g_i) \phi_i^\nu \tag{6.2}$$

The property at atom A_0 is defined, relative to the crystallographic axes, by the vector (a_0, b_0, c_0). It is is constructed by the action of the projection operator over the elements of $\mathbb{S}_0$, which map A_0 to itself or a position related by a lattice translation. As noted in section 2.13, Izyumov (1990) has developed a complete formalism for the reduction and projection operators in terms of the stabilizers of the 0^{th} atom.

$\mathbb{S}_0$ is a group and thus divides the space around A_0 into invariant subspaces. By selecting our trial vectors to lie within lines and planes of invariance of $\mathbb{S}_0$ we naturally simplify projection of that position, and hence the relationships between BVs. In many cases the invariants of the stabilizer group will be obvious. When they are not, they can be found by projection from the point group $\mathbb{H}_k$ using the trial vectors ϕ_1=$(1,0,0)$, ϕ_2=$(0,1,0)$, ϕ_3=$(0,0,1)$. In either case, the invariants can be used as "symmetry adapted trial functions" from which the system basis-vectors are projected.

> e.g.
> If the stabilizers of a position are $\{E, C_{4x}, C_{4x}^2, C_{4x}^3\}$, then its invariants are the line $(1,0,0)$ and the plane $[1,1,1]$ perpendicular to it. The symmetry adapted trial functions for this position would lie parallel and perpendicular to $(1,0,0)$.

This technique is particularly appropriate when the lowering of a system's symmetry divides related positions into several distinct orbits. Consider the position $A_i = g_i A_0$ which is related to A_0 by an operation of $\mathbb{G}_0$ not in $\mathbb{G}_k$. If $\mathbb{S}_i$ is the group of operations "stabilizing" A_i then $\mathbb{S}_i = g_i \mathbb{S}_0 g_i^{-1}$ (section 2.13). Thus, if two orbits are related by the operation g_i, then appropriate trial functions are also related by g_i.

$$\phi_{orbit_i} = g_i \phi_{orbit_0} \tag{6.3}$$

The next section will work through an example where standard trial functions produce an excess of solutions, and determine the symmetry adapted trial functions. This example splits into two orbits under $\vec{k}$ and Eq 6.3 defines appropriate trial functions for the second orbit.

Worked example

Consider the space group $I4_132$ (214), ordering under the k-vector $\vec{k} = (\frac{1}{2}, \frac{1}{2}, \frac{1}{2})$, with an atom at the position $(0, 0, 0)$. Under the operations of the little group, G_k, there are three equivalent positions at $(\frac{1}{2}, \frac{1}{2}, 0)$, $(0, \frac{1}{2}, \frac{1}{2})$, and $(\frac{1}{2}, 0, \frac{1}{2})$. Using SARA$h$ (Wills, 2000), the decomposition of possible atomic displacements is given as:

$$\Gamma_{Polar} = 2\Gamma_1 + 2\Gamma_2 + 2\Gamma_3 \tag{6.4}$$

The IRs are labelled using the numbering scheme of Kovalev (1993), and each is of order 2; correspondingly, we expect $2 \times 2 = 4$ BVs to be projected from each IR.

The basis vectors generated for Γ_1 using the standard trial vectors ϕ_1=$(1, 0, 0)$, ϕ_2=$(0, 1, 0)$, ϕ_3=$(0, 0, 1)$ are listed in Table 6.1, using the notation:

$$\psi^n_{ij}(x, y, z) = \begin{pmatrix} a_0 \\ b_0 \\ c_0 \end{pmatrix} A_0 + ... \tag{6.5}$$

The BV $\psi^n_{ij}(x, y, z)$ has been projected from the IR Γ_n, using the ij^{th} matrix element of each IR matrix, and the trial vector (x, y, z) at the position $A_0 = (0, 0, 0)$. It consists of a series of vectors (a_n, b_n, c_n), defined with respect to the crystallographic axes, at the positions A_n. Projection using the standard trial functions generates six apparently distinct BVs, rather than the four required by the reduction formula. It

can be shown, by solution of simultaneous equations, that:

$$\begin{aligned}\psi^1_{11}(0,0,1) &= e^{\frac{2}{3}\pi.i}\psi^1_{11}(1,0,0) + e^{-\frac{2}{3}\pi.i}\psi^1_{11}(0,1,0)\\ \psi^1_{21}(0,0,1) &= e^{\frac{2}{3}\pi.i}\psi^1_{21}(1,0,0) + e^{-\frac{2}{3}\pi.i}\psi^1_{21}(0,1,0)\end{aligned} \tag{6.6}$$

For this system, two of the six basis vectors must be eliminated and the four retained must form a set of basis sets. Following the strategy of section 6.3.1, we will determine a set of symmetry-adapted trial functions that simplify the BV relationships and eliminate one of the trial functions.

BV	$A_0=(0,0,0)$	$A_1=(\frac{1}{2},\frac{1}{2},0)$	$A_2=(0,\frac{1}{2},\frac{1}{2})$	$A_3=(\frac{1}{2},0,\frac{1}{2})$
$\psi^1_{11}(1,0,0)$	$\begin{pmatrix}1\\ -0.183-0.683i\\ -0.183+0.683i\end{pmatrix}$	$\begin{pmatrix}0+i\\ -0.683+0.183i\\ 0.683+0.183i\end{pmatrix}$	$\begin{pmatrix}0\\ 0.683-0.183i\\ -0.183+0.683i\end{pmatrix}$	$\begin{pmatrix}0\\ 0.183+0.683i\\ -0.683-0.183i\end{pmatrix}$
$\psi^1_{11}(0,1,0)$	$\begin{pmatrix}-0.183+0.683i\\ 1\\ -0.183-0.683i\end{pmatrix}$	$\begin{pmatrix}-0.683-0.183i\\ 0-i\\ -0.683+0.183i\end{pmatrix}$	$\begin{pmatrix}-0.183+0.683i\\ 0\\ -0.683+0.183i\end{pmatrix}$	$\begin{pmatrix}0.683+0.183i\\ 0\\ -0.183-0.683i\end{pmatrix}$
$\psi^1_{11}(0,0,1)$	$\begin{pmatrix}-0.183-0.683i\\ -0.183+0.683i\\ 1\end{pmatrix}$	$\begin{pmatrix}0.683-0.183i\\ 0.683+0.183i\\ 0-i\end{pmatrix}$	$\begin{pmatrix}-0.683+0.183i\\ 0.183-0.683i\\ 0\end{pmatrix}$	$\begin{pmatrix}0.183+0.683i\\ 0.683+0.183i\\ 0\end{pmatrix}$
$\psi^1_{21}(1,0,0)$	$\begin{pmatrix}0\\ -0.183-0.683i\\ -0.683-0.183i\end{pmatrix}$	$\begin{pmatrix}0\\ -0.683+0.183i\\ -0.183+0.683i\end{pmatrix}$	$\begin{pmatrix}1\\ -0.683+0.183i\\ 0.683+0.183i\end{pmatrix}$	$\begin{pmatrix}0-i\\ -0.183-0.683i\\ -0.183+0.683i\end{pmatrix}$
$\psi^1_{21}(0,1,0)$	$\begin{pmatrix}-0.683-0.183i\\ 0\\ -0.183-0.683i\end{pmatrix}$	$\begin{pmatrix}0.183-0.683i\\ 0\\ -0.683+0.183i\end{pmatrix}$	$\begin{pmatrix}0.683+0.183i\\ -1\\ 0.683-0.183i\end{pmatrix}$	$\begin{pmatrix}0.183-0.683i\\ 0-i\\ 0.183+0.683i\end{pmatrix}$
$\psi^1_{21}(0,0,1)$	$\begin{pmatrix}-0.183-0.683i\\ -0.683-0.183i\\ 0\end{pmatrix}$	$\begin{pmatrix}0.683-0.183i\\ -0.183+0.683i\\ 0\end{pmatrix}$	$\begin{pmatrix}0.683-0.183i\\ -0.683-0.183i\\ 1\end{pmatrix}$	$\begin{pmatrix}-0.183-0.683i\\ 0.183-0.683i\\ 0+i\end{pmatrix}$

TABLE 6.1. The projected basis vectors for the position $(0,0,0)$ in the space group $I4_132$, ordering under $\vec{k}=(\frac{1}{2},\frac{1}{2},\frac{1}{2})$. In this projection, the trial vectors lie parallel to the crystallographic axes.

The stabilizer group of the position A_0 is the group of C_3 rotations about $(1,1,1)$, whose invariant subspaces are the line $(1,1,1)$ and the perpendicular plane $[1,1,1]$. Thus, we select one trial vector to lie along $(1,1,1)$ and the other two to lie in $[1,1,1]$ such that they form a right-hand set: ϕ_1=$(1,1,1)$, ϕ_2=$(1,-1,0)$, ϕ_3=$(1,1,-2)$ all

BV	$A_0=(0,0,0)$	$A_1=(\frac{1}{2},\frac{1}{2},0)$	$A_2=(0,\frac{1}{2},\frac{1}{2})$	$A_3=(\frac{1}{2},0,\frac{1}{2})$
$\frac{1}{\sqrt{3}}\psi^1_{11}(1,1,1)$	$\begin{pmatrix} .366 \\ .366 \\ .366 \end{pmatrix}$	$\begin{pmatrix} .366i \\ -.366i \\ -.366i \end{pmatrix}$	$\begin{pmatrix} -0.5+0.5i \\ 0.5-0.5i \\ -0.5+0.5i \end{pmatrix}$	$\begin{pmatrix} 0.5+0.5i \\ 0.5+0.5i \\ -0.5-0.5i \end{pmatrix}$
$\frac{1}{\sqrt{2}}\psi^1_{11}(1,-1,0)$	$\begin{pmatrix} 0.837-0.483i \\ -0.837-0.483i \\ 0+0.966i \end{pmatrix}$	$\begin{pmatrix} 0.483+0.837i \\ -0.483+0.837i \\ 0.966 \end{pmatrix}$	$\begin{pmatrix} 0.129-0.483i \\ 0.483-0.129i \\ 0.354+0.354i \end{pmatrix}$	$\begin{pmatrix} -0.483-0.129i \\ 0.129+0.483i \\ -0.354+0.354i \end{pmatrix}$
$\frac{1}{\sqrt{6}}\psi^1_{11}(1,1,-2)$	$\begin{pmatrix} 0.483+0.837i \\ 0.483-0.837i \\ -0.966 \end{pmatrix}$	$\begin{pmatrix} -0.837+0.483i \\ -0.837-0.483i \\ 0+0.966i \end{pmatrix}$	$\begin{pmatrix} 0.483+0.129i \\ 0.129+0.483i \\ -0.354+0.354i \end{pmatrix}$	$\begin{pmatrix} 0.129-0.483i \\ -0.483+0.129i \\ -0.354-0.354i \end{pmatrix}$

TABLE 6.2. The projected basis vectors for the position $(0,0,0)$ in the space group $I4_132$, ordering under $\vec{k}=(\frac{1}{2},\frac{1}{2},\frac{1}{2})$. In this projection, symmetry adapted trial vectors were used.

upon the position A_0. In Table 6.2, these trial vectors have been renormalized to have modulus 1, and the BVs generated from these trial functions are listed. Inspection of the alternate basis vectors reveals that: $\frac{1}{\sqrt{2}}\psi^1_{11}(1,-1,0) = -i.\frac{1}{\sqrt{6}}\psi^1_{11}(1,1,-2)$. Hence, we can eliminate either $\phi_2=(1,-1,0)$ or $\phi_3=(1,1,-2)$ from our projection; symmetry adapted trial functions have produced a set of BVs in which equivalent trial functions are readily discernable and discarded.

Our example is split into two orbits, the second orbit being related to the previously considered set of atomic positions by the operation:

$$g_5 = \begin{pmatrix} 0 & 1 & 0 & 0.25 \\ 1 & 0 & 0 & 0.75 \\ 0 & 0 & -1 & 0.75 \\ 0 & 0 & 0 & 1 \end{pmatrix} \tag{6.7}$$

The trial vectors for this orbit are derived from Eq. 6.3: ϕ_1=$(1,1,-1)$, ϕ_2=$(-1,1,0)$, ϕ_3=$(1,1,2)$ upon the position $A_4=(\frac{1}{4},\frac{3}{4},\frac{3}{4})$. The BVs calculated for the *second* orbit are presented in Table 6.3. Inspection reveals that $\frac{1}{\sqrt{2}}\psi^1_{11}(-1,1,0) = i.\frac{1}{\sqrt{6}}\psi^1_{11}(1,1,2)$, and again we can eliminate either ϕ_2 or ϕ_3.

BV	$A_4 = (\frac{1}{4}, \frac{3}{4}, \frac{3}{4})$	$A_5 = (\frac{3}{4}, \frac{3}{4}, \frac{1}{4})$	$A_6 = (\frac{3}{4}, \frac{1}{4}, \frac{3}{4})$	$A_7 = (\frac{1}{4}, \frac{1}{4}, \frac{1}{4})$
$\frac{1}{\sqrt{3}}\psi^1_{11}(1,1,-1)$	$\begin{pmatrix} 1.366 \\ 1.366 \\ -1.366 \end{pmatrix}$	$\begin{pmatrix} 1.366i \\ -1.366i \\ 1.366i \end{pmatrix}$	$\begin{pmatrix} -0.5-0.5i \\ 0.5+0.5i \\ 0.5+0.5i \end{pmatrix}$	$\begin{pmatrix} -0.5+0.5i \\ -0.5+0.5i \\ -0.5+0.5i \end{pmatrix}$
$\frac{1}{\sqrt{2}}\psi^1_{11}(-1,1,0)$	$\begin{pmatrix} -0.224+0.129i \\ 0.224+0.129i \\ 0.259i \end{pmatrix}$	$\begin{pmatrix} -0.129-0.224i \\ 0.129-0.224i \\ 0.259 \end{pmatrix}$	$\begin{pmatrix} -0.483-0.129i \\ -0.129-0.483i \\ -0.354+0.354i \end{pmatrix}$	$\begin{pmatrix} -0.129+0.483i \\ 0.483-0.129i \\ -0.354-0.354i \end{pmatrix}$
$\frac{1}{\sqrt{6}}\psi^1_{11}(1,1,2)$	$\begin{pmatrix} 0.129+0.224i \\ 0.129-0.224i \\ 0.259 \end{pmatrix}$	$\begin{pmatrix} -0.224+0.129i \\ -0.224+0.129i \\ -0.259i \end{pmatrix}$	$\begin{pmatrix} -0.129+0.483i \\ -0.483+0.129i \\ +0.354+0.354i \end{pmatrix}$	$\begin{pmatrix} 0.483+0.129i \\ -0.129+0.483i \\ -0.354+0.354i \end{pmatrix}$

TABLE 6.3. The projected basis vectors for the position $(\frac{1}{4}, \frac{3}{4}, \frac{3}{4})$ in the space group $I4_132$, ordering under $\vec{k} = (\frac{1}{2}, \frac{1}{2}, \frac{1}{2})$. In this projection, symmetry adapted trial vectors were used.

6.3.2. Testing for bad projections using SARA*h*

Our method of symmetry adapted trial functions was tested using SARA*h*'s "batch mode". This mode allows users to define a range of space groups, k-vectors and atomic positions for which SARA*h* projects the basis vectors for every combination of these variables. When SARA*h* is unable to define the correct number of basis vectors during a calculation an error code is printed to the output file.

A batch test was run over all the space groups, using more than 30 k-vectors with 30 atomic positions. Points and k-vectors were chosen to represent possible points of symmetry, e.g. $(0,0,0)$, $(\frac{1}{2},0,0)$, $(\frac{1}{4},0,0)$, etc, including systems known to cause over-generation errors when the standard trial functions are used. When using the method presented above to select trial functions, no cases of over- or under- generation were found by SARA*h*.

6.4. Other considerations in the choice of trial functions

Simplifying the determination of equivalent basis vectors is not the only consideration when selecting trial functions. Observe the basis vectors of a water molecule, as projected using standard trial functions (Fig. 6.1). While they have the correct symmetry, the vibrational motions are not parallel or perpendicular to the hydrogen-oxygen bonds as might be expected. An atom's stretching and bending modes are usually considered to be largely distinct (e.g. Choudhury, 2009), but are mixed in the vibrational modes determined by these trial vectors.

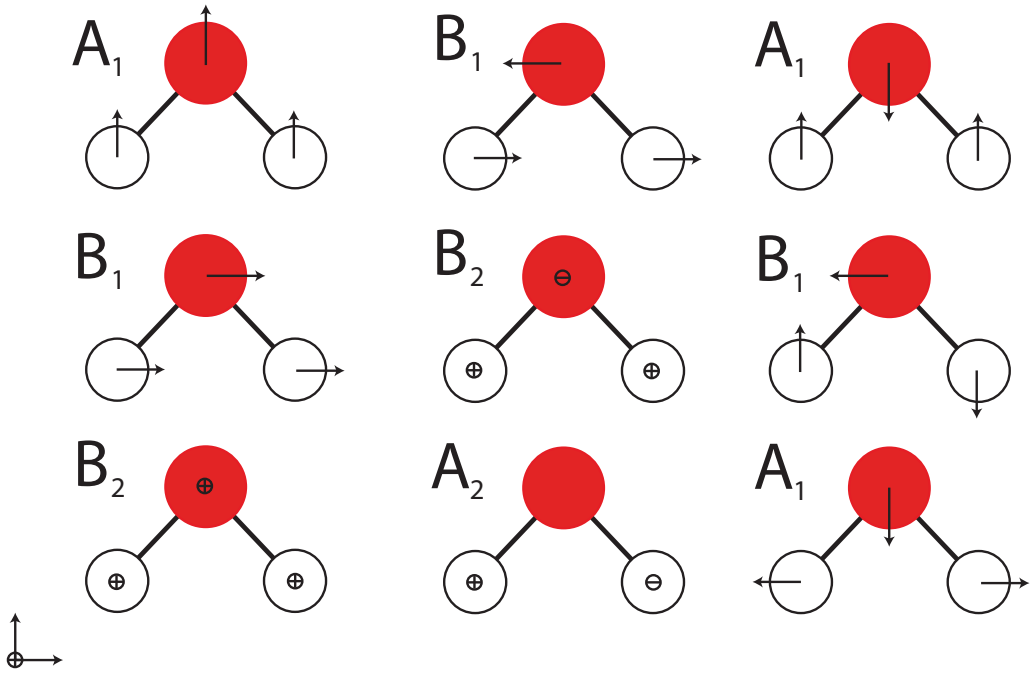

FIGURE 6.1. The basis vectors of water, as projected from trial functions that lie parallel to the axis system defining C_{2v} symmetry: + and − indicate motion into and out of the plane of the page. The left column depicts the translational modes, the middle rotational modes, and the right column vibrational modes. While these basis vectors have the correct symmetry properties, they poorly represent the motions of the atoms because they do not consider the influence of the OH bond.

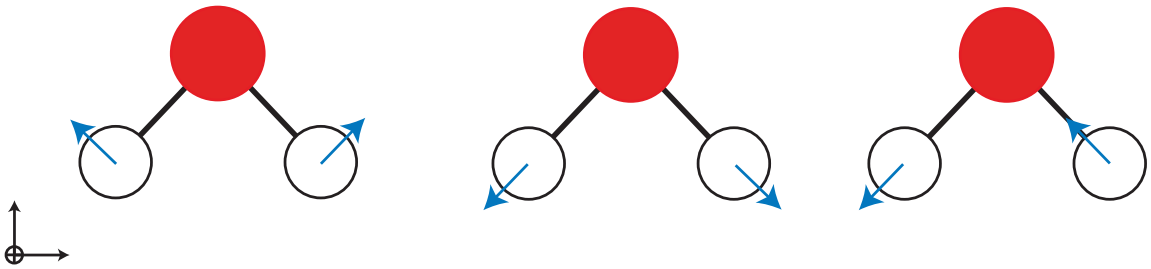

FIGURE 6.2. The vibrational motions of water, projected from trial functions that lie parallel to the OH bonds. These better represent the system, but are equivalent to, the basis vectors in Fig. 6.1.

Motions that correspond to stretching and bending vibrational motions can be obtained by projection from a set of trial functions lying parallel or perpendicular to the OH bonds (Fig. 6.2). This occurs because basis sets from the same IR, although they are not degenerate, they can be freely mixed to generate new basis sets of the correct symmetry. We cannot uniquely define, *a priori*, the basis set of an IR, only its symmetry[4].

The role of local symmetry is an important, but often overlooked, problem in the application of representation theory to magnetic ordering and displacive phase transitions. The local environment of an atom has a strong influence upon its behaviour, but not the form of its basis vectors which derive from the crystal symmetry. One approach is to select trial vectors in a manner that represents interactions such as directional bonding, and crystal field anisotropy. Currently there is no software that will generate basis vectors from user-defined trial functions, and we consider this a significant omission from existing tools for representation theory.

[4]Except in the case of a 1 dimensional IR which occurs exactly once in the reduction of the system representation

6.5. Under-generation

Under-generation is the apparent inability to generate sufficient basis vectors to fully span a system's decomposition. For the projection operator W_{ij}^{μ} changing μ generates a basis set with a different symmetry, while varying i generates further members of the same basis-set. Hence, the only free variable which to generate new basis sets is j. This point has been thoroughly explored by Stokes *et. al* (1991), who define when varying the column index j will generate new basis vectors. Here, we briefly discuss the problem using basis sets to complete our understanding the method of projection operators.

Basis vectors occur in basis sets which transform under two relations:

$$\begin{aligned} g\psi_i^{\mu} &= \sum_{j}^{d^{\mu}} \mathfrak{d}_{ji}^{\mu}(g)\psi_j^{\nu} \\ W_{ij}^{\mu *}\psi_j^{\mu} &= \psi_i^{\mu} \end{aligned} \tag{6.8}$$

From consideration of these two equations, it is apparent that the enumeration of BVs is not arbitrary; it defines how they inter-relate *within the basis set to which they belong.* Further, in a system spanning the reduction $\Gamma = \sum_{\nu} C^{\nu}\Gamma_{\nu}$, there are C^{ν} basis sets with the symmetry of each Γ_{μ}. Within each basis set the BV's will be labelled $1, 2, ..., d^{\nu}$, and so their numbering is neither arbitrary nor unique.

The action of $W_{i1}^{\mu *}$ on a general vector ϕ is to project the component of ϕ parallel to ψ_1^{μ} into ψ_i^{μ}; similarly, $W_{i2}^{\mu *}$ projects the component along ψ_2^{μ} into ψ_i^{μ}. However, *there is no restriction that ψ_1 and ψ_2 are from the same basis set.* Hence, by varying j we can project two basis vectors, ψ_i^{μ}, which may belong to different basis sets.

We now understand the influence of each term in the projection operator. Varying the row-index i generates another member of the same basis-set, while varying the column-index j generates a BV from a different basis set (which may be equivalent). Varying μ changes the symmetry of the projected basis vectors, and changing the

trial vectors generates basis sets that are linearly related to any other choice of trial vectors.

6.6. Conclusions

The role of trial vectors in defining symmetry modes of a system is a long-neglected subject, often relegated to the single word "suitable". In this chapter we have applied an understanding of the method of projection operators, and in particular stabilizers, to resolve the problems of over-generation that occur when trial functions are not carefully chosen. Moreover, we have developed an *algorithm* which has been implemented in SARA*h* and tested using the batch mode. Our new approach makes the calculation of a systems' basis vectors significantly more reliable.

The importance of trial functions is not only limited to simplifying the results of basis vector calculation. They also represent an opportunity to include the influence of covalent bonds and local symmetry; indeed, they are the only way to do this when using the method of projection operators. Currently, the ability to define trial functions in this way is not supported in any existing software and we consider this a significant area for development.

References

[1] Bertaut, E. F. (1962). *J. Apply. Phys.* **33(3)**, 1138-1143.

[2] Bertaut, E. F. (1981). *J. Mag. Mag. Materials* **24**, 267-278.

[3] Choudhury, J. *et. al.* (2009). *Chin. Phys. Lett.*, **26**(2), 020308.

[4] Hamermesh, M. (1990).*Group Theory and its Application to Physical Problems*, **Addison-Wesley Publishing Company** (Reading, 1964).

[5] Izyumov, Y. A and Syromyatnikov, V. N. (1990). *Phase Transitions and Crystal Symmetry*, **Kluwer Academic Publishers** (Dordrecht).

[6] Izyumov, Y. A. and Naish, V. E., (1991). *Neutron Diffraction of Magnetic Materials*, **Consultants Bureau** (New York).

[7] Kovalev O. V., *Representations of the Crystallographic Space Groups: Irreducible representations, Induced representations and Corepresentations (2nd Ed)*, **Gordon and Breach Science Publishers** (Amsterdamn. 1993).

[8] Kenzelmann, *et. al.* (2006). *Phys. Rev. B*, **74**, 014429.

[9] Rodriguez-Carvajal, J. (2004). *ftp://ftp.cea.fr/pub/llb/divers/BasIreps*

[10] Sikora, W. *et. al* (2004). *J. App. Crys* **37**, 1015-1019.

[11] Stokes, H. T. *et. al* (1991). *Phys. Rev. B* **43**, 11010-11018.

[12] Wills, A. S. (2000). *Physica B* **276**, 680.

[13] Wills, A. S. (2005). *J. Mater. Chem.*, **15**, 245.

CHAPTER 7

Normal Mode Parameterization of Powder Diffraction Data: A New Module for SARA*h* GSAS

Part of the inhumanity of the computer is that, once it is competently programmed and working smoothly, it is completely honest.

Isaac Asimov

7.1. Introduction

Displacive phase transitions are characterised by small, symmetry breaking, distortions of a crystal. During such a phase transition, the mean position of each atoms is displaced by a softening phonon whose frequency tends to zero lowering the symmetry of the crystal (Putnis, 1992; Dove, 1997a, 2003). Classic examples of second- or almost second-order displacive transitions include quartz (Dolino, 1990), and $SrTiO_3$ (Cowley, 1996). The aim of this thesis is to develop the use of representation theory in defining displacive phase transitions. In particular, we aim to express how a system changes during a phase transition in terms of a linear combination of basis vectors:

$$\Delta = \sum_{\nu} \sum_{i}^{d^{\nu}} C_i^{\nu} \psi_i^{\nu} \tag{7.1}$$

So far, this thesis has focused on developing tools for constructing all of the ψ for any system. What remains is determination of the basis vector coefficients. The structure of crystalline systems is usually investigated using diffraction techniques, and it is from diffraction patterns that we will extract the basis vector coefficients.

In particular we focus upon powder diffraction experiments, as these are common in the study of complex magnetic systems for which single crystals are often difficult to synthesize.

This chapter will briefly review popular software for constructing the basis vectors of physical systems, and for using these modes to analyze powder-diffraction data. We then present a new module for the SARA*h*-Refine (Wills, 2000) software suite that performs Monte-Carlo Rietveld refinement of displacive phase transitions using normal-mode coefficients, within the GSAS programme suite. Also presented are three example refinements, based upon simulated data, and a discussion of the software's limitations.

Simultaneous to our work on symmetry mode refinements in GSAS, other groups independently developed software for the TOPAS and Fullprof refinement engines (Campbell, 2007, 2008; and Rodriguez-Carvajal, 2008). The net result of these works is that symmetry-mode parameterisation is now supported by three of the most popular powder-diffraction refinement routines.

7.1.1. Determinable properties of the phase transition

When discussing the symmetry-mode approach to phase transitions, it is important to be clear exactly what new information such an analysis can determine. In section 6.4 we noted that basis vectors cannot be uniquely assigned to each occurence of an IR[1]. If the distortion of an atom involves many basis vectors of the same symmetry, then the basis vectors can always be redefined such that, under the new definitions, the distortion is defined a single basis vector of that symmetry[2]. Therefore, we can

[1]The exception to this is when a 1-dimensional IR occurs exactly once. It this case it must be uniquely defined, as there are no other basis vectors of the same symmetry.

[2]It is interesting to note that, though this basis transformation is always possible it may *not* appropriate. For example, it may be desirable to separate the stretching and bending components of a molecular ion species. As always, the axis system should be appropriate to the problem being investigated.

only *uniquely* define the number of irreducible representations that are components of the displacement of each position, and the vector defining the distortion.

With this in mind, during the example symmetry-mode refinements presented within this chapter we focus our attention upon determining the number of distinct IR symmetries involved in each distortion: i.e. does Landau theory (section 1.5) allow this transition to be second order. We also consider the "shape" of the distortion, and the position of the atoms within the daughter phase. There is no emphasis placed upon the coefficients of individual distortion modes.

7.2. Powder diffraction experiments

Powder diffraction experiments are relatively simple when compared to single crystal work; the sample does not need to be aligned with any great care and powdered samples are usually less challenging to prepare (IUCr, 2002). Conversely, the analysis of powder-diffraction data can be far more difficult. While the diffraction pattern of a single crystal comprises a pattern of discrete intensity spots, in a powdered sample each particulate generates its own diffraction pattern and is orientated randomly relative to all of its neighbours. Resultantly, the diffraction pattern consists of concentric spheres, observed as circles upon a two dimensional detector (Fig. 7.2). As the diffraction pattern is radially symmetric, data is usually collected along a single radius as a one-dimensional plot of intensity against d-spacing (the distance between planes of atoms in the crystal).

7.2.1. Rietveld refinement

In a diffraction experiment, the cell parameters and space group can be determined from the spatial distribution of diffraction peaks, while the position of atoms within the unit cell is encoded in the peak intensities. For a single crystal experiment, the peaks are sufficiently spread in reciprocal space that the integrated intensity

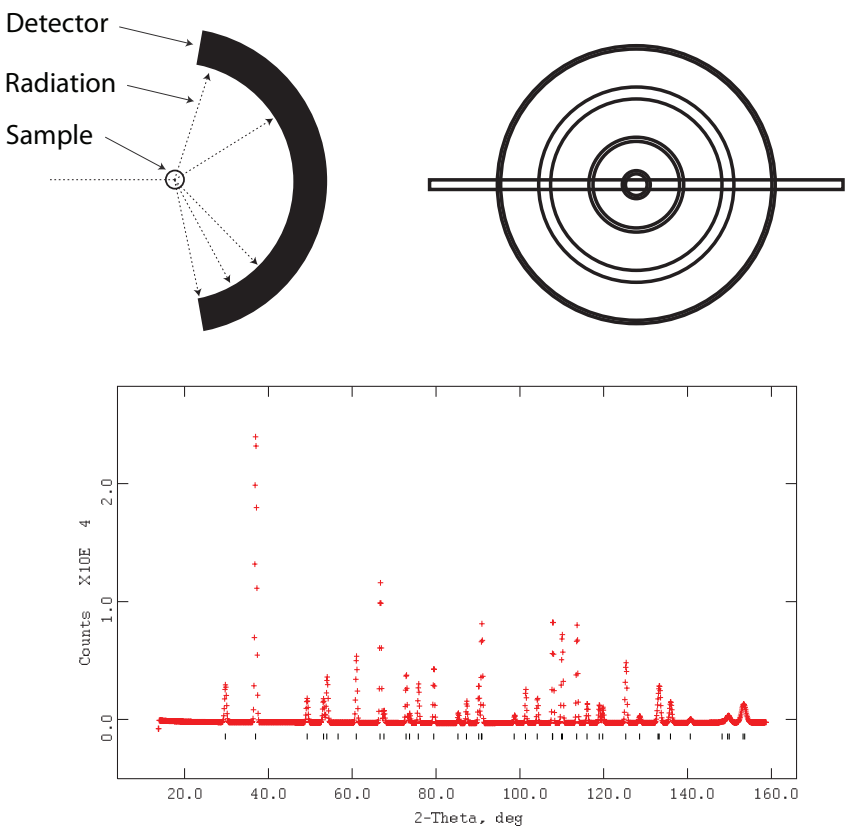

FIGURE 7.1. In a powder diffraction experiment, the sample is placed in the path of a radiation beam and before a detector (top-left). The diffraction pattern of powders, as observed by a 2-dimensional detector, consists of concentric circles (top-right). Each radius of the pattern is identical, and the path along one can be described by a graph of intensity against angular position (main).

of individual diffraction peaks can be calculated, allowing the position of atoms and other crystallographic parameters to be determined. Direct methods (Woolfson, 1971; Hauptman, 1986) and analytic methods such as charge-flipping (Oszlányi, 2008) solve single-crystal data from integrated peak intensities.

When using powder diffraction data, the determination of individual peak intensities is often impossible, because the overlapping of many peaks within the diffraction pattern correlates their integrated intensities. The number of independent intensities is usually insufficient to define the large number of the structural parameters using

algebraic or analytical methods. Instead, structures are resolved using model-fitting, also known as Rietveld refinement in this context (Rietveld, 1967). Rather than attempting to separate the individual contributions to each peak, Rietveld methods model the whole of the diffraction pattern simultaneously. To do this, the Rietveld method models not only the system, but also the shape of diffraction peaks, which is a function of both the radiation source and sample parameters such as strain and preferential orientation of the crystallites.

In crystallography, model-fitting involves the generation of an initial model of the system using chemical and crystallographic knowledge, and methods such as Le Bail extraction (Le Bail, 1988). The diffraction pattern of this model is then calculated using Rietveld methods, and the model is iteratively "refined" to match its calculated pattern to the observed diffraction data. Refinement involves varying the model parameters, such as the position of atoms and the cell parameters, and the fidelity of the calculated diffraction pattern is measured by "goodness of fit" parameters. These parameters quantify the statistical quality of the match between the calculated and observed diffraction data.

There are several approaches to the iteration process. Least-squares is a specialized technique for rapidly optimising models already close to the "true" structure using parameter derivatives. All of a model's free parameters are refined simultaneously, leading to a rapid convergence in the calculations. However, least-squares refinements are often unstable and may "diverge", with the goodness of fit parameter becoming worse after each step. Alternatives to the least-squares method include the Monte-Carlo (Metropolis, 1949; 1963)[3] and Simulated Annealing (Kirkpatrick, 1983; Cerny, 1985) techniques. These methods optimise structure through a serious of random distortions, rather than by calculating parameter derivatives.

[3]More strictly, for data refinement *reverse* Monte-Carlo methods are applied. Monte-Carlo methods select a large number of randomly determined *initial* conditions, and then minimize that system in a deterministic way (such as least squares refinement). This generates a range of solutions, which occur with some well defined statistical distribution. Reverse Monte Carlo involves using a number of random steps to reach a pre-defined goal; in this case to fit the observed diffraction pattern.

Use of Rietveld methods in the analysis of powder-diffraction data has been popularized by a number of software programs based upon them. The most commonly encountered refinement engines for the analysis of powder diffraction data are: GSAS (Larson, 1994); FullProf (Rodriguez-Carvajal, 1993); and TOPAS (Cheary, 1990). Of these GSAS is currently the most widely used, followed by Fullprof; TOPAS is largely supported by users in industry. Refinements are usually perfomed using the crystallographic axes, however the use of symmetry modes has become established for magnetic structures (e.g. Wills, 2002; Kenzelmann, 2005; Poole, 2008) since its establishement by SARA*h* (Wills, 2000) and later support in Fullprof (Rodriguez-Carvajal, 2001). The extension of representation theory to atomic displacements has been discussed in the literature (Dove, 1997a; Wills, 2001, 2005), but has not been supported by any of the popular data analysis tools until recently.

Currently, two software routines support the calculation and use of normal-modes in Rietveld refinement in the Fullprof and TOPAS engines and are reviewed in the next section. Our goal was to write a new module for SARA*h* that would extend this functionality to the GSAS software suite, by defining the position of a system's atoms in the lower-symmetry phase as a distortion from its co-ordinates in the higher symmetry phase:

$$\begin{aligned} x' &= x_0 + c_1\psi_1 + ... \\ &= x_0 + \sum_{\nu}\sum_{i}^{d^\nu} C_i^\nu \psi_i^\nu \end{aligned} \tag{7.2}$$

The distortion from the initial position, x_0 is parameterized by the coefficients, C_i^ν, of each normal mode, ψ_i^ν. Defining a phase transition in this way allows us to identify the irreducible representations active during a displacive phase transition.

7.3. Review of existing software

The calculation of basis vectors by hand is an arduous process, consequently a number of algorithms exist to perform this work. These routines vary slightly in their construction and many (as noted in chapter 6) are known to have a problems in a small number of instances. In this section, we review the most popular of these programs, along with existing support for representation theory in defining displacive transitions.

MODY (Sikora *et al.*, 2004), generates magnetic BVs using Izyumov's method of stabilizers (Izyumov, 1960; section 2.13) and Kovalev's table of irreducible representations (Kovalev, 1993). SARA*h* (Wills, 2005) uses both the tables of Kovalev and IRs generated by a modified routine from KAREP (Hovestreydt, 1992) to calculate magnetic and atomic BVs using the method of projection operators. BASIREPS (Rodríguez-Carvajal, 2004) also uses KAREP, along with the methods of Izyumov (1991) to generate a system's basis vectors. The IRs of both KAREP and Kovalev were constructed using Zak's method (Zak, 1960; Klauder, 1968).

ISODISPLACE (Stokes, 2007a) differs from other basis-vector calculators in that it does not define all the basis vectors of the parent phase. Instead, the symmetry of the daughter phase and k-vector of the distortion are pre-defined, and only those BVs compatible with the symmetry of the daughter phase are returned. These modes are retrieved from pre-prepared tables, based upon the so-called *physically* irreducible representations (Stokes, 1987). A printed version these tables have been published by Stokes (1988), along with an electronic version (Stokes, 2007b). AMPLIMODES (Aroyo et al., 2003, 2006a, 2006b) approaches phase transitions in a similar manner to ISODISPLACE. From a defined parent and daughter phase, the structural distortion

is calculated by bringing both phases into the same axis system. The possible k-vectors and IRs which can bring about such a symmetry reduction are then read from pre-prepared tables[4].

While there are numerous options for generating basis vectors, the opportunities to use them in data refinement are more limited. The parameterization of a general refinement using symmetry modes was first supported by SARAh and is now well developed in magnetic refinement, but extension of this technique to atomic distortions has only become possible in the last two years. It is now supported in TOPAS using ISODISPLACE (Campbell, 2007, 2008), and in Fullprof using AMPLIMODES (Rodriguez-Carvajal, 2008). Both routines perform least-squares Rietveld refinement upon a daughter phase of defined symmetry. In the next section we report a new application which makes this approach practical for GSAS users for the first time. Our routine performs reverse Monte-Carlo Rietveld refinement, taking a distinctly different and more general approach to symmetry mode refinement.

7.4. Structural refinement in SARAh

SARAh-Refine is a modular front-end to GSAS and Fullprof that manipulates their runfiles to parameterize refinements using symmetry modes. We have developed a new module which refines structural distortions in GSAS, complimenting SARAh's existing magnetic structure routines. A schematic overview of how this module performs structural refinements is given in Figure 7.2.

During each refinement cycle, the module generates a random set of basis-vector coefficients that define a distortion. This distortion is applied to the existing structural model and the new structure is written to a *name*.EXP file, which is read by

[4]These are presented using the notation of ISOTROPY (Stokes 2007b), and presumably the ISOTROPY tables are used in the calculations.

the GENLES applet within GSAS. GENLES performs a least-squares Rietveld refinement upon the distorted structure, to determine how well it fits the diffraction data; during this refinement almost all of the model parameters are fixed[5]. The refined model and the χ^2 goodness of fit parameter for the least-squares refinement are then passed back to SARA*h*; if the fit has improved the new structure is accepted, otherwise it is rejected.

$$\chi^2 = \frac{\sum w(I_o - I_c)^2}{N_{obs} - N_{var}} \tag{7.3}$$

Here I_o, I_c are the observed and calculated intensities at each point, N_{obs}, N_{var} are the number of observations and variables and w is a weighting for that data point.

Overall, our refinement strategy comprises a reverse Monte-Carlo walk through the coefficient space of a system. In order to concentrate the majority of these steps about any refinement minima, the size the distortion changes dynamically. During each cycle, the generated distortion is reduced in magnitude by a function of χ^2; it is also controlled by a slider in the graphical user interface. Several functions are used for different ranges χ^2 and these were determined empirically by studying the evolution of example refinements.

The step functions were tailored by observing a large number of refinements. In particular, the functions were "smoothed" over several ranges when refinements were regularly observed to become "stuck". They were also designed to become flat as χ^2 approached 0: small values of χ^2 are assumed to be close to a minima. The set of functions used was that which appeared to converge in the fewest average number of steps, and is presented in Table 7.1. Figure 7.3 plots the step size as a function of χ^2, and a hypothetical walk for a 2-dimensional refinement.

[5]The scale factor and background function are usually allowed to refine. 3-5 least-squares cycles are sufficient when there are very few free parameters.

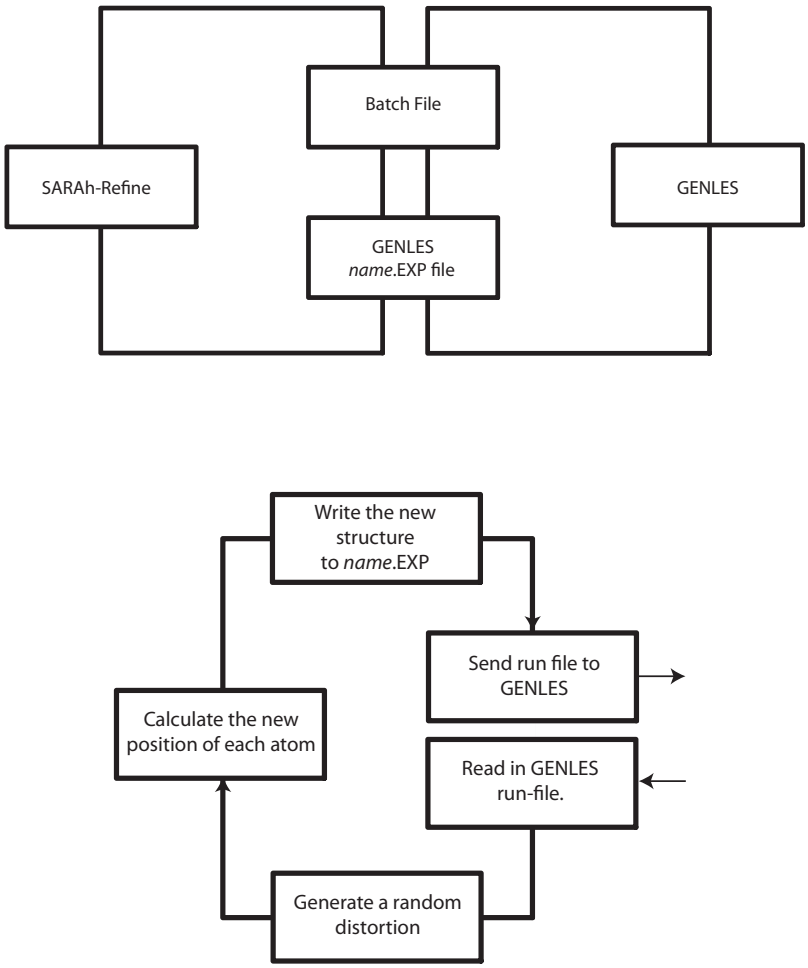

FIGURE 7.2. Schematic representations of SARA*h*, and her interaction with GENLES via the *name*.EXP file (top). During each cycle, the new module generates a structural distortion which is written to an *name*.EXP file, GENLES performs a least-squares Rietveld refinement upon on the run-file before it is passed back to SARA*h* for the next cycle (bottom). The batch-file is used to call GENLES during each cycle.

χ^2	Divisor	Step Size
$\chi^2 > 220$	1	1
$97 < \chi^2 < 220$	$3 \times 1.005^{-\chi^2}$	$\frac{1}{3} \times 1.005^{\chi^2}$
$\chi^2 < 97$	$900 \times 1.07^{-\chi^2}$	$\frac{1}{900} \times 1.07^{\chi^2}$

TABLE 7.1. The effect of χ^2 upon step size. Each distortion is reduced in magnitude by a function of χ^2, as given above. Reducing the step size when χ^2 is small concentrates most of the random walk around any minima.

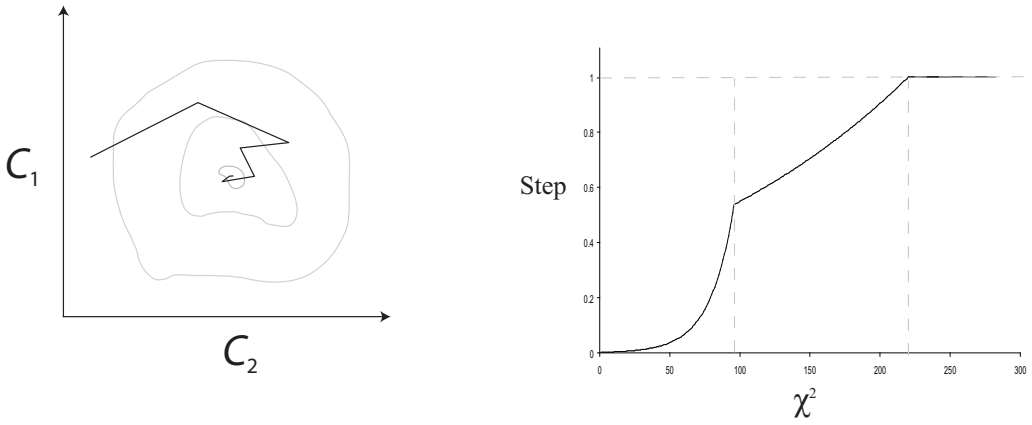

FIGURE 7.3. (Left) A possible random walk through the coefficient space of a two basis-vector refinement, the contours represent points of equal χ^2. Note that, the step size decreases as a function of χ^2. (Right) The step-size reduces smoothly and continuously, as defined by the functions in Table 7.1.

SARA*h* has a simple graphical user interface (GUI), allowing users to select which basis-vectors to include in a refinement and other details such as the number of cycles to perform (Figure 7.4). Basis vectors and system information are loaded from two pre-prepared files: a *name*.MAT generated by SARA*h*-Representational Analysis; and a *name*.EXP generated in GENLES and containing the position of all the atoms in the parent phase. The undistorted low-symmetry phase is generated in the *name*.EXP by a supporting routine that calculates the position of every atom in the unit cell using the symmetry operations of the parent space group.

Our approach to refinements within SARA*h* is significantly different to those of ISODISPLACE and AMPLIMODES. First, it is not a least-squares refinement, but a reverse Monte-Carlo walk; this makes refinements significantly more computationally expensive. Second, SARA*h* makes no assumptions about the symmetry of the daughter phase: the refinement is performed using a $P1$ cell and every possible distortion mode of the parent phase. Both ISODISPLACE and AMPLIMODES define the symmetry of the daughter phase before refining the diffraction data, and limit their focus to the "obvious" modes that maybe involved. The examples in this chapter will highlight potential weaknesses in this approach.

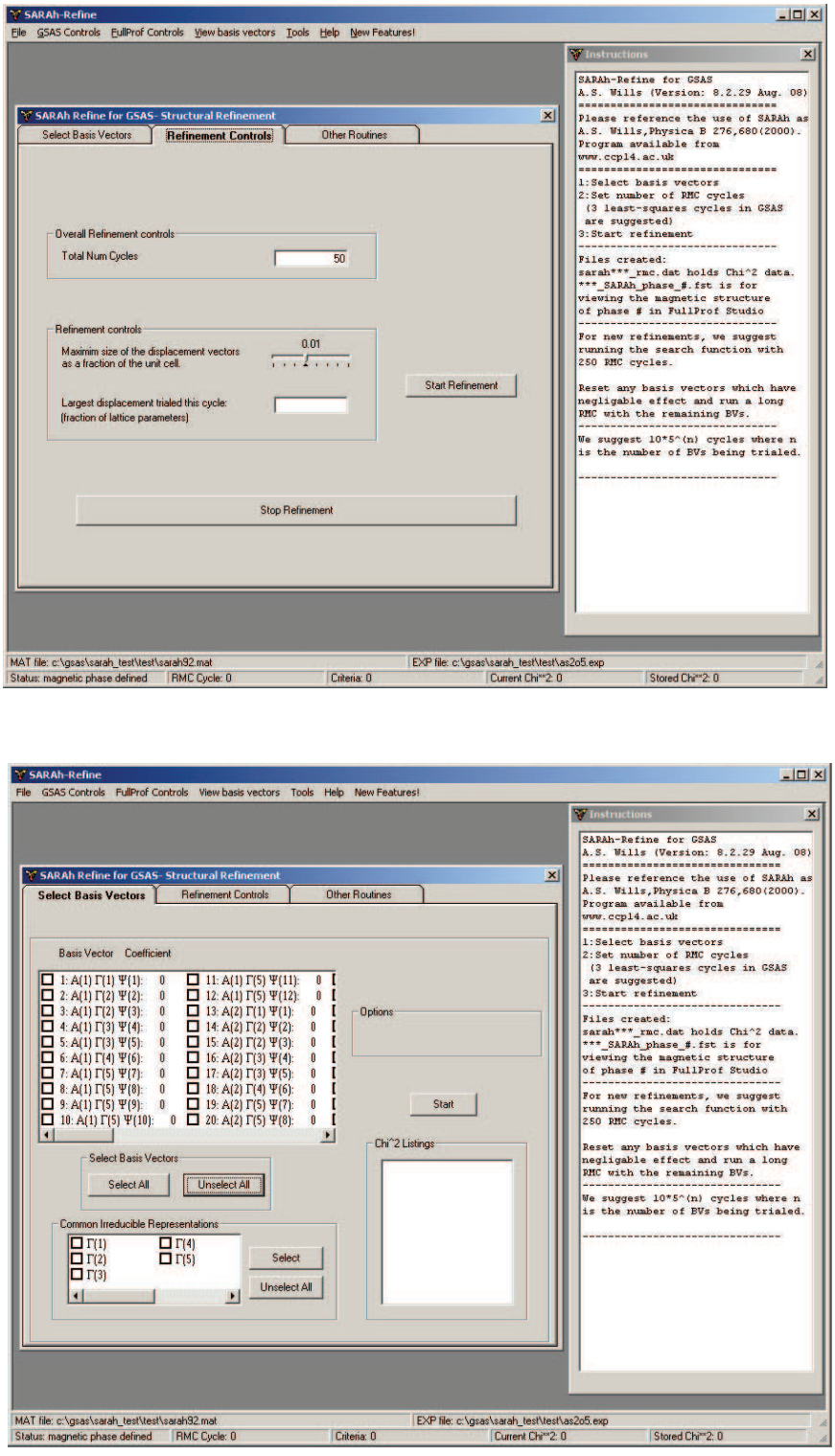

FIGURE 7.4. The two main tabs for using SARA*h*-GSAS. (Top) The displacements tab contains the scale slider along with the number of cycles field. (Bottom) The main tab is where users select or de-select basis-vectors for inclusion in a refinement.

7.4.1. Limitations

SARA*h*-Refine edits *name*.EXP runfiles, which are then computed upon by GENLES. As such, it inherits a number of GENLES' limitations. Most significantly, because the refinement is formally performed using a unit-cell with P1 symmetry, refinement of cell parameters and atomic thermal parameters must be restrained to prevent them diverging[6]. Further, as atomic positions are not refined within GENLES, refinements do not return any uncertainties.

A more significant problem is that the χ^2 minima is often shallow and/or broad, and the refinement can fail to find the best model. In particular, some BVs have only a very small influence on the goodness of fit parameter. When a refinement contains weakly correlated modes then there are many structural models with the same χ^2, broadening the structural minima. This also makes it uncertain as to whether or not a such modes are present in the distortion. Further, SARA*h*-GSAS is prone to becoming trapped in local-minima as there is no route by which the routine can "climb" out of them; this is also true of least-squares Rietveld methods.

7.5. Determination of the dominant k-vector and basis vectors

Systems have an infinite number of possible k-vectors and associated basis vectors. In order to reduce this set to a manageable size we must employ qualitative symmetry arguments to minimize the number of basis vectors and k-vectors considered during a refinement. This requires prior knowledge of the low-symmetry, "daughter" phase as well as the high-symmetry "parent" phase.

The k-vector of a perturbation defines the translational symmetry of the daughter phase relative to its parent. In particular it defines the reciprocal space periodicity of the distortion, and when this differs from that of the underlying lattice the

[6]In practise, if the cell parameters of the daughter-phase are known, the cell parameters are usually fixed and thermal parameters assumed to be the same in both the daughter and parent phase.

cell parameters of the system in direct space are enlarged (its translational period increases).

> E.g
> A k-vector of $(\frac{1}{2}, 0, 0)$ induces modes which double the cell parameter in the a direction.
> A k-vector of (0,0,0) would leave the translational symmetry of a system unchanged.

Reversing this argument, we can determine the k-vector by considering the change in lattice parameters of the *primitive* unit cell during a phase change, disregarding the small changes caused by thermal expansion.

We can deduce the irreducible representation likely to define a phase transition using the arguments of section 3.8: for a symmetry operation to persist after a phase transition, it must be represented by the identity matrix within that IR. If the symmetry group of the daughter phase is already known, it is possible to define which IRs (and hence which basis vectors) are compatible with the phase transition. This approach may still return a large number of BVs, therefore a routine to determine the effect of each BV on the refinement has been provided. The procedure identifies which BVs which generate the largest improvement in χ^2, as those basis-vectors which have a marked influence on χ^2 are more likely to be involved in the final structure.

During a refinement users can add or remove BVs and, when the refinement has converged, weakly correlated modes (those which have negligible influence on χ^2) should be removed. These modes contribute insignificantly to the quality of the final fit, while complicating the distortion model. Identification of such modes is aided by another routine, which determines the effect on χ^2 of removing each BV from the refinement. Those BVs which can be removed without a significant change in χ^2 (less than 1%) can usually be ignored.

The final outputs from each refinement are: a filename.EXP file which contains the final structure in P1 symmetry; a filename.MAT file which stores the BVs and their refined coefficients; and two filname.FST files which contain fullprof-studio structures of the cell and of the distortion. The fullprof-studio files can be used to visualize the distortion and final structure.

7.6. Examples

To test SARA*h*-Refine, a number of powder-diffraction spectra were simulated using the GSAS software suite. All of the structures used were taken form the Inorganic Crystallographic Database Service (Allen, 2002). Powder diffraction patterns of structures were simulated using the GSAS, by outputting the calculated spectra via POWPLOT. The POWPLOT outputs were then run through a custom conversion routine, SIMGEN (Supporting Material), to generate a new histogram file.

Simulated histograms were refined using GSAS to ensure their fidelity, and to generate a target value[7] for χ^2. χ^2 is a function of counting statistics (usually referred to as the scale factor): if both I_o and I_c are increased, then χ^2 also increases. By simulating data using very large scale-factors we were able to make minima in the χ^2-space deeper, improving the speed at which calculations converged.

The first two examples were chosen based upon a number of criteria. First, they were selected to have a small number of atoms in the unit cell: this kept the number of basis vectors low, improving the speed at which calculations converged. Second, they were chosen to be well studied systems for which high-quality data had been collected and whose structures are "known" with confidence. Third, they were chosen to be transitions which were nearly second-order, to test how reliably SARA*h* could

[7]Although N_{var} differs for GSAS and SARA*h* refinements, in general $N_{obs} > 10,000$ while $N_{var} < 100$ hence the effect upon χ^2 is negligible

identify the number of distinct symmetries present within the phase transition. The third transition was chosen because it had a non-zero k-vector.

7.6.1. Quartz

One of the oldest known, and most widely discussed, phase transitions is the quartz α-β transition, from $P6_222(180)$ to $P3_222(154)$, which has been subject to great interest since its discovery (Le Chatelier, 1889, 1890a, 1890b; Dolino, 1990). Despite the large body of work on this sytem, there is still disagreement over the short and long-range nature of this phase transition. The diffraction pattern of the lower-symmetry β-phase was simulated from using the structure reported by Kihara (1990), GSAS refinement of the simulated data gave a χ^2 of 1.575.

The volume of the primitive cell does not change significantly during the phase transition, therefore we assign to it the k-vector $(0, 0, 0)$. Refinement was initially performed using the basis vectors of Γ_3, the only IR of $P6_222$ which generates a daughter phase with the symmetry $P3_222$, resulting in a fit of $\chi^2 = 2.506$ (Figure 7.5, top). To improve the fit, modes associated with Γ_1 were added to the refinement as these do not lower the symmetry of the daughter phase. This lowered χ^2 to 1.575 (Figure 7.5, bottom). The final atomic positions are compared with those reported in the literature in Table 7.2, and the distortions are depicted in Figure 7.6. The distortion was completely defined using 4 basis vectors from two irreducible representations and convergence was achieved in less than 1000 cycles.

Atom	x_{obs}	y_{obs}	z_{obs}	x_{calc}	y_{calc}	z_{calc}	δx	δy	δz
Si	0.48547	0.00000	0.16667	0.48547	0.00000	0.16667	0.00000	0.00000	0.00000
O	0.41732	0.23956	0.30889	0.41735	0.23950	0.30892	-0.00003	0.00006	-0.00003

TABLE 7.2. A comparison of the atomic positions in β-quartz as reported by Kihara (1990, denoted by *obs*), and those refined using SARA*h*-refine (denoted by *calc*). All of the co-ordinates are reported the $P3_221$ axis system

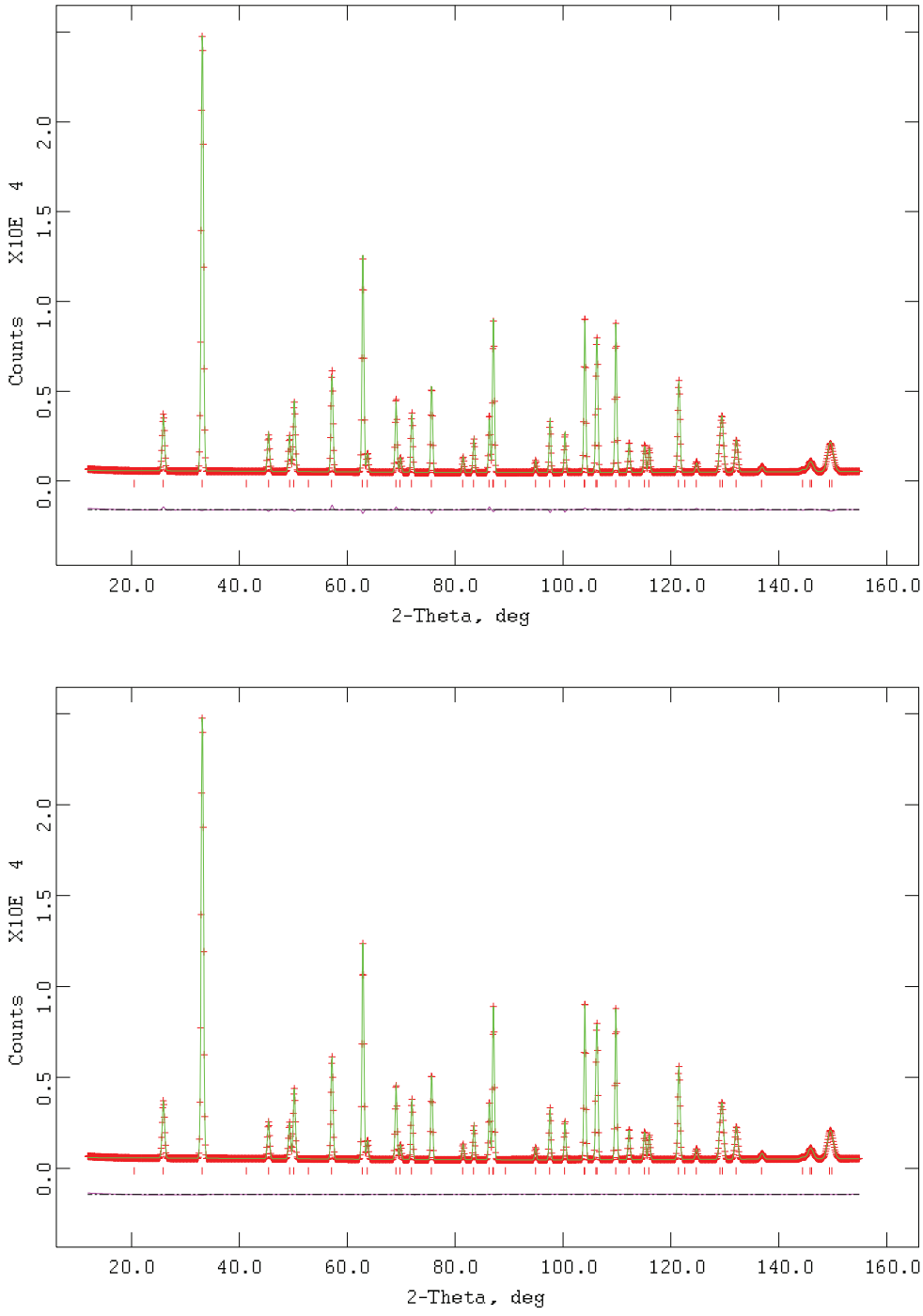

FIGURE 7.5. Refinement plots of simulated neutron diffraction data for β-quartz, space group $P3_222(154)$. The structure was refined in SARA*h* using Γ_3 (upper) and $\Gamma_1 + \Gamma_3$ (lower). The lower line in each plot indicates the difference between the observed and the calculated diffraction patterns.

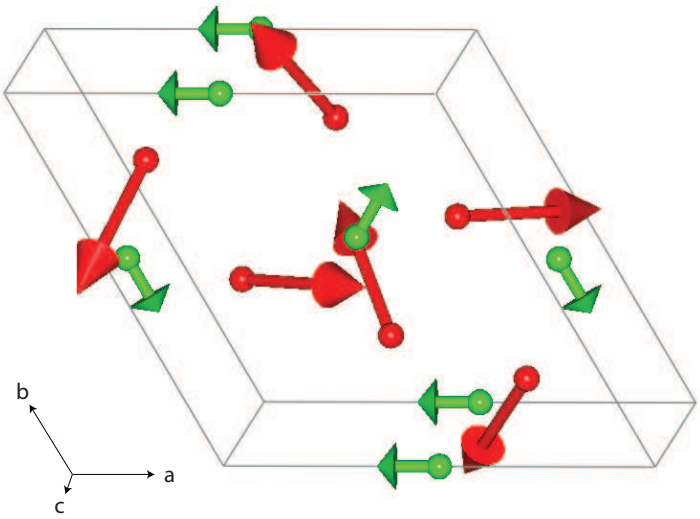

FIGURE 7.6. This figure represents the atomic displacements that occur in the quartz α-β phase transition. The red spheres and arrows represent the initial position of the oxygen atoms, and their displacement; the green arrows and spheres represent the silicon atoms and displacements. Arrows have been increased in magnitude by a factor of 10 for clarity.

Historically, quartz was believed to go through a single, second-order phase transition, mediated by soft-phonon modes of the high-symmetry phase (Axe, 1970). However, it has been shown that quartz passes through a short-lived (c.a. 1.4K) incommensurate phase (Heaney, 1991) which is responsible for the observed opalescence (Dolino, 2001), and that one of these transitions is first-order. Our analysis demonstrates that, for an idealized data set, it is possible to detect elements of a second-IR in the phase transition and so confirm that, according to Landau theory (section 1.5), the transition could not be second order. However, it is questionable whether the influence of Γ_1 would be distinguishable in a real data set; difference between the plots in figure 7.5 is very small. The refined structure is in very close agreement to that used in the histogram simulation.

7.6.2. Arsenic Oxide

Arsenic oxide undergoes a phase change consisting of a small distortion from $P4_12_12(92)$ (Igartua, 1996) which has been considered to be a model for the ideal ferro-elastic transition (Redfern, 1990). A simulated spectra of the $P2_12_12_1(19)$ daughter phase was generated from the structures of Jansen (1979), and refinement in GSAS gave a target χ^2 of 0.3891.

During this transition the volume of the primitive cell is approximately constant and is assigned k-vector $(0, 0, 0)$. Γ_3 is the only IR of $P4_12_12(92)$ to precipitate a group-subgroup transition to $P2_12_12_1$, and refinement of the data using these basis vectors gave an initial χ^2 of 27.95 (Figure 7.7, top), which fell to 0.2620 when the modes of Γ_1 were added. This rose to 0.3044 when those BVs which contributed less than 1% of the displacement were culled (Figure 7.7, bottom). Table 7.3 reports the final atomic positions, and compares them with those reported in the literature. The distortion are depicted in Figure 7.8, and was defined using 19 coefficients from two distinct irreducible representations. Convergence was achieved in less than 5,000 cycles.

The important role of the introduction of a second IR upon reducing χ^2 is more apparent in the displacive phase transition of As_2O_5 than in quartz, although visually the difference between the two refinement plots is even more vanishing. The arithmetic result agrees with the work of Redfern; although second-order Landau behaviour of the system is observed over a large temperature range, the transition is not described by a single irreducible representation. Again, the refined structure was in very close agreement to that used in the histogram simulation.

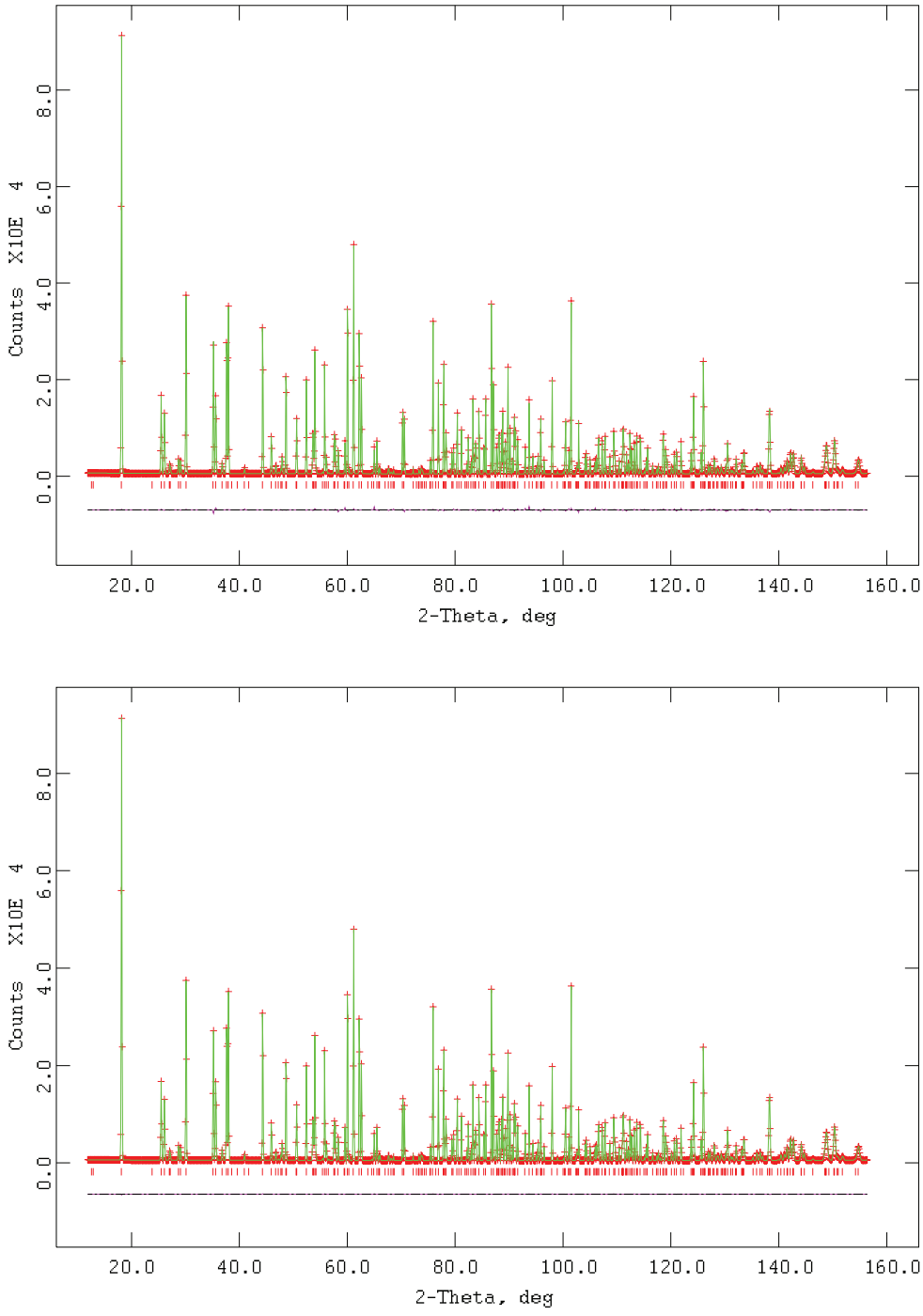

FIGURE 7.7. Refinement plots of simulated neutron diffraction data for As_2O_5. The structure was refined in SARA*h* using the Γ_3 (upper) and $\Gamma_3 + \Gamma_1$ (lower) irreducible representations. The lower line in each plot indicates the difference between the observed and the calculated diffraction patterns.

Atom	x_{obs}	y_{obs}	z_{obs}	x_{calc}	y_{calc}	z_{calc}	δx	δy	δz
As	0.4016	0.4024	0.003	0.40187	0.40213	0.00358	-0.00027	0.00027	-0.00058
As	0.7838	0.7827	0.0088	0.78366	0.78254	0.00896	0.00014	0.00016	-0.00016
O	0.5400	0.4349	0.7197	0.53983	0.43495	0.71927	0.00017	-0.00005	0.00043
O	0.7465	0.1426	0.4865	0.74625	0.14256	0.48686	0.00025	0.00005	-0.00036
O	0.8318	0.2668	-0.042	0.8318	0.26694	-0.04158	0	-0.00014	-0.00042
O	0.7487	0.4737	0.3363	0.7465	0.47382	0.33573	0.00220	-0.00012	0.00057
O	0.5254	0.2555	0.1774	0.52529	0.2535	0.17694	0.00011	0.00200	0.00046

TABLE 7.3. A comparison of the atomic positions in As_2O_5 as reported by Jansen (1979, denoted by *obs*), and those refined using SARA*h*-refine (denoted by *calc*). All of the co-ordinates are reported the $P4_12_12$ axis system

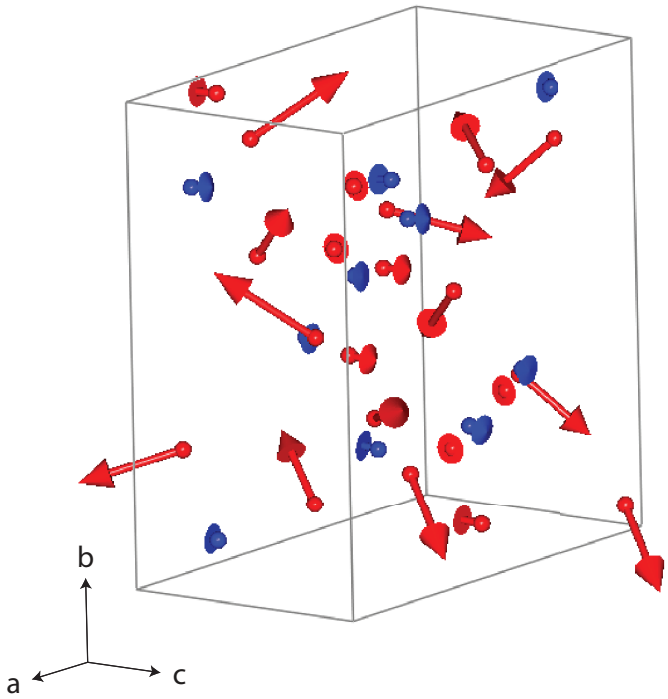

FIGURE 7.8. This figure represents the atomic displacements that occur in the arsenic oxide phase transition. The red spheres and arrows represent the initial position of the oxygen atoms, and their displacement; the blue arrows and spheres represent the arsenic atoms and displacements. The arrows have been increased in magnitude by a factor of 10 for clarity.

7.6.3. Cristobalite

Cristobalite undergoes a phase transition from $Fd\bar{3}m$ (227) to $P4_12_12$ in the region of ca. 500-550K (Swainson, 2003), during which the volume of the primitive cell increases significantly. GSAS refinement of the simulated $P4_12_12$ phase (Schmahl *et. al* 1992) provided a reference χ^2 of 0.2679.

The k-vector relating the primitive cells of $Fd\bar{3}m$ and $P4_12_12$ is $k_{Prim} = (\frac{1}{2}, \frac{1}{2}, 0)$ in the primitive setting[8], and this corresponds to a doubling of the crystallographic primitive cell in two directions. The k-vector also indicates that adjacent primitive unit-cells of the high-symmetry phase show anti-symmetric distortions. Thus, the twist/anti-twist rotations observed in this structure, and related structures such as the distorted perovskites, arise naturally from the k-vector. Indeed, anti-phase relations must occur during this group-subgroup transition, a result only obtained when a k-vector is used to define the distortion.

There are no IRs of $\mathbb{G}_k$ which correspond to a transition between the literature parent and daughter space groups, so we utilized the basis vector search routine which indicated that only the basis vectors of Γ_2 had a strong influence on χ^2 . Symmetry-mode refinement using these basis vectors converged on a χ^2 of 3.775 (Fig. 7.9). Combinations of Γ_2 with the remaining IRs, Γ_1, Γ_3 and Γ_4 all showed small improvements in χ^2. However, the change in $\chi^2$was less than 10% ($\chi^2 > 3.4$), after more than 200,000 cycles.

Inspection of the refinement plot indicates that Γ_2 is unlikely to completely define the distortion in cristobalite, even when making allowance for noise in real data. Therefore, the parameterization of this distortion was performed by-hand (Tables 7.4, 7.5, 7.6), and derived two results. First, the displacement of the silicon atoms is defined by a single basis vector. Second, the motion of the oxygen atoms is defined by

[8]Corresponding to $k = (0, 0, 1)$ in the face-centered setting.

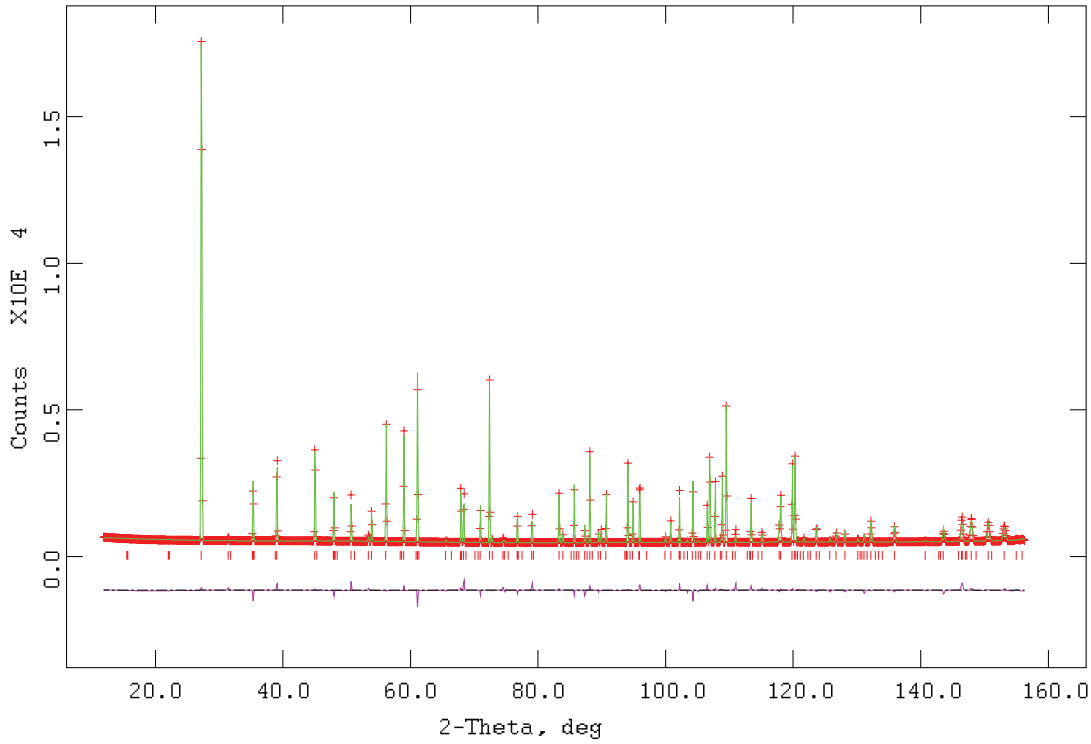

FIGURE 7.9. Refinement plots of simulated neutron diffraction data for low-symmetry Cristobalite. The structure was refined in SARA*h* using using the Γ_2 irreducible representation. The lower line indicates the difference between the observed and the calculated diffraction patterns for that refinement.

no less than eight modes in the *ab* plane, but only one in the *c*-axis. The refinement failed to converge because, while χ^2 is strongly correlated to Γ_2, there are many weakly correlated modes present in the distortion. The convolution in the *ab*-plane, can be interpreted as an averaging of rotational disorder about the *c* axis. This is consistent with the suggestion that β cristobalite is orientationally disordered (Dove, 1997b).

Our analysis disagrees with that of Hatch (1994) who found that the system ordered under a single six-dimensional irreducible representation. We find that there are no 6 dimensional representations for this little group and the lowering of symmetry occurs according to the two-dimensional representations Γ_1, Γ_2, Γ_3 and Γ_4.

Atom	x_{obs}	y_{obs}	z_{obs}	x_{cal}	y_{cal}	z_{cal}	δx	δy	δz
Si	0.125	0.125	0.125	0.125	0.1707	0.125	0.00000	0.04570	0.00000
Si	0.375	0.375	0.875	0.4207	0.375	0.875	0.04570	0.00000	0.00000
O	0	0	0	-0.0433	-0.0528	0.0497	0.05280	0.04330	-0.04970
O	0.75	0.75	0	0.7933	0.8028	0.0497	0.04330	0.05280	0.04970
O	0.75	0	0.75	0.7933	-0.0528	0.7003	0.04330	-0.05280	-0.04970
O	0	0.75	0.75	0.0528	0.7067	0.7997	0.05280	-0.04330	0.04970

TABLE 7.4. A comparison of the atomic positions in the $P4_12_12$ and $Fd\bar{3}m$ phases of cristobalite Schmahl (1992). All of the co-ordinates are reported the $Fd\bar{3}m$ axis system

	Distortion			$\psi^2_{1,1}$			C	$C \times \psi$		
	δx	δy	δz	x	y	z		x	y	z
Si	0.0000	0.0457	0.0000	0.0000	1.0000	0.0000	0.0457	0.0000	0.0457	0.0000
Si	0.0457	0.0000	0.0000	1.0000	0.0000	0.0000		0.0457	0.0000	0.0000
					ψ^2_{11}					
O	0.0528	0.0433	-0.0497	0.0000	0.0000	2.0000	-0.0249	0.0000	0.0000	-0.0497
O	0.0433	0.0528	0.0497	0.0000	0.0000	-2.0000		0.0000	0.0000	0.0497
O	0.0433	-0.0528	-0.0497	0.0000	0.0000	2.0000		0.0000	0.0000	-0.0497
O	0.0528	-0.0433	0.0497	0.0000	0.0000	-2.0000		0.0000	0.0000	0.0497

TABLE 7.5. Comparison of silicon and oxygen distortions with single modes of Fd$\bar{3}$m cristobalite. The distortion of each atom is defined along with a single basis vector for the silicon and oxygen positions. The distortion of the silicon atoms is defined completely by assigning to these basis vectors the coefficient C, as is the distortion of the oxygen atoms parallel to the c.

		Distortion	Symmetry mode								Total
			ψ^1_{11}	ψ^1_{21}	ψ^2_{11}	ψ^2_{21}	ψ^3_{11}	ψ^3_{21}	ψ^4_{11}	ψ^4_{21}	
Coeff			0.02403	0.00238	0.00238	0.02403	0.02165	-0.02640	-0.02165	0.02640	
	x	0.0528	0.02403	0.00238	0.00238	0.02403	0.02165	0.00000	-0.02165	0.00000	0.0528
O	y	0.0433	-0.02403	-0.00238	0.00238	0.02403	0.02165	0.00000	0.02165	0.00000	0.0433
	z	-0.0497	0.00000	0.00000	0.00000	0.00000	0.00000	0.00000	0.00000	0.00000	0.0000
	x	0.0433	0.02403	-0.00238	-0.00238	0.02403	0.00000	-0.02640	0.00000	0.02640	0.0433
O	y	0.0528	0.02403	-0.00238	0.00238	-0.02403	0.00000	0.02640	0.00000	0.02640	0.0528
	z	0.0497	0.00000	0.00000	0.00000	0.00000	0.00000	0.00000	0.00000	0.00000	0.0000
	x	0.0433	0.02403	-0.00238	-0.00238	0.02403	0.00000	0.02640	0.00000	-0.02640	0.0433
O	y	-0.0528	0.02403	-0.00238	0.00238	-0.02403	0.00000	-0.02640	0.00000	-0.02640	-0.0528
	z	-0.0497	0.00000	0.00000	0.00000	0.00000	0.00000	0.00000	0.00000	0.00000	0.0000
	x	0.0528	0.02403	0.00238	0.00238	0.02403	-0.02165	0.00000	0.02165	0.00000	0.0528
O	y	-0.0433	-0.02403	-0.00238	0.00238	0.02403	-0.02165	0.00000	-0.02165	0.00000	-0.0433
	z	0.0497	0.00000	0.00000	0.00000	0.00000	0.00000	0.00000	0.00000	0.00000	0.0000

TABLE 7.6. Parameterization of oxygen distortions in the ab-plane using symmetry modes of Fd$\bar{3}$m cristobalite. The final solution is highly convoluted, with 7 terms. This is consistent with there being considerable disorder in the low-symmetry phase.

7.7. Conclusions

Description of displacive phase transitions is a complex and contentious issue. The examples discussed show that the use of symmetry modes can give significant insight into the symmetry of these phase transitions, though there are experimental limitations upon the precision of this analysis. In each case, we determine that the phase transition is not second order, however, legitimate questions remain as to whether these conclusions would be supported by experimental data. In general, our results agree with earlier work, though we disagree with the symmetry analysis of the α-β cristobalite transition performed by Hatch.

The importance of this work is, perhaps, best demonstrated by independent and simultaneous work of three groups to develop this method. Use of a particular refinement engine (TOPAS, Fullprof, GSAS, etc.) often amounts to a choice of familiarity or convenience, making cross-platform support for basis vector analysis is a significant advancement in the accessibility of this technique. We hope that, together, these programmes will encourage broader use of representation theory of when analysing powder diffraction data.

Finally, we have discussed the limitations of our method. SARA*h* is an effective tool for analysing phase transitions when the parent phase is well defined, and the cell parameters of the daughter phase known. However, the reverse Monte-Carlo approach is computationally expensive, and system properties such as the cell parameters must be tightly constrained or not refined. Further, the ability to identify or exclude basis vectors which make only small contributions to a distortion is limited, even for highly ideal data.

In the next two chapters, both structural and magnetic transitions are analysed from powder diffraction data using SARA*h*. We also make extensive use of the qualitative arguments from this chapter and chapter 3.

7.8. Acknowledgements

We acknowledge the help of I. P. Swainson, who suggested all of the example systems and many others. His ideas were a great aid in testing SARA*h*-refine.

References

[1] Allen, F. H (2002). *Acta Cryst.* **B58**, 380-388.

[2] Aroyo, M. *et. al* (2003). *Phase Transitions: A Multinational Journal* **76**(1-2), 155-170.

[3] Aroyo, M. I. , Kirov, A., Capillas, C., Perez-Mato, J. M., and Wondratschek, H. (2006a). *Acta Cryst.* **A 62**, 115-128.

[4] Aroyo, M. I. , Kirov, A., Capillas, C., Perez-Mato, J. M., Wondratschek, H., Kroumova, E., Ivantchev, S., Madariaga, G., Kirov, A., (2006b). *Zeit. f ur Krist.*, **221**, 15-27.

[5] Axe, J. D, Shirance, G. (1970) *Phys. Rev.* **B 1**, 342 - 348.

[6] Campbell B. J, Evans J. S. O. , Perselli F. , and Stokes H. T. (2007). *IUCr Computing Commission Newsletter* **8**, 81-95.

[7] Campbell B. J, Evans J. S. O. , Perselli F. , and Stokes H. T. (2008). *Acta. Cryst.* **A 64**, C216.

[8] Cerny, V. (1985). *J. Optimization Theory and Applications*, **45**, 41.

[9] Cheary, R. W., Coelho, A. A. (1992). *J. Appl. Crystallogr.* **25**, 109.

[10] Cowley,R. A. (1996). *Phil. Trans.: Math., Phys. Eng.*, **354**, 2799.

[11] Dove, M. T. (1997a). *American Mineralogist* **82**, 213-244.

[12] Dove, M. T., *et. al.* (1997b) *Journal of Physics and Chemistry of Minerals* **24**, 311-317.

[13] Dove, M. T. (2003). *Structure and Dynamics: An Atomic View of Materials* **Oxford University Press**.

[14] Dolino, G. (1990). *Phase Transitions* **21**, 59-72.

[15] Dolino, G. (2001). *J. Phys.: Condens. Matter* **13**, 11485-11501.

[16] Hatch, D. M., Subrata, G. and Bjorkstam, J. L. (1994). *Physics and Chemistry of Minerals* **21**, 67-77.

[17] Hauptman, H. (1986). *Science*, **233**, 178.

[18] Heaney, P. J, Veblen, D. R. (1991). *American Mineralogist* **76**, 1018-1032.

[19] Hovestreydt, E, Aroyo, M., Sattler, S., WondratschekJ, H. (1992) *J. Appl. Cryst.* **25**, 544.

[20] Igatua, J. M., Aroyo, M. I., and Perez-Mato, J. M. (1996), *Phy. Rev.* **B54**, 12744-12752.

[21] Izyumov, Y. A. and Syromyatnikov V. N. *Phase Transitions and Crystal Symmetry*, **V. N. Kluwer Academic Publishers** (1960).

[22] Izyumov, Y. A. and Naish, V. E. (1991). *Neutron Diffraction of Magnetic Materials*, **Consultants Bureau**, (New York, 1991).

[23] IUCr, (2002). *Structure Determination from Powder Diffraction Data* Ed. W. I. F. David *et. al.* **Oxford University Press**, USA.

[24] Jansen, M. (1979) *Zeit. f ur Naturforschung, Teil B. Anorg. Chemie, Organ. Chemie* **24**, 10-13.

[25] Kenzelmann, *et. al.* (2005). *Phys. Rev. Lett.* **95**, 087206

[26] Kihara, K. (1990) *European J. of Mineralology* **2**, 63-77.

[27] Kirkpatrick, S., Gelatt, C. D., Vecchi, M. P. (1983).*Science. New Series*, **220**, 4598.

[28] Kovalev O. V., *Representations of the Crystallographic Space Groups: Irreducible representations, Induced representations and Corepresentations (2nd Ed)*, **Gordon and Breach Science Publishers** (Amsterdamn. 1993).

[29] Klauder Jr., L. T. and Gay J., J. G. (1968). *Math. Phys.*, **9**, 1488.

[30] Larson, A.C. and Von Dreele, R.B. (1994) *Los Alamos National Laboratory Report* **LAUR** 86-748.

[31] Le Bail, A., Duroy, H. and Fourquet, J. L. (1988). *Mater. Res. Bull.*, **23**, 447.

[32] Le Chatelier, H. (1889). *C. R. Acad. Sci., Paris* **108**, 1046.

[33] Le Chatelier, H. (1890). *Bull. Soc. Mineral.* **13**, 112.

[34] Le Chatelier, H. (1890). *Bull. Soc. Mineral.* **13**, 119.

[35] Metropolis, N., *et. al.* (1953). *J. Chem. Phys.*, **21** (6), 1087.

[36] Metropolis, N., Ulam, S. (1949). *J. Am. Statistical Association*, **44** (247), 335.

[37] Rietvled, H. M. (1967). *Acta Crys. A*, **22**, 151.

[38] Redfern, S. A. T., *Ferroelectrics* **106**, 219-224.

[39] Rodriguez-Carvajal, J. (1993). *Physica B.* **192**, 55-69.

[40] Rodriguez-Carvajal, J. (2001) *Fullprof News* **January**, http://www.ill.eu/sites/fullprof/php/Fullprof_News_2001.htm

[41] Rodriguez-Carvajal, J. (2004). *ftp://ftp.cea.fr/pub/llb/divers/BasIreps*

[42] Rodriguez-Carvajal, J. (2008) *Fullprof News* **August**, http://www.ill.eu/sites/fullprof/php/Fullprof_News_2008.htm

[43] Oszlányi, G. and S utohttp, (2008). *Acta Cryst. A* **64**, 123.

[44] Poole, A., Wills, A. S., Lelièvre-Berna, E. (2007). *J. Phys.: Condens. Matter* **19**, 45 452201.

[45] Putnis, A. (1992). *Introduction to mineral sciences*, **Cambridge University Press**.

[46] Schmahl, W.W., Swainson, I.P., Dove, M.T., Graeme-Barber, A. (1992) *Zeit. f ur Krist.* **201**, 125-145.

[47] Sikora, W. *et. al* (2004). *J. App. Crys* **37**, 1015-1019.

[48] Stokes, H. T., Hatch, D. M. and Kim, J. S. (1987). *Acta Cryst. A*, **43**, 81.

[49] Stokes, H. T., Hatch, D. M., *Isotropy subgroups of the 230 crystallographic space groups*, **World Scientific Publishing** (Sigapore, 1988).

[50] Stokes, H. T. *et. al* (2007a). **Isodisplace**, stokes.byu.edu/isodisplace.html

[51] Stokes, H. T. *et. al* (2007b). **Isotropy**, stokes.byu.edu/isotropy.html

[52] Swainson, I. P., Dove, M. T., Plamer, D. C., (2003). *Physics and Chemistry of Minerals* **30**, 353-365.

[53] Wills, A. S. (2000). *Physica B* **276**, 680.

[54] Wills, A. S. (2001). *Appl. Phys. A*, **74**, 856.

[55] Wills, A. S. (2002). *Appl. Phys. A*, **74**(Suppl. 1), 1432.

[56] Wills, A. S. (2005). *J. Mater. Chem.*, **15**, 245.

[57] Woolfson, M. M. (1971). *Rep. Prog. Phys.*, **34** 369.

[58] Zak, J. (1960). *J. Math. Phys.*, *1*, 165.

CHAPTER 8

Experimental application: Iron oxyborate

"Measure what is measurable, and make measurable what is not so."

Galileo

8.1. Introduction

Chapters 8 and 9 present examples in which the methods of representation theory are used to analyse real systems and, in particular, neutron powder diffraction data collected from them. First, we investigate the structural, electronic and magnetic transitions of iron oxyborate, using both qualitative and quantitative methods to determine its magnetic and charge-ordered structure. Chapter 9 will study the structural distortion of potassium selenate during its transition to a ferroelectric phase.

8.2. Iron oxyborate, Fe_2OBO_3

The influence of a material's electronic structure upon its physical properties is profound. The Verwey transition, in which magnetite (Fe_3O_4) becomes insulating upon becoming charge ordered (Verwey, 1939), is the classic example of this relationship. Charge ordering, and its role in the emergence of properties such as colossal magnetoresistance and high temperature super-conductivity, is of great current interest (e.g. Salkola, 1996; Emerya, 1996; Vojta, 2000; Howald, 2003).

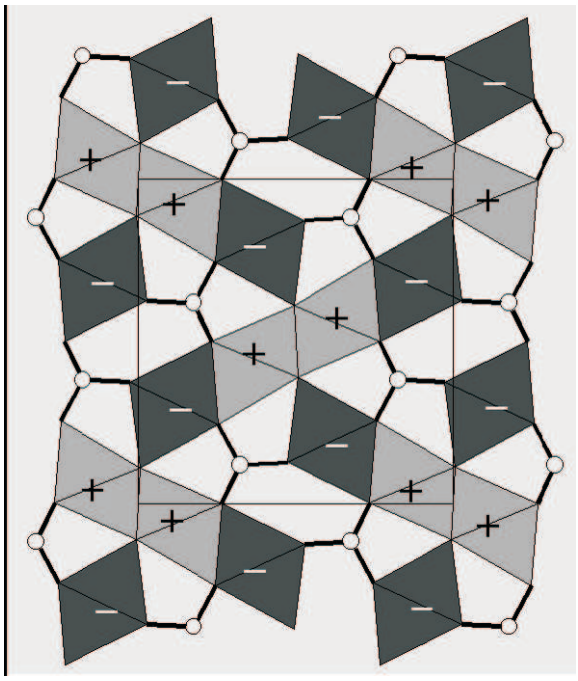

FIGURE 8.1. The suggested structure of Fe_2OBO_3 below 155K from Attfield *et. al* (1998a). Iron atoms exist in two symmetry distinct sites, shaded in light and dark grey respectively. The + and - symbols denote the relative orientations of the magnetic moments parallel to the a-axis.

Iron-oxyborate (Fe_2OBO_3) shows structural and magnetic phase transitions which, like magnetite, are thought to be driven by charge ordering upon the iron atoms. At high temperature it is an orthorhombic semiconductor with the Warwickite structure, consisting of ribbons of four edge sharing octohedra running parallel to the a-axis (Bertaut, 1950; Fig 8.1). Upon cooling, iron oxyborate displays a number of distinct transitions. The structural phase transition, from $Pmcn$ (62) to $P21/c$ (14), occurs at 317K, roughly in the middle of a broad semi-conductor to semi-conductor transition (Attfield, 1999).

Magnetic order emerges at 155K and was first described as antiferromagnetic (Attfield, 1992), then later as ferrimagnetism (Attfield, 1998a). The ferrimagnet model is based upon SQUID magnetometry data which indicates a saturation magnetic

moment of around $0.14\mu_B$ per formula unit (Continentino, 2001). More recently, a canted antiferromagnetic structure has been proposed on the basis of Mössbauer data and features in the susceptibility curve near T_C (Suda, 2003). This has brought back into question the true magnetic structure of this system.

Initial Mössbauer studies suggested that the structural phase transition was concomitant with the onset of short-range charge ordering (Douvalis, 2000), and that charge ordering became long-ranged at the magnetic transition (Rivas-Murias, 2006). However, super-structure peaks corresponding to charge-ordering have been observed using X-rays at 270K, above the magnetic transition temperature (Angst, 2007a). There also exists an incommensurately charge-ordered phase from 280K to 340K (Angst, 2007b), that is likely to arise from frustration within the pseudo-triangular lattices along the length of the ribbon (Leanov, 2005).

There remain significant unanswered questions about this system, in particular: whether the magnetic moments order in a ferrimagnetic or canted antiferromagnetic manner; the intra-layer motif of the charge-ordered structure; and the relationship between the magnetic and charge-ordering. The aim of this experiment was to investigate, using neutron powder diffraction and symmetry analysis, the magnetic, structural and charge-order transitions of iron oxyborate.

The chapter is structured as follows: in sections 8.3 and 8.4 we report the method of synthesis and data collection, the results of which are analysed using Rietveld refinement in section 8.5. In section 8.6 we perform a full symmetry analysis of all the phase transitions and discuss the results.

8.3. Synthesis

A powdered sample of iron oxyborate was synthesised following the method of Attfield *et. al.* (1998), in two-steps:

$$Fe_2O_3 + 2H_3BO_3 \longmapsto \text{“}FeBO_3\text{”} + 3H_2O$$
$$3\text{“}FeBO_3\text{”} + Fe + Fe_2O_3 \longmapsto 3Fe_2OBO_3$$

Naturally occurring boron has a high-neutron absorbance due to the ^{10}B isotope; the neutron absorbance of ^{11}B is six orders of magnitude smaller (3835barn vs 0.0055barn for 2200 m/s neutrons (Sears, 1992)). To minimise the sample absorbance, thereby improving the counting statistics during data collection, 99.95% isotopically enriched $H_3{}^{11}BO_3$ (supplied by Cambridge Isotope Laboratories[1]) was used in the synthesis.

32.2mmol of powdered Fe_2O_3 was ground in an agate pestle and mortar with 64.3mmol of H_3BO_3, placed in a crucible boat and heated to 700°C using a muffle furnace. On reaching 700°C the heater element was turned off and the mixture left in the closed furnace to cool. The intermediate formed was analysed by X-ray diffraction on a D5000 laboratory diffractometer, in a flat plane geometry using cobalt K_α radiation[2] ($\lambda = 1.7902$Å). Comparison of the diffraction data with the D5000's diffraction library (ICCD, 2009) showed it to consist predominately of B_2O_3 and Fe_2O_3 with a small amount of mixed iron borates; pelleting the mixture did not have any measurable effect on the product's diffraction pattern.

The intermediate mixture was ground with stoichiometric amounts of Fe and Fe_2O_3 powder in a ball mill and separated (initially) into 2g samples that were heated in evacuated, sealed silica tubes at 1050°C for 4 days. The black product of this step was ground and any Fe_3O_4 by-product removed using a magnet. Analysis of

[1] http://www.isotope.com
[2] Copper K_α is not appropriate for iron containing samples as it lies close to an absorption edge.

the product on the D5000, using the diffractometer's library, showed the remaining product to be primarily iron-oxyborate with a significant impurity phase identified as the Ludwigite $Fe_3O_2BO_3$.

The second step of the synthesis was significantly more difficult than anticipated, largely due to the nature of the borate mixture intermediate. Boron oxide melts at 440°C forming a liquid that can react with silica to form the more brittle and lower melting-point boro-silicate glass. Combined with the vapour pressure of liquefied boron oxide at 1050°C this caused many of the silica tubes to fail.

A number of steps were taken to prevent tube explosions. First, the reactants were wrapped in a platinum foil jacket to keep the boron oxide off the surface of the silica. Second, pressure within the tube was moderated by using smaller samples in each silica tube (0.5g). Third, 10mm thick silica was used to form the tubes (twice the standard 5mm). While these steps stabilized the reaction, the synthesis generated significant amounts of two by-products; Fe_3O_4 and $Fe_3O_2BO_3$. The iron-oxide impurity was removed using a permanent magnet, but the Ludwigite could not be separated and formed an impurity phase in the collected diffraction data. Due to these synthetic problems each sample was kept separately.

8.4. Experimental

Several samples were taken to the D2B diffractometer at the Institut Laue Langevin and diffraction data was collected from them for 1 hour. After inspecting the collected data, and under advice from the instrumental support staff, the samples were determined to be sufficiently different that they should not be mixed. Instead, the product showing the smallest impurity phase fraction was used.

The experimental sample weighed 0.240g and its small size had a significant negative impact upon the statistics of our data. It was loaded into a cylindrical vanadium

canister with an internal diameter of 3mm, and data was collected at four temperatures (140K, 200K, 330K, 350K) using a standard crystat/cryofurnace. Diffraction data was collected at each temperature using neutrons with a wavelength of 1.6Å for 8 hours. The magnetic phase (140K) was then scanned a second time using neutrons with a wavelength of 2.4Å as this gave a greater resolution at large d-spacing.

8.5. Results and analysis

The diffraction data collected on D2B were analysed using FullProf (Rodriguez-Cavajal, 1993). Refinement showed that there were two significant contaminants in the data: peaks from the cryostat's aluminium sample container; and peaks from a second phase, identified as iron Ludwigite: $Fe_3O_2BO_3$ (*Pbam*, a=9.42, b=12.299, c=3.073) , Mir (2006). The diffraction peaks from the impurities, combined with the poor counting statistics from a small sample, made the analysis considerably more difficult. Further, the narrow peaks were not well modelled by any of Fullprof's peak profile functions. We attempted to fit the data using the alternate peak profile functions in GSAS (Larson, 1994), however GSAS refinements proved unstable with respect to both atomic positions and thermal parameters.

Reasonable fits to the data sets at each temperature were achieved, and are presented in Tables 8.3 - 8.2, Figures 8.2-8.5. The final χ^2 parameters for the 350K, 330K and 200K data were: 2.5, 2.518 and 2.482 (Table 8.1). We had hoped to observe some change in the structure of the oxyborate at the incommensurate charge-ordering phase transition at around 340K. However there is no significant difference between the structures refined using data at 330K and 350K. The structure of Fe_2OBO_3 at each temperature was in good agreement with that of previous work (Attfield, 1992), as were the structures of $Fe_3O_2BO_3$ (Mir, 2006) and Al. The thermal parameters of Al are large at every temperature because the aluminium can was poorly crystalline, causing its diffraction peaks to be broad and diffuse.

$T(K)$	Phase	Brag R (%)	RF-factor(%)	χ^2
350	Fe_2OBO_3	7.560	5.833	
	$Fe_3O_2BO_3$	14.87	9.363	
	Al	3.169	0.259	2.50
330	Fe_2OBO_3	7.467	5.751	
	$Fe_3O_2BO_3$	15.90	9.572	
	Al	1.859	0.168	2.518
200	Fe_2OBO_3	7.480	4.977	
	$Fe_3O_2BO_3$	11.95	7.082	
	Al	3.248	0.371	2.482
140	Fe_2OBO_3	4.964	3.307	
	Magnetic Phase	8.602	–	
	$Fe_3O_2BO_3$	7.801	5.060	
	Al	3.004	0.352	2.134

TABLE 8.1. The goodness of fit parameters for the data refinements of the iron oxyborate sample at each experimental temperature. χ^2 is a measure of the fit of the overall data set, while the R and RF-factors measure the statistical fit of individual phases.

$T(K)$	Phase	S. G.	a(Å)	b(Å)	c(Å)	$\alpha(^\circ)$	$\beta(^\circ)$	$\gamma(^\circ)$
350	Fe_2OBO_3	$Pmcn$	3.17381(3)	9.39019(9)	9.24376(9)	90	90	90
	$Fe_3O_2BO_3$	$Pbam$	9.4520(3)	12.2992(5)	3.0728(1)	90	90	90
	Al	$Fm\bar{3}m$	4.0108(4)	4.0108(4)	4.0108(4)	90	90	90
330	Fe_2OBO_3	$Pmcn$	3.1738(1)	9.3902(1)	9.2438(1)	90	90	90
	$Fe_3O_2BO_3$	$Pbam$	9.4519(4)	12.2989(6)	3.0728(1)	90	90	90
	Al	$Fm\bar{3}m$	4.0108(5)	4.0108(5)	4.0108(5)	90	90	90
200	Fe_2OBO_3	$P2_1/c$	3.16921(3)	9.37398(9)	9.23398(9)	90	90.4255(6)	90
	$Fe_3O_2BO_3$	$Pbnm$	9.4381(1)	12.2726(2)	6.1446(2)	90	90	90
	Al	$Fm\bar{3}m$	3.9968(4)	3.9968(4)	3.9968(4)	90	90	90
140	Fe_2OBO_3	$P2_1/c$	3.16716(3)	9.37486(7)	9.240191	90	90.4141(6)	90
	$Fe_3O_2BO_3$	$Pbnm$	9.4415(5)	12.2711(7)	6.1457(3)	90	90	90
	Al	$Fm\bar{3}m$	3.9932(4)	3.9932(4)	3.9932(4)	90	90	90

TABLE 8.2. The space groups and refined lattice parameters all phases identified in the diffraction data.

Atom	x	y	z	B_{iso}
Fe(1)	0.7500	0.0679(4)	0.1177(5)	1.41(7)
Fe(2)	0.2500	0.1960(5)	0.3990(5)	1.47(7)
B(1)	0.7500	0.3787(9)	0.1654(5)	0.65(8)
O(1)	0.2500	0.118(1)	0.9871(7)	1.8(1)
O(2)	0.2500	0.0084(8)	0.2645(9)	1.6(1)
O(3)	0.7500	0.2507(7)	0.2423(8)	1.6(1)
O(4)	0.7500	0.371(1)	0.0181(7)	1.8(1)

Atom	x	y	z	B_{iso}
Al(1)	0.00000	0.00000	0.00000	42(6)

Atom	x	y	z	B_{iso}
Fe(1)	0.0000	0.0000	0.0000	4.1(7)
Fe(2)	0.5000	0.0000	0.5000	0.4(4)
Fe(3)	0.999(3)	0.270(2)	0.0000	3.3(4)
Fe(4)	0.741(2)	0.392(1)	0.5000	0.9(2)
B(1)	0.266(2)	0.368(2)	0.5000	0.0(4)
O(1)	0.649(4)	0.433(3)	0.5000	1.2(4)
O(2)	0.395(3)	0.073(2)	0.0000	0.8(4)
O(3)	0.621(3)	0.132(2)	0.5000	1.3(5)
O(4)	0.106(5)	0.154(4)	0.0000	2.1(7)
O(5)	0.841(3)	0.241(2)	0.5000	0.5(4)

TABLE 8.3. The refined atomic parameters of Fe_2OBO_3, $Fe_3O_2BO_3$ and Al (top, middle, bottom) at 350K. Lattice parameters are given in Table 8.2.

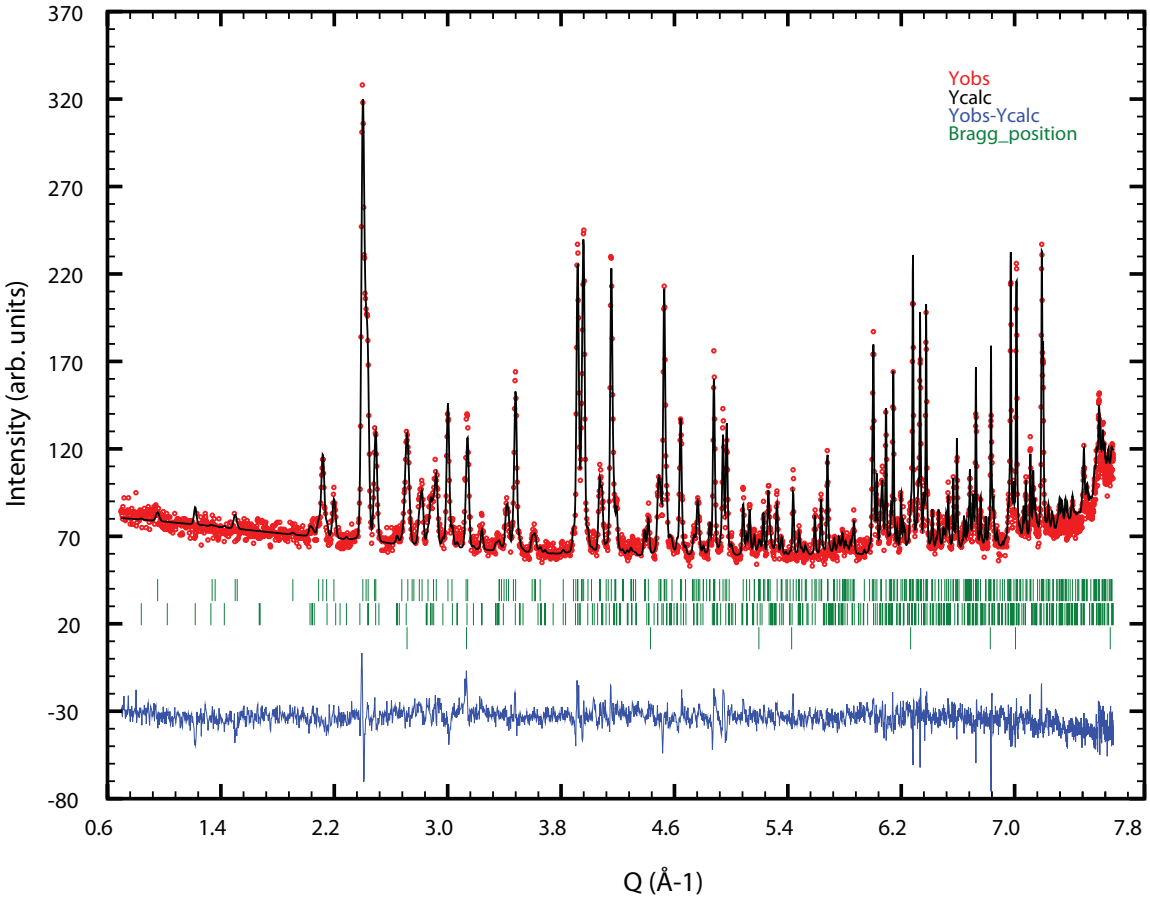

FIGURE 8.2. The Rietveld refinement of neutron diffraction data collected on the D2B diffractometer at 350K, $\lambda = 1.6$Å. The refined values of the sample parameters are listed in Tables 8.3 and 8.2.

Atom	x	y	z	B_{iso}
Fe(1)	0.7500	0.0676(4)	0.1176(6)	1.39(8)
Fe(2)	0.2500	0.1960(5)	0.3989(6)	1.47(7)
B(1)	0.7500	0.379(1)	0.1653(6)	0.61(8)
O(1)	0.2500	0.119(1)	0.9870(8)	1.8(1)
O(2)	0.2500	0.0086(8)	0.264(1)	1.7(1)
O(3)	0.7500	0.2508(8)	0.2421(9)	1.5(1)
O(4)	0.7500	0.371(1)	0.0186(8)	1.8(1)

Atom	x	y	z	B_{iso}
Fe(1)	0.0000	0.0000	0.0000	3.4(9)
Fe(2)	0.5000	0.0000	0.5000	0.4(4)
Fe(3)	0.995(5)	0.278(3)	0.0000	2.5(6)
Fe(4)	0.740(2)	0.391(5)	0.5000	0.5(3)
B(1)	0.267(3)	0.367(3)	0.5000	0.3(3)
O(1)	0.646(5)	0.433(3)	0.5000	0.9(5)
O(2)	0.395(3)	0.075(2)	0.0000	1.2(5)
O(3)	0.622(3)	0.132(3)	0.5000	1.7(4)
O(4)	0.104(5)	0.157(4)	0.0000	1.9(5)
O(5)	0.841(3)	0.241(2)	0.5000	0.5(4)

Atom	x	y	z	B_{iso}
Al(1)	0.00000	0.00000	0.00000	43(8)

TABLE 8.4. The refined atomic parameters of Fe_2OBO_3, $Fe_3O_2BO_3$ and Al (top, middle, bottom) at 330K. Lattice parameters are given in Table 8.2.

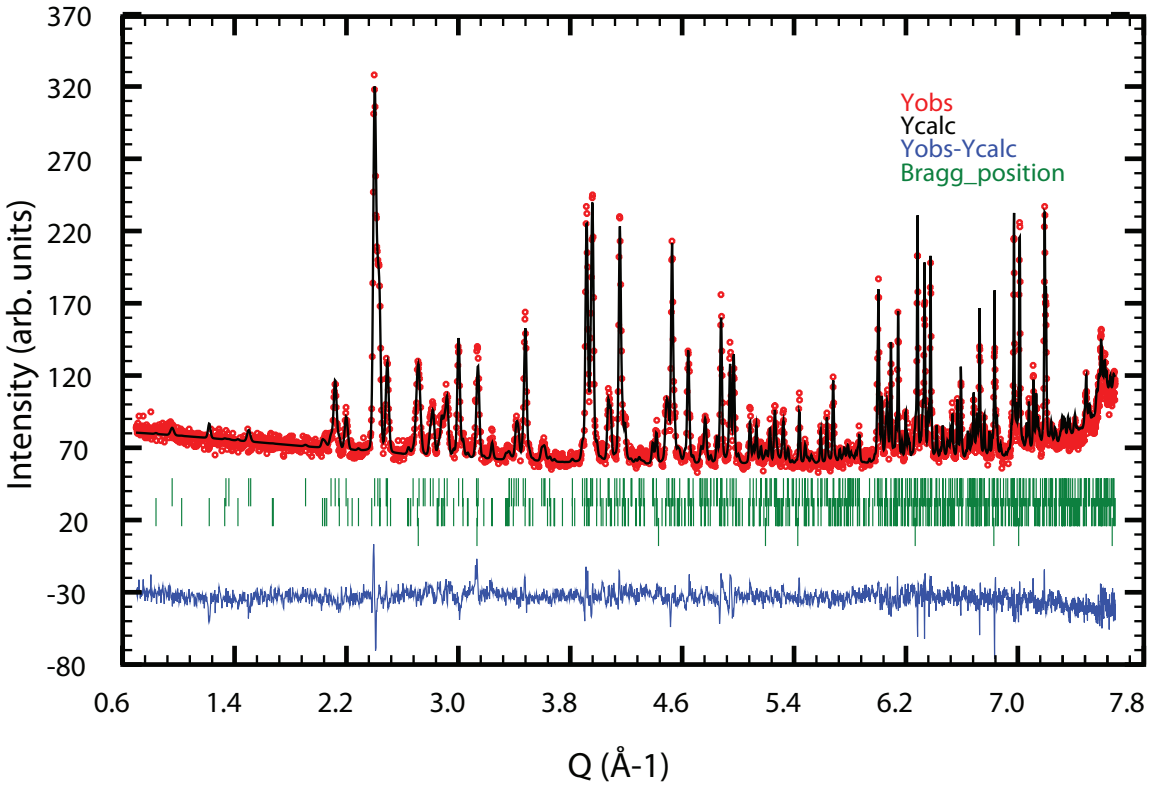

FIGURE 8.3. The Rietveld refinement of neutron diffraction data collected on the D2B diffractometer at 330K, $\lambda = 1.6$Å. The refined values of the sample parameters are listed in Tables 8.4 and 8.2.

Atom	x	y	z	B_{iso}
Fe(1)	0.755(2)	0.0683(4)	0.1173(5)	0.37(6)
Fe(2)	0.248(2)	0.1986(4)	0.3963(6)	0.81(7)
B(1)	0.743(2)	0.3733(8)	0.1635(6)	0.19(8)
O(1)	0.239(2)	0.118(1)	0.9892(9)	1.3(1)
O(2)	0.242(4)	0.0120(7)	0.269(1)	1.3(1)
O(3)	0.752(3)	0.2510(6)	0.2425(8)	0.7(1)
O(4)	0.747(2)	0.3720(9)	0.0176(6)	0.5(1)

Atom	x	y	z	B_{iso}
Al(1)	0.0000	0.0000	0.0000	50(8)

Atom	x	y	z	B_{iso}
Fe(1)	0.5000	0.5000	0.0000	3.3(4)
Fe(2)	0.979(4)	0.50201	0.2500	2.9(5)
Fe(3)	0.997(3)	0.72360	0.005(9)	4.4(5)
Fe(4a)	0.740(7)	0.40663	0.2500	3(1)
Fe(4b)	0.271(3)	0.62228	0.2500	2.4(5)
B(1)	0.748(5)	0.65806	0.2500	2.9(8)
B(2)	0.267(3)	0.371(2)	0.2500	0.3(3)
O(1a)	0.637(3)	0.551(2)	0.2500	0.3(3)
O(1b)	0.354(5)	0.432(4)	0.2500	0.8(8)
O(2)	0.136(2)	0.580(2)	0.988(6)	0.7(3)
O(3a)	0.857(6)	0.643(6)	0.2500	1.8(3)
O(3b)	0.083(5)	0.373(4)	0.2500	1.4(8)
O(4)	0.588(3)	0.366(3)	0.023(3)	1.9(4)
O(5a)	0.87(1)	0.240(8)	0.2500	5(1)
O(5b)	0.176(7)	0.756(5)	0.2500	5.2(8)

TABLE 8.5. The refined atomic parameters of Fe_2OBO_3, Al and $Fe_3O_2BO_3$ (top left, bottom left, right) at 200K. The lattice parameters are given in Table 8.2.

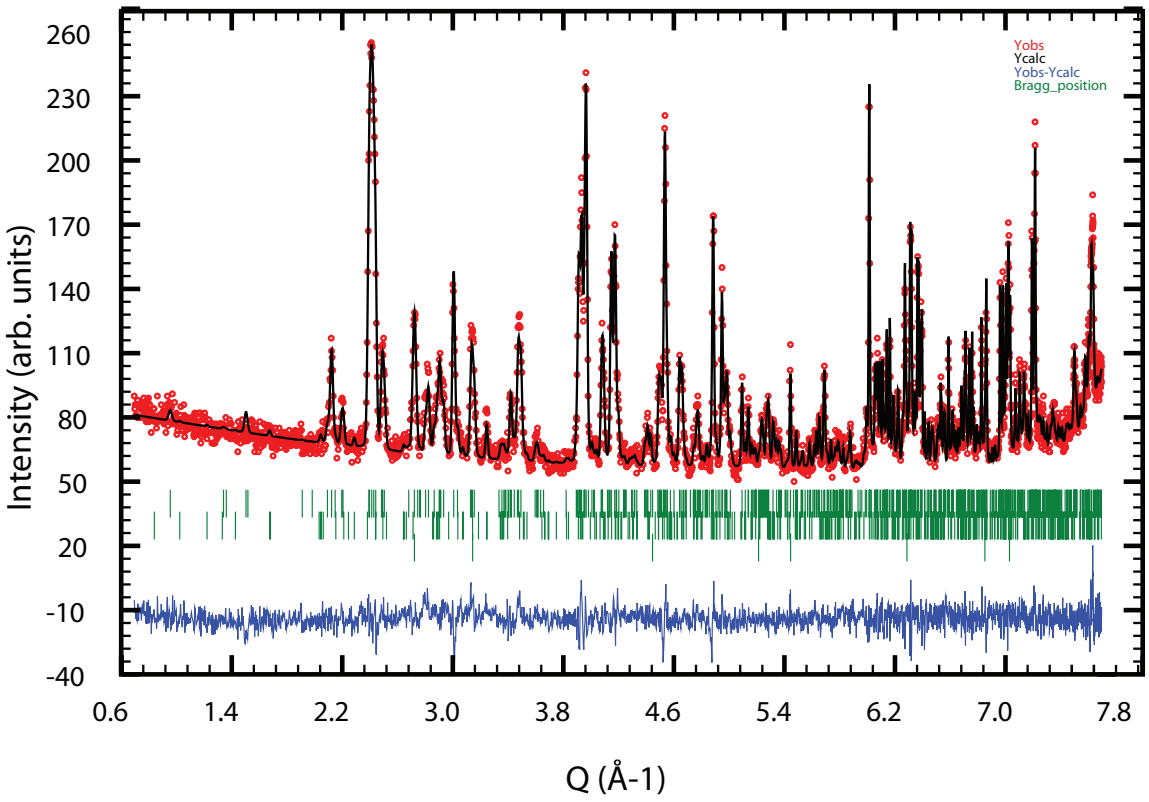

FIGURE 8.4. The Rietveld refinement of neutron diffraction data collected on the D2B diffractometer at 200K, $\lambda = 1.6$Å . The sample parameters are listed in Tables 8.5 and 8.2.

8.5.1. Determination of the magnetic ordering

The diffraction data collected at 140k was initially compared to the nuclear-only structural model refined from the 200K diffraction data. As iron oxyborate does not undergo a structural phase transition over this temperature range, any additional diffraction peaks, or peak intensity, can be attributed to long-range magnetic order. This step revealed three distinct "magnetic"[3] peaks in the range $Q = 0.6$ to 1.6 Å $^{-1}$ (Fig. 8.5). Our analysis of the magnetic ordering focused on fitting these peaks using symmetry modes from SARAh (Wills, 2000) within Fullprof.

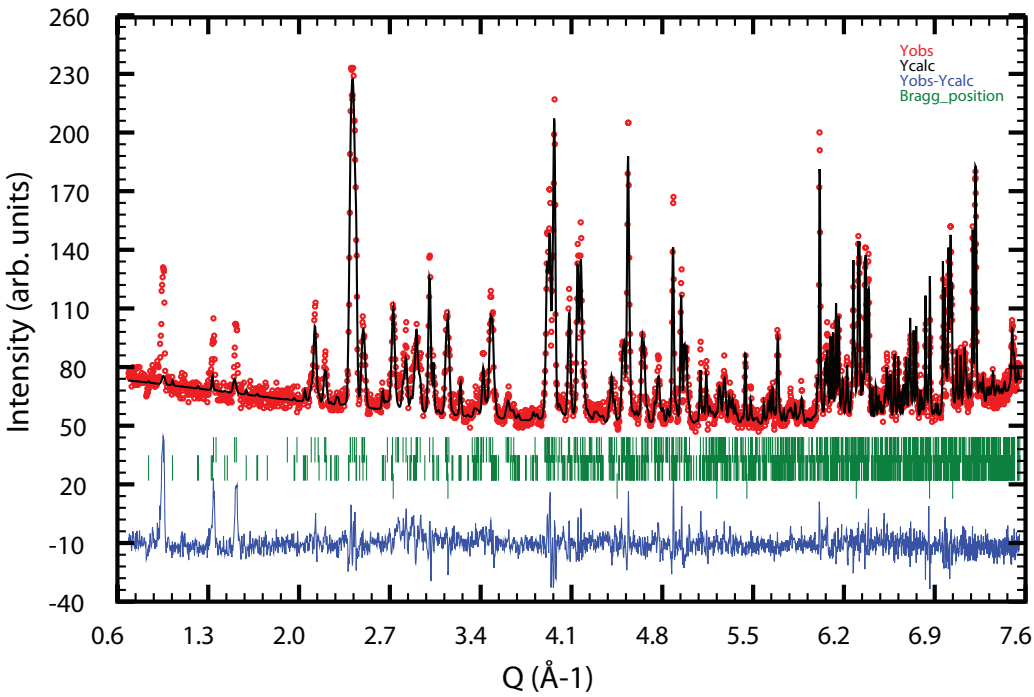

FIGURE 8.5. The Rietveld refinement of neutron diffraction data collected on the D2B diffractometer at 140K, $\lambda = 2.4$Å . The structural parameters from the 200K refinement, Table 8.5, were used without a magnetic phase. Three distinct magnetic peaks are observed in the range $Q = 0.6$ to 1.6Å $^{-1}$.

[3]These are not magnetic peaks in the usual sense: that they arise from an increase in the system's unit cell parameters. In this case they correspond to peaks for which almost all of the intensity can be attributed to the long-range magnetic order and not nuclear diffraction.

I.R.	E	C_{2x}	C_{2y}	C_{2z}	I	σ_x	σ_y	σ_z
Γ_1	1	1	1	1	1	1	1	1
Γ_2	1	1	1	1	−1	−1	−1	−1
Γ_3	1	1	−1	−1	1	1	−1	−1
Γ_4	1	1	−1	−1	−1	−1	1	1
Γ_5	1	−1	1	−1	1	−1	1	−1
Γ_6	1	−1	1	−1	−1	1	−1	1
Γ_7	1	−1	−1	1	1	−1	−1	1
Γ_8	1	−1	−1	1	−1	1	1	−1

TABLE 8.6. The irreducible representations of the space group $Pnma$, ordering under $\vec{k} = (0, 0, 0)$. These are the small irreducible representations from the tables of Kovalev (1993).

The parent, non-magnetic phase has the symmetry $P2_1/c$ and the observation of an uncompensated magnetic moment (Attfield *et. al.*) requires the magnetic k-vector to be $(0, 0, 0)$. This k-vector corresponds to the little group $\mathbb{G}_k = \mathbb{G}_0$, as $\vec{k}$ is invariant under every operation in the point-group $\mathbb{H}_0$. The operators and irreducible representations of this group are given in Table 8.6 and, as the little group contains the inversion operator, anti-unitary symmetry does not expand the group or alter the basis vectors. For the $P12_1/c1$ phase, both iron atoms are in the (x, y, z) Wyckoff position and so have the same decomposition and basis vectors. The basis vectors that define axial vectors upon the (x, y, z) position are listed in Table 8.7, corresponding to the decomposition (the IR notation follows Kovalev, 1993):

$$\Gamma = 3\Gamma_1^{(1)} + 3\Gamma_2^{(1)} + 3\Gamma_3^{(1)} + 3\Gamma_4^{(1)}$$

Four refinements of the 140K data were performed within Fullprof, each using all the basis vectors from a single irreducible representation (Fig 8.6). From these refinements it was clear that Γ_3 was sufficient to fit the magnetic phase. Refinements using Γ_1 and Γ_2 generated too litte intensity upon the $(0, 2, 0)$ peaks. The Γ_4 refinement left small but significant residuals at three peaks, while refinement using the Γ_3 closely matched the observed data at all of the peaks in this Q range.

B.V.	A_1	A_2	A_3	A_4	*B.V.*	A_1	A_2	A_3	A_4
$\psi^1_{11}(x)$	$\begin{pmatrix}1\\0\\0\end{pmatrix}$	$\begin{pmatrix}\bar{1}\\0\\0\end{pmatrix}$	$\begin{pmatrix}1\\0\\0\end{pmatrix}$	$\begin{pmatrix}\bar{1}\\0\\0\end{pmatrix}$	$\psi^3_{11}(x)$	$\begin{pmatrix}1\\0\\0\end{pmatrix}$	$\begin{pmatrix}1\\0\\0\end{pmatrix}$	$\begin{pmatrix}1\\0\\0\end{pmatrix}$	$\begin{pmatrix}1\\0\\0\end{pmatrix}$
$\psi^1_{11}(y)$	$\begin{pmatrix}0\\1\\0\end{pmatrix}$	$\begin{pmatrix}0\\1\\0\end{pmatrix}$	$\begin{pmatrix}0\\1\\0\end{pmatrix}$	$\begin{pmatrix}0\\1\\0\end{pmatrix}$	$\psi^3_{11}(y)$	$\begin{pmatrix}0\\1\\0\end{pmatrix}$	$\begin{pmatrix}0\\\bar{1}\\0\end{pmatrix}$	$\begin{pmatrix}0\\1\\0\end{pmatrix}$	$\begin{pmatrix}0\\\bar{1}\\0\end{pmatrix}$
$\psi^1_{11}(z)$	$\begin{pmatrix}0\\0\\1\end{pmatrix}$	$\begin{pmatrix}0\\0\\\bar{1}\end{pmatrix}$	$\begin{pmatrix}0\\0\\1\end{pmatrix}$	$\begin{pmatrix}0\\0\\\bar{1}\end{pmatrix}$	$\psi^3_{11}(z)$	$\begin{pmatrix}0\\0\\1\end{pmatrix}$	$\begin{pmatrix}0\\0\\1\end{pmatrix}$	$\begin{pmatrix}0\\0\\\bar{1}\end{pmatrix}$	$\begin{pmatrix}0\\0\\\bar{1}\end{pmatrix}$
$\psi^2_{11}(x)$	$\begin{pmatrix}1\\0\\0\end{pmatrix}$	$\begin{pmatrix}\bar{1}\\0\\0\end{pmatrix}$	$\begin{pmatrix}\bar{1}\\0\\0\end{pmatrix}$	$\begin{pmatrix}1\\0\\0\end{pmatrix}$	$\psi^4_{11}(x)$	$\begin{pmatrix}1\\0\\0\end{pmatrix}$	$\begin{pmatrix}1\\0\\0\end{pmatrix}$	$\begin{pmatrix}\bar{1}\\0\\0\end{pmatrix}$	$\begin{pmatrix}\bar{1}\\0\\0\end{pmatrix}$
$\psi^2_{11}(y)$	$\begin{pmatrix}0\\1\\0\end{pmatrix}$	$\begin{pmatrix}0\\1\\0\end{pmatrix}$	$\begin{pmatrix}0\\\bar{1}\\0\end{pmatrix}$	$\begin{pmatrix}0\\\bar{1}\\0\end{pmatrix}$	$\psi^4_{11}(y)$	$\begin{pmatrix}0\\1\\0\end{pmatrix}$	$\begin{pmatrix}0\\\bar{1}\\0\end{pmatrix}$	$\begin{pmatrix}0\\\bar{1}\\0\end{pmatrix}$	$\begin{pmatrix}0\\1\\0\end{pmatrix}$
$\psi^2_{11}(z)$	$\begin{pmatrix}0\\0\\1\end{pmatrix}$	$\begin{pmatrix}0\\0\\\bar{1}\end{pmatrix}$	$\begin{pmatrix}0\\0\\\bar{1}\end{pmatrix}$	$\begin{pmatrix}0\\0\\1\end{pmatrix}$	$\psi^4_{11}(z)$	$\begin{pmatrix}0\\0\\1\end{pmatrix}$	$\begin{pmatrix}0\\0\\1\end{pmatrix}$	$\begin{pmatrix}0\\0\\\bar{1}\end{pmatrix}$	$\begin{pmatrix}0\\0\\\bar{1}\end{pmatrix}$

TABLE 8.7. Basis vectors of the $P12_1/c1$ phase, $\vec{k} = (0,0,0)$. These basis vectors represent the ordering of axial vectors on the Wyckoff position: $A_1 = (x,y,z)$, $A_2 = (\bar{x}+\frac{1}{2},\bar{y},z+\frac{1}{2})$, $A_3 = (\bar{x},\bar{y},\bar{z})$, $A_4 = (x+\frac{1}{2},y,\bar{z}+\frac{1}{2})$.

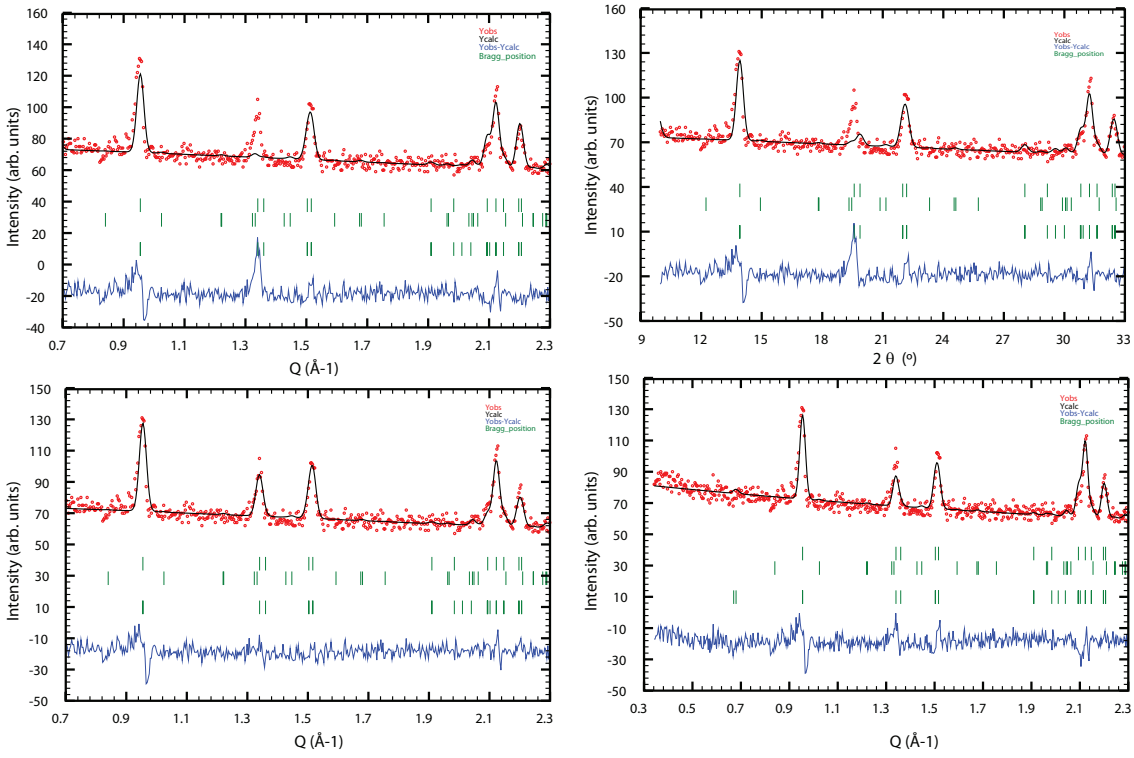

FIGURE 8.6. These plots show the best fits for the three distinct magnetic peaks in the 140K data set, using basis vectors from only a single irreducible representation. The fits made use of Γ_1, Γ_2, Γ_3 and Γ_4 (top-left, top-right, bottom-left, bottom-right). It is clear that Γ_3 is sufficient to fit these peaks.

Further refinements showed that the $\psi^3_{11}(y)$ basis-vector was sufficient to define the magnetic order at both iron positions, with coefficients 2.5(1) and -1.9(1) upon Fe(1) and Fe(2) (Figure 8.8). This corresponds to a ferrimagnetic arrangement of spins aligned parallel to the a-axis (Figure 8.7). Once the magnetic ordering was determined, the other structural parameters were allowed to refine simultaneously, and the refined structure is reported in Table 8.8.

Other models of the magnetic ordering, having non-zero k-vectors, were considered using SARAh-Refine's k-vector search function (Wills, 2009). This routine performs a Monte-Carlo type search for possible magnetic ordering with each k-vector type in the Brillouin zone. Performing 500 cycles at each special point in the Brillouin zone failed to generate any feasible alternative magnetic structures. From this we conclude that the k-vector assigned on the basis of SQUID data best fits the observed powder-diffraction data.

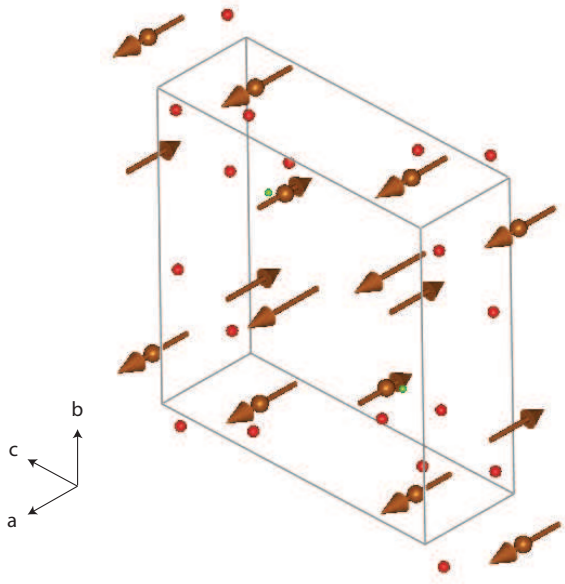

FIGURE 8.7. A graphical representation of the ferrimagnetic structure of iron oxyborate, with moments parallel to the a-axis.

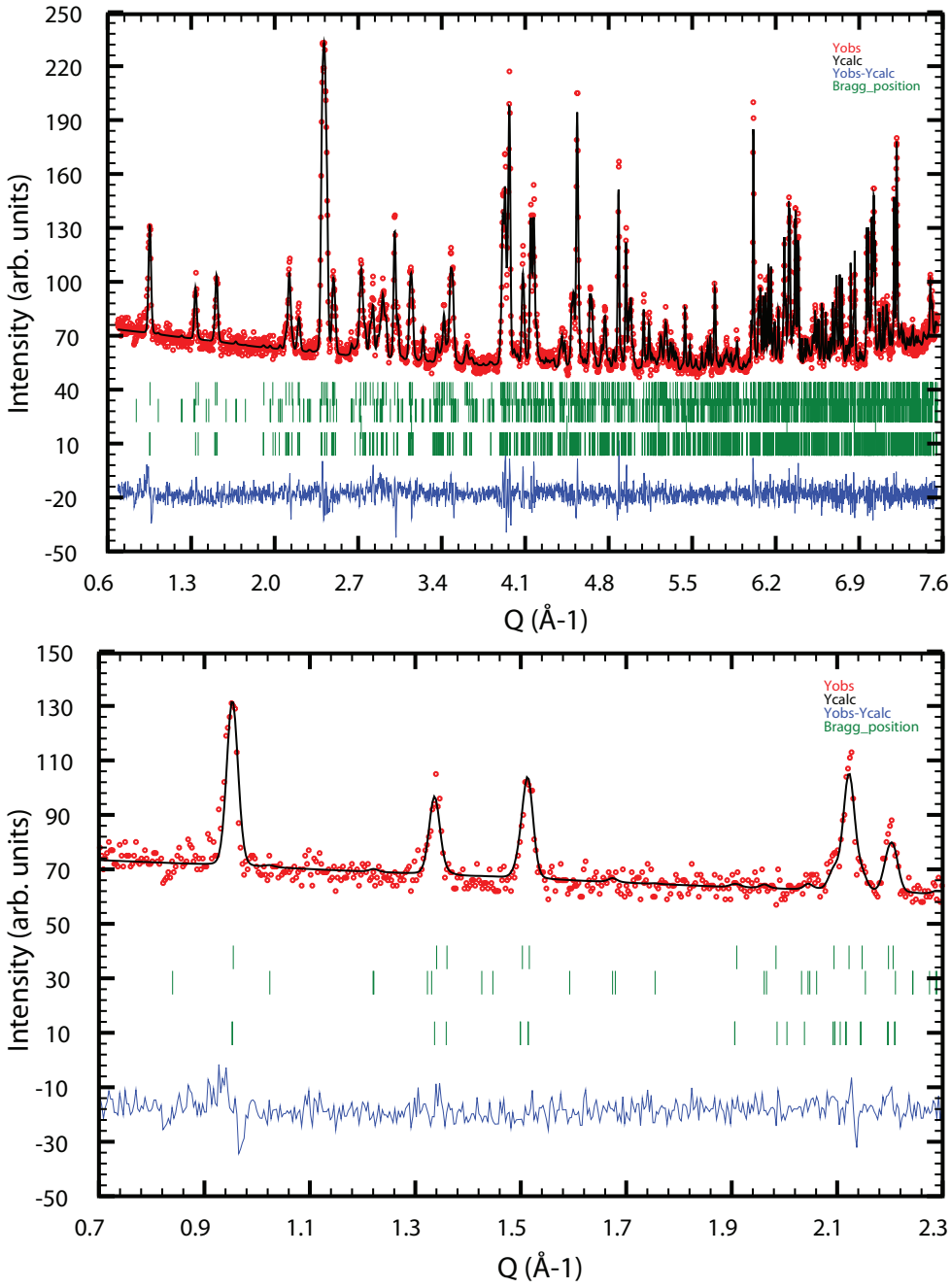

FIGURE 8.8. The Rietveld refinement of neutron diffraction data collected on the D2B diffractometer at 140K, $\lambda = 2.4$Å , modelling the magnetic phase defined with the basis vector $\psi^{\nu}_{11}(y)$ at both iron atoms. The refined values of the sample parameters are listed in Tables 8.8 and 8.2.

Atom	x	y	z	β_{11}	β_{22}	β_{33}	β_{12}	β_{13}	β_{23}
Fe(1)	0.751(2)	0.0673(6)	0.1179(8)	0.018(6)	0.0012(6)	0.0014(7)	0.000(2)	0.000(2)	0.0004(6)
Fe(2)	0.248(3)	0.1970(6)	0.3985(8)	0.000(8)	0.0188(6)	0.0012(8)	0.000(2)	0.005(2)	0.0000(7)
B(1)	0.742(3)	0.378(3)	0.1650(9)	0.024(1)	0.000(7)	0.0001(9)	0.000(4)	0.000(2)	0.0000(9)
O(1)	0.248(4)	0.117(2)	0.986(1)	0.03(1)	0.003(1)	0.003(1)	0.000(4)	0.003(3)	0.003(1)
O(2)	0.253(5)	0.011(1)	0.262(1)	0.05(1)	0.002(1)	0.004(1)	0.000(4)	−0.009(3)	0.001(1)
O(3)	0.754(5)	0.2501(9)	0.242(1)	0.05(1)	0.002(1)	0.004(1)	−0.001(3)	−0.002(3)	−0.003(1)
O(4)	0.744(4)	0.375(2)	0.0192(9)	0.034(8)	0.003(1)	0.003(1)	0.000(4)	0.000(3)	0.003(1)

Atom	x	y	z	β_{11}	β_{22}	β_{33}	β_{12}	β_{13}	β_{23}
Fe(1)	0.5000	0.5000	0.0000	0.00(7)	0.007(5)	0.01(1)	0.003(5)	−0.010(9)	−0.008(9)
Fe(2)	0.98(1)	0.50(1)	0.2500	0.01(1)	0.004(5)	0.02(1)	−0.005(8)	0.0000	0.0000
Fe(3)	0.005(4)	0.725(3)	0.986(7)	0.011(6)	0.003(2)	0.02(1)	−0.004(3)	−0.013(9)	0.006(5)
Fe(4a)	0.746(9)	0.399(5)	0.2500	0.005(9)	0.003(4)	0.03(2)	0.000(5)	0.0000	0.0000
Fe(4b)	0.264(8)	0.616(2)	0.2500	0.012(2)	0.000(3)	0.02(2)	0.00(4)	0.0000	0.0000
B(1)	0.75(1)	0.649(6)	0.2500	0.008(9)	0.000(3)	0.2(1)	0.010(2)	0.0000	0.0000
B(2)	0.270(9)	0.370(7)	0.2500	0.00(1)	0.001(5)	0.01(2)	−0.003(6)	0.0000	0.0000
O(1a)	0.650(9)	0.558(5)	0.2500	0.001(1)	0.005(4)	0.001(4)	0.003(4)	0.0000	0.0000
O(1b)	0.34(1)	0.457(6)	0.2500	0.00(9)	0.006(5)	0.22(9)	0.002(5)	0.0000	0.0000
O(2)	0.124(9)	0.57(2)	0.00(1)	0.02(1)	0.013(4)	0.00(1)	−0.003(6)	0.00(1)	0.010(9)
O(3a)	0.88(1)	0.658(8)	0.2500	0.00(1)	0.004(6)	0.02(3)	0.004(5)	0.0000	0.0000
O(3b)	0.11(1)	0.369(6)	0.2500	0.03(1)	0.02(3)	0.02(2)	0.00(6)	0.0000	0.0000
O(4)	0.587(2)	0.37(6)	0.96(1)	0.01(1)	0.01(1)	0.01(4)	−0.01(1)	0.01(2)	−0.01(2)
O(5a)	0.87(5)	0.20(4)	0.2500	0.4(2)	0.3(1)	0.02(5)	−0.3(1)	0.0000	0.0000
O(5b)	0.143(9)	0.755(2)	0.2500	0.00(1)	0.000(4)	0.03(1)	0.010(5)	0.0000	0.0000

Atom	x	y	z	B_{iso}
Al(1)	0.00000	0.00000	0.00000	42(10)

TABLE 8.8. The refined atomic parameters of Fe_2OBO_3, $Fe_3O_2BO_3$ and Al (top, middle, bottom) at 140K. The lattice parameters are given in Table 8.2.

The refined magnetic structure is in agreement with that of Attfield *et. al*, but with reduced moment size. For a system of mixed Fe^{2+} and Fe^{3+} we would expect a moment size of of 4-5μ_B, rather than the 2-2.5μ_B observed. Possible explanations of this reduced moment are delocalization of the electron density on the iron, or a dynamic spin state in which the moments precess about the a-axis. Further work, possibly using inelastic neutron scattering or muon spin resonance, is required to identify cause of the reduced moments.

Analysis of our diffraction data has confirmed the atomic structure of iron borate above and below the magnetic transitions to be that presented by Atfield *et. al*. In particular the structure shows no evidence of the canted-magnetic structure suggested by Suda (2003), but is well modelled by a ferrimagnetic ordering parallel to the a-axis, with a reduced moment at each iron atom. In the next section we make use of the experimental data from this and previous studies to make a full symmetry

analysis of the structural phase transition and the charge-ordering at 140K. We also compare the irreducible representations that the system orders under at each phase transition.

8.6. Symmetry analysis of the phase transitions

Having confirmed the atomic and magnetic structure of iron oxyborate using powder diffraction data, we performed a symmetry analysis of the structural, magnetic and charge-ordering phase transitions and discuss their relations. This section makes use of both current and previous work.

8.6.1. The structural phase transition

Previous studies of iron oxyborate have used the space group $Pmcn$, a non-standard setting of $Pnma$ (62). As SARAh and the tables of Kovalev use the standard settings, some manipulation of the settings is required. Careful consideration of these steps allows identification of the symmetry of the displacive phase transition.

The structural phase transition in iron oxyborate at around 320K does not change the volume of the primitive unit cell, and so is assigned the k-vector $(0, 0, 0)$. The maximal sub-groups of $Pmna$, as listed in the International tables of crystallography - A (2002), reveal two possible paths from $Pmna$ to $P12_1/c1$:

$$Pnma \longmapsto P112_1/a$$
$$\longmapsto P2_1/n11$$

Both $P112_1/a$ and $P2_1/n11$ are alternate settings for $P12_1/c1$, related by opposite rotations of the axis set: $\{z, x, y\}$ and $\{y, z, x\}$ respectively, in the Jones faithful representation. These can be expressed as group sub-group relations, allowing us to

determine the irreducible representations that can represent these transitions. Listing the elements of each space group in the same manner as above:

$$\{E, C_{2x}, C_{2y}, C_{2z}, I, \sigma_x, \sigma_y, \sigma_z\} \supset \{E, C_{2z}, I, \sigma_z\}$$
$$\supset \{E, C_{2x}, I, \sigma_x\}$$

Referring to the irreducible representations of $Pnma$, for $\vec{k} = (0, 0, 0)$ (Table, 8.6), the possible symmetry reductions correspond to Γ_7 and Γ_3 respectively. From the positions of atoms in the lower phase it is clear that there is no redefinition of the axis system during the phase transition. Hence, the axes of $P12_1/c1$ and $Pmcn$ must coincide and we can distinguish between the two possibilities. Consider the following scheme, where $\mathfrak{M}$ is represented by the left-to-right mappings and is the same axis transformation in each case:

$$\begin{array}{ccc} & \mathfrak{M} & \\ P112_1/a & \longmapsto & P12_1/c1 \\ \uparrow & & \uparrow \\ Pnma & \longmapsto & Pmcn \\ \downarrow & & \\ P2_1/n11 & \longmapsto & P112_1/a \end{array}$$

Under $\mathfrak{M}$, $P112_1/a$ becomes $P12_1/c1$ with the same axis system as $Pmcn$, while $P2_1/n11$ becomes $P112_1/a$. The distortion of the system must result in a daughter phase with the symmetry $P112_1/a$ and, therefore, corresponds to Γ_7.

8.6.2. Magnetic ordering

We have already determined that the magnetic moments order under $\psi_{11}^3(x)$ (Table 8.6) from the powder diffraction data. This corresponds to ferrimagnetic ordering, with moments of differing sizes parallel to the a-axis at each of the two iron sites. Table 8.9 lists the axial basis-vectors of the $(x, 0.25, z)$ position in $Pnma$, these are the

same for both iron sites and so are listed only once. The a-axis of $Pmcn$ corresponds to the b-axis in $Pnma$, thus the mode $\psi_{11}^5(y)$ of $Pnma$ is equivalent to $\psi_{11}^3(x)$ in Table 8.6. This is confirmed by their IR tables (taking note of the change of axis for Γ_3, $P112_1/a$):

$I.R.$	E	C_{2x}	C_{2y}	C_{2z}	I	σ_x	σ_y	σ_z
$\Gamma_5, Pnma$	1	-1	1	-1	1	-1	1	-1
$\Gamma_3, P112_1/a$	1			-1	1			-1

We can conclude that, using the basis vectors of $Pnma$, the magnetic structure is ordered ferrimagnetically under the representation Γ_5, according to $\psi_{11}^5(y)$. By bringing the displacive and magnetic phase transitions into equivalent settings we deduce that they order under differing IRs.

8.6.3. Charge ordering

The charge ordering of iron oxyborate is particularly interesting because of the incommensurate phase observed by Angst (2007b), however we cannot determine the charge-ordering motif from the collected powder diffraction data. Instead we will use symmetry arguments based upon the SQUID data reported in previous work to identify the charge-ordering motif in the commensurately charge-ordered phase. If the iron atoms were charge-uniform then the observed anti-parallel magnetic structure would be antiferromagnetic.Consideration of which charge-order motifs can give rise to a net magnetic moment is sufficient to determine the symmetry of the charge ordering.

The presence of charge-order has been confirmed by single-crystal diffraction (Angst 2007a, 2007b). However, the observed k-vector was $(\frac{1}{2}, 0, 0)$ and such a charge-ordering *can not* give rise to a net ferrimagnetic moment. Under $\vec{k} = (\frac{1}{2}, 0, 0)$ any moment arising in a plane from charge-order will be cancelled by the plane above in

B.V.	*Pos.*1	*Pos.*2	*Pos.*3	*Pos.*4
$\psi^1_{11}(y)$	$\begin{pmatrix}0\\2\\0\end{pmatrix}$	$\begin{pmatrix}0\\\bar{2}\\0\end{pmatrix}$	$\begin{pmatrix}0\\2\\0\end{pmatrix}$	$\begin{pmatrix}0\\\bar{2}\\0\end{pmatrix}$
$\psi^2_{11}(x)$	$\begin{pmatrix}2\\0\\0\end{pmatrix}$	$\begin{pmatrix}2\\0\\0\end{pmatrix}$	$\begin{pmatrix}\bar{2}\\0\\0\end{pmatrix}$	$\begin{pmatrix}\bar{2}\\0\\0\end{pmatrix}$
$\psi^2_{11}(z)$	$\begin{pmatrix}0\\0\\2\end{pmatrix}$	$\begin{pmatrix}0\\0\\\bar{2}\end{pmatrix}$	$\begin{pmatrix}0\\0\\\bar{2}\end{pmatrix}$	$\begin{pmatrix}0\\0\\2\end{pmatrix}$
$\psi^3_{11}(x)$	$\begin{pmatrix}2\\0\\0\end{pmatrix}$	$\begin{pmatrix}2\\0\\0\end{pmatrix}$	$\begin{pmatrix}2\\0\\0\end{pmatrix}$	$\begin{pmatrix}2\\0\\0\end{pmatrix}$
$\psi^3_{11}(z)$	$\begin{pmatrix}0\\0\\2\end{pmatrix}$	$\begin{pmatrix}0\\0\\\bar{2}\end{pmatrix}$	$\begin{pmatrix}0\\0\\2\end{pmatrix}$	$\begin{pmatrix}0\\0\\\bar{2}\end{pmatrix}$
$\psi^4_{11}(y)$	$\begin{pmatrix}0\\2\\0\end{pmatrix}$	$\begin{pmatrix}0\\\bar{2}\\0\end{pmatrix}$	$\begin{pmatrix}0\\\bar{2}\\0\end{pmatrix}$	$\begin{pmatrix}0\\2\\0\end{pmatrix}$
$\psi^5_{11}(y)$	$\begin{pmatrix}0\\2\\0\end{pmatrix}$	$\begin{pmatrix}0\\2\\0\end{pmatrix}$	$\begin{pmatrix}0\\2\\0\end{pmatrix}$	$\begin{pmatrix}0\\2\\0\end{pmatrix}$
$\psi^6_{11}(x)$	$\begin{pmatrix}2\\0\\0\end{pmatrix}$	$\begin{pmatrix}\bar{2}\\0\\0\end{pmatrix}$	$\begin{pmatrix}\bar{2}\\0\\0\end{pmatrix}$	$\begin{pmatrix}2\\0\\0\end{pmatrix}$
$\psi^6_{11}(z)$	$\begin{pmatrix}0\\0\\2\end{pmatrix}$	$\begin{pmatrix}0\\0\\2\end{pmatrix}$	$\begin{pmatrix}0\\0\\\bar{2}\end{pmatrix}$	$\begin{pmatrix}0\\0\\\bar{2}\end{pmatrix}$
$\psi^7_{11}(x)$	$\begin{pmatrix}2\\0\\0\end{pmatrix}$	$\begin{pmatrix}\bar{2}\\0\\0\end{pmatrix}$	$\begin{pmatrix}2\\0\\0\end{pmatrix}$	$\begin{pmatrix}\bar{2}\\0\\0\end{pmatrix}$
$\psi^7_{11}(z)$	$\begin{pmatrix}0\\0\\2\end{pmatrix}$	$\begin{pmatrix}0\\0\\2\end{pmatrix}$	$\begin{pmatrix}0\\0\\2\end{pmatrix}$	$\begin{pmatrix}0\\0\\2\end{pmatrix}$
$\psi^8_{11}(y)$	$\begin{pmatrix}0\\2\\0\end{pmatrix}$	$\begin{pmatrix}0\\2\\0\end{pmatrix}$	$\begin{pmatrix}0\\\bar{2}\\0\end{pmatrix}$	$\begin{pmatrix}0\\\bar{2}\\0\end{pmatrix}$

TABLE 8.9. The basis vectors of Pnma, ordering under $\vec{k} = (0, 0, 0)$. The basis vectors represent the ordering of an axial vector on the equivalent positions $(0.1176, 0.75, 0.0676)$ and $(0.3989, 0.25, 0.1960)$, both of which have four distinct images under the operations of the space group.

which the charge-order (and so the ferrimagnetism) is reversed. Indeed, only charge-ordering under $\vec{k} = (0, 0, 0)$ could give rise to a net ferrimagnetic moment. Such an ordering would be almost unobservable because the diffraction cross-sections of Fe^{2+} and Fe^{3+} are nearly identical, and it would not give rise to any new peaks in the diffraction pattern.

By calculating the possible charge-ordering schemes using the basis-vectors for a *scalar* property, we can determine which IR the charge orders under. The possible charge-ordering schemes are depicted in Fig. 8.9, and it is clear that only Γ_1 gives rise to a net ferrimagnetic moment within the plane; all the other symmetry modes form a pattern of charge for which there is no net-magnetic moment. The net-magnetisation must, therefore, arise from a charge-ordering phenomena with a k-vector of $(0, 0, 0)$ and the symmetry of Γ_1.

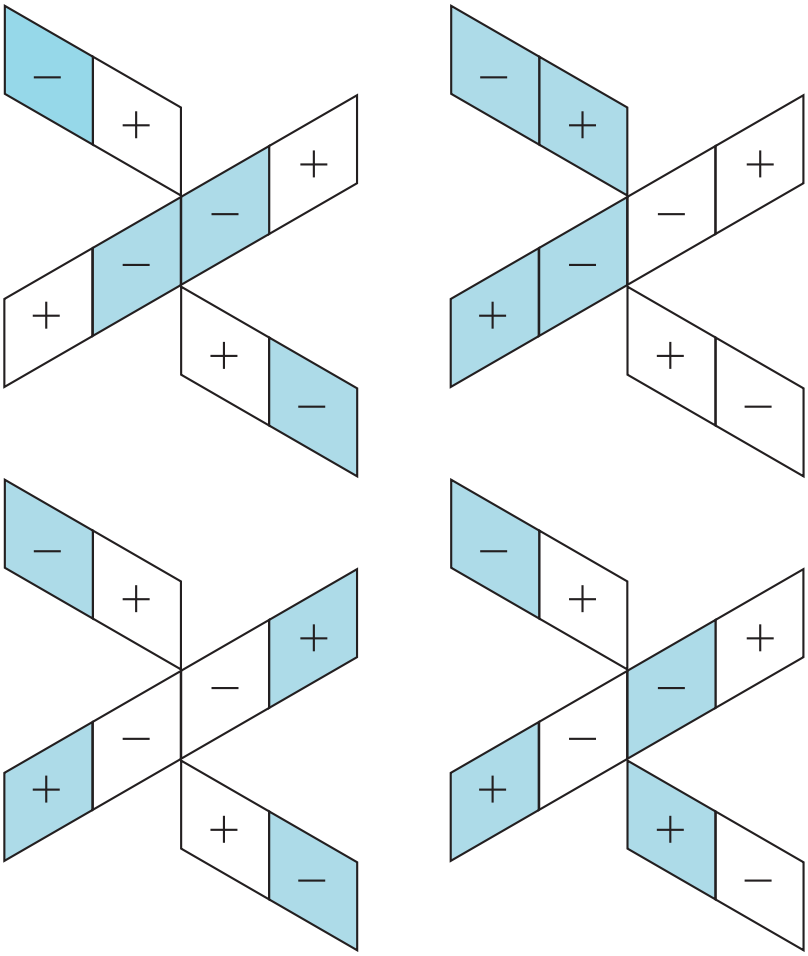

FIGURE 8.9. Possible charge-order motifs of the iron oxyborate structure under the k-vector $(0, 0, 0)$. There is only a single basis vector for each irreducible representation. The $+/-$ refer to relative orientations of the magnetic moments, relative to one another. The colour schemes denote the nominally $+2/+3$ iron ions. From left to right, top to bottom; Γ_1, Γ_2, Γ_3, Γ_4.

8.6.4. Symmetry relations

Our symmetry analysis has revealed that the structural, magnetic and charge-ordering phase transitions are all dominated by different irreducible representations. However, while the charge and magnetic ordering of iron borate do not occur within the same irreducible representations, this does not mean they are unrelated. At a naive level, the net ferrimagnetic moment arises from the excess of charge at positions with a specific moment orientation; the magnetic and charge ordering are distributed through the system in the same manner, despite their differing IR labels.

If the distribution of charge and moment orientation are coincident, how can they have differing symmetries? The divergence of charge and magnetic labelling arises because they behave in fundamentally different ways under symmetry operations: charge is a scalar and therefore invariant under all operations of the point group, while magnetic moments act as axial vectors. At a, perhaps, more fundamental level the charge and spin are differentiated not by how they are physically ordered, but how mathematics formally represents that order, and this can be seen if we consider only the permutation representation. Both the charge and magnetic ordering are permuted according to Γ_1.

$$\begin{aligned} \Gamma &= \Gamma_{Perm} \otimes \Gamma_{Rot} \\ \Gamma_{Scalar} &= \Gamma_1 \otimes \Gamma_1 \\ \Gamma_{Axial} &= \Gamma_1 \otimes (\Gamma_1 + 2\Gamma_3) \end{aligned} \tag{8.1}$$

The equivalence of their permutation representations implies that both charge and magnetic moment are distributed in the same way amongst the various iron atoms. Where they differ is how their representations transform under the symmetry operations of the space group (Γ_{Rot}).

This abstraction back to the permutation representation has been considered in a different context by Izyumov (1991), who notes that the energetics of simple exchange

are unchanged by a global rotation of every spin about a parallel local axes. If exchange is expressed as:

$$S_i.S_j = |S_i||S_{ij}|cos\Theta_{ij} \tag{8.2}$$

Then, as a global rotation changes neither the magnitude of any moment nor the angles between them, one could view this as another symmetry element of the Hamiltonian. This is, mathematically, same the abstraction we have performed above, and it draws together basis vectors that come from the same IR of the permutation representation (so called "exchange multiplets").

In fact, Izyumov's arguments are unphysical. While in theory the global rotation is a symmetry operation, it is not observed as one in real systems. Magnetic atoms do not exist *in vacuo*, and their local environment will cause particular orientations of the moments to represent an energetic minima. Were this not true then the system would be an ordered paramagnet; every orientation of the ordered spin state relative to the lattice would be degenerate and the system would move freely about that space. For any system with static moment ordering, crystal field anisotropy and spin orbit coupling determine the moment orientations, and this effect can be enormous.

In contrast, our arguments in the case of iron borate rest not upon the isotropy of space, but the scalar nature of charge density waves. The rotation of a scalar at a point in space is meaningless and therefore cannot cost energy, unlike the rotation of a moment.

8.7. Conclusions

We have used representation theory to analyze the phase transitions of iron oxyborate, and to interpret data collected from a powdered sample using the D2B diffractometer at the ILL. The synthesis was significantly more taxing that previous literature had reported, and the product was not 100% pure. Despite synthetic difficulties,

both the $Pmcn$ and $P12_1/c1$ phases were refined and the magnetic ordering shown to be ferrimagnetic. Further, we have shown that the ferrimagnetic moment must arise from a $\vec{k} = (0, 0, 0)$ charge-ordering that has not been previously discussed. Consideration of the basis vectors describing such an ordering has allowed us to unambiguously determines the charge-ordering motif.

Symmetry analysis of the structural, magnetic, and charge ordering transitions reveals that charge and magnetic ordering are related when considered them within an appropriate symmetry frame-work. This involves recognizing that charge and magnetism are fundamentally different in behaviour and that it is not sufficient to just consider their IR labels. Within the permutation representation both charge and magnetic moments are distributed amongst the atomic positions in the same manner, a result that is self-evident when considering the physical origin of ferrimagnetism in iron oxyborate.

Finally, the magnetic moments observed by powder diffraction were approximately half their expected value. Further work is required, using other techniques such as inelastic neutron scattering and muon spin resonance, to explain this observation. Without an explanation for the reduced moments our model remains unphysical.

References

[1] Angst, M. *et al.* (2007a). *Phys. Rev. Let.* **99**, 086403.

[2] Angst, M. *et al.* (2007b). *Phys. Rev. Let.* **99**, 256402.

[3] Attfield, J. P., Clarke, J. F., Perkins, D. A., (1992). *Physica B* **180**, 581.

[4] Attfield, J. P., *et al.* (1998a). *J. Mat. Chem.* **9** , 205.

[5] Attfield, J. P., *et al.* (1998b). *Nature* **Dec** , 655.

[6] Bertuat, E. F. (1950). *Acta. Crys.* **3**, 473.

[7] Continentino, M. A. *et. al.* (2001). *Phys. Rev. B*, **64**, 014406.

[8] Cambridge Isotope Laboratories. *www.isotope.com/.*

[9] Douvalis, A. P., *et al.* (2000). *J. Phys.: Con. Mat.* **12**, 177.

[10] *International tables for crystallography. Vol. A. (5th edition.)* (2002). Ed. Th. Hahn, **Springer**, Dordrecht.

[11] Emerya, V. J. and Kivelson, S. A. (1996). *Proc. Int. Symp. Front. High - Tc Superconductivity*, **263**, 44.

[12] Howald, C., *et. al.*. (2003) *PNAS*, **100**, 9705.

[13] Izyumov, Y. A. and Naish, V. E. (1991) *Neutron Diffraction of Magnetic Materials*, **Consultants Bureau** (New York and London).

[14] Kovalev, O. V. (1993). *Representations of the Crystallographic Space Groups: Irreducible representations, Induced representations and Corepresentations (2nd Ed)*, Ed. H. T. Stokes and D. M. Hatch, **Gordon and Breach Science Publishers** (London, 1993).

[15] Larson, A.C. and Von Dreele, R.B. (1994) *Los Alamos National Laboratory Report* **LAUR** 86-748.

[16] Leonov, I. *et al.* (2005). *Phys. Rev. B* **72**, 014407.

[17] Mir, M., Janczak, J., and Mascerenhas, Y. P. (2006). *J. Appl. Cryst.* **39**, 42-45.

[18] ICCD, (2009). PDF-2 Database, *http://www.icdd.com/products/pdf2.htm.*

[19] Rivas-Murias, B. *et al.* (2006). *Chem. Mat.* **18**, 4547.

[20] Rodriguez-Carvajal, J. (1993). *Physica B.* **192**, 55-69.

[21] Salkola, M.I., Emery, V.J., and Kivelson, S.A. (1996). *Phys. Rev. Lett.*, **77**(1), 155.

[22] Suda, N., Kohn, K., and Nakamura, S. (2003). *Ferroelectrics* **286**, 155.

[23] Sears, V. F. (1992). *Neutron News*, **3**(3), 29.

[24] Verwey, W., (1939). *Nature* (London) **144**, 327.

[25] Vojta, M., Zhang, Y., and Sachdev, S. (2000). *Phys. Rev. B*, **62**, 6721.

[26] Wills, A. S. (2000). *Physica B* **276**, 680.

[27] Wills, A. S. (2009). *Zeit. fur Krist.* **In print**.

CHAPTER 9

Experimental application: Potassium selenate

"I love fools' experiments. I am always making them."

Charles Darwin

9.1. Introduction

The second system studied experimentally in this thesis is potassium selenate, which undergoes two displacive phase-transitions thought to be driven by soft phonon modes. Potassium selenate is particularly important for two reasons: the softening of phonon branches at the transition temperature has been directly observed using inelastic neutron scattering techniques (Iizumi, 1977); and the second transition appears to be a k-vector transition, where the only change of symmetry is a discontinuous jump in $\vec{k}$. Such symmetry-transitions are only describable using representation theory and may be important in a wide range of systems (Cowley, 1980).

9.2. Potassium Selenate

Potassium selenate, along with its structural isomorphs, has been extensively studied over the past 30 years. In particular, the work by Iizumi *et al.* (1977) has formed the basis of many computational studies into this and related systems (e.g Mashiyama, 1983; Kunz, 1992; Zinenko, 1998). At room temperature K_2SeO_4 is isomorphic to β-K_2SO_4, with space group $Pnam$[1] (Kálmán, 1970): this is referred to as the P-

[1]This is an alternative setting of $Pnma$(62)

or paraelectric-phase of potassium selenate. Upon cooling, K_2SeO_4 undergoes phase transitions at 129.5K and 93K (Aiki; 1969a, 1969b). The first of these is to an incommensurately modulated structure (Iizumi, 1977; Yamada, 1984), termed the I-phase. Observation of a strongly-softening phonon mode at the P→I phase transition, by Iizumi *et al.*, has generated much work towards the identification of this mode and its involvement in the phase transitions of the system (e.g. Dvorak, 1978; Sannikov, 1978; Fleury, 1979; Massa, 1983; Pérez-Mato, 1985).

Below the P→I transition, the k-vector of the incommensurate modulation is $(\frac{1-\delta}{3}, 0, 0)$, where δ varies continuously with temperature over the range $0.04 - 0.08$ (Iisumi, 1977). At 93K δ jumps, discontinuously to the commensurate value 0. This low temperature phase is ferroelectric and its symmetry was hotly debated (Shimoaka, 1972; Yamada, 1984; Aiki 1969b), but is now accepted as being $Pna2_1$. The behaviour of the system at the ferroelectric (or F-phase) transition is notable because both $\vec{k} = (q, 0, 0)$ and $\vec{k} = (\frac{1}{3}, 0, 0)$ have the same little group. Therefore, if the distortions in both the I- and the F- phases are described by the same irreducible representation, there may be no formal change of symmetry associated with the F→I phase transition.

In this chapter we highlight flaws in previous symmetry analysis performed by Iizumi (1977) and Pérez-Mato (1985) and show there is no single phonon mode that can give rise to a distortion with the symmetry $Pna2_1$. Having derived the correct irreducible representations and basis vectors for this system, the symmetry of the F-phase and the modes generating its ferroelectric distortion are determined from new powder neutron diffraction data using the SARA*h*-GSAS routines developed as part of this thesis (chapter 7).

9.3. Symmetry analysis

Symmetry analysis of the K_2SeO_4 phase transitions was first performed by Iizumi *et al.*(1977), who experimentally determined that in the I- and F-phases the system ordered under a distortion with wave-vector $k \approx (\frac{1-\delta}{3}, 0, 0)$. In the I-phase δ ranges from $0.04 - 0.08$Å jumping to 0 at the I→F transition. Observation, using inelastic neutron scattering, of a soft phonon with the symmetry of Γ_2 at the P→I transition lead to the assignment of Γ_2 symmetry to the distortion of the I- and F-phase[2]. This assessment was challenged by PérezMato *et al.* (1985), who performed a symmetry mode analysis of both the I- and F- phase structures reported by Iizumi and found elements of the I-phase distortions had Γ_1 symmetry. Further, the I→F phase transition was reported to be driven by Γ_3 and Γ_4. In this section we highlight significant errors in the analysis by both Iizumi and PérezMato, before performing a new co-representational analysis of potassium selenate in section 9.3.1.

Careful inspection of the literature reveals that Iizumi *et al.* mistakenly performed their analysis using the loaded irreducible representations (LIRs) of Kovalev[3]. Correct irreducible representations for this little group are significantly different from those reported in their work (Table 9.1); in particular, the daughter phases associated with each IR are much less symmetric. From the IRs, it is clear that any distortion involving only Γ_2 must reduce the system to P1 symmetry (section 3.8). These incorrect representations also appear in the work of Pérez-Mato *et al.* and, as a result, their symmetry modes are significantly more symmetric than they should be.

The symmetry-mode analysis of K_2SeO_4 by Pérez-Mato *et al.* concluded that the I phase ordered under two IRs; the "completely symmetric" Γ_1 and the low-symmetry Γ_2. The F-phase was reported to order under elements of all the IRs of $\mathbb{G}_k$. However,

[2]In the original work the branches are labelled as Σ_2, but with the same meaning.
[3]See chapter 5.

	$\{E\|0\}$	$\{C_{2x}\|\frac{1}{2}\vec{a}+\frac{1}{2}\vec{b}+\frac{1}{2}\vec{c}\}$	$\{\sigma_z\|\frac{1}{2}\vec{a}+\frac{1}{2}\vec{c}\}$	$\{\sigma_y\|\frac{1}{2}\vec{b}\}$
LIR				
Γ_1	1	1	1	1
Γ_2	1	1	-1	-1
Γ_3	1	-1	1	-1
Γ_4	1	-1	-1	1
SIR				
Γ_1	1	$e^{-q\pi}$	1	$e^{-q\pi}$
Γ_2	1	$e^{-q\pi}$	-1	$-e^{-q\pi}$
Γ_3	1	$-e^{-q\pi}$	1	$-e^{-q\pi}$
Γ_4	1	$-e^{-q\pi}$	-1	$e^{-q\pi}$
SIR				
Γ_1	1	$e^{-\frac{\pi}{3}}$	1	$e^{-\frac{\pi}{3}}$
Γ_2	1	$e^{-\frac{\pi}{3}}$	-1	$-e^{-\frac{\pi}{3}}$
Γ_3	1	$-e^{-\frac{\pi}{3}}$	1	$-e^{-\frac{\pi}{3}}$
Γ_4	1	$-e^{-\frac{\pi}{3}}$	-1	$e^{-\frac{\pi}{3}}$

TABLE 9.1. The top table lists the LIRs of *Pnam*, for $\vec{k}=(q,0,0)$; incorrectly listed as the IRs for this group by Iizumi (1977) and Pérez-Mato (1985). Middle and bottom list the SIRs for $\vec{k}=(q,0,0)$, and the case $q=\frac{1}{3}$.

his basis vectors were incorrect, due to an incorrect use of the LIR tables presented by Kovalev. As a result his conclusions are brought in to doubt and we have performed a new symmetry mode analysis using fresh experimental data. Further, due to the complex nature of the basis vectors projected from $\mathbb{G}_k$, we have extended our consideration to the anti-unitary operations of this system (section 3.6).

9.3.1. Co-representational analysis of potassium selenate

The irreducible corepresentations (ICRs) of *Pmna*, $\vec{k}=(\frac{1}{3},0,0)$ are all of type *A* (Table 9.2). In our analysis we have chosen $\beta=1$, however the choice of phase factor does not affect our discussion or quantitative results (see sections 3.6.3, 3.7). Inversion is a symmetry operation of $\mathbb{G}_0$ but not $\mathbb{G}_k$, so we take I as our anti-unitary generating element and it doubles the size of the symmetry group.

	E	C_{2x}	σ_y	σ_z	I	σ_x	C_{2y}	C_{2z}
Γ_{1+1}	1	$e^{-\frac{\pi}{3}}$	1	$e^{-\frac{\pi}{3}}$	1	$e^{-\frac{\pi}{3}}$	1	$e^{-\frac{\pi}{3}}$
Γ_{1-1}	1	$e^{-\frac{\pi}{3}}$	1	$e^{-\frac{\pi}{3}}$	-1	$-e^{-\frac{\pi}{3}}$	-1	$-e^{-\frac{\pi}{3}}$
Γ_{2+2}	1	$e^{-\frac{\pi}{3}}$	-1	$-e^{-\frac{\pi}{3}}$	1	$e^{-\frac{\pi}{3}}$	-1	$-e^{-\frac{\pi}{3}}$
Γ_{2-2}	1	$e^{-\frac{\pi}{3}}$	-1	$-e^{-\frac{\pi}{3}}$	-1	$-e^{-\frac{\pi}{3}}$	1	$e^{-\frac{\pi}{3}}$
Γ_{3+3}	1	$-e^{-\frac{\pi}{3}}$	1	$-e^{-\frac{\pi}{3}}$	1	$-e^{-\frac{\pi}{3}}$	1	$-e^{-\frac{\pi}{3}}$
Γ_{3-3}	1	$-e^{-\frac{\pi}{3}}$	1	$-e^{-\frac{\pi}{3}}$	-1	$e^{-\frac{\pi}{3}}$	-1	$e^{-\frac{\pi}{3}}$
Γ_{4+4}	1	$-e^{-\frac{\pi}{3}}$	-1	$e^{-\frac{\pi}{3}}$	1	$-e^{-\frac{\pi}{3}}$	-1	$e^{-\frac{\pi}{3}}$
Γ_{4-4}	1	$-e^{-\frac{\pi}{3}}$	-1	$e^{-\frac{\pi}{3}}$	-1	$e^{-\frac{\pi}{3}}$	1	$-e^{-\frac{\pi}{3}}$

TABLE 9.2. The irreducible co-representations of $Pnam$, for $\vec{k} = (\frac{1}{3}, 0, 0)$. The subscripts denote the IRs of $\vec{k}$ and $-\vec{k}$ that are mixed by anti-linear symmetry, and how they combine. I.e. Γ_{1-1} is a short-form notation for $\Gamma_{\Gamma_1^{\vec{k}}-\Gamma_1^{-\vec{k}}}$.

The ICRs of this group are complex, and so the reduction and projection operators can not be used. Instead, we must perform a "simple" symmetry reduction and form the co-representations from the IRs spanned (section 3.7); normal representation analysis was performed using SARAh (Wills, 2000). Atoms upon the Wyckoff position $(x, 0.25, z)$ split into two orbits under $\mathbb{G}_k$ and, using polar vectors to represent possible displacements, each orbit spans the reduction:

$$\Gamma = 2\Gamma_1 + 1\Gamma_2 + 2\Gamma_3 + 1\Gamma_4 \tag{9.1}$$

For this system, the anti-unitary generating operator brings the split orbits together under A co-representations, forming the combinations $\mathfrak{d}_k(g) \pm \mathfrak{d}_{-k}(g)$ (again, we chose $\beta = 1$ for convenience). Hence, the $(x, 0.25, z)$ position spans the following ICRs:

$$\Gamma = 2\Gamma_{1+1} + 2\Gamma_{1-1} + 1\Gamma_{2+2} + 1\Gamma_{2-2} + 2\Gamma_{3+3} + 2\Gamma_{3-3} + 1\Gamma_{4+4} + 1\Gamma_{4-4} \tag{9.2}$$

This analysis can be repeated for the (x, y, z) position, generating the reduction:

$$\Gamma = 3\Gamma_{1+1} + 3\Gamma_{1-1} + 3\Gamma_{2+2} + 3\Gamma_{2-2} + 3\Gamma_{3+3} + 3\Gamma_{3-3} + 3\Gamma_{4+4} + 3\Gamma_{4-4} \tag{9.3}$$

	$(x, 0.25, z)$	$(x, -0.25, -z)$	$(x, -0.25, z)$	$(x, 0.25, -z)$
$\psi^{1+1}(x)$	$(2,0,0)$	$(1,0,0)$	$(1,0,0)$	$(\bar{1},0,0)$
$\psi^{1+1}(z)$	$(0,0,2)$	$(0,0,\bar{1})$	$(0,0,1)$	$(0,0,1)$
$\psi^{1-1}(x)$	$(2,0,0)$	$(1,0,0)$	$(\bar{1},0,0)$	$(1,0,0)$
$\psi^{1-1}(z)$	$(0,0,2)$	$(0,0,\bar{1})$	$(0,0,\bar{1})$	$(0,0,\bar{1})$
$\psi^{2+2}(y)$	$(0,2,0)$	$(0,\bar{1},0)$	$(0,1,0)$	$(0,1,0)$
$\psi^{2-2}(y)$	$(0,2,0)$	$(0,\bar{1},0)$	$(0,\bar{1},0)$	$(0,\bar{1},0)$
$\psi^{3+3}(x)$	$(2,0,0)$	$(\bar{1},0,0)$	$(1,0,0)$	$(1,0,0)$
$\psi^{3+3}(z)$	$(0,0,2)$	$(0,0,1)$	$(0,0,1)$	$(0,0,\bar{1})$
$\psi^{3-3}(x)$	$(2,0,0)$	$(\bar{1},0,0)$	$(\bar{1},0,0)$	$(\bar{1},0,0)$
$\psi^{3-3}(z)$	$(0,0,2)$	$(0,0,1)$	$(0,0,\bar{1})$	$(0,0,1)$
$\psi^{4+4}(z)$	$(0,2,0)$	$(0,1,0)$	$(0,1,0)$	$(0,\bar{1},0)$
$\psi^{4-4}(z)$	$(0,2,0)$	$(0,\bar{1},0)$	$(0,1,0)$	$(0,1,0)$

TABLE 9.3. Basis vectors of the position $(x, 0.25, z)$ in $Pnma$, ordering under $\vec{k} = (\frac{1}{3}, 0, 0)$. These have been projected from the type A ICRs for this group, and made real by linear combination with their $-\vec{k}$ conjugates (section 3.4). For the position (x, y, z), there are 24 basis vectors spanning 8 equivalent positions.

In total there are 84 basis vectors for the system, this differs noticeably from the 63 calculated by Pérez-Mato *et al.* whose analysis is flawed in two ways. First it assumes that the F-phase symmetry $Pna2_1$, limiting itself to motions with that symmetry. Second, they use 21 atoms to define their proposed structure. As the distortion is periodic, with a well defined k-vector, there are only 7 independent atoms in the $Pna2_1$ structure; the distortion of the remaining atoms is defined by $\vec{k}$. "Co-basis vectors" for the position $(x, 0.25, z)$, $\beta = \pm 1$ are presented in Table 9.3; these describe every atom in the potassium selenate structure, except for $O(1)$[4].

In concluding our qualitative analysis of this system, we note that $Pna2_1$ contains the operations:

$$Pna2_1 = \left\{ \{E|0\}, \{C_{2z}|\frac{1}{2}\vec{a} + \frac{1}{2}\vec{b} + \frac{1}{2}\vec{c}\}, \{\sigma_y|\frac{1}{2}\vec{a} + \frac{1}{2}\vec{c}\}, \{\sigma_x|\frac{1}{2}\vec{b}\right\} \} \tag{9.4}$$

[4]The co-basis vectors of O(1) have not been included for brevity, and in consideration of the comments in section 3.7 and 6.4. Our interest lies in the IRs/ICRs spanned and the distorted structure rather than the form of the symmetry modes (see section 7.1.1).

Or, in the same setting as $Pnma$:

$$Pn2_1a = \left\{ \{E|0\}, \{C_{2y}|\frac{1}{2}\vec{a} + \frac{1}{2}\vec{b} + \frac{1}{2}\vec{c}\}, \{\sigma_z|\frac{1}{2}\vec{a} + \frac{1}{2}\vec{b}\}, \{\sigma_x|\frac{1}{2}\vec{c}\right\} \} \tag{9.5}$$

Considering the ICRs presented in table 9.2 reveals that there is no single-IR, route from $Pnma$ to $Pna2_1$. The non-zero phase difference associated with $\mathfrak{d}(\sigma_z)$ in every ICR prohibits the retention of this operation. Hence, there is no single distortion symmetry that can give rise to a $Pna2_1$ phase from $Pnma$.

9.4. Experimental and results

A polycrystalline sample of approximately 15g of 99.95% pure[5] K_2SeO_4 (Absco Materials[6]) was scanned on the High-Resolution Powder Diffraction (HRPD) time-of-flight (ToF) instrument at ISIS. The sample was held in a vanadium can, and data was collected at three different temperatures (150K, 110K, 50K). Each experiment lasted 8 hours, the long exposure ensured the statistical quality of the data despite the mild neutron absorbance of selenium (11.7barn at 2200m/s). From this data, the P- and F- phases were refined using GSAS (Larson, 1994) with the space groups $Pnma$ and $Pna2_1$ respectively (Iizumi, 1977).

During the refinements, a number of peaks generated by the sample environment were excluded, in the ranges: 1.239 - 1.239Å ; 1.642 - 1.652Å ; 2.128 - 2.138Å [7]. Further, for both refinements a small correction for absorption was included in the model, using GSAS function 0 (Coefficient_1 = 0.150). Refinement of the P-phase structure (Fig 9.1, Table 9.5) converged with a χ^2 of 1.924 (Table 9.4), using 57 model parameters. For the F-phase, a goodness of fit of $\chi^2 = 6.275$ was achieved using 83 model parameters, including isotropic thermal parameters and a unit-cell tripled in

[5]Metal-base.
[6]http://www.abscomaterials.com/
[7]The peak at 2.128 - 2.138Å was *not* excluded in the F-Phase refinement, as it overlapped with a large peak from the selenate.

	χ^2	wR_p	R_p
150K	1.924	3.60%	3.71%
50K	6.275	4.61%	4.49%

TABLE 9.4. The goodness of fit parameters for the structural models at 150K and 50K, refined from powder diffraction data.

the a direction (Fig 9.2, Table 9.6). Isotropic thermal parameters were used in the F-phase refinement, as anisotropic thermal parameters made it unstable.

The F-phase refinement was challenging for two reasons: the large number of atoms in the tripled unit cell; and the peak profiles. The peak-shapes varied with d-spacing and none of the GSAS peak profiles were able to accurately reproduce their shape over the full range of d. In particular, there was evidence of a broad Lorentzian component at the base of peaks at large d-spacing (Fig. 9.3) that was not well modelled. FullProf (Rodriguez-Carvajal, 1993) and TOPAS (Cheary, 1990) were also unable to model this peak shape over the full range of d.

We had hoped to fit the I-phase data from HRPD using JANA (Petříček, 1985), however previous versions of JANA are not compatible with time of flight data (such as that from HRPD). The newest version, JANA2006 (Petříček, 2006), will support ToF data, but was not brought into a workable state in time to complete this analysis. A considerable amount of time was spent communicating with the author of JANA2006 to help develop support for HRPD data.

Overall, the refined structures were in a good agreement with those previously reported (Iizumi, 1977). The broadening of the peak-bases could be an instrument artefact, or be indicative of a short-range ordering superimposed upon the long-range structure; data from a second instrument might help establish its origin.

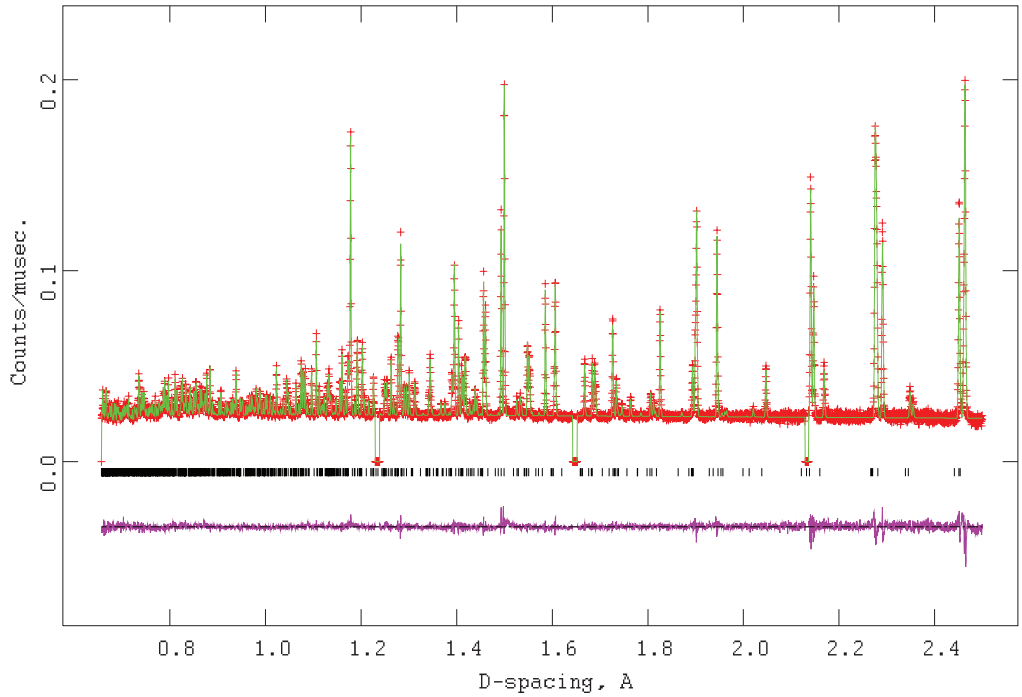

FIGURE 9.1. The Rietveld refinement of neutron diffraction data collected on the HRPD diffractometer from K_2SeO_4at 150K. The refined structure had symmetry *Pnma* and the sample parameters are listed in Tables 9.5

	x	y	z	U_{11}	U_{22}	U_{33}	U_{12}	U_{13}	U_{23}
Se	0.2230(1)	0.25	0.4195(1)	0.77(3)	0.33(3)	0.63(3)	−0.14(3)	0	0
$K(1)$	−0.0041(2)	0.25	−0.2921(1)	1.06(8)	0.70(7)	0.88(7)	0.11(6)	0	0
$K(2)$	0.1674(1)	0.25	0.0826(1)	1.00(7)	1.27(8)	1.46(7)	0.23(7)	0	0
$O(1)$	0.2922(1)	0.0268(1)	0.3442(1)	2.61(4)	2.20(4)	1.21(4)	1.18(4)	0.10(4)	−0.64(3)
$O(2)$	0.3078(1)	0.25	−0.4361(1)	1.62(6)	0.90(5)	2.76(5)	−0.55(5)	0	0
$O(3)$	0.0096(1)	0.25	0.4271(1)	0.65(5)	2.37(6)	3.78(7)	−0.05(6)	0	0
Cell	7.57657(3)	5.94662(2)	10.36115(5)						

TABLE 9.5. The structural parameters of K_2SeO_4 (*Pnma*), refined from neutron powder diffraction data collected at 150K. All of the thermal parameters are in units of $\times 10^{-2}$.

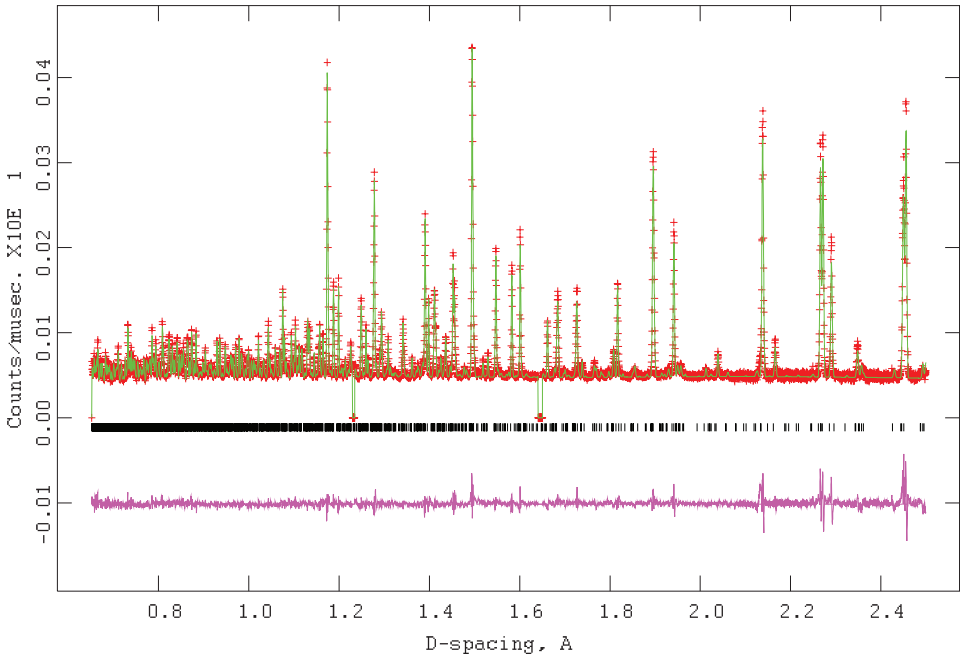

FIGURE 9.2. The Rietveld refinement of neutron diffraction data collected on the HRPD diffractometer from K_2SeO_4at 50K. The refined structure had symmetry $Pna2_1$ and the sample parameters are listed in Tables 9.6

	x	y	z	$U_{iso}(\times 10^{-2})$
$Se(1a)$	0.0753(2)	0.4114(5)	0.2482(8)	0.75(9)
$Se(1b)$	0.4059(2)	0.4203(5)	0.2675(9)	0.83(9)
$Se(1c)$	0.7400(2)	0.4217(5)	0.2456(8)	0.7(1)
$K(1a)$	0.0577(5)	0.078(1)	0.263(2)	1.9(2)
$K(1b)$	0.3844(4)	0.076(1)	0.253(2)	1.5(2)
$K(1c)$	0.7232(4)	0.0828(7)	0.253(2)	0.0(1)
$K(2a)$	0.0009(5)	0.7109(8)	0.269(1)	0.1(2)
$K(2b)$	0.3314(5)	0.711(1)	0.226(2)	1.1(2)
$K(2c)$	0.6677(5)	0.699(1)	0.251(2)	1.7(2)
$O(1a)$	0.0995(3)	0.3431(9)	0.026(1)	2.4(2)
$O(1b)$	0.4273(2)	0.3391(7)	0.036(1)	1.1(1)
$O(1c)$	0.7531(3)	0.3252(7)	0.032(1)	1.6(1)
$O(1d)$	0.0902(3)	0.3352(8)	0.470(1)	1.1(1)
$O(1e)$	0.4345(2)	0.3386(6)	0.474(1)	0.6(1)
$O(1f)$	0.7708(2)	0.3549(6)	0.478(1)	1.2(1)
$O(2a)$	0.1075(3)	0.5576(6)	0.290(1)	0.8(1)
$O(2b)$	0.4370(3)	0.5649(6)	0.270(1)	0.6(1)
$O(2c)$	0.7703(4)	0.5619(7)	0.220(1)	2.0(2)
$O(3a)$	0.0033(3)	0.4382(7)	0.208(1)	1.8(1)
$O(3b)$	0.3361(2)	0.4259(6)	0.280(1)	0.9(1)
$O(3c)$	0.6701(3)	0.4316(8)	0.291(1)	1.5(1)
Cell	22.70589(7)	10.32936(5)	5.97230(3)	

TABLE 9.6. The structural parameters of F-K_2SeO_4 ($Pna2_1$), refined from neutron powder diffraction data collected at 50K.

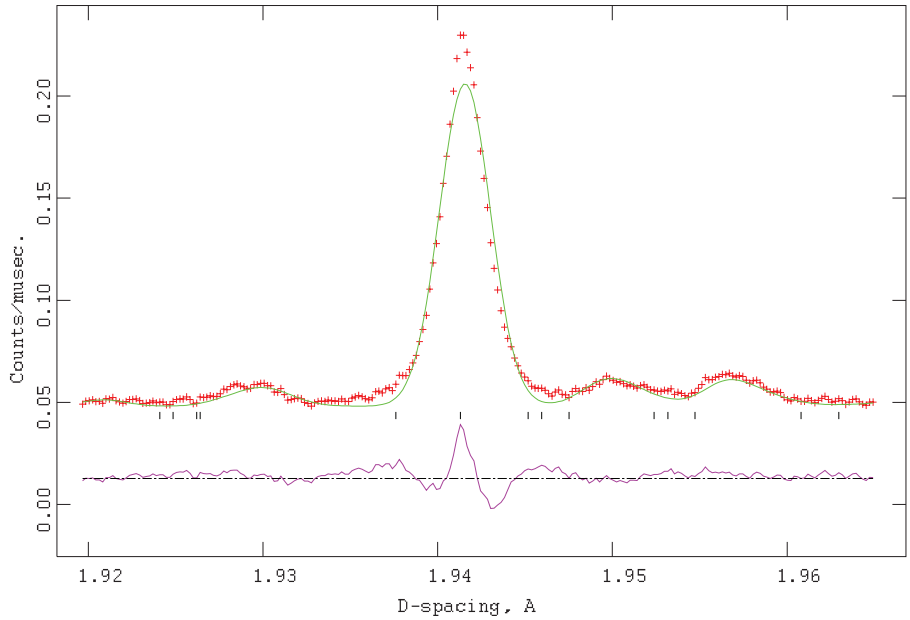

FIGURE 9.3. An illustration of GSAS's inability to model the peak profiles at high *d*-spacings. The peak shape used, function 1, is too narrow at the base and too broad at the top leading to a characteristic "W" in the difference plot.

9.5. Analysis of the phase transition using SARA*h*-GSAS

The flaws in previous work prompted a new analysis of potassium selenate and the role of phonon modes in the distortion of the F-phase, using SARA*h*-GSAS. P-K_2SeO_4 has 84 "co-basis" vectors, and (as discussed in section 9.3.1), the ICR indicates that no single phonon mode can give rise to a daughter phase with symmetry $Pna2_1$. To determine which symmetry modes had the greatest influence upon the refinement's goodness of fit, an initial search over all of the basis vectors was performed using the search routine in SARA*h*-GSAS. This indicated clearly that, while no one ICR dominated the refinement, Γ_{2+2} and Γ_{2-2} had the greatest effect upon χ^2.

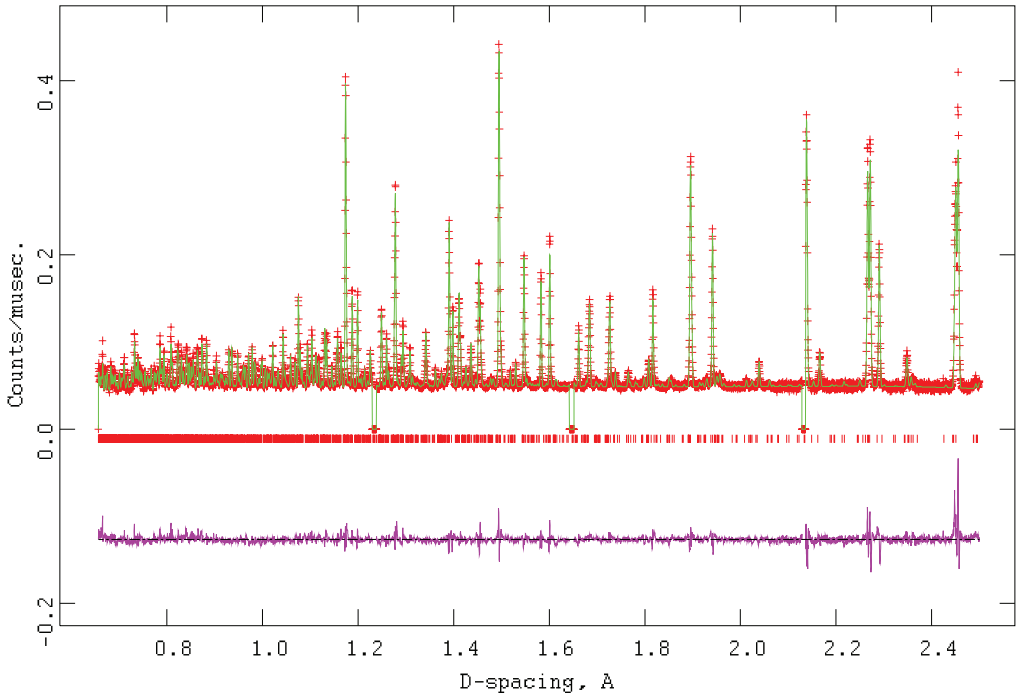

FIGURE 9.4. The SARA*h*-GSAS refinement of neutron diffraction data collected on HRPD at 50K.

From the initial (undistorted) structure defined by the GSAS refinement of the 150K powder diffraction data, distortions with the symmetry of Γ_{2+2} and Γ_{2-2} improved the goodness of fit to $\chi^2 = 18.97$, far above the fit achieved by GSAS. More modes were gradually added to the refinement, until all 84 modes had been included. The final refinement was performed using 200,000 cycles, with the background and scale parameters allowed to refine during each cycle for 3 least-squares steps (section 7.4). The refinement converged upon $\chi^2 = 7.621$, with $wRp = 5.12\%$, $Rp = 4.69\%$ (Fig, 9.4).

The final refinement used 84 basis vectors, none of which were removed by the elimination routine in SARA*h*-GSAS (section 7.4). This indicates that the distortion of the F-Phase involves elements of every possible ICR symmetry.

Atom	SARA*h*			GSAS			Δ		
	x	y	z	x	y	z	δx	δy	δz
$Se(1a)$	0.0740	0.2446	0.4232	0.0753	0.2476	0.4118	0.0014	0.0030	−0.0114
$Se(1b)$	0.4084	0.2555	0.4157	0.4057	0.2659	0.4203	−0.0027	0.0105	0.0046
$Se(1c)$	0.7415	0.2552	0.4158	0.7401	0.2449	0.4215	−0.0014	−0.0103	0.0057
$K(1a)$	0.0542	0.2419	0.0853	0.0573	0.2619	0.0783	0.0031	0.0200	−0.0070
$K(1b)$	0.3909	0.2586	0.0786	0.3850	0.2520	0.0770	−0.0059	−0.0066	−0.0015
$K(1c)$	0.7242	0.2585	0.0787	0.7230	0.2288	0.0825	−0.0012	−0.0298	0.0038
$K(2a)$	0.0009	0.2533	0.7006	0.0005	0.2689	0.7109	−0.0004	0.0155	0.0103
$K(2b)$	0.3311	0.2463	0.7154	0.3318	0.2276	0.7108	0.0007	−0.0187	−0.0046
$K(2c)$	0.6674	0.2534	0.7004	0.6680	0.2491	0.6994	0.0006	−0.0043	−0.0010
$O(1a)$	0.0992	0.3413	0.0324	0.0998	0.3425	0.0211	0.0006	0.0012	−0.0113
$O(1b)$	0.4290	0.3469	0.0213	0.4270	0.3392	0.0381	−0.0021	−0.0077	0.0168
$O(1c)$	0.7624	0.3467	0.0212	0.7526	0.3272	0.0367	−0.0099	−0.0194	0.0154
$O(1d)$	0.0982	0.3543	0.4831	0.0910	0.3338	0.4755	−0.0072	−0.0205	−0.0076
$O(1e)$	0.4293	0.3339	0.4636	0.4341	0.3383	0.4747	0.0048	0.0044	0.0111
$O(1f)$	0.7627	0.3337	0.4632	0.7710	0.3557	0.4733	0.0083	0.0220	0.0101
$O(2a)$	0.1021	0.5675	0.2140	0.1080	0.5578	0.2908	0.0059	−0.0097	0.0768
$O(2b)$	0.4378	0.5612	0.2860	0.4371	0.5641	0.2714	−0.0007	0.0029	−0.0146
$O(2c)$	0.7712	0.5613	0.2860	0.7700	0.5621	0.2219	−0.0012	0.0008	−0.0640
$O(3a)$	0.0044	0.4267	0.2359	0.0035	0.4377	0.2102	−0.0009	0.0111	−0.0257
$O(3b)$	0.3354	0.4282	0.2638	0.3359	0.4261	0.2790	0.0005	−0.0021	0.0151
$O(3c)$	0.6690	0.4282	0.2640	0.6701	0.4312	0.2907	0.0011	0.0030	0.0267

TABLE 9.7. A comparison of the GSAS (Left), and SARA*h* (Middle) refinements of K_2SeO_4, from neutron powder diffraction data collected at 50K. The right-most column lists the differences.

9.6. Discussion

While the SARA*h* refinement was, numerically, worse than that achieved by GSAS, the structures are in good agreement (Table 9.7). This is strong evidence that, to a first approximation, the systems symmetry is indistinguishable from $Pna2_1$, with k-vector $(\frac{1}{3}, 0, 0)$. The F-phase distortion is a mixture of all the possible distortion symmetries of the parent phase, and can arise from a single IR or ICR.

Inspection of the refined distortions reveals further incompatibilities between our distortion model and that presented by Iizumi*et al.*. First, we note that the displacements of the potassium atoms are clearly orientated in a number of directions. Around half of the potassium atoms have been displaced approximately in the *a*-*b* plane while some displacements lie in the *a*-*c* plane, and others at obtuse angles to any of the crystallographic axes (Fig 9.5). In contrast, the displacements reported by Iizumi all lay parallel to the crystallographic axes.

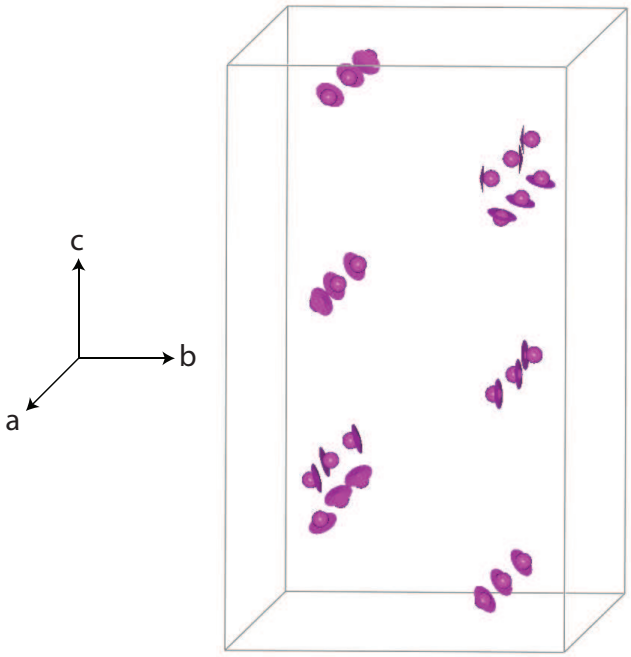

FIGURE 9.5. A view of the distortions of each potassium ion in the F-phase of K_2SeO_4 relative to its position in the P-phase. These distortions were defined from powder-diffraction data using SARA*h*-GSAS.

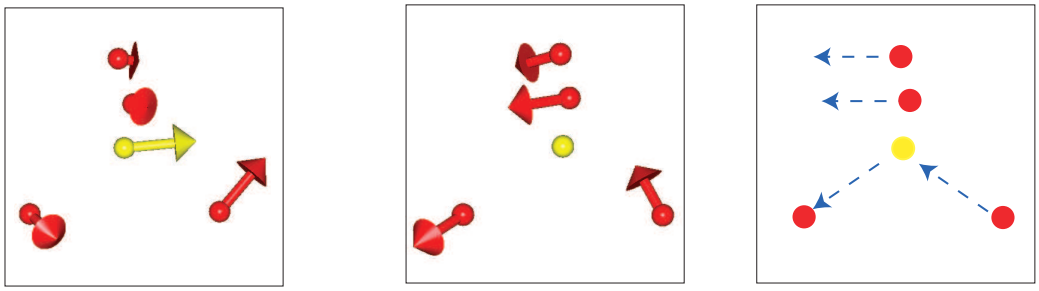

FIGURE 9.6. The distortions of a single selenate unit in the F-phase of K_2SeO_4 relative to its position in the P-phase, refined from powder-diffraction data using SARA*h*-GSAS. (Left) There is a clear component that displaces the entire unit to the right as viewed. (Middle) Under a "rigid-body" approximation, the motion of the selenate atom has been subtracted from each position, revealing the motion of the oxygen ions relative to the selenium. (Right) A cartoon of the anti-symmetric stretch and the symmetric bending modes of a tetrahedral molecular ion, these show a striking similarity to the observed displacements.

Further, the distortions of the selenate tetrahedra are quite complex and show signs of both translation and stretching/bending displacements (Fig 9.6). Isolating one of the tetrahedra from the rest of the material and inspecting the distortions at each atom reveals that the largest distortion is at the selenate, and not the oxygens. Indeed, in a "rigid body" approximation, there is clear evidence of a displacement of the selenate tetrahedra. Further, if we "remove" the translational component of the displacements there is clear evidence of symmetric and anti-symmetric bending modes in the oxygen displacements. This contrasts starkly with the model of selenate rotations about the a-axis put forward previously.

9.7. Conclusions

In this chapter we have revisited earlier work on potassium selenate and highlighted flaws in the symmetry analysis performed. A more careful approach demonstrates that, despite evidence of soft phonon modes at the first phase transition, the F-phase structure can *not* be brought about by a single IR. Full co-representational analysis of the $Pnma$ phase generates 8 irreducible co-representations which are all involved, to a lesser or greater extent, in the structure of the F-Phase.

New powder-diffraction data from this system, collected on the high-resolution powder-diffractometer instrument at ISIS, was refined using both GSAS and SARAh-GSAS. The symmetry mode refinement of SARAh is in good agreement with the $Pna2_1$ based refinement of GASAS, allowing us to conclude that all the co-representations are involved in the structure of the ferroelectric phase. Further, the internal-displacements of the selenate bear a close resemblence to bending/stretching modes, rather than the rotational motions previously reported.

We were unable to analyse the incommensurate phase as time-of-flight data is not yet supported in JANA. Further, no refinement routines support the use of symmetry

modes for incommensurate structures and this represents an obvious absence in the tools of representation theory. However, the flaws in previous symmetry analysis extend to the I-phase and warrent further investigation.

References

[1] Aiki, K., Hukunda, K. and Matumura, O. (1969a). *J. Phys. Soc. Japan*, **26**, 1064.

[2] Aiki, K. and Hukunda, K. (1969b). *J. Phys. Soc. Japan*, **26**, 1066.

[3] Cheary, R. W., Coelho, A. A. (1992). *J. Appl. Crystallogr.* **25**, 109.

[4] Cowley, R. A. (1980). *Adv. Phys.* **29**, 1.

[5] Dvorka, V. and Ishibashi, Y. (1978). *J. Phys. Soc. Japan*, **45**, 755.

[6] Fleury, P. A., Chiang, S. and Lyons, K. B. (1979). *Solid State Commun.*, **31**, 1021.

[7] Iizumi, M., Axe, J. D. and Shirane,G. (1977). *Phys. Rev. B*, **15**, 4392.

[8] Kovalev, O. V. (1993). *Representations of the Crystallographic Space Groups: Irreducible representations, Induced representations and Corepresentations*, (2nd Ed). Ed. H. T. Stokes and D. M. Hatch, **Gordon and Breach Science Publishers** (London).

[9] Kálmán, A., Sterhens, J. S. and Cruickshank, D. W. J. (1970). *Acta Cryst. B*, textbfB26, 1451.

[10] Kunz, M. and Armbruster, T. (1992). *Acta Cryst. B*, *48*, 609.

[11] Larson, A.C. and Von Dreele, R.B. (1994) *Los Alamos National Laboratory Report* **LAUR** 86-748.

[12] Mashiyama, H. and Unruh, H -G (1983). *J. Phys. C*, **16**, 5009.

[13] Massa, N. E., Ullman, F. G. and Hardy, J. R. (1983). *Phys. Rev. B*, **27**, 1523.

[14] Peŕez-Mato, J. M. *et al.* (1985). *J. Phys. C*, **19**, 1923.

[15] Petříček, V., Coppens, P. and Becker, P. (1985). *Acta Cryst. A*, **41**, 478.

[16] Petříček, V., Dusek, M. and Palatinus, L. (2006).*Jana2006. Structure Determination Software Programs*, Institute of Physics, Praha, Czech Republic.

[17] Rodriguez-Carvajal, J. (1993). *Physica B.* **192**, 55.

[18] Sannikov, D. G. and Levanyuk, A. P. (1978). *Sou. Phys. Solid State*, **20**, 580.

[19] Shimaoka, K., Tsuda, N. and Yoshimura, Y. (1972). *Acta Cryst. A*, **28 Suppl.**, 187.

[20] Wills, A. S. (2000). *Physica B* **276**, 680.

[21] Yamada, N. and Ikeda, T. (1984). *J. Phys. Soc. Japan*, **53**, 2555.

[22] Zinenko, V. I. and Zamkova, N. G. (1998). *Phys. Rev. B*, **57**, 211.

CHAPTER 10

Conclusions

"Any fool can make things bigger, more complex, and more violent. It takes a touch of genius - and a lot of courage - to move in the opposite direction."

Albert Einstein

10.1. Review of thesis

Symmetry is a powerful tool for understanding displacive phase transitions; as shown in chapter 4, even qualitative symmetry arguments can derive important results. Representation theory is the most general framework for considering the symmetry of crystalline systems and it provides an insight into the energetics of phase transitions through Wigner's theorem (chapter 2).

The aims of this thesis were set out in the conclusion of chapter 1:

(1) Development of a reliable method for generating all the basis-vectors of any crystalline system.
(2) Development of a method for analysing powder diffraction data using symmetry modes.
(3) Application of the representation theory technique to a number of example phase transitions.

These represent separate elements of an overall goal: making the technique of representation theory more reliable and accessible. Towards this goal we verified the

tables of Kovalev (1993) in chapter 5 and developed reliable algorithms for constructing appropriate trial functions (chapter 6). Representation theory often involves the arduous execution of complex vector arithmetic and the ability to reliably automate these calculations is, possibly, the most important step in opening up this field of analysis to a broader community.

The work presented in chapters 5 and 6 has been implemented within the SARA*h* software suite (Wills, 2000), forming a reliable source of basis vectors for use with Fullprof (Rodriguez-Carvajal, 1993) and SARA*h*-Refine. We hope that this work will be incorporated into other routines such as MODY (Sikora *et al.*, 2004) and BASIREPS (Rodríguez-Carvajal, 2004)[1].

We also discussed the role of anti-unitary symmetry and co-representations in physical systems. This symmetry is already, unknowingly, used widely in the construction of completely real symmetry modes from complex basis vectors. While anti-linear symmetry is fundamental, in practical calculations it has a limited influence upon the form of basis vectors. Indeed, we argue that only type A ICRs can change the form of basis vectors (section 3.7); in contrast, type B and C ICRs define additional degeneracies in the system.

10.2. Qualitative and quantitative analysis

This thesis has discussed and applied qualitative symmetry arguments to explore the relationship between a system's IRs, its possible distortions and the symmetry of resulting daughter phases. Clear understanding of the symmetry of irreducible representations can provide a great deal of information qualitatively. These arguments were used in chapter 8 to determine the structural distortion and charge-ordering

[1]It is not clear whether ISODISPLACE (Stokes, 2007) and AMPLIMODES (Aroyo; 2006a, 2006b) calculate basis vectors, or reproduces them from the printed tables of Stokes (1988).

in iron oxyborate; including the identification of a previously undiscussed charge-ordering with k-vector $(0, 0, 0)$. They were further applied in the refinements of chapters 7 and 9, and a generally underline all the work presented.

Quantitatively, the new module for SARAh-Refine (Chapter 7) is a unique tool for analysis of powder-diffraction data. Simultaneous independent development of ISODIPLACE (Campbell, 2007, 2008), AMPLIMODES (Rodriguez-Carvajal, 2008) and SARAh-GSAS for the Rietveld programs TOPAS (Cheary, 1990), Fullprof (Rodriguez-Carvajal, 1993), and GSAS (Larson, 1994) highlights an increasing appreciation of representation theory by the crystallographic community. SARAh-Refine is unique amongst the three; it makes no assumption about the symmetry of the daughter phase, instead using reverse Monte Carlo techniques to refine data. As such it is the most general, if also the slowest/least reliable, application of representation theory to structural phase transitions. Our work also highlights the problem of weakly correlated variables; weak correlation between structure parameters and the goodness of fit is an inherent part of the Rietveld method, yet the estimated errors are often (flatteringly) small.

While SARAh-GSAS can determine the coefficients of symmetry modes in a displacive phase transition, we have seen that individual basis vector coefficients are, surprisingly perhaps, of little significance on their own as basis vectors are not unique[2] (section 6.4). Indeed, redefinition of basis vectors allows them to represent the influence of an atoms local symmetry or directional bonding. The significant contribution of representation theory is the determination of which irreducible representations are present in displacive phase transitions

Finally, we have applied the theory and tools of representation theory to the phase transitions of iron borate (chapter 8) and potassium selenate (chapter 9). In iron

[2]Except in the case of a 1-dimensional representation occurring exactly once

oxyborate we identified the magnetic and charge-ordering motifs using both qualitative and quantitative symmetry analysis. The work on potassium selenate showed that even apparently simple phase transitions can be highly-complex, and how easily mistakes in symmetry analysis can occur.

10.3. Publications

Much of the work presented from chapter 3 onwards has been prepared, submitted or accepted for publication in peer reviewed journals; two topics have been published to date. The work on validating the tables of Kovalev, presented in chapter 5, was published in part in the proceedings of the European Conference on Neutron Scattering (ENCS): Davies, 2008. The discussion of the role of phase displacements in multi-ferroic systems (chapter 4) was published as part of the proceedings of the Highly Frustrated Magnetism (HFM) meeting: Davies, 2009.

10.4. Future work

There is ample opportunity to expand upon the work presented in this thesis, and the use of representation theory in general. Some areas we hope to see explored further include: the application of these symmetry analysis to many more systems, both old and new; development of tools for analysing single-crystal data using representation theory; and development of a programme to apply representation theory to incommensurate structures.

For the two systems studied, further work is needed to complete our understanding. For iron oxyborate, the "missing" magnetic moment on the iron sites needs to be investigated and explained. Further, an investigation of the charge-ordering motif within the plane (perhaps using surface techniques) could refute or confirm our proposed structure as it is the only structure that would *not* show distinct charge

striping. For potassium selenate, there remains the analysis of I-phase powder diffraction data. It could also be revealing to perform analysis of this system using basis vectors projected form trials parallel to the Si-O bonds, which would reflect the influence of silicate bonding. More generally, we would like to see support for custom trial functions within popular basis-vector generating routines.

There are also significant areas in which the SARA*h*-Refine module could be developed. In particular it would benefit from an analysis algorithm that is faster, and that scales more efficiently (SARA*h*-Refine scales pseudo-exponentially with the number of refined basis vectors). It would also benefit from a step-size profile derived from a theoretical foundation, rather than the current profile which was determined empirically.

10.5. Concluding remarks

Symmetry is a powerful tool when defining physical systems, yet its deceptive simplicity could lead to the erroneous assumption that the problems with which it is concerned are trivial. In fact, the symmetry of a system is entirely fundamental, and there are many pitfalls that lie in wait for the incautious user. Only by a clear understanding of group and representation theory can we hope to reach the right answers.

Conversely, for a technique to be widely used it must be accessible. It is our hope that, by developing a simple, straightforward approach to applying representation theory along with software supporting its use, this thesis has made the technique more useable. Further, we hope that this will promote wider use of these methods in future work.

References

[1] Aroyo, M. *et. al* (2003). *Phase Transitions: A Multinational Journal* **76**(1-2), 155-170.

[2] Aroyo, M. I. , Kirov, A., Capillas, C., Perez-Mato, J. M., and Wondratschek, H. (2006a). *Acta Cryst.* **A 62**, 115-128.

[3] Aroyo, M. I. , Kirov, A., Capillas, C., Perez-Mato, J. M., Wondratschek, H., Kroumova, E., Ivantchev, S., Madariaga, G., Kirov, A., (2006b). *Zeit. f ur Krist.*, **221**, 15-27.

[4] Campbell B. J, Evans J. S. O. , Perselli F. , and Stokes H. T. (2007). *IUCr Computing Commission Newsletter* **8**, 81-95.

[5] Campbell B. J, Evans J. S. O. , Perselli F. , and Stokes H. T. (2008). *Acta. Cryst.* **A 64**, C216.

[6] Cheary, R. W., Coelho, A. A. (1992). *J. Appl. Crystallogr.* **25**, 109.

[7] Davies, Z., Wills, A. S. (2009). *J. Phys: Conf* **145**, 012072.

[8] Hatch, D. M., Subrata, G. and Bjorkstam, J. L. (1994). *Physics and Chemistry of Minerals* **21**, 67-77.

[9] Kovalev O. V., *Representations of the Crystallographic Space Groups: Irreducible representations, Induced representations and Corepresentations (2nd Ed)*, **Gordon and Breach Science Publishers** (Amsterdamn. 1993).

[10] Larson, A.C. and Von Dreele, R.B. (1994) *Los Alamos National Laboratory Report* **LAUR** 86-748.

[11] Rodriguez-Carvajal, J. (1993). *Physica B.* **192**, 55-69.

[12] Rodriguez-Carvajal, J. (2001) *Fullprof News* **January**, http://www.ill.eu/sites/fullprof/php/Fullprof_News_2001.htm

[13] Rodriguez-Carvajal, J. (2004). *ftp://ftp.cea.fr/pub/llb/divers/BasIreps*

[14] Rodriguez-Carvajal, J. (2008) *Fullprof News* **August**, http://www.ill.eu/sites/fullprof/php/Fullprof_News_2008.htm

[15] Sikora, W. *et. al* (2004). *J. App. Crys* **37**, 1015-1019.

[16] Stokes, H. T., Hatch D. M., *Isotropy subgroups of the 230 crystallographic space groups*, **World Scientific Publishing** (Sigapore, 1988).

[17] Stokes, H. T. *et. al* (2007). **Isodisplace**, stokes.byu.edu/isodisplace.html

[18] Wills, A. S. (2000). *Physica B* **276**, 680.

Appendicies

Appendix 1: Lagrange's theorem

Lagrange's theorum of subgroups states that the order of every subgroup $\mathbb{H}$ of a finite group $\mathbb{G}$ subdivides the order of $\mathbb{G}$.

The proof of this theorem begins with showing that cosets are disjoint. Suppose that $g_1\mathbb{H} \cap g_2\mathbb{H} = 0$:

$$\begin{aligned} \therefore \exists g_1 h_1 &= g_2 h_2 \\ g &= g_2 h_2 h_1^{-1} \\ \therefore g_1 &\in g_2\mathbb{H} \qquad (10.1) \\ \text{Further,} \qquad g_1 h &\in g_2\mathbb{H}h \qquad \forall h \in \mathbb{H} \\ \therefore g_1\mathbb{H} &\subset g_2\mathbb{H} \end{aligned}$$

However, we can reverse the argument and thus:

$$\begin{aligned} g_1\mathbb{H} &\subset g_2\mathbb{H} \\ g_2\mathbb{H} &\subset g_1\mathbb{H} \qquad (10.2) \\ \therefore g_1\mathbb{H} &= g_2\mathbb{H} \end{aligned}$$

The left cosets of $\mathbb{H}$ form a partition of $\mathbb{G}$, they are mutually disjoint, and therefore we need only to show that every left coset has the same number of elements and we are done, since $\mathbb{H}$ is itself a coset of $\mathbb{H}$. If $a\mathbb{H}$ and $b\mathbb{H}$ are two cosets of $\mathbb{H}$ then there

exists a map between them:

$$\begin{aligned} f &: a\mathbb{H} \mapsto b\mathbb{H} \\ f(x) &= ba^{-1}x \end{aligned} \tag{10.3}$$

There also exists a map:

$$\begin{aligned} f &: b\mathbb{H} \mapsto a\mathbb{H} \\ f(x) &= ab^{-1}x \end{aligned} \tag{10.4}$$

Therefore, the mapping has an inverse and must be *bijective*. Thus we have proved that every coset has the same order, and that order divides the order of $\mathbb{G}$

Appendix 2: Maps

Maps associate each element of a set $\mathbb{C}$ with a *single* element of a set $\mathbb{D}$. The set $\mathbb{C}$ over which a function f is defined is termed the the domain, and the set $\mathbb{D}$ the co-domain. There are several categories of mapping:

- Injective: $f(c) = f(c') \implies c = c' \qquad \forall c \in \mathbb{C}$

  A mapping is injective if the image of each element $c \in \mathbb{C}$ is unique: no two elements have the same image.

- Surjective: $\exists f(c) = d \qquad \forall d \in \mathbb{D}$

  The image of a surjective map spans the whole of the co-domain.

- Bijective

  A mapping is bijective if it is *both* injective and surjective. That is, every element in $\mathbb{C}$ has a unique image, and the image of $\mathbb{C}$ is the set $\mathbb{D}$. Bijective functions have an inverse mapping from $\mathbb{D}$ to $\mathbb{C}$.

- Homomorphic: $f(c_1)f(c_2) = f(c_1 \circ c_2) \qquad \forall c_1, c_2 \in \mathbb{C}$

  A homomorphic mapping is a map between two groups in which the structure of the domain is retained.

All transformations considered in this work are isomorphisms of Euclidean spaces.

Appendix 3: Maschke's theorem

Mashke's theorem is central to representation theory and states that every representation of a finite group is completely reducible. That is, if we construct any faithful, finite representation of a finite group, then it is reducible to a direct sum of irreducible representations. It is, of course, critical to our application of representation theory to phase transitions that we can reduce a system representation to a direct sum of irreducible representations. However, the space groups are *infinite* groups, and thus appear to be excluded from Maschke's theorem. Fortunately Mashke's theorem has a more general formulation [**1**]:

> Let $\mathbb{A}$ be a finite group and $\mathscr{K}$ a field whose characteristic does not divide the order of $\mathbb{A}$. Then $\mathscr{K}\mathbb{A}$, the group algebra of $\mathbb{A}$, is a semisimple algebra.

In the case of space groups, $\mathbb{A}$ is the finite group $\mathbb{G}_0$ and $\mathscr{K}$ is $\mathbb{T}$, the set of all primative translations. Thus our space group is represented by the group algebra $\mathscr{T}\mathbb{G}0$, and is *semisimple* which implies it is reducible. These results follow from the fact that our space group is, in fact, a *module*; this fact is used more explicitly in the formulation of superspace group theory.

References

[1] Maschke's theorem,
http://en.wikipedia.org/w/index.php?title=Maschke%27s_theorem&oldid=267859266

Appendix 4: Schur's lemma

Shur's lemma is a generic name applied to several related theorums from different branches of mathematics, and with a correspondingly wide number of proofs. In its most intuitive form it states: for an irreducible representation of a group $\mathbb{G}$, the only matrices which commute with the representation of every element are scalar multiples of the identity matrix. This is useful as a test of irreducibility.

Proof

Consider a representation of some group $\mathbb{G}$, with a symmetric basis ψ_s $(s = 1, ..., n)$:

$$\mathfrak{T}(g)\psi_k^\nu = \sum_{k=1}^{n} \psi_t^\nu D_{ks}^\nu(g) \tag{10.5}$$

Presume that ψ_s^ν is reducible, such that it can be written as the linear sum of a smaller set of vectors $\langle\phi_1^\nu, \phi_2^\nu, \ldots, \phi_m^\nu|$:

$$\begin{aligned} \psi_s^\nu &= \sum_{t=1}^{m} \phi_t^\nu a_{ts} \\ \mathfrak{T}(g)\phi_t^\nu &= \sum_{l=1}^{m} \phi_l^\nu D_{lt}^{\nu'}(g) \end{aligned} \tag{10.6}$$

Hence,

$$\begin{aligned} \mathfrak{T}(g)\psi_s^\nu = \mathfrak{T}(g)\sum_{t=1}^{m} \phi_t^\nu a_{ts} &= \sum_{t=1}^{m}\sum_{l=1}^{m} \phi_l^\nu D_{lt}^{\nu'} a_{ts}(g) \\ = \sum_{k=1}^{n} \psi_k^\nu D_{ks}^\nu(g) &= \sum_{k=1}^{n}\sum_{t=1}^{m} \phi_t^\nu a_{tk} D_{ks}^\nu(g) \end{aligned} \tag{10.7}$$

Thus,

$$\sum_{t=1}^{m}\sum_{l=1}^{m}\phi_l^\nu D_{lt}^\nu(g)a_{ts} = \sum_{k=1}^{n}\sum_{t=1}^{m}\phi_t^\nu a_{tk}D_{ks}^{\nu'}(g) \tag{10.8}$$

Now, as the ϕ_i^ν are linearly independent:

$$\begin{aligned}\sum_{t=1}^{m} D_{lt}^\nu(g)a_{ts} &= \sum_{k=1}^{n} a_{tk}D_{ks}^{\nu'}(g)\\ D^\nu A(g) &= AD^{\nu'}(g)\end{aligned} \tag{10.9}$$

Thus if D^ν is reducible we can find some matrix A which commutes with $D^\nu(g)$ for all $g \in \mathbb{G}$.

If there exists A such that it satisfies our condition, then:

$$\begin{aligned}\sum_{t=1}^{m} D_{lt}^\nu(g)a_{ts} &= \sum_{k=1}^{n} a_{tk}D_{ks}^{\nu'}(g)\\ \sum_{l=1}^{m}\sum_{t=1}^{m}\psi_l^\nu D_{lt}^\nu(g)a_{ts} &= \sum_{t=1}^{m}\mathfrak{T}(g)(\psi_l^\nu a_{ts})\end{aligned} \tag{10.10}$$

Thus the m vectors:

$$\phi_s^\nu = \sum_{t=1}^{n}\psi_t^\nu a_{ts} \tag{10.11}$$

form a basis of the space $D^{\nu'}$ which obeys our restriction.

$$\mathfrak{T}(g)\phi_s^\nu = \sum_{t=1}^{n}\psi_t^\nu D_{ts}^\nu(g) \tag{10.12}$$

Consider the case that D is an irreducible representation. Then we have a contradiction unless $A = 0$, *or* $D = AD'A^{-1}$ and the two representations are equivalent. Further it can be shown that if $A \neq 0$ then it must be a multiple of the identity matrix; $A = c\mathfrak{T}(E)$.

Appendix 5: Zorns lemma

This appendix is a summary of wikipedia articles:
http://en.wikipedia.org/w/index.php?title=Zorn%27s_lemma&oldid=262758135
http://en.wikipedia.org/w/index.php?title=Well-ordering_theorem&oldid=267651043
http://en.wikipedia.org/w/index.php?title=Axiom_of_choice&oldid=270377362

Zorn's lemma is a proposition of set theory, that is related to the well-ordering theory or the axiom of choice. All of these are equivalent in that each is sufficient to prove the other two, but none have been independantly proven.

The simplest of the three is the axiom of choice which states:

> Let $\mathbb{S}$ be a set of non-empty sets;
> we can chose a single element from each set in $\mathbb{S}$

This may appear a self evident statement, but it has not been proven in the case that the order of X is infinite. Indeed the axiom of choice can lead to some apparently absurd results such as the *Banach-Tarski paradox*, which demonstrates that if the axiom of choice is true, then we can decompose a three dimensional Euclidean space into two identical spaces. Thus using only rotations and translations we can transform an object into two copies of itself.

The well-ordering theorem states that every set can be well ordered in the sense that: it is totally ordered; and every non-empty subset has a smallest element. For

a totally ordered set, the following statements are true for all elements of the set:

$$\begin{aligned} a \leq b \quad &, b \leq a \implies a = b \\ a \leq b \quad &, b \leq c \implies a \leq c \\ a \leq b \quad &\text{or} \quad b \leq a \quad \text{or} \quad a = b \end{aligned} \tag{10.13}$$

This theorem is more obviously counter-intuitive than the axiom of choice if we consider the meaning of the set of real numbers $\mathbb{R}$ being well-ordered.

Zorn's Lemma states that for a set $\mathbb{S}$ in which every non-empty, totally ordered subset has a largest element, the group itself has a largest element. It occurs in the proof of several crucial theorems, including the theorem that every vector space has a basis.

A simple outline of the proof, using the axiom of choice, is as follows. Consider the lemma to be false, then there exists a partially ordered set $\mathbb{P}$ such that every subset has an upper bond, and for every element there exists a larger one. Consider that $\mathbb{P}$ is a subset of itself, then for every element $p \in \mathbb{P}$ we may define a bigger element $f(p)$. If we index the elements defined by $f(p)$ we find that the indices span not just the natural numbers, but all *ordinal* numbers. The number of elements is thus greater than the largest possible order of $\mathbb{P}$ (although a counter-intuitive concept, infinite sets can be contained within *larger* infinite sets), and thus contradicts our assumption that every totally ordered subset has an upper bound.

Appendix 6: Scalar products under affine transformations

Here we present a proof of this equation for matricies of dimension 3:

$$\vec{v}_a \mathfrak{P}.\mathfrak{P}^{-1}\vec{v}_b = \vec{v}_a.\vec{v}_b \tag{10.14}$$

For a 4 dimensional matrix on a 4 dimensional vector the proof would be somewhat lengthier and harder to follow. However, generality may be assumed from a simple consideration. A change of basis is an isometry of the n-dimensional vector space V_n, so lengths and angles are unchanged. The dot product of two vectors $\vec{v}_a$, $\vec{v}_b$ can be expressed:

$$\vec{v}_a.\vec{v}_b = |\vec{v}_a||\vec{v}_b|\cos\Theta \qquad \Theta = \arccos\left(\frac{\vec{v}_a.\vec{v}_b}{|\vec{v}_a||\vec{v}_b|}\right) \tag{10.15}$$

Thus a change of basis must leave the dot product unchanged.

The case V_3

$$k = (k_1, k_2, k_3) \qquad v = \begin{pmatrix} v_1 \\ v_2 \\ v_3 \end{pmatrix} \qquad \mathfrak{P}^{-1} = \begin{pmatrix} a_{11} & a_{12} & a_{13} \\ a_{21} & a_{22} & a_{23} \\ a_{31} & a_{32} & a_{33} \end{pmatrix}$$

$$\therefore \mathfrak{P} = C \begin{pmatrix} (a_{22}a_{33} - a_{32}a_{23}) & -(a_{12}a_{33} - a_{32}a_{13}) & (a_{12}a_{23} - a_{22}a_{13}) \\ -(a_{21}a_{33} - a_{31}a_{23}) & (a_{11}a_{33} - a_{31}a_{13}) & -(a_{11}a_{23} - a_{21}a_{13}) \\ (a_{21}a_{32} - a_{31}a_{22}) & -(a_{11}a_{32} - a_{31}a_{13}) & (a_{11}a_{22} - a_{21}a_{12}) \end{pmatrix}$$

$$C = \frac{1}{a_{11}(a_{22}a_{33} - a_{32}a_{23}) - a_{21}(a_{12}a_{33} - a_{32}a_{13}) + a_{31}(a_{12}a_{23} - a_{22}a_{13})}$$

$$\begin{aligned} k\mathfrak{P} =& (k_1(a_{22}a_{33} - a_{32}a_{23}) - k_2(a_{21}a_{33} - a_{31}a_{23}) + k_3(a_{21}a_{32} - a_{31}a_{22}), \\ & - k_1(a_{12}a_{33} - a_{32}a_{13}) + k_2(a_{11}a_{33} - a_{31}a_{13}) - k_3(a_{11}a_{32} - a_{31}a_{13}) \\ & k_1(a_{12}a_{23} - a_{22}a_{13}) + k_2(a_{11}a_{23} - a_{21}a_{13}) + k_3(a_{11}a_{22} - a_{21}a_{12}) \end{aligned}$$

$$\mathfrak{P}_{-1}v = C \begin{pmatrix} a_{11}v_1 + a_{12}v_2 + a_{13}v_3 \\ a_{21}v_1 + a_{22}v_2 + a_{23}v_3 \\ a_{31}v_1 + a_{32}v_2 + a_{33}v_3 \end{pmatrix}$$

We now have everything in place to demonstrate equality:

$k\mathfrak{P}.\mathfrak{P}_{-1}v$

$$\begin{aligned} =& C\big([k_1(a_{22}a_{33} - a_{32}a_{23}) - k_2(a_{21}a_{33} - a_{31}a_{23}) + k_3(a_{21}a_{32} - a_{31}a_{22})][a_{11}v_1 + a_{12}v_2 + a_{13}v_3] \\ & + [-k_1(a_{12}a_{33} - a_{32}a_{13}) + k_2(a_{11}a_{33} - a_{31}a_{13}) - k_3(a_{11}a_{32} - a_{31}a_{13})][a_{21}v_1 + a_{22}v_2 + a_{23}v_3] \\ & + [k_1(a_{12}a_{23} - a_{22}a_{13}) + k_2(a_{11}a_{23} - a_{21}a_{13}) + k_3(a_{11}a_{22} - a_{21}a_{12})][a_{31}v_1 + a_{32}v_2 + a_{33}v_3]\big) \\ =& C(k_1v_1[a_{11}(a_{22}a_{33} - a_{32}a_{23}) - a_{21}(a_{12}a_{33} - a_{32}a_{13}) + a_{31}(a_{12}a_{23} - a_{22}a_{13})] \\ & - k_2v_2[a_{11}(a_{22}a_{33} - a_{32}a_{23}) - a_{21}(a_{12}a_{33} - a_{32}a_{13}) + a_{31}(a_{12}a_{23} - a_{22}a_{13})] \\ & + k_3v_3[a_{11}(a_{22}a_{33} - a_{32}a_{23}) - a_{21}(a_{12}a_{33} - a_{32}a_{13}) + a_{31}(a_{12}a_{23} - a_{22}a_{13})]) \\ =& C\left(k_1v_1 + k_2v_2 + k_3v_3\right)C^{-1} \\ =& k_1v_1 + k_2v_2 + k_3v_3 \end{aligned}$$

Q.E.D

Supporting Material

Documents

WignerTheory.pdf

Pfister, O., *http://www.math.virginia.edu/Institute/MathSeminar2003_04_23.pdf.*

A detailed derivation of Wigner's theory and discussion of its importance in quantum mechanics.

Programs

SARA*h*-Representational Anaylsis, SARA*h*-Refine

Wills, A. S., *ftp://ftp.ucl.ac.uk/pub/users/uccaawi/setup.exe*

Compiled versions of SARA*h* which utilize the verified tables of Kovalev and his settings, and which incorporate options for normal-mode refinement of powder-diffraction data. Also included is an uncompiled copy of the normal-mode refinement module for independent validation.

KovCheck

Davies, Z. L.

Compiled and uncompiled versions of the validation routine used in chapter 5.

SimGen CW

Davies, Z. L.

Compiled and uncompiled versions of routine used in chapter 7.

Experimental

Potassium Selenate

This folder includes the histogram files from HRPD for K_2SeO_4, along with refinements in GSAS, and SARA*h*-Refine.

Iron Borate

This folder includes the histogram files from D2B for Fe_3OBO_3, along with refinements in Fullprof.